AN INTEGRATED APPROACH OF DETERMINING SHALE GAS POTENTIALITY OF CARBONACEOUS SHALE OF THE PERMIAN TULI BASIN, LIMPOPO PROVINCE OF SOUTH AFRICA

Name: George Oluwole Akintola

Student Number: 16014356

Supervisor: Dr. F. Amponsah-Dacosta

Co-Supervisor: Prof. S.M Rupprecht

Co-Supervisor: Dr. S.E Mhlongo

A Thesis Submitted to the Department of Earth Sciences, Faculty of Science, Engineering and Agriculture, University of Venda, in Fulfilment of the Requirements for the Doctor of Philosophy Degree in Environmental Sciences (Geology)

May 2022

DEDICATION

To

The Almighty God for making it possible to complete this milestone degree.

To my father, Pastor Jacob. A. Akintola

To my late mother of blessed memory, Deaconess Comfort. A. Akintola

To my beloved family members

To my Promoters

And

To my priceless and adorable wife, Olutosin Phebean Akintola

To my great son, David Olusola Toluwani Akintola

DECLARATION

I at this moment declare that this thesis entitled "Source-rock and reservoir quality of the Tuli basin for potential shale gas generation in Limpopo Province of South Africa" is my work except where sources are otherwise cited and acknowledged in references. In addition, it has not been previously, in whole or in part, submitted to any examination or university for any degree.

Signed:

………………………………………………….
Student: George Oluwole Akintola

This ……23rd...... day of ……May…… 2022

ABSTRACT

Shale gas displays signs of future potential for energy generation. Apart from the fluctuating prices of liquid fuel and energy resources, the recent national load shedding of electricity supply is probably the most obvious sign of the energy security crisis in South Africa. To expand energy security, there is a need for an energy mix to complement existing sources. Despite extensive studies on stratigraphic, sedimentology, and coal investigations, the source rock potential of organic-rich shale for gas generation remains elusive in the Permian Tuli Basin. As a result, this research aims to investigate the shale gas potentiality of the carbonaceous shale of Madzaringwe and Mikambeni Formations in the Tuli Basin of Limpopo Province, South Africa.

A total of Twenty (20) representative core samples are selected to determine the whole rock major and trace elements using X-ray fluorescence (XRF) and Laser Ablation Inductively Coupled Mass Spectrometry (LA-ICP-MS) respectively. In addition to the mineralogical characterisation using X-ray diffraction (XRD), the functional groups of organic compounds in studied samples are identified using Fourier Transform Infrared Spectrometry (FTIR). Furthermore, the porosity networks of the shale samples are determined using the Scanning Electron Microscopy-Energy Dispersive X-Ray Analysis (SEM-EDX). Lastly, the total organic carbon content (TOC), Kerogen type and thermal maturity of the studied samples to generate hydrocarbon are determined using the Rock-Eval 6 programmed pyrolysis.

The major oxides results indicate a varying amount of Al_2O_3 (19.37–20.32%), CaO (0.20-0.22%), Fe_2O_3 (0.85-0.94%), K_2O (1.59-1.66%), MgO (0.25-0.28%), Na_2O (0.12-0.15%), P_2O_5 (0.04%), SiO_2 (50.37-51.90%), TiO_2 (0.69-0.73%) in the studied Mikambeni samples. The compositional trend of other major components is comparable, except for the lower average value of loss-on-ignition (LOI), which averages 15.04% in the Madzaringwe shale, indicating a lower TOC content. The average LOI values of Mikambeni shales (25.02%) show a higher TOC content which correspond to the actual TOC test. The elemental ratio K_2O / Al_2O_3 (0.08) of the studied samples showed values ≤ 0.5, which suggests a moderately mature shale since a significant amount of Al_2O_3 is typical of immature sediments.

The LA-ICP-MS analysis reveals trace elements Ba (294.16-560.88 ppm), Zn (57.46-121.63 ppm), Zr (189.02–341.72 ppm), Rb (67.69-102.26 ppm), V (81.24-156.88 ppm), Sr (92.02-344.91ppm), Cr (47.50–86.66 ppm), Pb (11.25-35.22ppm) in all studied samples. The presence of Ba suggests the dissolution of mineral barite in the black shale by the action of sulphate-reducing bacteria while Zn indicates paleo-productivity of abundant organic matter. Furthermore, Mo concentration > 2.5ppm of Mikambeni, suggests a marine sediment input in

the Mikambeni samples apart from terrigenous sources in all studied samples. The interpretation of the anoxic environment is consistent with the V/(V+Ni) average value of 0.84ppm which exceeds the 0.54 limit for anoxic conditions for all studied samples.

The XRD analysis shows the presence of montmorillonite, mixed illite/smectite (I/S), illite, chlorite, and non-clay minerals such as dolomite, albite, microcline, pyrite, and quartz in the studied samples. The presence of pyrite suggests activities of sulphide-reducing bacteria on parent organic matters to generate biogenic gas. The presence of illite and chlorite suggests illitisation and chloritization at greater depths of Madzaringwe samples, suggesting a high thermal alteration level for sediments.

The functional group of all studied samples shows infrared absorption peaks between 2800 and 3300cm^{-1} wavelength attributed to an aliphatic C-H stretching vibrations. The sp^2 C-H hybridization found with absorption peak between 3000-3100 cm^{-1} wavelength indicates the aliphatic methane gas stretching of methyl and methylene vibration.

Bubble-like porosity resulting from organic matter decomposition typifies most of the studied samples, suggesting a gaseous release from organic matters. However, isolated-irregular pattern of matrix-mineral pores are displayed apart from preferred-oriented linear pores exhibited by the micro-fracture pore types in all studied samples. The EDX elemental compositions indicate intragranular grains composed of quartz, feldspars, carbonate, and pyrite minerals to form interconnected matrix. Furthermore, a non-spherical, closely packed polyframboidal-pyrite is observed, having multiple presence of Fe contents on the EDX composition. Thus, this suggests an anaerobic condition that favours organic matter degradation that initiates methanogenesis.

The Rock-Eval 6 programmed pyrolysis and TOC of the studied shale samples revealed a TOC content that exceeds threshold limit of 5.0 wt %, indicating an excellent source rock in both formations. The hydrocarbons produced from the thermal breakup of kerogen (S2) ranged from 101.64 to 122.75mg HC/grock with an average value of 115.7mg HC/g rock in the Mikambeni samples. The S2 content of Madzaringwe shale ranged from 15.25 to 16.47 mg HC/g rock averaging at 1.82 mg HC/g rock. The plot of Hydrogen Index (HI) against TOC indicates a mixed kerogen TYPE II-III for the Mikambeni samples and TYPE-III for the Madzaringwe samples, which is gas prone. The maximum temperature, Tmax, corresponding to the peak of hydrocarbon yield (S2) range between 430 to 434°C, averaging at 431.8°C thus indicating a thermally immature source in the Mikambeni samples. On the other hand, the Madzaringwe shale samples yield a thermally mature condensate wet-gas, with Tmax values (464 - 470°C) averaging at 467.2°C. The studied samples have an average Productivity Index

(PI) value of 0.1 which indicates a moderately mature source, generating a mixed biogenic-thermogenic gas. As such, the petroliferous indicators of the studied Mikambeni shale generates thermal immature biogenic gas while Madzaringwe shale produces a matured condensate wet-gas in the Tuli Basin.

ACKNOWLEDGEMENT

First and foremost, I acknowledge the Almighty God and Jesus Christ, my Saviour and Lord, who enabled me to complete this Ph.D. programme. With His strength and help, I was able to accomplish this feat.

Secondly, my overflowing gratitude goes to my Promoter, Dr. Francis Amponsah-Dacosta, and Co-Promoter, Prof. Steven Rupprecht, whose supervisory works transcend academic mentoring but life-imparter. Specifically, I am grateful for the confidence and freedom you gave me to conduct this research under your educational guidance and unparalleled supervision. Your words of encouragement when research pressure and challenges overwhelmed me are always inspiring and motivate me not to throw in the towel. These are rare attributes a supervisor can possess and demonstrate.

My special thanks go to my wife, Olutosin Phebean, and son, Olusola David, for their support. Your encouragement, understanding, prayers, and love inspire me to complete this Ph.D. I cannot but thank my siblings: Advocate Olusegun, Mr. Adekunle, Dr. Akintunde, Mr. Olawale, Mrs. Adeola, and other family members for their encouragement and prayers for the success of this work. At the same time, I would want to appreciate my father and mother-in-law, Pastor and Deaconess Oyebode, for their support morally and prayerfully.

My immense appreciation Mr. Mahlaule Ally for his selfless support during sample collection. Furthermore, my thanks goes to Dr. Joshua Edokpayi, Prof. Wilson Gitari, Dr. Nithyadharseni Palaniyandy, Dr. Akin Olaleru, Prof. Jegede and Prof. Emma Anyasi for their financial support, generosity and contribution, particularly, towards the sample analyses. I am indebted to Dr. Muyiwa Obijole, Dr. Tonna Anyasi, Dr. Comfort Edokpayi, Dr. Israel Ekanade, and Dr. Moses Oyebanjo for their immeasurable supports. Finally, my special thanks go to the leadership of Christ Tabernacle Church and all the members for providing a healthy and homely spiritual family for me.

University of Venda

TABLE OF CONTENTS

Contents   **Page**

LIST OF FIGURES

University of Venda

LIST OF TABLES

LIST OF ABBREVIATIONS AND ACRONYMS

HI	Hydrogen Index
OI	Oxygen Index
PI	Production Index
S1	Volatile hydrocarbon content
S2	Remaining hydrocarbon generative potential
S3	Carbon (IV) oxide amount released
GIS	Gas In-Situ
TM	Thermal Maturity
TOC	Total Organic Carbon Content
TDS	Total Dissolve Solid
EGR	Enhanced Gas Recovery
EOR	Enhanced Oil Recover
BB	Backbulge Basin
NORM	Naturally Occurring Radioactive Material
Tmax	Temperature of Maximum Pyrolysis Yield for HC Generation
Bsm	Billion Square Meters
Mcf	Million Cubic Feet
EIA	Energy Information Administration
SACS	South African Committee of Stratigraphy
MPRDA	Mineral and Petroleum Resources Development Act
DMR	Department of Mineral Resources
DWS	Department of Water and Sanitation
DOE	Department of Energy
DEA	Department of Environmental Affairs

PUBLICATIONS FROM THE THESIS

Journal Publications

- **George Oluwole Akintola**, Amponsah-Dacosta, F., Rupprecht, S., Palaniyandy, N., Mhlongo, S. E., Gitari, W. M., & Edokpayi, J. N. (2021). Methanogenesis Potentials: Insights from Mineralogical Diagenesis, SEM and FTIR Features of the Permian Mikambeni Shale of the Tuli Basin, Limpopo Province of South Africa. *Minerals*, *11*(6), 651: https://doi.org/10.3390/min11060651

Conference Proceedings

- **George Oluwole Akintola**, Amponsah-Dacosta, F., Rupprecht, S., Mhlongo, S. E. (2021). Stable Isotopic Characteristics of the Permian Tuli Basin: Implication for Shale Gas Potentiality, South Africa. **Springer Published Proceedings** of 3rd International Conference of Mediterranean Geosciences Union, Turkey 25-28 November 2021.

- **George Oluwole Akintola**, Amponsah-Dacosta, F., Rupprecht, S., Mhlongo, S. E. (2022). Shale Gas Potential of the Permian Tuli Basin in Limpopo Province, South Africa: Insight from Mineralogical, SEM and Organic Isotopic Constraints. **Univen Research Open-Day Proceeding** 1 March 2022.

Submitted Manuscript

- **George Oluwole Akintola**, Amponsah-Dacosta, F., Rupprecht, S., Mhlongo, S. E., Edokpayi, J. N. (2022). Kerogen Type, Stable Isotopic and Geochemical Evaluation of the Permian Mikambeni Black Shale of Tuli Basin South Africa: Implication for Shale Gas Potential. *Journal of African Earth Sciences Under – peer- review*

- **George Oluwole Akintola**, Amponsah-Dacosta, F., Rupprecht, S., Mhlongo, S. E., (2022). Petrographic, mineralogical, morphological and organic constraints of the Permian Shale in Limpopo-Area Karoo Basin, South Africa: Implication for Potential Shale Gas Generation. **Arabian Journal of Geosciences-Under peer-review.**

- **George Oluwole Akintola**, Amponsah-Dacosta, F., Rupprecht, S., Mhlongo, S. E. (2022). Stable Isotopic, FTIR, and Geochemical Characteristics of the Permian Madzaringwe Shale of Tuli Basin, South Africa: Implications for organic-rich shale provenance. *MDPI, in peer-review.*

CHAPTER ONE

INTRODUCTION

This chapter introduces the shale gas study and its associated petrophysical characteristics, as well as the problem statement, goal and specific objectives, hypothesis, significance, and study motivation. The latter sections of this chapter give specific operational terms and the structure of the thesis, in addition to a description of the subject area.

1.1   Background of the Research

Shale gas displays signs of future potential for energy generation. In contrast to the conventional gas reservoirs, shale gas is marked by self-generation and self-storage mechanisms because it does not migrate nor diffuse over a long distance due to the extremely low permeability of the shale (Chen et al., 2019, Du et al., 2020). Low permeabilities ranging from 1-100nDarcy have been observed in the Whitehill and Prince Albert Formations of Ecca Group in South Africa (Mosavel et al., 2019, Nolte et al., 2019). Despite the micro-pores retaining the fluid or gas, there is an unease flow of fluid between pore spaces due to the low permeabilities. As a result, shale gas recovery at its best would require enhancing driver mechanisms to increase the reservoir pressure during exploitation from impermeable organic-rich shales. The enhancement mechanism such as horizontal well-drilling and hydraulic fracturing technologies are recently used to extract natural gas impregnated in an impermeable organic-rich shale rock (Wang et al., 2018b). The successful and commercial application of these techniques for shale gas production in the United States and other countries such as Canada and China have spurred interest in searching for natural gas deposits in porous but impermeable organic-rich shale formations (Xi et al., 2018).

Accumulation of shale gas in most shale basins such as Barnett, Marcellus, and Hayneville Basins in the United States is dependent on the availability of carbonaceous organic matter in respect of quantity, quality, and level of thermal maturity (Mastalerz et al., 2018a). Basically, the organic matter with high total organic carbon (TOC) content greater than 2% indicates a good prospect for gaseous source rock (Jarvie et al., 2007). Organic materials can accumulate in shale sediments due to an erosional or an allochthonous process. Furthermore, it may form as an in-situ deposit during an autochthonous process from land or the aquatic environment until diagenesis is attained (Dai et al., 2020a). An increase in burial depth, temperature, and pressure over geological time results in a physical and chemical transition in organic matter to humin and kerogen under an anoxic condition (Akintola et al., 2021). Kerogen is an insoluble organic matter made up of algae, pollens, spores, and woody plants that influences the type

and quality of hydrocarbon that accumulates. According to some studies (Cai et al., 2020, Dai et al., 2020b, Froidl et al., 2021) higher plants with vascular tissues, leaves, and cell walls of woody tissues can undergo heat change to create Kerogen prone to gas generation

In shale reservoir rock, the generated gas is stored in shale strata in the form of free gas within inherent fracture or lamina between the layers (Xi et al., 2018). It can also be stored as adsorbed gas in pores of organic matters (OM) and clay minerals because of high specific surface area that provides adsorption sites for gas. The presence of high content of free gas in pores, fracture or lamina is considered to increase production rate of shale gas although it may be controlled by porosities and gas saturation (Wang et al., 2018c, Feiyu et al., 2013). According to a report (Pan and Connell, 2015) on shale gas extraction from the Barnett and Hayneville shale, a considerable amount of total in-situ gas is stored as free gas rather than adsorbed gas or dissolved gas. However, to accelerate gas recovery from low-porous shale formations, an artificial crack or porosity is generated using high-pressure hydraulic fracturing technique (Kazak and Kazak, 2020). As such, shale porosity has been considered as a veritable reservoir parameter to predict and evaluate shale gas content, as well as its recoverable volume (Theloy et al., 2019, Srinivasan et al., 2019).

The reservoir quality of shale gas with low permeability critically depends on the porosity mechanism for storing hydrocarbon gas (Al-Selwi and Joshi, 2015, Zhang et al., 2018c). Organic-matter porosity has been reported to promote TOC, thermal maturity and possible generation of shale gas (Zhang et al., 2018c). The mineral components and organic matter influence the behaviour of shale as a storage host for natural gas by offering a sorption site on the organic surface as void filing (Fort Worth, 2008). However, biological precursors preserve cavernous micropores. However, little original porosity exists within most mineral grains that influence the hydrocarbon displacement phenomena and hydrodynamic solubility. Due to the coexistence of minerals and organic matter, gas shales are generally stored both in an adsorbed state in contact with organic matter and in a free gas state in intergranular porosity and fractures (Jarvie et al., 2007, Boruah et al., 2019). This stands in contrast to conventional reservoirs that contain gas mainly in a free state, and it also differs from coal where coalbed gas is predominantly sorbed on abundant organic matter (Clarkson and Bustin, 1996). Moreover, due to different pore sizes, gas flow in shales is expected to occur via both Knudsen diffusion and slip flow in nanometer-size pores and Darcy-like flow in larger pores (Kuila and Prasad, 2011) as opposed to Darcy-like flow in micrometer or even larger pore sizes in a conventional reservoir.

Historically, coal has been the dominant contributor to the Southern African power grid and will continue to dominate in the next decade (Nhamo, 2011, Eskom, 2010). Considering the

depletion of coal reserves and a global paradigm shift towards a cleaner energy economy, shale gas represents an opportunity to strengthen energy security while cutting down greenhouse gas emissions. At present, South Africa's carbon emission from coal-fired power plants stands at an average of 460 million metric tonnes of CO_2 equivalent yearly according to Postsdam Institute for Climate Impact Research (Jakob and Steckel, 2014). Meanwhile, the US greenhouse gas emissions from fossil-fuel combustion have declined by 390 million metric tons CO_2 in consecutive years since 2006 more than any other country (Wang et al., 2014). In contrast to the conventional gas reservoir, natural gas is trapped within shale formations under relatively low pressure. It largely consists of methane which has a high heat value (15MJ) though less than coal (25 MJ) but greater than wind and solar heating value (Chen et al., 2019). Apart from methane, shale gas may also contain an insignificant proportion of ethane and a lesser amount of non-hydrocarbon compounds and efficient compliance with the use of "carbon capture storage technology" to capture any carbon emission (Zhiltsov and Semenov, 2016a, Zhiltsov and Semenov, 2016b, Wang et al., 2011).

In South Africa, several studies on shale gas have concentrated on the lower Ecca Group in the main Karoo Basin. The concentration of recent research work on this region might have resulted from the need to understand the natural gas that escapes from the Whitehill Formation at Loeriesfontein after drilling a borehole 30 years ago (De Kock et al., 2017, Van Vuuren et al., 2011). After petroliferous characterisation of the lower Ecca group, the work of Geel *et al.* (2013) indicated the presence of an overmatured kerogen-type that could partly generate gaseous hydrocarbon in shale deposit associated with the Whitehill and Collingham Formations. However, the underlying Prince Albert Formation of Ecca group showed kerogen typed II-III hosted shale which implied gas prone source with limited liquid hydrocarbon but resource estimate was not quantified.

The work of De Kock et al (2017) have suggested a potential resource estimate of 12 to 48 trillion square meters (tsm) for the Ecca group, particularly the Whitehill Formation in contrast to an initial estimate of 450 tsm (Administration and Kuuskraa, 2011, Decker and Marot, 2012). The work argued that the dolerite intrusion that resulted from Cape Orogeny 250 Million years ago has been responsible for the heat flow causing degassing, thus deflating the initial gas estimate of 450 tsm. Although the study of Decker and Marrot (2012) predicts gas resource between 25- 410 tsm; the Administration and Kuuskraa (2011) estimated the reserve base of Karoo Basin at 360 tsm b of which the Whitehill Formation was noted to contribute 211 tsm. Meanwhile, there are incongruous reports on shale gas estimates in this karoo basin and the real gas potential remains unclear.

Although several investigations (Mosavel et al., 2019, Baiyegunhi et al., 2018b, De Kock et al., 2017, Black et al., 2016, Geel et al., 2013) have been carried out on the shale gas potentiality of the Ecca group, nothing is known about the shale gas potential of the Tuli Basin situated in the north-eastern part of South Africa. Meanwhile, coal deposits, sedimentology, and stratigraphic studies have been substantially conducted in the region (Denge and Baiyegunhi, 2021, Malaza, 2014, Kataka et al., 2018). To resolve this knowledge gap, this study investigates the source and reservoir quality of the carbonaceous shales in the Tuli Basin for the potential gas generation to expand and strengthen the energy security of the country and reduce greenhouse gas emissions from coal-fired power plants. This study significantly improves the current understanding of the extent of the shale gas resources and the status of the local reservoir capacity in which such developments are to take place. To address this gap, core samples of organic-rich shale are collected and subjected to various petroliferous characterisation to better understand their diagenetic transformation, depositional environment, paleo-productivity, reservoir quality and gas generation potential.

1.2 Statement of the Problem

Recently, South Africa has been experiencing an energy supply crisis, rolling out a managed blackout across the country according to schedule – "load shedding" (Andreasson, 2018, Bohlmann et al., 2016, Baker et al., 2014a). The chronic shortage in electricity supply was first experienced in 2008 and it has lingered up to date on regular basis (Trollip et al., 2014). This national load shedding of electricity supply is the most obvious sign of energy insecurity in South Africa. Possibly, technical problems or cable theft may have been attributed to the load shedding crisis but the prior announcement of load shedding timetable, provided by the national energy supplier, Eskom, is most likely an attempt to avoid a total shutdown of the power grid. The challenge of load shedding at various parts of the country remains critical and partly connected with the rise in demand for energy consumption for domestic and industrial uses (Department of Energy, 2016). This report is consistent with the electricity demand trend that grows steadily at around 3.5% per year (Eskom, 2010). In the past few decades, South Africa has been enjoying reliable, secure, and cheap electricity but household energy demand between 1994 and 2015 has increased from 34% to 88% (Eberhard and Naude, 2016). In South Africa, an endeavour to increase the energy supply in the next decade and reduce greenhouse emission has spurred the interest in the aggressive search for alternative energy of which shale gas has been identified as part of the "5- points Energy-Plan" (Pollet et al., 2015).

In addition, the increasing greenhouse gas emission in South Africa has posed a significant threat or barrier to achieving a lower carbon economy. South Africa's carbon emission from

coal-fired power plants stands at an average of 460 million metric tonnes of CO_2 equivalent yearly according to Potsdam Institute for Climate Impact Research (Jakob and Steckel, 2014). Given that the 15 coal-power plants supply about 90% of South African's energy, it also contributes approximately 1.4% of global greenhouse gas emissions which compound climate change challenges (Pradhan and Mbohwa, 2014, EIA, 2011). Consequently, South Africa is not only the largest and leading carbon emitter in Africa but ranked the 14th highest emitting country in World (Merven et al., 2014). Following the 2015 Paris Climate Agreement, South Africa pledge an equitable contribution to the climate targets of limiting the global temperature increases below 2[o]C. In response, the country intends to aggressively reduce its carbon emission hence setting a target of 30% reduction to achieve a greener economy by 2040 (Department of Energy, 2016). Heavy greenhouse gas emissions from coal-fired power plants devastate the climate and exacerbate global warming hence a need to shift from a brown economy to a greener economy by exploring shale gas as alternative energy to coal (Scholvin, 2014, Andreasson, 2018).

To expand energy security through an energy mix and achieve a low carbon economy in South Africa, there is a need to explore unconventional shale gas resources as an alternative energy source. The weakness of renewable energy sources such as solar plants includes their inability to deliver sufficient energy for the energy-intensive consuming mining companies, automobile, and other extractive industries (Steyn, 2015). As a result, the petroliferous potential of organic-rich shale strata in the Tuli Basin for energy alternative uses in South Africa was explored to determine reservoir maturity for natural gas generation.

1.3 Aim and Specific Objectives

This research investigates the source and reservoir quality of the carbonaceous shales associated with the Tuli Basin for natural gas generation potential. The implication of the study was to expand the energy-mix, strengthening the energy security in South Africa, thus reducing the greenhouse gas emissions from the coal-fired power plants.

The **specific objectives** set out to achieve this aim include:

- To ascertain the diagenetic alteration of the carbonaceous shale.
- To determine the origin of organic matter associated with the carbonaceous shale.
- To examine the reservoir pore network of the studied shale samples.
- To evaluate the source rock and reservoir quality of the studied shale.

1.4   Research Hypothesis

The intelligibly assumptions or theories that are tested to achieve the objectives of this research include:

- The degree of diagenetic alteration of organic matter in carbonaceous shale determine their conversion to kerogen prone to gas generation.
- Shale rocks found in a highly reducing anoxic environment are enriched in sufficient amount of total organic carbon to expel natural gas.
- The reservoir quality of shale rock depends largely on the porosity network to host the generated shale gas.
- The generation of shale gas is determined by the thermal maturity, sufficient quantity, quality of organic matter in the shale rock.

1.5   Motivation for the Study

The rationale underlying this study is the availability of vast deposits of organic matter rich in indigenous land plants that are expected to be an excellent source rock for shale gas generation. The heterogeneous nature of the geological setting and structural complexity of this basin could be responsible for the variation of its associated organic matters in comparison to other basins. In contrast to the pre-Devonian age, the Tuli Basin consist of a post-Devonian shale sequence marked with a significantly higher land plant having cellulose and lignin (Kenrick and Crane, 1997; Chesshire et al., 2017). Under suitable diagenetic and catagenetic and meta-genetic processes, the organic matter converts to kerogen type III or II/III depending on its amount and quality to generate shale gas. To date, there is no available information on this basin's potentiality for shale gas generation. Based on its available carbonaceous shale sequence which is a fundamental prerequisite for gaseous source rock (Malaza, 2014; Luyt, 2017), there is a need to investigate its source rock potentiality.

Furthermore, the drastic decline in shale gas resource estimate raises serious concern hence the need to investigate more potential reservoirs for natural gas for energy mix. According to Kuuskraa et al. (2011), an original shale gas resource estimate at 475 tsm for Karoo Supergroup remains highly speculative and grossly inflated due to insufficient data necessary to conduct the assessment. De Kock et al. (2017) used a probabilistic technique to deflate the initial resource estimate to a smaller cautious figure of 45 tsm. Because of the dramatic drop in South Africa's prospective shale gas potential, additional viable source rocks in other parts of the country must be identified.

1.6   Significance of the Study

The exploration of the country's potential for unconventional shale gas development as an energy mix can complement existing energy sources, thus, expanding the energy security of South Africa. Addressing energy insecurity in South Africa is possible by widening domestic resources other than coal which may not satisfy the country's current demand for energy supply that grows steadily around 3.5% annually with increasing variation in some years. Presently, coal is the dominant primary energy source in South Africa and accounts for 95% of electricity production (Dunmade et al., 2019). Aside supplying electricity, the coal resource is synthesized into liquid fuel such as petrol, diesel, paraffin, and polymer at Sasol and PetroSA refineries, accounting for about 35% of the country's liquid energy (Department of Energy, 2013; Trollip et al., 2014). Despite its multifarious benefits to supply various forms of energy, proposition for more coal-fired power plants at Kusile and Medupi, and the conventional gas reserve in Ibhubesi West Coast are insufficient to justify energy independence due to widespread domestic, regional, and international demands.

With respect to climate change mitigation, the development of shale gas will promote a short-term accelerated action to achieve the 2015 Paris agreement climate targets of limiting the global temperature increases below 2°C (Bohlmann et al., 2019). According to some studies (Andreasson, 2018, Wang et al., 2014) shale gas revolution in the US from 2006 to 2017 reduced CO_2 emissions by around 430 million metric tonnes. Greenhouse gas emissions into the environment have been blamed for global warming, which has resulted in climate change challenges. The South Africa government plans to aggressively reduce greenhouse gas emissions from coal-fired plants owing to climate changes vulnerability (Department of Environmental Affairs DEA, 2016). Due to its heavy reliance on coal, South Africa ranks among the dirtiest energy producer in the globe. As such, harnessing shale gas can transform the carbon level landscape from a brown to a green environment, thus, encouraging a low carbon economy.

The economic benefits of shale gas development have a potential impact on the commercial and socio-economic viability of the country through tax revenue and services related to shale gas production. Severance tax accruable from the removal of shale gas and its sale tax can promote the prosperity and economic stability of the province of production as well as the entire country. According to Mohtar et al. (2019), shale gas taxes constitute the major revenue source for the Texas economy accounting for over 30% of its fiscal financial years. Furthermore, shale gas development will positively impact jobs and wages through employment provision. A sizeable number of employees will be required at different stages of

shale gas production in a given site for different activities. Activities related to construction, drilling, fracking, completion of wells will require skilled, semi-skilled, and labourer personnel.

1.7   Description of the Study Area

The study area is described in terms of geographical location, topography and drainage pattern, vegetation, climate condition and local geology.

1.7.1 Geographical location of the study area

The Tuli Basin is a trans-frontier depozone that straddles the triple junction of South Africa, Zimbabwe, and Botswana (Bordy, 2000). Figure 1.1 shows the location of boreholes from which carbonaceous shale of Madzaringwe and Mikambeni Formation in the Tuli Basin are retrieved.
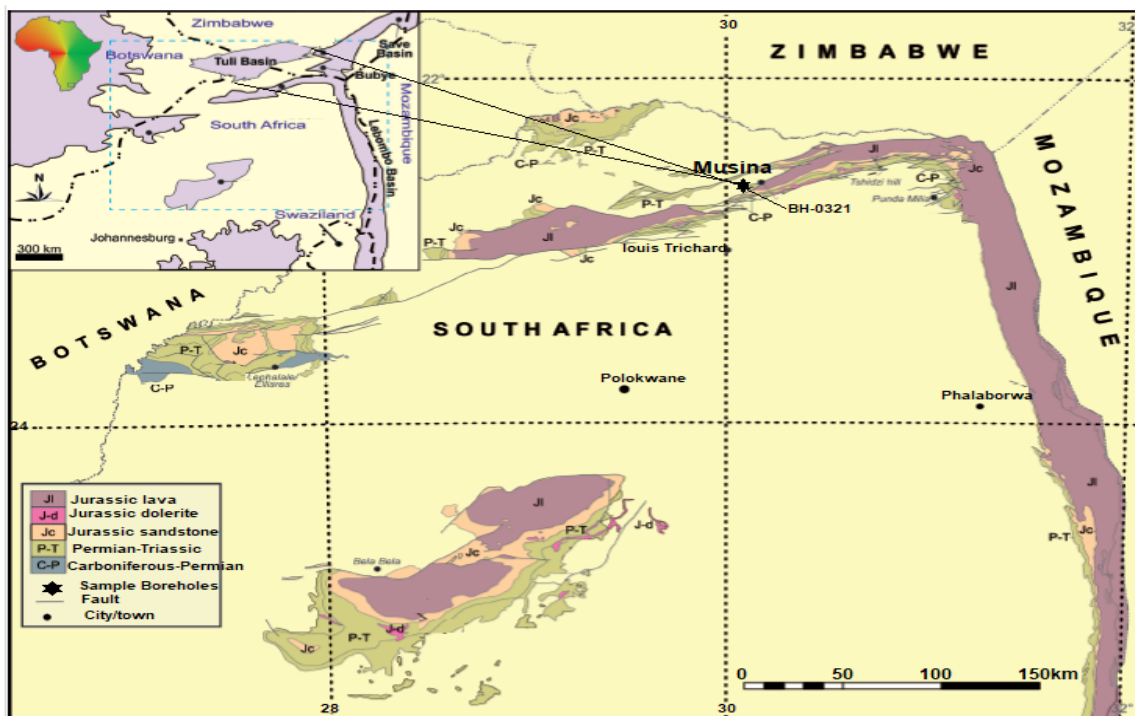
Figure 1.1: Geological map showing the location of the study area (modified after Bordy, 2018)

The South African Tuli Basin has both the Limpopo area Karoo-aged sedimentary rocks. The estimated thickness of the sedimentary sequence ranged from 950 to 1050 m (Chidley, 1985). This Northern Karoo-aged Basin lies between 21°00´00″S and 22°30´00″S and longitude 28°28´00″E and 30°15´00″E as shown in Figure 1.1. It is situated at the extreme north-east of Limpopo Province near the border of Zimbabwe and Mozambique and about 150 Km north of Thohoyandou town. It lies north of Soutpansberg Mountain Range and stretches about 200Km from Waterpoort in the west to Kruger National Park in the east (Brandl, 2002). The proximity of Louis Trichardt and Musina towns relative to the study area are approximately 20

km south and 25 km north respectively. The topography of the study area is characterised by the Soutpansberg mountain range. This regional topographic structure extends for approximately 200 Km, giving rise to a prominent east-west striking mountains and valleys. The landform is moderately undulating and characterized by scattered outcrops of relatively small hills towards the East and the West. The access roads leading to the study area are good and easily navigated. The topography of the Tuli basin is undulatingly ranging from 600 to 900 m above the main sea level (Nemakundani, 2009).

According to Middleton and Bailey (2009), the Limpopo River is the major river that drained the study area. However, six main river systems are tributaries to the Limpopo River and have different sources. Luvuvhu, originating from the east of Louis Trichardt; Mutale originating in Thathe Vondo; Mutamba originating on the farm Buelgum Poort; Nwanedzi originating near Mavhode; Nzhelele originating in Thathe vondo and Sandrivier originating between Potgietersrus and Pietersburg.

1.7.2 Land-use and vegetation cover

In Musina, land use is mainly for mining and agricultural activities. Mining of coal by Coal of Africa (now MC mining) and Venetia diamond mining are the major anthropogenic activities found in the study area. The quality of coal being mined may be imparted by the depositional environment, plant communities, climatic variation, and Jurassic dolerite intrusion (Brandl, 2002). Pottery manufacturing, livestock rearing, and plantain plantations, as well as construction, are some of the other land-use activities. The research region is comprised of open grasslands with scattered trees and bushes in the Venda dry Mountain Bushveld and Mopani woods (Ramaano, 2021a). However, a semi-deciduous forest prevails along the streams. Some types of trees that dominate the study area are Acacias and a Baobab tree. At a relatively low proportion Poinciana (flamboyants), Jacandas, Frangipani and Bougainvillea flourish trees are also identified (Ramaano, 2021b).

1.7.3 Climatic condition of the study area

The study area is situated in a dry savannah sub-region marked with open grassland and scattered trees and shrubs. The regional climate is strongly influenced by the east-west orientated mountain range which represents an effective barrier between the south- easterly maritime climate influences from the Indian Ocean and the continental climate influences (predominantly the Inter-Tropical Convergence Zone and the Congo Air Mass) coming from the north. Summer rainfall in the area comes in the form of strong thunderstorms or light rain, with rainfall ranging between 450 and 890 mm (Cory-Toussaint et al., 2021). It is hot and dry, resulting in high evaporation rates. Cool, dry winters (May to August) and warm, wet summers

(October to March) characterise the region, with April and September serving as transition months. Temperatures in elevated places and the entire region range from 18 to 39.9°C, respectively, although the area is normally frost free (Kobylkin et al., 2019)

1.7.4 Sedimentary sequence of the study area

The sedimentary sequence of the Tuli Basin can attain a maximum thickness of about 920 m but have an average estimate thickness ranging from about 450 to 500 m that occupies an area extent of about 1000 Km^2. It comprises an alternating clastic sedimentary rocks and chemical deposits that unconformably overlies the high-grade metamorphic rocks of the Limpopo Mobile Belt (Johnson et al., 2006a). Figure 1.2 shows the stratigraphic sequence of lithologies in the Tuli Basin in comparison with the Main Karoo Basin (MKB) and other Limpopo area sedimentary basins.
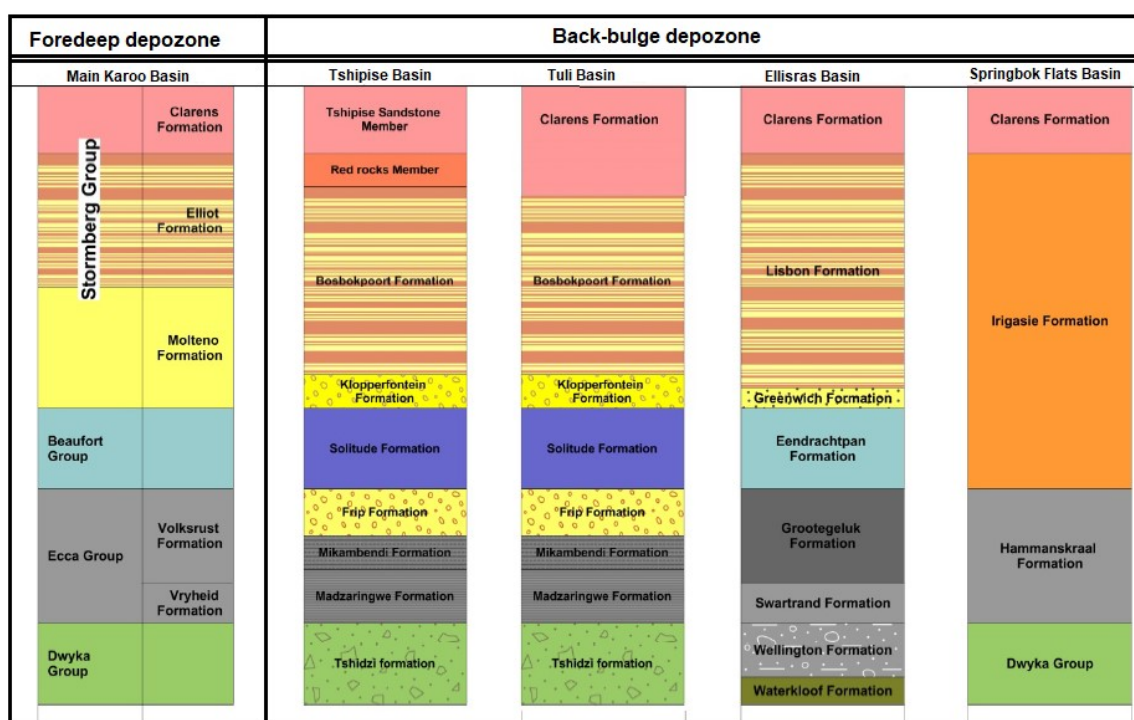
Figure 1.2: Sedimentary sequence of the Tuli Basin correlated with Main Karoo Basin and neighbouring Basins (modified after Johnson et al., 2006a)

The basin has a strike length of ± 200 km while its chronological succession from oldest to youngest are the Tshidzi, Madzaringwe, Mikambeni, Fripp, Solitude, Klopperfontein, Bosbokpoort and Clarens Formations as shown Figure 1.2 (Bordy and Catuneanu, 2002b). Given the overall lithofacies, the basin is considered to be deposited by fluvial processes from Permian to the Jurassic Period (Johnson et al., 2006a). The Permian black organic-rich shales are mainly deposited in Madzringwe and Mikambeni Formations with alternating sandstone, siltstone and coal seam (Bordy, 2018). The shale colour and content suggest a reducing

condition associated with oxygen deficiency causing decay of fauna and flora or plant organisms. Plant remains such as *Dicroidium*, which are deposited may be responsible for the main coal seam that developed above the carbonaceous shale of Madzringwe Formation (Chidley, 1985, Bordy, 2018). The thickness of this carbonaceous shale is generally above 25 m but increases northeast above 50 m. Variation in shale thickness could be controlled by basin tectonics and differential subsidence or depositional trends as transporting river flowed from the northwest to deposit more sediments towards the southeast direction of the basin (Cadle et al., 1993). In contrast to lithofacies of Madzringwe and Mikambeni, the Tshidzi Formation shows non-sorted to poorly sorted argillaceous or sandy sediments with particles size up to 2 m in diameter. This argillaceous diamictite suggests a glacial or fluvioglacial environment resulting from a low energy level of mudflow to deposit well-sorted sediments. There are progressive changes from an anoxic to oxidizing environment as shale formations become older. The Triassic black shale at the lower unit of Solitude Formation was observed to become dark grey shale and grey shale towards overlying Bosbokpoort and Clarens Formations (Johnson et al., 2006a). This may reflect a progressive fall in water level where sediments are deposited on floodplains of meandering rivers under dry and oxidizing conditions. The preponderance of red calcareous concretions of overlying Bosbokpoort further supports oxidizing environment towards the upper Tuli Basin.

1.8   Operational Terminology and Definitions

Certain terms and definition must be specified properly for a better comprehension of the work given in this thesis. The major concepts and terminologies utilized in the thesis are defined and explained in this part.

- *Source rock:* An organic-rich shale rock which can generate natural gas if heated sufficiently.
- *Shale Gas:* An unconventional hydrocarbon resources characterized by co-existing source rock and reservoir with no obvious trap seal.
- *Reservoir:* It is same rock as the source rock in this unconventional resource system.
- *Reservoir Quality:* This refers to pore space types that trap the generated gas in the same rock or shale formation without migration to adjacent formation.
- *Effective/Excellent Source Rock*: A source rock that has a minimum value of 5% total organic carbon by weight.
- *Kerogen*: This refers to an insoluble organic matter
- *Condensate-Wet Gas*: This refers to natural gas that contain about 85 % methane and liquid hydrocarbon such as ethane and propane.

- ***Thermal Maturity:*** It refers to the degree of heating a source rock in the process of transforming kerogen into gaseous hydrocarbon, evaluated by pyrolysis and vitrinite reflectance methods.

1.9   Structure of the Thesis

The thesis is divided into seven chapters which are discussed under different sections and sub sections.

The first chapter includes background information on the research thrust, delivers the study problem statement, and highlights the research's aim and specific objectives. The research hypothesis, purpose, and significance of the study are also included. The final section of this chapter described the local study region as well as the operational terms and definitions employed in this research.

The second chapter provides a comprehensive evaluation of the current and existing state of knowledge about shale gas reservoirs, noting gaps in past research and the need for new study. This chapter contains various pertinent comments on the Tuli Basin's deposition, sequence stratigraphy, organic matter depositional environment, and diagenesis of organic matter, inorganic minerals, and kerogen types. Furthermore, subjects such as porosity, permeability, quantification techniques, and functional groups in connection to reservoir quality are examined. The second half of this chapter covers the global history of the shale gas play, the development and current state of shale gas in South Africa, shale gas recovery, potential restrictions, and mitigating options.

The third chapter presents the materials and methods used to achieve the objectives of this study. In addition to providing information on sample collection and preparation, this chapter discussed how the mineralogical, geochemical, stable isotopic fractions, functional groups, and morphological compositions of the examined shale samples were carried out. The latter section of this chapter provides a detailed information on how the total organic carbon content (TOC) and source-reservoir potential are evaluated using the Rock-Eval-6 programmed pyrolysis.

The fourth chapter reports the findings and discussion on mineralogical and geochemical analysis of the studied shale sample. The initial section provides information on the background and purpose of this chapter. In addition to the results and interpretations presentation, this chapter also discusses their significance in respect of diagenetic, paleo-redox condition and paleo-productivity. The last section of this chapter offers the summary of the chapter.

The fifth chapter provides the findings and discussion on the stable isotope of carbon and oxygen and functional groups of the organic-rich studied shales. In addition, an information on the examined porosity types of the studied samples are provided. Meanwhile, the scientific implications of these analysis in relation to organic matter origin, methanogenesis potentials, and reservoir porosity quality are explained. The latter part of the chapter presents the chapter's summary.

The sixth chapter presents the findings and discussion on the organic richness, quality and thermal maturity of kerogen to generate shale gas. The earlier section of this chapter provides the background and purpose of the chapter. Afterwards, the results and interpretations of the analysed samples are provided. A thorough explanation of source rock and reservoir quality is presented before the final section on the chapter's summary.

The seventh chapter focuses on the summary and conclusions taken from the data analysis findings and results. It also highlights the research's contribution to knowledge as well as the constraints that hampered the research. This chapter concludes with recommendations for future or further research to improve and develop this study.

CHAPTER TWO

LITERATURE REVIEW

The investigation of shale reservoir maturity for the potential generation of natural gas requires a contextual understanding of organic shale formations and their kerogen types. This chapter provides a critical discussion of the current and existing level of knowledge on shale gas reservoir and generation and the research gap in the Tuli Basin of South Africa. A comprehensive review and critical analysis of the regional geology and tectonic development of the Tuli Basin has been conducted comprehensive. Sequence stratigraphy and sedimentology of the Basin was described, revealing the organic-rich formations. Detailed information on global shale gas occurrences and its current status quo in South Africa is discussed. The potential prospect and pitfall of shale gas development are provided as well as the proposed mitigation to the perceived concerns about shale gas productions.

2.1   Geological Setting

This section provides the geological settings of the Limpopo Belt under various sub-sections, including the regional geology of the Tuli Basin and its development, tectonic and thermal development, and stratigraphic sequence and sedimentation of the Tuli Basin.

2.1.1 Regional geology and tectonic development

The sedimentary strata of the Karoo Supergroup in South Africa are commonly regarded to have influenced the tectonic formation of the Tuli Basin. The deposition of Karoo sedimentary rocks in South Africa between the Late Carboniferous and Middle Jurassic periods was a response to the break-up of the Gondwana Craton circa 540 Ma in terms of tectonic event sequence. The Pan African Orogenic event, which occurred between 600 and 450 Ma, is thought to have produced this cratonic break-up. Due to the widespread of tectonothermal effect, the orogeny resulted to several fold belts, intracratonic thermal sag basin or rift basin which controls depositional patterns of sediments (Groenewald et al., 1991).

However, different models have been proposed for the development of the Tuli Basin. According to Rust (1975), the Karoo sedimentary sequence is deposited in two different tectonic settings which are separated by the Limpopo River. The Tuli Basin, to the north of the river, is suggested by sedimentation that occurred in a separate fault-controlled basin, whereas a comparatively stable miogeosynclinal depression is found south of the Limpopo

River. Implicitly, these localised Limpopo fault and depression structures were likely to be formed without volcanic activity and their sediments deposited in shallow water environment. In line with the theory of continental drifting, miogeosyncline troughs are associated with quiescent volcanism (Mitchell and Reading, 1969, Rolf et al., 2012). In other word, Rust (1975) implied that the Limpopo lineament formation is not related to volcanism but attributed in part to the lineament, Sabi and Nuanestsi synclines, to the intense Karoo volcanic eruption between 200 and 175 Ma ago. This proposition spurred a question as to the possibility of the two parts of the Limpopo lineament being formed by volcanism while the third part, Tuli syncline, could have been formed by crustal drifting. In spite of this, some studies (Groenewald et al., 1991, Cox et al., 1965) alluded that the Tuli and Nuanetsi synclines combined to form an east-west trending lineation on the north of Messina Block and meet the Sabi monocline, but Cox (1965) attributed the Tuli syncline to the Limpopo orogenic belt. To infer, the age and tectono-volcanic structural relationships for the evolution of the Tuli basin were not provided by this model.

Furthermore, Cloos (1939) proposed another theory, claiming that plume-generated triple rift junction mechanisms were responsible for the formation of the Tuli syncline. It was proposed that the hot plume underneath the continental plates of Sabi, Lebombo monocline, and Limpopo rift upwelled and ruptured along a three rifts junction about in 2 Ga (Cloos, 1939). In response, the Lebombo and Sabi crustal blocks spread out following the plate tectonic regime while the Limpopo crust did not spread, hence became a failed arm of the triple junction. This hypothesis was consistent with previous study (Burke and Dewey, 1973), recognizing that every plume-generated triple junction is less than 2.0 Ga old, which may be associated to the earliest incident of the Gondwana continental break-up. Figure 2.1 illustrates the theory of plume generated triple junctions and rift valley development of the Tuli Basin.
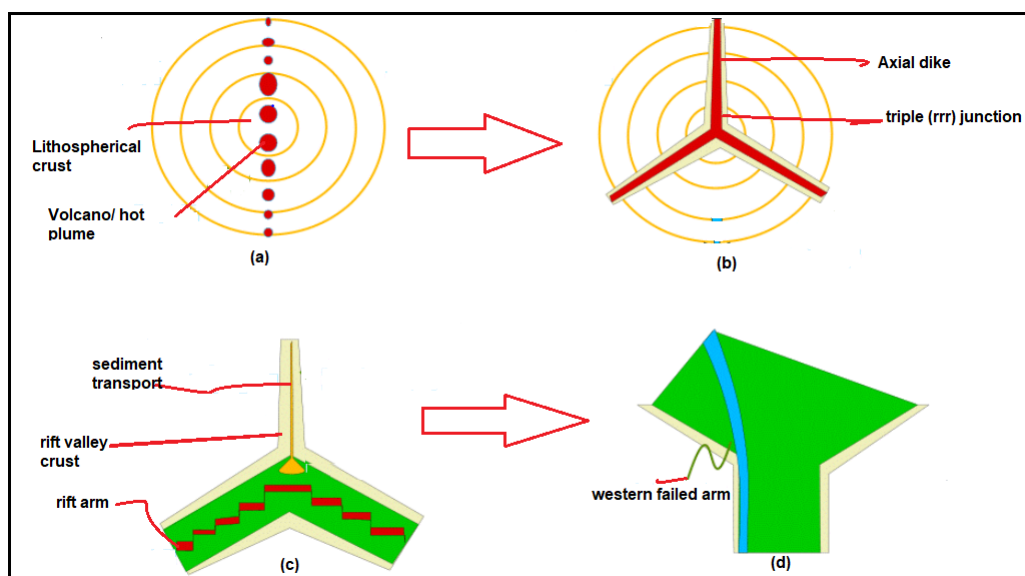
Figure 1.1:Plume – generated triple junctions (a) uplift develop over plume with crestal volcano (b) three rift valleys develop meetings at the triple rift junction of Tuli Basin (c) sediment transport to rift valley crust (d) two crustal blocks spread and one failed to spread and one failed to spread

A different model from the pull-apart rhombochasm model suggested an episodic subduction of the paleo-pacific plate beneath the Gondwana plate between the late Paleozoic and Early Mesozoic periods (Watkeys and Sweeney, 1988, Catuneanu et al., 1998). Catuneanu et al. (1999) suggested a combination of tectonic episodes for the basin's evolution, based on an extensional rift model presented by Watkeys and Sweeney (1988) for the Basal Unit of Tuli Basin.

Recent research (Catuneanu et al., 2005, Catuneanu, 2004) on the history of the Tuli Basin proposed a structural back-bulge foreland depozone model. It was proposed that in the Late Palaeozoic–Early Mesozoic, flexural subsidence coupled with subduction of the Paleo-Pacific Plate beneath the Gondwana plate resulted in the formation of a foreland system towards the north of the Cape Fold Belt (CFB). Despite the development of the forebulge and foredeep, the back-bulged setting finally migrated between 1500 and 1800 Km to form the Tuli Basin in Northern Limpopo. While the retroarc foreland model for evolution of the main Karoo Basin (MKB) has been interpreted as the foreland system consisting of the foredeep and forebulge provinces, the back-bulged flexural subsidence has been observed to conserve sediments that accumulated in the Tuli Basin of South Africa (Catuneanu et al., 1998, Catuneanu et al., 1999, Bordy, 2000). Measurements on the Tuli Basin's paleo-current system show an ENE-WSW flow direction, which coincides to the strike orientation for the back-bulged flexure, implying this back-bulge hypothesis (Bordy, 2000). Figure 2.2 shows the development of the Tuli Basin as a back-bulge basin in the Karoo retro-arc foreland system in comparison to MKB and other Limpopo-aged Karoo Basins in the Limpopo Province of South Africa.
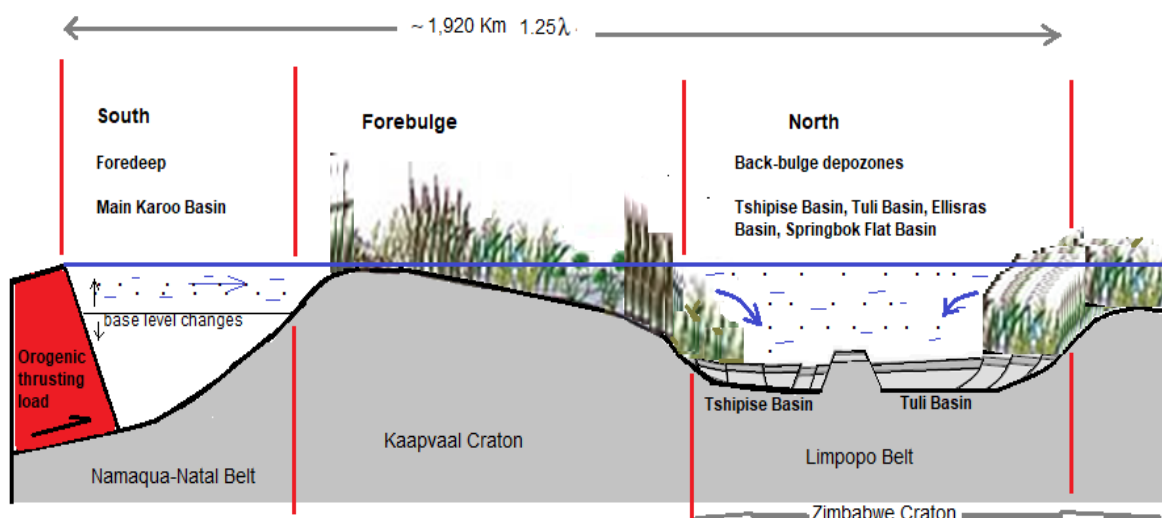
Figure 2.2: Tuli Basin development as a back-bulge depozone in the Karoo Retro-arc foreland system (Modified from Catunueanu 1998)

16

Unlike the MKB, the Tuli Basin includes sedimentary sequence piles that are comparatively thinner, with thickness and spatial area estimates of 980-1050 m and 15,000 Km^2 respectively (Bordy, 2000). The back-bulge is a structural depression which results from crustal subsidence caused by tectonic regimes adjacent to the CFB orogenic belt and controls the accommodative space that preserves the Carboniferous-Jurassic sedimentary sequence of the Tuli Basin in South Africa (Catuneanu et al., 1998, Bordy and Catuneanu, 2002a).

2.1.2 Lithostratigraphic sequence of the Tuli Basin.

The South African Committee of Stratigraphy (SACS) recognises the lowermost and oldest sedimentary sequence of the Tuli Basin as the Tshidzi Formation after the work of Hendrik Jacobus (1980). The formation is regarded as the lowermost sedimentary rock unit of the Karoo supergroup because of its stratigraphic position, age and genetic mode (Du Toit, 1939, der Berg and Jacobus, 1980, Brandl, 2002, Bordy, 2018). The genesis of Tshidzi Formation is influence by Paleo-glacier flow as evident by deposition of massive diamictite facies which are glacially-striated (Bordy and Catuneanu, 2002a). The glaciogenesis is related to the divergence of Africa and Antarctica plates during the Gondwana break-up event in 500 Ma. This tectonic divergence resulted in a climatic shift from glacier-cold region to desert region and deposited sediments with correlative vertical lithology that is highly variable and limited in thickness in different basins (Groenewald et al., 1991, Johnson et al., 1996). Although, there is no available report on radiometric age, the relative age determination of the formation was based on palaeontology, stratigraphic position and lithostratigraphic correlation which showed Permo-Carboniferous age (Bordy, 2000, Barbolini and Bamford, 2014). Figure 2.3 shows correlation of stratigraphic sequence correlation of the Tuli Basin in comparison to MKB and other Limpopo-aged Karoo Basins in the Limpopo Province of South Africa.
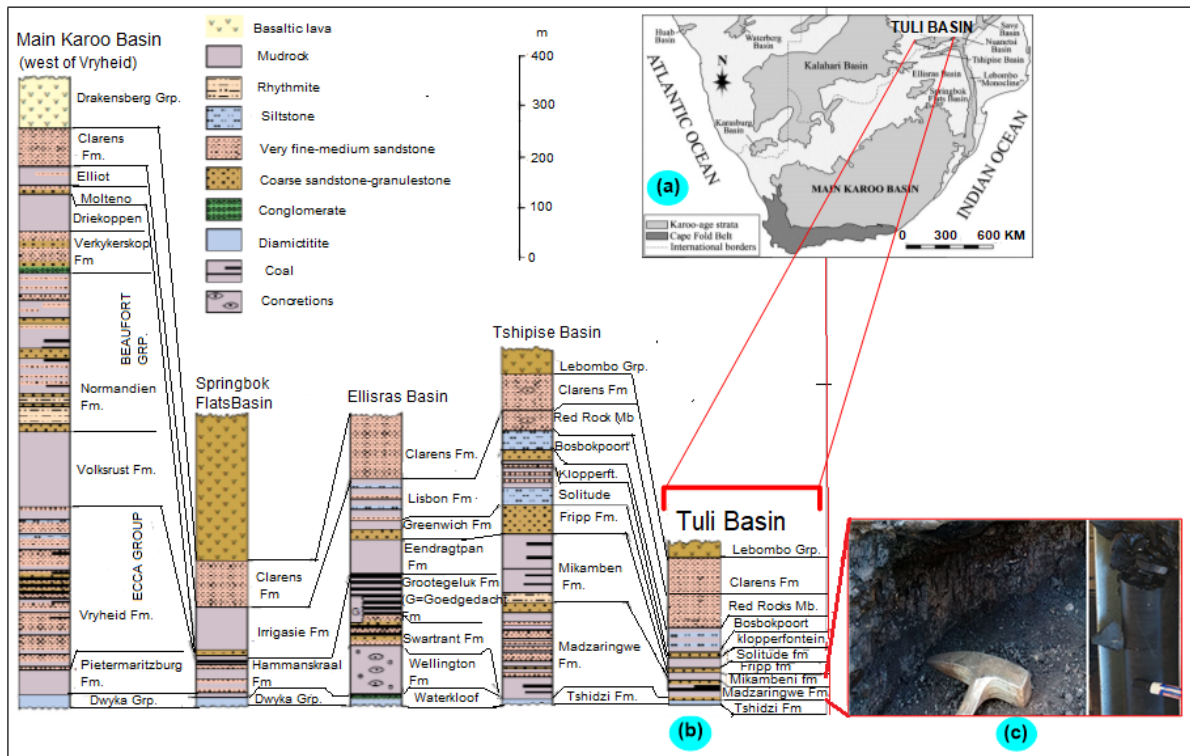
Figure 2.3:Stratigraphy and correlation of Karoo Supergroup strata in Limpopo part of Main Karoo Basin (modified after Johnson, 2006)

In terms of lithological description, the Tshidzi Formation of Tuli Basin displayed a poorly sorted diamictite textural feature which contain breccia clast with a diameter up to 80 cm embedded in argillaceous matrix (Chidley, 1985, Bordy, 2000). It is important to note that the exposure of the Tshidzi Formation is rare however it may attain a maximum thickness of 2m. Unlike the Tshidzi Formation of the Tshipise Basin, the Tshidzi Formation of Tuli basin contains less pebble clast embedded in mudstone matrix although displays more conglomerate clast which are poorly sorted and set in micaceous sandy matrix. Stratigraphically, the Tshidzi Formation of the Tuli Basin overlies an uneven Archaean granitoid-greenstone terrain in an unconformable manner but conformably overlain by Permian coal-bearing formation of Madzaringwe Formation. This stratigraphic position further revealed the unifying identical feature with other basal Karoo rocks, such as the Dywka Group in the main Karoo Basin and Springbok Flats Basin, the Waterkloof Formation of Ellisras Basin, and the Tshidzi Formations of the Tshipise and Lebombo Basins. The Tshidzi Formation is characterized with facies association lacking striated clasts, varvite, and polymict clast fabric. However, the presence of laminated matrix suffices its interpretation as glaciogenic diamictite.

Above the glaciogenic diamictitic Tshidzi Formation in the Tuli Basin is the Madzaringwe Formation (Chidley, 1985). This formation is overlain by a red hematitic micaceous sandstone

while the vertical lithofacies analysis revealed succession of thick shale and coal seams. This facie constitute the coal-bearing strata of the Tuli Basin due to its economic significance of the coal seam of up to 300 m thick near the Limpopo River (Ortlepp, 1986). Although recent studies have reported varied thickness of coal seams, no distinct thickness is less than 20 m with six continuous coal seams interbedded with grey to black shale in a rhythmic manner (Mtimkulu, 2010, Bordy, 2000). It is not unlikely that the plant-organic-rich-shale has potential for natural gas resources because the evolutionary pathway for coal and shale gas has similar origin but different endpoints. Based on stratigraphic position, Paleo-current directions and sedimentary facies, the formation is regarded as an equivalent deposit of some Karoo-age deposits, such as Ecca Group, Vryheid, Wellington and Madzaringwe Formations of the main Karoo Basin, Ellisras and Tshipise Basins respectively (Faure et al., 1996, Johnson et al., 1996, Bordy, 2000, Chidley, 1985).

Despite, considerable studies (Geel et al., 2013, Geel et al., 2015, De Kock et al., 2017) have reported the potential resources of shale gas in the Permian black shales of the Prince Albert, Whitehill and Collingham Formations of the Ecca Group in the main Karoo Basin, no study has been conducted on the equivalent Limpopo area-Karoo-age deposits of Madzaringwe and Mikambeni Formations of the Tuli Basin. Furthermore, the normal grading exhibited by the vertical profile of Madzaringwe Formation shows an upward fining, up to 120 m thick, which could serve as a possible reservoir for shale gas accumulation. The grain sizes prograde from conglomerate stringers to bedded sandstones to siltstones to shale at the lower part of the informally-termed-Basal Unit (Bordy and Catuneanu, 2002c). Earlier work by the authors identified four lithostratigraphy which are the Basal, Lower, Middle, Upper Units and Clarens Formation but not yet recognised by the SACS. Hence, regarded as informal nomenclature for the Tuli Basin (Bordy, 2000). However, the depositional pattern of the formations portrays a relatively low fluvial energy milieu transported by meandering or braided stream in relation to a gradual peneplanation or denudation processes (Miall, 1977).

Having reported (Bordy and Catuneanu, 2002c) the upward-fining facies to contain abundant plant debris, fossil leaves impressions of *glossopteris sp.* and seed bearing plants, the Mikambeni Formation, which overlies the Madzaringwe, is associated with black organic-rick shale and coal seams. The Mikambeni Formation is considered as a fine-grained strata composed of massive or laminated structure of shales, siltstones and mudstone. The depositional environment has been interpreted as a braided lacustrine deposit based on the Paleo-current directions and facies pattern analysis. Fluvial structures, such as point-bars and channel lags, indicate a relatively low fluvial energy and typical of meandering fluvial or braided stream. Although similar in depositional setting with the Madzringwe Formation, the internal

architectural facies analysis of the Mikambeni Formation revealed carbonaceous shales and siltstones with sporadic coal seamlets with no conglomerate stringers (Bordy and Catuneanu, 2002c). The recognisable 50 m thick middle unit of black carbonaceous shale with occasional bright coal seams has been attributed to Mikambeni Formation (Chidley, 1985). However, besides coal, more potential economic significance of this formation is the possible shale gas resources because studies (Bordy, 2000, Bordy and Catuneanu, 2002b, De Kock et al., 2017) have revealed its compositional similarity with the Ecca Group of the main Karoo Basin identified with unconventional gas resources.

Based on the bio- and chrono-stratigraphic study, the succeeding Fripp Formation is the youngest of these four Permian-aged Formations with thickness up 10 m but varies in other locations to somewhat 30 m thick (Chidley, 1985). The architectural description of lithofacies comprises well-sorted, medium to coarse-grained, feldspathic fossilised sandstone. By implication, fluvial transport system is believed to have rapidly deposited feldspathic minerals from granitic rocks in a point-bar and channel-lag bedforms. Inferentially, the whitish panorama of the sediments could be attributed to the leukocratic nature of feldspathic minerals. Although there is no equivocal evidence of fossilisation, similarity in lithology and stratigraphic position suggest a time-equivalent with the *Dicroidium*-bearing strata of the Tshipise Basin, Molteno and Beaufort Formations in the main Karoo Basin (Chidley, 1985, Catuneanu et al., 2005, Bordy and Catuneanu, 2002b). To date, there is little or no study that documents the geo-economic importance of this formation despite the economic significance of its correlative Triassic coal- Molteno Formation in the main Karoo Basin (Cadle et al., 1993). In addition, the petrochemical study for shale gas in areas of high probability near Beaufort Formation speculated a higher thermal maturity of organic (De Kock et al., 2017). The Fripp Formation, which corresponds to these organic-rich deposits in the main Karoo, is believed to have geo-economic significance, but this has yet to be studied.

The Triassic-aged-deposit of Solitude Formation overlies the chronologically older Fripp Formation with a conformable contact and grades upwards into the klopperfontein Formation. Although without abrupt change in lithology, the sediments of Solitude Formation differ in colouration, thickness and structures. Retrospective studies (Chidley, 1985, Brandl, 2002, Bordy, 2000) have revealed that lithology consists of siltstones and sandstone which akin to the underlying Fripp Formation but differs in colour. The reddish colour of Solitude lithofacies suggest an reducing depositional environment where plant material accumulation may be presumably present with less leukocratic minerals contrary to the whitish sediments of underlying formation. Due to the lack of carbonaceous and coal seams, this formation may probably fit the description of the lower boundary of the Middle Unit which represents the

regional hiatus surface associated with the Tuli Basin (Bordy and Catuneanu, 2002b). Unlike the underlying formation, the depositional structure of Solitude Formation showed crevasse-splay features with climbing sediments over levee onto adjoining. Many studies have indicated that the crevasse-splay structures ensued from a high energetic sinuous flow of a river or stream system.

The succeeding conformable Klopperfontein Formation is characterised with subordinate intraformational conglomerates besides the coarse sandstone that are deposited ubiquitously in a cross-bedded pattern (Chidley, 1985). Owing to its coarse-grain, distinctive lithological character, Klopperfontein is proposed to have resulted from resurgence of uplift and erosion of a fault. Based on textural distribution, this formation represented rapid braided deposit settling from proximal bedload of a fluvial flow and attained a thickness of about 12 m (Bordy and Catuneanu, 2001, Catuneanu et al., 2005). Analysis of the internal structure revealed a fluvial trough cross-bedding which suggest a channel-fill origin from high-energy stream (Bordy, 2000). Paleo-current measurement from dip angles showed that the denudation and sediment dispersal patterns trend from roughly west to east direction (Bordy, 2000).

The Bosbokpoort Formation overlies the underlying previous formation conformably and grades upwards into the Clarens Formation with a disconformable contact. Its depositional setting represents a transitional zone marked with progressive warming and aridity from subaerial floodplain milieu. The aeolian condition is evidenced by the friable brick-red to purplish mudstones which suggest deposition on the floodplains of matured meandering stream under oxidising condition. Due to aridity, the meandering river level reduces as revealed by preponderance of calcareous nodules and concretions precipitating under an oxidizing state. The lithofacies contain mudstone, white siltstone layers and occasional intraformational conglomerates up to 60 m thickness.

The lower part of the Clarens Formation displayed a lithofacies marked with channel morphology which suggest fluvial depositional environment (Bordy and Catuneanu, 2002a). The lithofacies composed of medium to very coarse sand were reported to show repeated flood event instead of a single event hence suggesting a seasonal flow regime and transport condition. It was interpreted that the overriding climate conditions varied from wet with significant rainfalls to semi-arid and or arid areas (Bordy, 2000). The ephemeral streams provided evidence of the wet season although a semi-permanent water body could not accumulate due to aridification. Gradual disappearance of the water channel is explainable as some surface run off water rapidly percolate through the medium to very coarse sand lithofacies while others evaporated (Warren, 1983). It was reported that the internal sedimentary structure such as ripple marks were absent or not well developed while Paleo-

currents were limited (Bordy and Catuneanu, 2001). This might suggest that the bedforms or channel morphology were generated by a more dynamic flooding event associated with storm-induced run off or seasonal snow thaw than a turbulence variation that generated small scale ripple marks and lineament (Miall, 1985).

Furthermore, according to Johnson et al. (2006), the lower part of Clarens Formation is characterised with red argillaceous sandstone lithofacies, scaling from 5m up to 60m thick although covered with patches of white sandstone. The white streak could have developed from the dissolution of the calcium carbonate of dinosaur remains, Massospondylus and Syntarsus or accumulation of saline minerals such as halite and gypsum due to semiarid to arid climatic overprint (Johnson et al., 2006). Seasonal variation in climate was evident by the significant water content found in internal structure of fossil wood, *Agathoxylon* sp. wood type (Bordy and Catuneanu, 2001). The presence of oasis or thermal springs was suggested as a source of water supply for the wood specie to had flourished since an ephemeral stream is transient. Identification of the petrified wood was interpreted as indirect evidence of continuous water supply from wadi-type ephemeral stream. Hadley (1997) has shown that ephemeral stream is diagnostic of arid or semi-arid region where precipitation is parsimonious or scanty. The low sinuous flow is conveyed by geomorphic channel to form a low-angle-trough, cross-bedded sandstone features and horizontal bedded sandstone to medium-scale planar cross-bedded features in the lower Clarens Formation (Chidley, 1985, Bordy, 2000).

The Upper Clarens Formation displayed aeolian milieu due to progressive desertification and warming as indicated by dissipation of ichno - fossils and bedforms previously associated with the ephemeral stream system (Brandl, 2002). A regional Paleo-current from west to east is noted to had deposited the large-scale aeolian cross-stratified sandstone which varied in thickness from 5 to 140m at different locations but differs in grain size and colour from the underlying wet dune deposited by ephemeral stream. Studies (Chidley, 1985, Bordy, 2000, Bordy and Catuneanu, 2001) have reported that the lithofacies varies from cream to yellow, fine to very-fined sandstone with moderately rounded and well sorted textural features. The work of Bordy and Catuneanu (2002) noted that the Clarens Formation has wet aeolian sediments whose seasonal inundation might have supported organisms and plants alongside their bioturbation activities. Activities of the trace fossils are showed Figure 2.4 (a) vertical, cylindrical pipes with open apices (b) simple, mostly vertical shaft-like trace fossils (c) close up of the wall of the digit-like structure showing the extensively branching burrow system with random orientation (d) Large-scale trace fossils showing lateral bifurcations on a sub-horizontal surface.
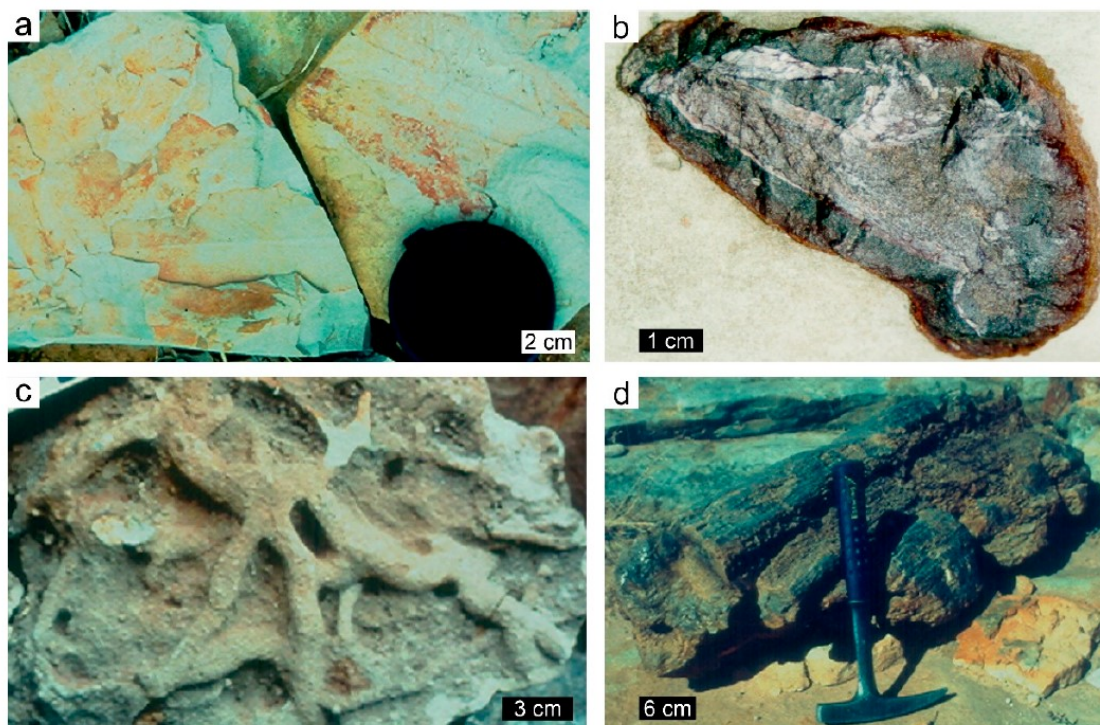
Figure 2.4: (a) vertical, cylindrical pipes with open apices (b) simple, mostly vertical shaft-like trace fossils (c) close up of the wall of the digit-like structure showing the extensively branching burrow system with random orientation (d) Large-scale trace fossils showing lateral bifurcations on a sub-horizontal surface (modified after Bordy and Catuneanu, 2002)

The study (Bordy and Catuneanu, 2002) identified an un-bifurcated ichno-fossils tentatively recognised as *Skolithosi* sp and other bifurcated trace fossils which were believed to had been produced by soft sediment burrowing organisms such as beetles and ants. Due to the similar biogenic, lithofacies and genetic features, the Clarens Formation of the Tuli Basin correlates with the main karoo Basin and other Karoo-age basins and represents the final phase of Karoo sedimentation (Eriksson, 1981, Malaza et al., 2016).

2.2   Shale and Shale Gas

Shale is a fissile or laminated sedimentary rock or mudrock with a fine-grained size less than 62.5m that can contain mineral grain and organic materials (Akintola, 2018). Shale rocks may contain significant amount of organic matter up to 30 wt.%, as well as grain minerals of clay, quartz, carbonate and feldspars (Liang et al., 2018b). It can be described as mudstone, silty shale, or clayey siltstone depending on the dominating fine-particle size and textural features and but it makes up more than two-thirds of all sedimentary rocks on the planet (Liu et al., 2019b). Meanwhile, it is a complex and heterogeneous porous media with complex inherent pore structures and low permeability that serves as both a source and a reservoir for natural gas. As a result, different storage and transmission of natural gas have emerged in a shale

© University of Venda

rock, making it difficult to anticipate the spatial distribution and availability of shale gas in a given region.

Shale gas is an unconventional resource composed of natural gas impregnated within impermeable shale. Some previous authors (Jarvie et al., 2007, Littke et al., 2011) define shale gas as gases trapped in a fine-grained sedimentary rocks, stored in complex pore and fracture, adsorbed on mineral particles or dissolved in pore fluids. It can emanates from biogenic or thermogenic processes and characterised with self-contained source and reservoir mechanism system. As such, controls the initial production and ultimately the recoverable shale gas content practical exploration of shale gas must be in accordance with reliable source and reservoir evaluations (Zhai et al., 2018). Additionally, mineral composition, pore structure, and gas sorption capacity are also the important parameters for evaluating shale gas reservoirs. Free gas can be stored in larger pores and fractures, while adsorbed gas is generally stored in micropores and fine mesopores that are in contact with organic matter (OM) and clay minerals; residual oil volume mainly controls gas in the solution (Bakshi and Vishal, 2021). The free gas content directly, while adsorbed gas mainly controls the late period of shale gas development (Lianhua et al., 2021). Knowing the major indicators for reservoir performance is crucial to effectively evaluate and anticipate shale gas volume and recoverable gas content when systematically evaluating a shale gas resource.

2.3   Production, Accumulation and Preservation of Organic Matter

The production, accumulation and preservation of organic matter in sediment are important requirement for hydrocarbon shale source rock. The production of organic material is influenced by a number of geological boundary factors (Chen et al., 2016a). It is almost exclusively limited to sediment deposited in aquatic environments, which must include a particular level of organic materials. This organic material might come in the form of dead or living particulate organic matter, or it can come in the form of dissolved organic matter (McCarthy et al., 2011). On one hand, the organic material may be autochthonous to the environment in which it is deposited, that is, it originated in the water column above or within the sediment in which it is buried (Tissot and Welte, 1978). On the other hand, it may be allochthonous, that is, it originated outside of its deposition environment (Tissot and Welte, 1978). It is essential that the energy level within the water body, as well as the quantity of sedimentary minerals, be such that a specific form of sedimentation can occur.

The accumulation and preservation of sedimentary organic matters initiate the evolution of gaseous hydrocarbon in shale rocks. Organic matter can be derived from the marine or terrestrial environment (Chen et al., 2020). According to Chen et al. (2020), the most

commonly marine organic matter source include pelagic calcareous (Protozoa, Planktonic Foraminifera) and siliceous-walled (Protozoa, Radiolarians) heterotroph protists, organic-walled and calcium carbonate cysts of heterotroph and autotroph dinoflagellates, siliceous-walled (Diatoms) and calcareous-walled autotroph protists (Coccolithophores), benthic protists (Benthic Foraminifera), and microscopic metazoa, Ostracods (Crustacea), as well as small fish teeth. The primary processes and pathways involving the element carbon concentrating in sediments in a marine environment are depicted in Figure 2.5. The figure shows the interplay of photosynthesis which form a basis for proliferation of terrestrial and marine- derived organic compound and favourable depositional environments. The majority of organic carbon generated by organisms is swiftly converted to CO_2 and recycled into atmospheric and hydrospheric CO_2 stores (Hohner et al., 2017). Organic-enriched shales in marine settings are believed to be controlled largely by combinations of phytoplankton blooms, nutrient supply and recycling, stratified oceanic waters, rising sea levels and anoxic events.
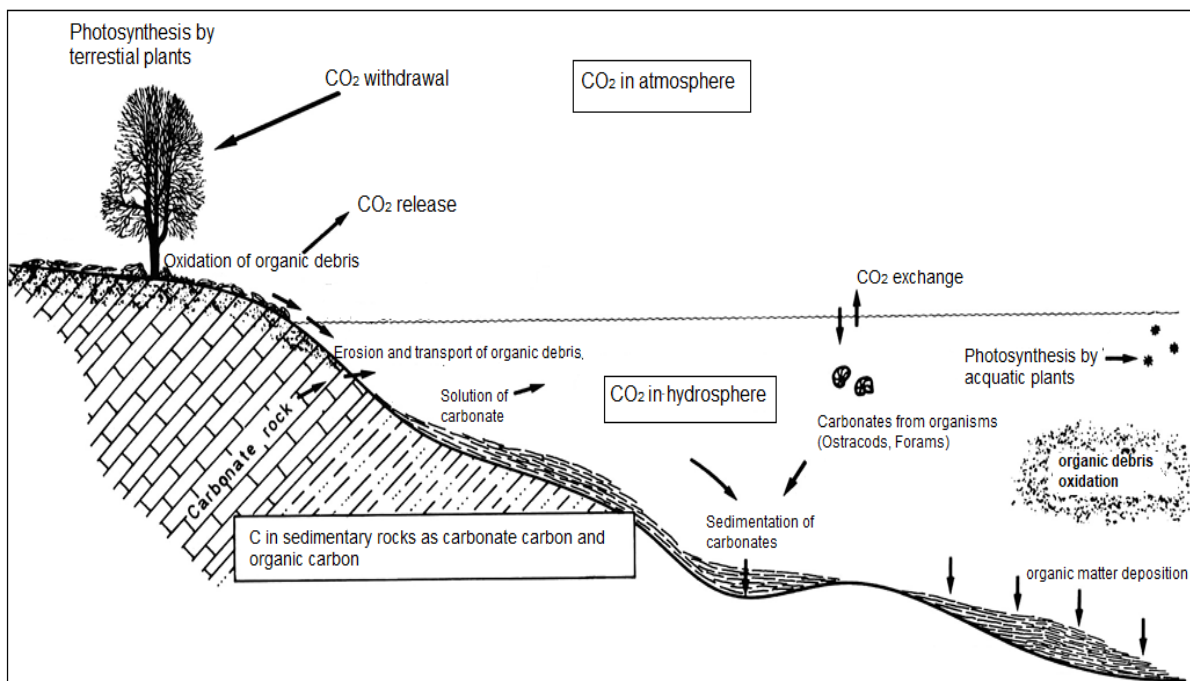
Figure 2.5: Sedimentary Process of organic matter production and accumulation in sediment (modified after Tissot and Welte, 1978)

2.4   Depositional Environment of Organic Matter and Thermogenic Pathways

This section focuses on organic matter's paleo-deposition habitats and the thermal mechanisms that lead to their formation. It also discusses methods for determining the paleo-deposition settings of organic-rich sediments. Furthermore, organic matter produced from terrestrial and marine ecosystems is fully covered in this section.

25

2.4.1 Terrestrial derived organic matter and their formations

Terrestrial organic matter disseminates in sediment of continental or brackish environment, having varying amount of hydrogen content and prone to generate hydrocarbon under favourable thermal maturity. Within the catagenesis thermal level of about 50 to 200ºC, an organic matter alters from solid to liquid to gaseous hydrocarbon as the hydrogen content increases (Hunt, 1991). However, land-derived organic matter can be transported and deposited in fluvial and lacustrine environments in form of particulate or dissolve organic matter (Sebag et al., 2006). Organic-rich sediments are thought to form and deposit in terrigenous environments. The carboniferous-Permian Formations, for example, are rich in organic materials and have been recognized as the most major source of shale gas in the Ordos and Sichuan Basins (Wang et al., 2019a). Since the Middle Triassic, most areas of China have been terrestrial depositional systems, except for a continuation of marine settings in portions of the Qinghai-Tibet regions into the Palaeocene . Several large inland lakes in the Ordos, Sichuan, Songliao, Bohai Bay, Qaidam, Junggar, Turpan-Hami and Tarim Basins characterised these landscapes during extended episodes during the Late Triassic to Cenozoic (Wang et al., 2020b)

However, organic-rich matters that form shale gas could originate or be deposited in marine, terrestrial or transitional environment (Elliott et al., 2017, Wei et al., 2021). According to Elliot et al. (2017), the organic matter which formed the studied bituminous sediments emanates from both marine and terrestrial sources based on the macerals compositions. Petrographic examination of the macerals reveals alginite and liptodetrinite which thrives in a low energy suboxic transitional environment. Furthermore, it was noted that the presence of epigenetic huminite macerals such as textinite, corpouminite and inertodetrinite are related to terrestrial plants. Table 2.1 shows the various origins for organic-rich shale of some shale gas producing rocks and shows basic highlights of the depositional environments.

Table 2.1:Marine and Terrestially derived Organic Matter and their Formations

Stratigraphy	Formation	Depositional Environment	Location	Kerogen Type	Maturity Processes	Basin	TOC (wt. %)/VR (R_o%)
Michigan	Antrim Shale	Marine	Northern Michigan	Type III	Biogenic	Michigan	25/0.4-0.6
Mississippian	New Albany	Marine	Illinois	Type II	thermogenic	Illinois	1.2-13/0.35-1.41
Mississippian	Barnett	Marine	Texas	Type III	thermogenic	Fort Worth	2.5-4.5/0.85-1.85
Devonian	Woodford	Marine	Oklahoma	Type III	thermogenic	Anadarko	4-5.5/0.51-6.4
Devonian	Marcellus	Marine	Pennsylvania	Type III	thermogenic	Appalachian	3.0-4.5/1.1-3.0
Jurassic	Kimmeridge	Marine	Yorkshire	Type II/III	thermogenic	Cleveland	2-3.5/0.25-1.10
Cambrian	Niutitang	Marine	China	Type II/III	thermogenic	Suchian	0.15-39.7/1.4-5.0
Ordovician-Silurian	Wufeng Longmaxi	Marine	China	Type III	thermogenic	Suchian	3-3.5/1.5-2.6
Permian-Triassic	Barakar/ Raniganj	Terrestrial	Indian	Type III	thermogenic	Raniganj	3.13-29.77/0.9-3.9
Jurassic-Cretaceous	Bredasdorp	Shallow Marine	South Africa	Type III/IV	Biogenic	Bredasdorp	0.14-7.03/0.60-1.2
Jurassic	Whitehill	Marine	South Africa	Type III/IV	thermogenic	Ecca Group	4.5/4.0

2.4.2 Marine derived organic matter and their formations.

Marine organic matter is dominated by autochthonous phytoplankton (Bibi et al., 2020). Nevertheless, allochthonous terrestrial organic matter can enter transitional facies and marine environments (Li et al., 2021). Meanwhile, preservation of marine phytoplankton consisting of calcareous-walled organisms such as dinoflagellates and coccolithophorids predominate due to compared to the less resistant organic-walled organisms of algae (Tuo et al., 2016). An organic matter derived from the marine is associated with oxygen deficiency, implying a reducing reaction. The Early Cambrian Niutitang Shale in Sichuan Basin of China indicates a black carbonaceous and siliceous deposition due to the reducing marine depositional environment (Xi et al., 2018). Given sea level regression, oxygen content increased in the late phase of Early Cambrian as a result of photosynthetic reaction with exposed organic matter thus changing sediment to grey-green or dark-gray coloured shale (Wu et al., 2019). In addition, the change in lithologic thickness may be controlled by the transgression and regression of the sea level (Zhang et al., 2018b). Sedimentary facies transiting from a deep shelf can be marked with black carbonaceous shale while the shallow-shelf facies is marked with dark grey silicic shale. Table 2.2 presents some depositional environments.

Table 2.2: Depositional Environment with Common Organic Matter

Depositional environment	Environment Name	Common sedimentary rock types	Common organic matters	Common structural features
Terrestrial or continental (include land, lakes and streams)	stream - channel	conglomerate, sandstone	high energy, oxidising environment with few fossils	cross-beds, ripple marks
	stream - floodplain	shale	terrestrial plants and animals	mud cracks
	alluvial fan	conglomerate, arkose	high energy, oxidising environment with few fossils	poorly sorted, cross-beds
	desert dune	sandstone	terrestrial reptile traces	well sorted, large scale cross-beds
	glacier - till	tillite	high energy environment with few fossils	angular to rounded grains, poorly sorted, unstratified (massive)
	glacier - outwash	sandstone, conglomerate	high energy, oxidising environment with few fossils	ripple marks, cross-beds, similar to stream channel
	swamp	coal	plant fossils	cross-beds, ripple marks, mud cracks
	lake	silt, shale, freshwater limestone	lake dwelling organisms	graded beds, thin beds, varves, ripple marks, mud cracks
Transitional (point where land and ocean meets)	delta or brackish	marine and nonmarine mudstone, siltstone, sandstone, coal	terrestrial plants, mollusk shells, bioturbation	possible cross-beds, ripple marks
	beach	sandstone	mollusk shells, bioturbation	fine to medium-grained, well-sorted, cross-beds
	tidal flat	mudstone, siltstone, sandstone, possible evaporites	mollusk shells, bioturbation	fine-grained, ripple marks, cross-beds, mud cracks
Marine (ocean)	shelf/platform	limestone, shale, sandstone	fish, coral, mollusk shells, sponges, echinoderms	cross-beds, ripple marks
	reef	limestone	coral	Massive
	slope/rise	mudstone, graywacke	microscopic plankton	graded beds, turbidites
	deep marine	chert, chalk, limestone, mudstone	microscopic plankton	thin beds
	shallow restricted circulation in arid hot climate	gypsum, anhydrite, halite	extreme chemical environment with few fossils	mud cracks, thin beds, salt casts

2.4.3 Thermo-genetic pathways of organic matter

The genetic source of shale gas has been constrained in terms of mechanism of formation and environment of deposition. Due to biogenetic and thermogenetic processes, gaseous hydrocarbon can be generated at shallow and deep burial in a depositional environment. The pyrolysis experiment performed by (Xiong et al., 2016) on stimulated kerogen in a closed gold-tube system revealed that thermogenetic process generates wet and dry gases composed mainly of methane. On the other hand, the C_{2+} hydrocarbon species are generally lacking in both shallow and deeply buried or matured shale (Xia et al., 2013, Golding et al., 2013) although ethane, carbon-dioxide and nitrogen may be present. However, condensate gas mixed with hydrocarbon liquid has been reported from shale rock rich in marine organic matter such as phyto-zooplanktons to produce wet gas and this is consistent with the organic geochemical characterisation of the source rock previously conducted by (Zhang et al., 2007). The study also noted that over-matured marine shale produces retained bitumen which could generate dry gas during secondary cracking of kerogen. It was inferred that an increase in temperature due to the depth of burial or thermal maturity of kerogen generates unconventional gas within organic rich shale rocks.

Microbial gas originates from organic matter which decomposes due to degrading actions of anaerobic microorganism such termites and ruminants at shallower depth compared to thermogenic gas (Strąpoć et al., 2011, Chai et al., 2016). Strąpoć et al. (2011) has demonstrated that the methanogenic gas accumulates as a result of enzymic break down of vascular plants due to microbial processes. Furthermore, it analysed the genetical changes in different organism during formation of methanogenic gas that could be broken down into methanogenic gas using phylogenetic sequencing and fluorescent *in-situ* hybridization. The study concluded that sedimentary Basin with low-mature Formation predominantly contain methanogenic gas while tectonically uplifted Formation could contain mixture of thermogenic and biogenic. The presence of thermogenic gas might have resulted from deep burial and afterwards migrated to shallow depth due to tectonic upliftment and subsequent anaerobic degradation.

2.4.4 Determination of depositional environment and shale gas origin

The recent advances in stable isotopic measurements provide definite information relating to source, alteration and deposition of geologic or organic materials. Despite difficulty to distinguish between thermogenic and biogenic gas inside the same closed system or Formation, phylogenetic sequencing, fluorescence, and stable isotopic techniques have been utilized to do so (Zumberge et al., 2012, Xia et al., 2013). The classic stable isotope

geochemistry is mass-independent, stemming from symmetry-based isotope effects and search for rare anomalies that show unfamiliar or unusual processes which occur only in a few species or environment.

Unlike the conventional stable isotope technique, the clumped isotope geothermometry consists multiply-substituted heavy rare isotopes that are not randomly distributed within molecules. It is concerned with state of order of the heavy rare isotopes such $\delta^{13}C$, $\delta^{18}O$, $\delta^{15}N$ in natural materials and their bonding nature with or near each other than numerous light isotopes present in same system. The thermodynamically controlled processes of isotopic fractionation of carbonate mineral through diffusion, isotope exchange and irreversible processes leads to distinctiveness in clumped isotope species. At thermodynamic equilibrium, carbonate mineral growth are constrained due to relative abundance of carbonate ion groups containing both $\delta^{13}C$ and $\delta^{18}O$ fractionations. In comparison to stable isotope analysis, the carbonate clumped isotope thermometer is independent of isotopic composition of water or any other phase that may co-exist with carbonate. As such, clumped isotopic approach can be used to reconstruct paleo-temperature of materials in marine and terrestrial sediments where the isotopic composition of water is not known. The primary temperature of geological materials which undergo diagenesis, weathering, burial depth and metamorphism can be preserved up to 200°C and constrained with carbonate clumped isotopic thermometry (Zaarur et al., 2013).

2.5   Diagenetic Evolution of Organic Matter and kerogen Types

Organic matter is a mixture of organic macerals rich in protein, carbohydrate, lipids and lignin (Liu and Masterlerz, 2018). Primary and secondary types of organic matter are recognised in which amorphous organic matter (AOM), vitrinite, alginate and inertinite are classified as primary while solid bitumen (SB) being classified as secondary type of organic matter. Alginite are oil-prone which are derived from algal organisms such Botryococcus, Tasmanites and Leiosphaeridia but usually represent Type I kerogen due to very high hydrocarbon generation potential (Liu et al., 2022). Amorphous Organic matter (AOM) which is also classify as amorphinites or bituminites are oil prone that are derived from microbial or physicochemical degradation of phytoplanktons such as diatoms and zooplanktons such as foraminera, radiolaria and crustacea (Teng et al., 2021). AOM could display either Type I or II kerogen but associated with medium to high hydrocarbon generation potential. Vitrinite refers to organic matter originating from higher terrestrial plants that has a low to medium hydrocarbon production capability and corresponds to gas-prone Type III kerogen (Ahmed et al., 2022). Inertinite refers to oxidized or burned terrestrial woody material that has no hydrocarbon production potential and is thus categorized as Type IV kerogen. As a result, the depositional

environment and degree of diagenetic modification of each shale source rock are major determinants of kerogen types and hydrocarbon generation potential as shown in Figure 2.6
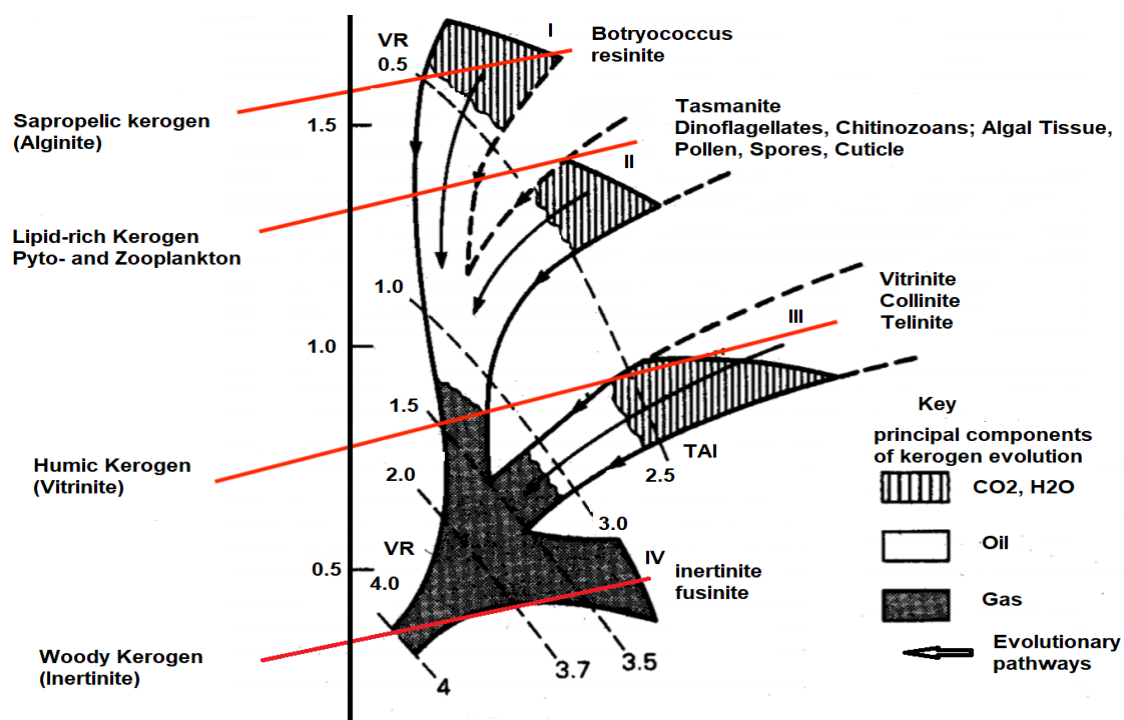
Figure 2.6: Kerogen Types and Thermal Maturity of Organic-rich sediment (adapted after Tissot and Welte, 1984).

The burial depth of organic-rich shale influences the thermal maturity of organic matter to generate gas or oil hydrocarbon (Liu et al., 2021a, Boruah and Ganapathi, 2015). There is a widely held notion that a shallow shale reservoir is unlikely to generate hydrocarbon oil or gas due to low thermal diagenetic changes. Boruah and Ganapathi (2015) indicated a T_{max} of 458˚C at a shallow depth of 350m-355m for organic-rich shale samples from the Raniganj Basin. This basin contains mature and overmatured kerogen, which is prone to gas generation. In the United States, the New Albany shale in Southern Indiana and the Antrim Shale in the Michigan Basin both produce shale gas from burial depths of less than 1000 meters (Liu et al., 2013, Martini et al., 1996). The Albany shale, which is prone to gas generation between 160 and 600 meters, contains more than 3% organic matter, but the Antrim shale produces gas from organic-rich mudstone buried at about 550 meters (Robert, 1991; Mastalerz and Schimmelmann, 2013). Temperature and pressure are thought to increase with burial depth, turning organic matter to hydrocarbon.

With increasing temperature and pressure within the earth's crust in terms of geothermal gradient, irreversible chemical reactions take place within the huminite/vitrinite network. This

process is termed maturation with subdivisions like diagenesis, catagenesis, and metagenesis, which eventually merge to low grade metamorphism (Mani et al., 2017). Table 2.3 presents the three stages of thermal maturity for an organic-rich sediment and their corresponding end products.

Table 2.3: Stages of Kerogen Maturation (After Mani et al., 2017)

Maturation Stage	Thermal Level	Alteration	End Product
Diagenesis	< 50˚C	Compaction, cementation, dissolution and precipitation	Hydrocarbon generation begins at this stage
Catagenesis	50˚C-150˚C	Chemical transformation: decarboxylation, dehydroxylation, demethylation, aromatization and polycondensation	Chemical bond breaks in kerogen and clays within shale to generate liquid HC. At peak of T ˚C range liquid HC undergo 2˚ cracking to generate gas molecule.
Metagenesis	150˚C-200˚C	Cracking	Dry gas and CH_4

In South Africa, some recent diagenetic studies (Adeniyi et al., 2018, Schulz et al., 2018, Baiyegunhi et al., 2017, Geel et al., 2015, Nengovhela et al., 2021) have concentrated on the Lower Ecca Group Shales of Karoo Basin to understand its reservoir properties. In view of understanding the anomalous thermal maturity of the black shale of Ecca Group, Adeniyi et al. (2018) revealed the significance of dolerite intrusion rather than the diagenetic effect. The study used $^{40}Ar/^{39}Ar$ radiometric dating and thermometric minerals of chlorite and illite to constrain the time of emplacement of the Jurassic-age dolerite around 180 Ma and attributed the over-maturity of Ecca Group to its proximity to the intrusion. In agreement with the findings of Adeniyi et al. (2018), the recent study of Nengovhela et al. (2021) characterised the thermal aureoles at the contact zone between the intrusive dolerite and the Ecca Group Shale. At various distance of 10 and 20 m of intrusive dolerite, the scanning electron imaging revealed metamorphic minerals of andalusite, cordierite and calcite.

2.6   Diagenetic Alteration of Inorganic Minerals in Carbonaceous Shale

The increase in temperature and pressure due to burial depth does not only transform organic materials but also inorganic materials. Inorganic constituents at shallow or deep subsurface undergo diagenetic alteration from deposition to solidification before metamorphism (Guo et al., 2021, Yu et al., 2018). As burial depth increase, the temperature and pressure increase although there is no consensus on the boundary temperature and pressure. Some studies

(Zhang et al., 2017b, Garner, 2019) reported diagenetic alteration clay minerals at temperature and pressure below 200˚C and 1 kbar respectively at a depth less than 1.5 km while some studies reported boundaries conditions above the aforementioned limits (Laubach et al., 2010).

Depending on the prevailing kinetic agents such as time, fluid-rock ratio, nature and geochemical condition, more than one precursor mineral can alter to form a diagenetic secondary mineral and on the contrarily, one precursor mineral can transform to form more than one secondary mineral (Yuan et al., 2019a, Worden et al., 2020). The diagenetic formation of chlorite minerals has been reported to have different starting minerals which include saponite, berthierine and kaolinite, however, the alteration pathway involves intermediate minerals as well. The intermediate minerals of corrensite and tosudite evolve from precursor minerals of saponite and kaolinite respectively to form chlorite but berthierine converts directly to diagenetic secondary chlorite mineral owing to solid state transformation mechanism (Beaufort et al., 2015). On the other hand, the dissolution mechanism has been ascribed to feldspar alteration to crystallise different secondary mineral depending of suitable geochemical environment and prevailing kinetic conditions (Baiyegunhi et al., 2017).

When clay minerals are exposed to greater temperatures and pressures under kinetic conditions, the chemical composition and structural framework of the minerals change. (Xu et al., 2021). Kinetic parameters that influence this transformation include time, fluid/rock ratio, precursor mineral type, and transformation mechanism. Moreover, clay minerals are phyllosilicate which are considered to be metastable at natural low-temperature systems but alterable when geochemical environment changes (Fulignati, 2020).

2.7   Quantification of Thermal Maturity of Organic-Rich Shale

The methods for quantifying the thermal maturation of an organic-rich shale are discussed in this section. The Rock-Eval programmed pyrolysis and vitrinite reflectance have been detailed in this section.

2.7.1 Rock-Eval Programmed Pyrolysis and Total Organic Carbon of Organic-rich shale

This petroliferous technique uses various parameter to determine the thermal maturity and hydrocarbon potential of source rock. The parameters provide information about free hydrocarbon (S1), residual hydrocarbon (S2), amount of CO_2 released (S3), and maximum temperature required to generate hydrocarbon during pyrolysis (Tmax). Furthermore, Tmax value is widely used as indicator of thermal maturity because it corresponds to different level

of hydrocarbon generation from insoluble organic matter (Boruah and Ganapathi, 2015). Shale gas with Tmax value lower that 435˚C is considered as immature organic matter while temperature above 470˚C shows overmatured organic matter or wet gas zone but in between these temperature range are matured (Geel et al., 2013). The Kerogen types, hydrocarbon maturation and generation are not only analytically measured during pyrolysis analysis but estimation of hydrogen (HI), oxygen(OI) and production indexes (PI) are determined as well.

2.7.2 Vitrinite Reflectance

Vitrinite is a group of macerals generated predominantly from the lignin, cellulose, and tannins found in the periderm (bark) and xylem (wood) tissues of vascular plants. It is the most abundant maceral in carbonaceous rocks, although it can also be found as distributed organic particles in a variety of sedimentary rocks, including some petroleum source rocks (Mukhopadhyay, 1993). The maceral "huminite," a low-rank equivalent of vitrinite, is created when plant biopolymers undergo physical and chemical changes as a result of temperature and pressure changes over geological time. The maceral "huminite" a low rank counterpart of vitrinite and both are formed when the biopolymers of plants are subjected to physical and chemical alteration due to increases in temperature and pressure through geological time. The increase in vitrinite reflectance is a physical reflection of the maturation process, which may include chemical transformations such decarboxylation, dehydroxylation, demethylation, aromatization, and lastly polycondensation of aromatic lamellae.

Vitrinite reflectance, the major maturity parameter, accurately establishes the effective maximum paleotemperature and its duration at any stage in geological time. Accordingly, vitrinite reflectance is often referred to as a paleo-geothermometer (Senftle et al., 2013; Whelan et al., 2013). The determination of maturity is the major building block for the determination of the boundary conditions of liquid and gaseous hydrocarbon generation, coke stability prediction in a coal, identification of various geological phenomena such as faulting, thrusting, intrusion, unconformity and temperature history in basin evolution (Mukhopadhyay, 2012; Teichmuller, 2012). The reasons for choosing vitrinite as the main parameter for the determination of maturity include (a) ubiquitous presence of vitrinite or vitrinite-like macerals in almost every organic-lean and organic-rich sedimentary or metasedimentary rock (b) vitrinite or vitrinite-like macerals appear homogenous when viewed under the incident light microscope (in most cases, vitrinite grains are large enough for maturity determination) and (c) vitrinite shows uniform physical and chemical changes under increasing thermal stress and other geological conditions.

2.8   The Unconventionality of Shale: A Source, Reservoir, and Seal Rock

Unconventional Shale gas differs from conventional gas because it has the capacity for self-generation and self-accumulation of hydrocarbon. The pore system for accumulating and generating hydrocarbon gas determines its productions from unconventional shale reservoirs marked with low permeability. Shale, generally, contains high clay size fraction and minerals and high organic matter.

Previous work suggested that the storage mechanism of shale as reservoir rock is not only influenced by the fractures but mineral components and organic matters which offer sorption sites on the organic surface areas of the voids (Mastalerz and Schimmelmann, 2013; Bustin et al., 2008; Bruant et al., 2002). Gas in shale can be stored in three states as an adsorbed gas in contact with organic matter and a free gas state in fracture and free gas state interstitial pores (Bakshi and Vishal, 2021) in Figures 2.7a and b.
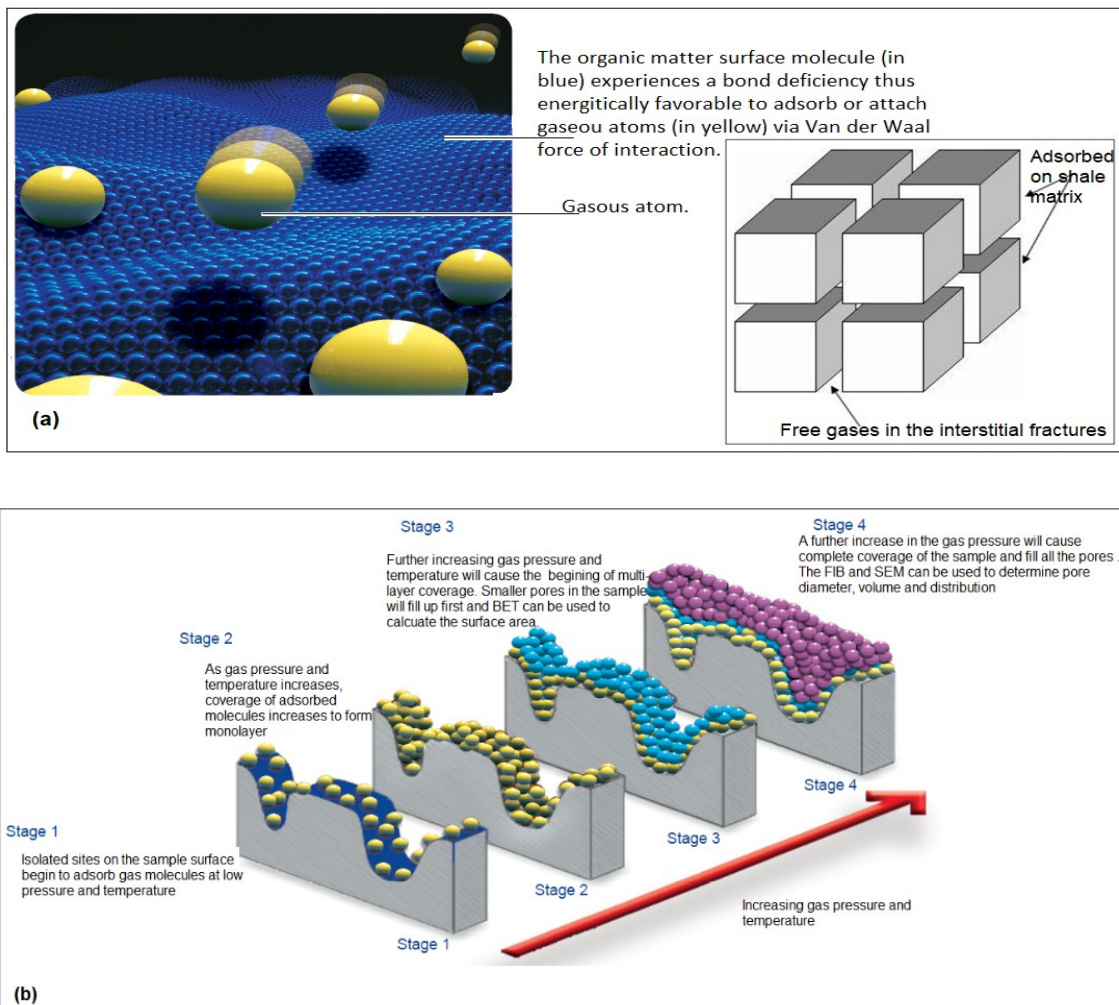
Figure 2.7:(a) Diagram showing the adsorption process of gas to organic matter's surface area (b) Diagram showing adsorption of gas within the organic matter during catagenesis process (modified Bakshi and Vishal, 2021)

The concept of gas being stored in an adsorbed state when in contact with solid kerogen is similar to surface tension theory, which is a consequence of surface energy. Most atoms, but not all the atoms that make up the kerogen or organic matter, are chemically bound to other atoms in the crystal lattice. However, the available reactive unbounded atom on the surface of the organic matter tends to attract or adsorb gas or fluid via Van der Waal forces of interaction to satisfy the imbalances of atomic forces, as shown in Figure 2.7a. Some studies have shown that a significant portion of gas in shale reservoir is stored in porosity developed within the organic matter by sorption and not only adsorbed their surfaces. It was explained that thermal decomposition of organic matter during catagenesis allows significant gas to reside within the organic matter. The catagenesis process transforms organic matter into hydrocarbon under increasing pressure and temperature, thus allowing the gas to condense in the pore of the organic matter, as shown in Figure 2.7b.

2.9   Porosity in Unconventional Shale Reservoir

The pore spaces that host the shale gas and permeability property of the shale rock reservoir are the subjects of this section. Different forms of porosity, as well as the methods used to quantify them, are also explored. Porosity is the percentage of void spaces or pore volume in a rock containing fluids, such as gas, oil, or formation water (Cheng, 2016). Generally, porosity is described as primary porosity when formed during the deposition of sediments, and void spaces between the grain are not thoroughly compacted together (Ali et al., 2010). The secondary porosity occurs alteration of the deposited sediments or existing or primary pores under increased temperature and pressure (Chima et al., 2018). These alterations may result in mechanical and geochemical changes such as vugs and fractures formation, brittle deformation, pore volume reduction, pore dissolution, and precipitation. Effective porosity differs from total porosity (Schieber, 1992). The void spaces are interconnected and contribute to the fluid flow in a rock while total porosity represents the total pore volume that may or not contribute to fluid flow as shown in Table 2.4. Porosity in organic matter is ubiquitous and heterogeneous due to myriad components and form network, along with fracture, to provide natural pathway for gas flow in unconventional shale source and reservoir rock.

Table 2.4: Description of Porosity in Shale Rock

Porosity Types	Example		Sizes	
Interparticle Porosity	Framework pores	Matrix pores	Intergrain-Intercrystal pores	Nanopores (<2nm) micropores, mesopores (2nm -50nm) and macropores(>50nm)
Intraparticle Porosity	Shelter pores	Organic matter pores	Intrafossil-moldic– shelter pores	Nanopores (<2nm)micropores, mesopores (2nm -50nm) and macropores(>50nm)
Fracture Porosity	Secondary dissolution pores	Solution-enlarged fracture	Cavernous fracture	Nanopores (<2nm)micropores, mesopores (2nm -50nm) and macropores(>50nm)

Figure 2.8 provides a schematic illustration of different grains of macerals and minerals, creating a network of pore spaces within a shale lamina. There are multiple cavities defined by organic matter pore, the shelter of phytoplankton, hollow fossil debris, and mineral grains which serve as sites or voids for infill by kerogen resulting from the maturation of organic matter.

Concerning organic pores, Schieber et al. (2012) observed a plethora of smaller pores between 10nm and 50nm superimposed by a few larger pores of 100nm–1000nm as associated porosity with organic matter the Eagle Ford Shale. It further suggested that these sponge-like smaller and larger pores, termed foam and bubble pores, respectively, were connected by pore throats revealed in SEM examination and confirmed by GATAN ILion ion mill instrumentation. Contrasting the observations made by Schieber et al. (2012) with earlier work of Loucks et al. (2009) on Mississippian Barnett shale showed a pattern of pore structure association within grains or phytoclast of organic matter. Pores within Barnett shale organic matter showed irregular, bubble-like, elliptical structures ranging from 5 to 750nm, but pore throats or interconnections were not observed or reported using SEM. However, Loucks et al. (2009) postulated that permeability or interconnectivity pathways are situated along the bedding-parallel layer of organic matter due to ubiquitous influence of the nanopores.
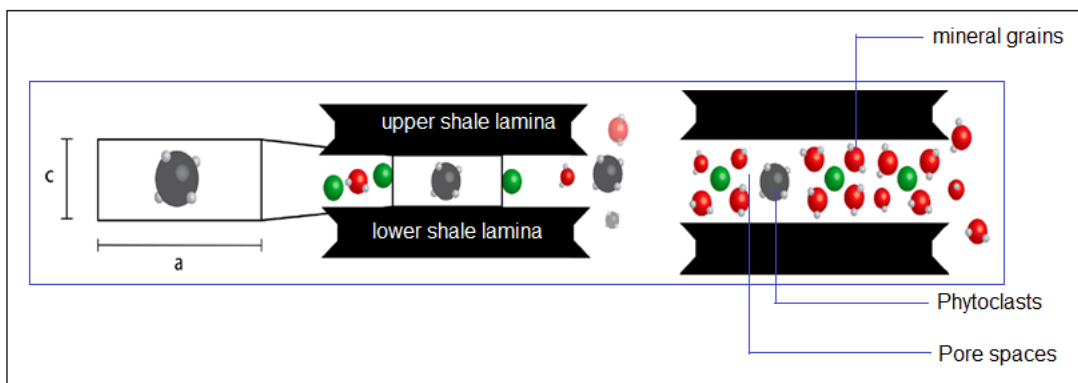
Figure 2.8: Schematic porosity in shale rock (modified after Schieber et al., 2012)

2.9.1 Porosity associated with hosted organic matter

Several workers have identified organic porosity as a significant contributor to the pore volume network in shale due to alterations in organic matter that increase with thermal maturity (Mastalerz et al., 2018b, İnan et al., 2016). Whist organic-matter pores occur mainly as intra-pores located within the organic matter. The groundmass-areas-matrix unassociated with organic matters are related to phytoclasts, hollowed fossils, and mineral grains. Unlike the organic pores, the groundmass-matrix-related pores commonly occur as interparticle between grain and crystal particles and as intraparticle pore located within particles of grains, minerals, or shelters (Loucks et al., 2012). This previous work reveals a sheet-like intra-pores size between 10nm and 1μm in compacted clay that were composed of loosely aggregated clay platelets. Distortion of sheet-like clay minerals were observed in SEM examination as bent around rigid grain like quartz thus forming cleavage-plane-pores within clay and mica mineral grains. On the other hand, Schieber et al. (2012) reported interparticle pores between clay and carbonate grains which was occupied by amorphous organic matter. Carbonate grains consist of scattered micro- and nano-fossils debris that forms supportive framework in fecal pellets and tends to form triangular interstitial pores when multiple carbonate grains agglomerate.

2.9.2 Porosity associated with mineral grains

Mineralogical grains such as quartz, clays, feldspars are another potential factor that may influence porosity and complicate the interpretation of porosity evolution with increasing maturity. Masterlerz et al. (2018) suggest that any influence on porosity by mineralogical composition is masked by the more substantial impact of changes in maturity. The authors explained that shale samples vary in their mineral compositions, but no significant correlations exist between total porosity and the contents of clays, carbonates, quartz, or feldspar. Total

porosity increases with clay and quartz contents and decreases with carbonate content in three shale samples when the least and most mature samples are ignored. The study revealed that Gas adsorption-derived microporosity increases with clay content, showing a weak positive correlation with the quartz content, and decreases with the carbonate content. Mesopore and macropore volumes do not show strong correlations with mineral contents, except for negative correlations between quartz content and mesopore volume, and possibly between clay content and macropore volume. However, It has been reported that high minerals such as quartz, feldspar and carbonate in shale tend to lower Poisson's ratio and increase Young's modulus points towards high brittleness (Boruah and Ganapathi, 2015). Being brittle, shale can easily fracture with external force and develop a conduit for gas or formation water to migrate and accumulate.

2.9.3 Fracture related porosity

Micro-fracture systems in organic-rich shales emanate from tectonic events or drilling activities, deforming the primary pore structures. Tectonically deformed shale (TDS) acts as a gas storage and transport pathway (Zhu et al., 2018). In China, the pore structures of a highly faulted and folded Lujiaping Shales of Yangtze area are characterised using a low pressured nitrogen adsorption, Helium, Nuclear Magnetic Resonance, and Scanning Electron Microscopy. The findings reveal that the syn-depositional of organic-rich shale has been deformed and destroyed by tectonism but enhanced the connectivity of pore networks (Zhu et al., 2018). As such, this finding alludes to the strong relationship between tectonic stress and fracture pores associated with the Wufeng- Longmaxi Formation of Sichuan Basin in China (Liang et al., 2017).

The fracture-related pore network reflects linear nano to micrometers cracks that commonly crosscut bedding planes. Among the factors that affect the structural orientation of fractured pores is the preponderance of brittle minerals such as quartz. Zone with quartz minerals having > 45% and clay minerals < 27% content in the Barnett Shale of Fort Worth Basin in Texas, USA, is prolific for shale gas production due to linear fracture network (Jarvie et al., 2007). Furthermore, the fractured shale of the Longmaxi Shale of Sichuan Basin in China has shown an ideal target for shale gas exploration due to the abundance of quartz and carbonate minerals exceeding 40% content compared with other minerals (Liang et al., 2017). Fracture-related pore structure in organic-rich shale emanates from tectonic stress or diagenetic alteration, controlled by brittle minerals, and reflected in a linear opening more than 5µm long and 0.5µm wide.

© University of Venda

2.9.4 Quantification of porosity in unconventional shale reservoir

Porosity and pore size distribution are crucial in shale rock resource evaluation. In organic-rich shale rock, a significant portion of the gas is stored not only in pores of the shale but within the organic matter pores and fractures, although they occur as adsorbed or free gas saturated with fluid phase. Quantification and characterisation of the total porosity of shale gas are therefore critical. Several analytical techniques such low pressure gas adsorption (LPGA), advance small angle x-ray scattering (ASAXS), environmental scanning electron microscope (ESEM), transmission electron microscope (TEM), Scanning electron microscope (SEM), mercury intrusion porosimetry (MIP) are used to quantify nano, micro, meso and macro pores present in shale source and reservoir rocks.

The SEM technique has experienced tremendous progress in investigating pores distribution in shale source and reservoir rock, but its validity as a sole analytical technique remained questionable (İnan et al., 2016). Studies (İnan et al., 2016; Masterlerz et al., 2018; Lawrence and Jiang, 2017; Liu et al., 2017) have reported successes in observation of pores with diameter ≥ 2nm using SEM. However, observing nanopores with a diameter <2nm is challenging. Observing smaller pores can be difficult with a nominal spatial resolution of SEM, approximately 2nm. In addition, porosity estimation solely based on SEM observation may not represent a holistic spectrum of pores distribution but a limited view of region or spot of interest. However, Sarkar et al.(2018) estimated porosity, pore size, and pore distribution of Gondwana shale Barren-Measure Formation for its gas potential using a combination of SEM and MIP with watershed segmentation and indicated their application for pore size <3nm. Despite the limitation of SEM observation of porosity as sole technique, Lazar et al. (2016) discriminated pore distributions and sizes among organic matter, grain minerals, and shelter with their pore throats during pore observation made on ion-milled surfaces.

2.10 Permeability in Unconventional Shale Reservoir

Permeability characteristics in shale reservoirs differ from that of tight sandstone reservoirs due to the structures and interconnectivity of the pores. Unlike conventional reservoirs, it is difficult to establish a reasonable flow rate in a shale reservoir, having extremely low permeability, particularly in a simple experimental configuration (Ghanizadeh et al., 2015). As such, a non-steady-state gas flow technique is commonly preferred to a steady-state approach than measuring permeability in unconventional shale source rock due to the non-laminar flow of gas. Previous studies (Zhang et al., 2020c, Tinni et al., 2012, Clarkson et al., 2012) have indicated that the non-steady-state gas method has different techniques, including pressure-decay profile permeability, pulsed-decay permeability, and pressure-decay crushed-rock

permeability techniques. While comparing these techniques, Ghanizadeh et al. (2015) recommend that the combined use of permeability techniques provides insight for heterogeneous sizes of shale rock reservoirs. The discrepancies observed between permeability values of the profile, pulsed-decay, and crushed rock techniques attributed to sampling size and stress-state (Ghanizadeh et al., 2015). The controlling factors on the non-steady-state include porosity, pore-fluid/salt, mineral compositions, and effective stress.

On the contrary, steady-state permeability of shale at reservoirs conditions are affected by factors that include net stress, pore pressure, temperature, and gas type (Hannon Jr et al., 2019). However, further studies (Guo et al., 2017; Zhou et al., 2016; Cao et al., 2016) have noted that the earlier mentioned factors are not sufficient to achieve accurate shale permeability measurement. Parameters such as adsorption, desorption, and formation water are crucial to determining shale permeability.

The propagation of gas molecules in shale reservoirs exhibits a non-laminar flow that deviates from a pressure-driven Darcy principle due to the low permeability less than 10^{-18} m^2 and low differential pore pressure (Davis et al., 2005, Tanikawa and Shimamoto, 2006). Some previous (Chen et al., 2016b, Duwiquet et al., 2021) studies indicate that sedimentary rocks display anisotropy in permeability due to various depth conditions, crack and fractures, and tectonic events, ranging from 10^{-12} to less than 10^{-23} m^2. Shale reservoirs with low permeabilities tend to deviate from Darcy's law, indicating that the amount of flow between two points is directly related to the difference in pressure, the distance, and the interconnectivity of pores pathways (Markl et al., 2018). While Darcy's law may not explain the observed deviation, Klinkenberg (1941) reveals that a slip flow of gas at pore walls enhances gas flow when pore sizes are below 10^{-18} m^2 (Tanikawa and Shimamoto, 2006, Guo et al., 2018).

2.11 Functional Groups associated with Organic-Rich Shale

Some functional groups are sensitive to infrared radiation, including aromatic and aliphatic carboxyl and carbonyls, aliphatic C-H's, and amides, which may be present in all Hydrogen Sulphide no matter their origin (Bestvater, 2017). Nevertheless, the aliphatic organic matter functional group has significantly determined gaseous hydrocarbon yield. Due to C-H stretching vibrations, hydrocarbons show infrared absorption peaks between 2800 and 3300 cm^{-1} (Chen et al., 2012). Although there can be an overlap of absorption peaks, the hybridisation of the carbon affects the exact position of the absorption. The explanation remains that the stiffer bonds vibrate at higher frequencies. The hybridisation of an aliphatic sp^3, sp^2, sp C-H has absorption peaks of 2800-3000 cm^{-1}, 3000-3100 cm^{-1}, 3300 cm^{-1} frequencies (Dutta, 2017). Several diagnostic infrared spectra bands, such as those for clays (3600-3750 cm^{-1}), aliphatic moieties (2800-3000 cm^{-1}), carbonates (1200-1550 cm^{-1}), and

silicates (900-1150 cm^{-1}), represent the presence of different mineral groups and organic matter content.

Fourier Transform Infrared (FTIR) data and multivariate chemometric analyses are veritable techniques that characterise an organic-rich shale's geochemical parameters. In shale gas studies, combining infrared spectrum and characteristics of organic shale remains a common technique to predict shale gas generation potentials (Washburn, 2015). Attenuated Total Reflectance (ATR) - FTIR has recently been integrated with principal component regression (PCR) for quantitative investigation of gas shale mineralogy (Palayangoda and Nguyen, 2012). Meanwhile, diffused reflectance FTIR (DRIFTS) has been combined with various chemometric approaches to estimate Fischer assay hydrocarbon output (Palayangoda and Nguyen, 2012). To date, infrared spectroscopy, morphological scanning electron microscopy, and stable isotopy have not been documented to model and predict the source and evolution of organic matter.

2.12   History of Shale Gas Play

The impermeable shale served as source rock and sealing rock while extracting oil and gas from permeable sandstone and limestone reservoirs. Still, advances in technology have favoured organic-rich-shale as reservoir rocks. Shale gas development was not economically viable until the Mitchell Energy and Development Corporation pioneered the hydraulic fracturing technique in 1981 to frack the impermeable Barnett Shale in North Texas for dry natural gas (Soeder, 2018). For 20 years, the company drilled experimental borewells and innovated the combined use of hydraulic fracturing and horizontal drilling to stimulate permeability in a naturally impermeable shale in an economical manner (Sinha and Sharma, 2016). The successful use of horizontal drilling and hydraulic fracturing technology makes shale gas extraction operational and economical (Suboyin et al., 2020). Interestingly, horizontal drilling has been employed in the conventional enhance oil (EOR) and gas recovery (RGR) to sweep oil and gas present in permeable sandstone or limestone reservoir formations but without applying the hydraulic fracturing technique (Alizadeh et al., 2017). This technique is worthwhile since it unlocks the gas trapped in impermeable shale through the fracturing concept to enhance the interconnectivity of pores and the transmission of gas flowage into shale wellbore.

2.13   Shale Gas Resources Development in South Africa

South Africa is one of the emerging shale gas players, although gas exploration is still in the early stages of appraisal for the entire technically recoverable gas potential (Wang et al., 2014, Mauter et al., 2014). The northern region basins Tuli, Tshipise, Ellisras, and Springbok Flat

Basins have been unexplored for shale gas despite their extensive deposit of organic-rich shale and coal-bearing strata (Luyt, 2017). Interestingly, these formations are identified as the current and largest virgin *in-situ* coal and shale bearing deposit with an estimate of about 40% of total reserve (Jeffrey, 2005). The northern region of South Africa has a vast potential for shale gas. It is poorly understood compared to the extensively studied on the Main Karoo Basin in the southern part.

The resource estimate for unconventional gas in the Main Karoo Basin (MKB), interpreted as the foredeep, has been declining in the southern region. At the same time, the corresponding formations in the northern back-bulge depozone are elusive. Given the decreasing estimate of technically feasible unconventional gas resources, thorough petroliferous assessments have been limited to a few shale formations from the MKB. The carbonaceous Prince Albert, Whitehill, and Collingham shales, which make up the Ecca Group of the Main Karoo Basin, are included in these formations. Initial petroliferous assessment of the Ecca Shale revealed an estimate of 475 tsm of shale gas (Administration and Kuuskraa, 2011, Kuuskraa et al., 2013). Figure 2.9 shows the technically recoverable shale gas resources trend in South Africa from 2017 to 2020.
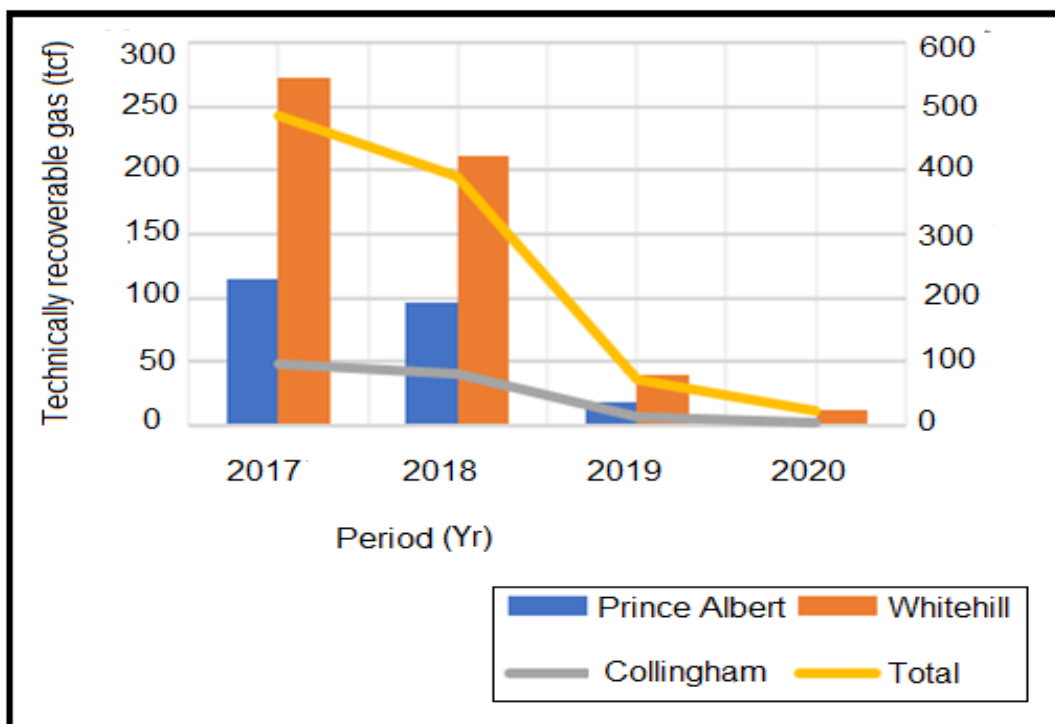
Figure 2.9:Trend of technically recoverable shale gas resources in SA from 2017 to 2020

Although this robust resource estimate positioned South Africa as the fourth-largest shale gas resource globally, subsequent studies (De Kock et al., 2017, Van Vuuren et al., 2011) have shown gradual decrement. The United States Energy Information Administration reported a

continuous reducing estimate of 370 tsm of shale gas. At the same time, the Whitehill Formation of the Ecca Group contributed over 50% of the gas resource (USEIA, 2013). An earlier study (Smithard et al., 2015) attributes volatilization caused by heat flow from dolerite intrusion to the gas decrement. The intrusion has liberated gas from the organic plant matters and leaked gas through fractures or solidified to overmatured organic matter.

Further explanation for shale gas deflation has been ascribed to the low organic content and thermal maturity of Waterford and Fort Brown shales of the Ecca Group. Alluding to the decrement, a recent study (De Kock et al., 2017) has argued that the most realistic resource estimate of shale gas for the Main Karoo Basin ranges from 12 to 45 bsm with the lower boundary value most feasible. It implies that more than a 60% proportion of technically recoverable shale gas from the Main Karoo Basin has deflated.

2.14   Status-Quo of Shale Gas Development in South Africa

In South Africa, shale gas development is emerging due to ongoing investigation of the total technically recoverable shale gas resource pending promulgation of appropriate legislative law and regulation framework to control hydraulic fracturing activities. According to Du Plessis (2015), current ongoing exploration activities for shale gas operate upon the previously issued permit by the Department of Mineral Resources and Energy (DMRE). Still, a moratorium has been imposed on issuing new exploration permits until an explicit framework on hydraulic fracturing of shale gas is promulgated. The Mineral and Petroleum Resources Development Act 28 of 2002 (MPRDA) has an explicit framework provision for exploration and exploitation of petroleum but an implicit implication for shale gas because it had only the offshore exploration in mind at the time of MPRDA promulgation (Du Plessis, 2015). However, the MPRDA definition of "petroleum" also referred to "gas," hence having direct application to gas exploration on which basis previous exploration permits for shale gas were issued.

In response, the South African government imposed a moratorium on the exploration of shale gas due to potential environmental concerns raised by some Karoo Action Group members against fracking. However, a larger group of the community embraced the economic, energy, and employment opportunities associated with shale gas development (Du Plessis, 2015, Pietersen et al., 2020). Divisive reactions to fracking are unsurprising as the experience is common elsewhere (United States (US) and Canada where shale gas boom becomes "gamechanger" of their economic and energy landscape. Drawing from the US, Canada, and Europe successes, the South African government has indicated an essential commitment to the public, their plan to pursue shale gas development seriously. This commitment aims to provide an effective policy, legislation, and sustainable condition under which shale gas

development could occur based on integrated assessment and decision-making framework (Du Plessis, 2015).

An update on shale gas exploration revealed that the restriction or moratorium on onshore gas and oil exploration and production right in South Africa had been recently lifted as gazetted on 20 December 2019 and announced by the Minister of Mineral Resources and Energy, Gwede Mantashe (Jali, 2019). In the gazette, no application of hydraulic fracturing for onshore gas production is emphasised until appropriate legislation and regulatory framework were finalised and promulgated. In terms of national legislation development, not only has the Department of Mineral Resources and Energy saddled with the responsibility of contributing to issues related to fracking but the Department of Environmental Affairs and Department of Water and Sanitation, as well to capture holistic interest from all stakeholders (Du Plessis, 2015). Instead of generalising the regulatory framework, the suggestion to contextualise risk, optimize risk, mitigation strategies, and compliances enforcement due to locality variation has been made (Konschnik and Boling, 2014). Thus, in specific cases, heterogeneous features such as faults, shear zones, dolerite, recharge zones, groundwater source zones, and water resources should be considered.

2.15   Shale Gas Recovery

Natural gas recovery from organic-rich shale formations with extremely low permeability has been uneconomical and impractical in the past but now technically and economically feasible due to advances in directional drilling and hydraulic fracturing techniques. Inclined drilling is a non-vertical well that hits underground target formations inclined toward horizontal drilling and multilateral and extended-reach drillings (Soeder, 2018). In contrast to the vertical drilling technique used for conventional oil and gas recovery, horizontal drilling can recover the same shale gas as vertical wells (Fink, 2020). Horizontal wells with an inclination greater than 80° are used to access natural gas within the shale formation. At the same time, hydraulic fracturing produces artificial ease of gas flow from the shale into the borewell (Fink, 2020, Barbot et al., 2013). Following the horizontal drilling, fracking water is injected into the targeted shale formation at a flow rate of about $0.3 m^3/s$ under high pressure ranging from 6,000 to 9,000 psi to frack the shale formation (Al-Muntasheri, 2014, Barbot et al., 2013).

Shale gas extraction requires fracking water and chemical additives such as polyacrylamide, bis (2-ethylhexyl), phthalate, and sand proppant. The additive reduces friction while the drilling perforates the sedimentary strata (Belyadi et al., 2019). The proppant keeps the fractured pores open, while water injection without proppant may produce good initial gas (Figure 2.10a and b). Still, the pores can close up due to overburden pressure over time from overlying

formations hence decreasing production(Wang and Du, 2018). According to Chesapeake Energy, shale gas production from the Barnett Shale is 5.0 billion square meters (bsm) , with a proven reserve of 4.0 billion square meters (bsm). However, this output has been eclipsed by the Haynesville Shale gas production of 4.5 bsm. In terms of total gas in place (GIP), the Marcellus Shale is estimated at 1,500 tsm with an area extent of 246,000km^2 and appears to be the most prolific shale reservoir although still at the initial stage of development (Smith and Montgomery, 2015). The shale gas revolution has translated to about 23% of United State energy consumption and contributed to a 50% increase in global energy demand (Ahmad, 2020).
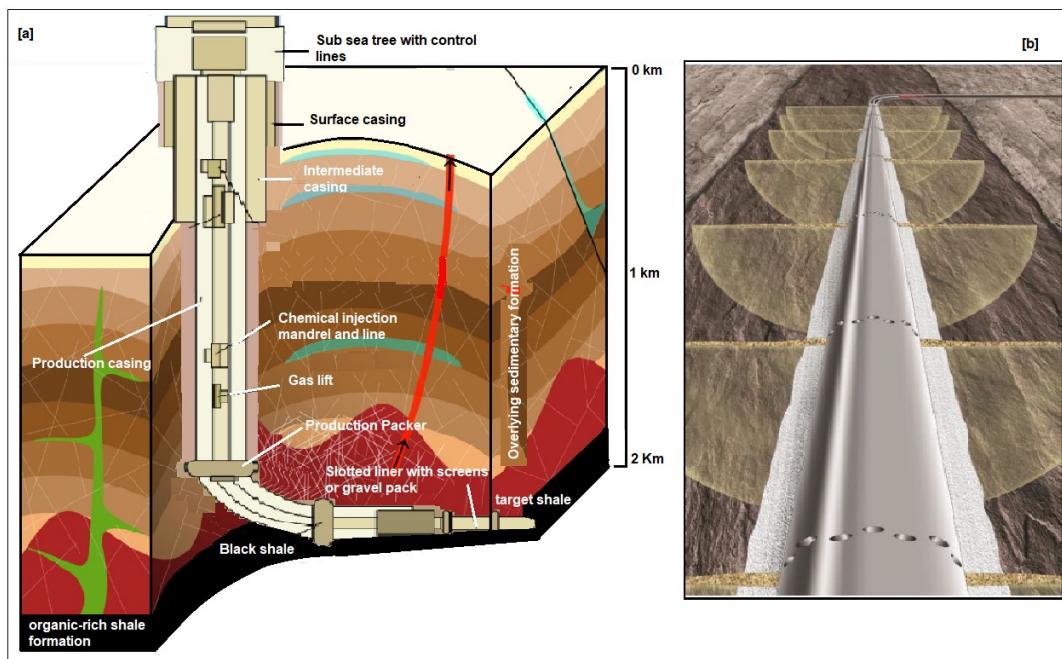
Figure 2.10:(a) Sand proppant suspended in hydraulic fluid with shale reservoir (b) Perforated Horizontal wellbore through fluid and gas is injected and extracted, respectively.

Given the successful and commercial use of hydraulic fracturing and horizontal drilling technology for Barnett shale gas production in the United States, shale gas has transcended from a corporation interest to globally sought-after energy. Globally, the technically recoverable shale gas estimate stands at 7,500 bsm, surpassing the conventional resource estimate reported by the Energy Information Administration (EIA) in 2015. However, this resource estimate changes since exploration and development of shale gas are ongoing globally, and the updated estimate up to 2020 is provided in this study (Table 2.5).

Table 2.5: World shale resource assessment (EIA 2015) and estimate from publications up to 2020

Region	Country	Shale gas (bsm)	Region	Country	Shale gas (bsm)
North America	Canada	572.9	Eastern Europe	Bulgaria	16.6
	Mexico	545.2		Lithuania/Kaliningrid	2.4
	United State	622.5		Poland	145.8
Australia	Australia	429.3		Romania	50.7
South America	Argentina	801.5		Russia	284.5
	Bolivia	36.4		Turkey	23.6
	Brazil	244.9		Ukraine	127.9
	Chile	48.5	Western Europe	Denmark	31.7
	Colombia	54.7		France	136.7
	Paraguay	75.3		Germany	17.0
	Uruguay	4.6		Netherlands	25.9
	Venezuela	167.3		Norway	0.0
North Africa	Algeria	706.9		Spain	8.4
	Egypt	100.0		Sweden	9.8
	Libya	121.6		United Kingdom	25.8
	Mauritania	0.0	Sub-Saharan Africa	Chad	44.4
	Morocco	11.9		South Africa	389.7
	Tunisia	22.7	Asia	China	1115.2
	West Sahara	8.6		India	96.4
Caspian	Kazakhstan	27.5		Indonesia	46.4
Middle East	Jordan	6.8		Mongolia	4.4
	Oman	48.3		Pakistan	105.2
	United Arab Emirates	205.3		Thailand	5.4
			Total		7,576.6

2.16   Potential Constraints to Shale Gas Recovery and Possible Mitigations

Besides the benefit of shale gas evolution, some studies (Estrada and Bhamidimarri, 2016, Wang et al., 2014, Mauter et al., 2014) have raised likely environmental risks associated with shale gas extraction. The primary concerns raised include the potential contamination of groundwater, surface water, and marine environment apart from worsening water crisis in some semi-arid or water-scarce regions (Vengosh et al., 2014, Burton Jr et al., 2014, Vengosh et al., 2013). These studies have divergent views on the impact of the returned water resulting from hydraulic fracturing on the immediate environment and groundwater resources. While some studies suggested that the concentration of chemical additives and dissolved formation salts in both injected water and returned water are hazardous, other studies argued that the flowback and produced water are harmless. The geochemical investigation of the freshwater injected during hydraulic fracturing of Marcellus Shale gas showed that the flowback water

increased in salinity content due to dissolution of halite and other salts present in the shale formation (Blauch et al., 2009).

Further proposed explanations for increased salinity content of the flowback and production water resulting from hydraulic fracturing of shale gas formation include osmotic diffusion of ions from impermeable shale formation and interaction of paleo-seawater with the injected freshwater fracturing fluid (Stewart et al., 2015, Rowan et al., 2015, Balashov et al., 2015, Engelder et al., 2014). Meanwhile, most geochemical investigations reported in the mentioned work used stable isotopes of oxygen and chloride content in the flowback water without detailed mineralogical and major elemental studies of the returned fluid. This gap may limit the compositional trend accuracy in shale formation and the produced water. The returned or effluent water refers to the flowback returned to the surface after freshwater is introduced under high pressure during the fracturing stage. At the same time, the produced water contains dissolved natural gas during the production stage.

On the other hand, groundwater contamination-related risk associated with shale gas extraction using hydraulic drilling suggests an inverse proportionality (Jackson et al., 2013). In contrast to groundwater contamination concerns, the study revealed that the impermeable Fayetteville Shale lacks pore connectivity with groundwater. Hence, thermogenic methane gas could not migrate into the far distance aquifer. It may be implausible to conclude that the water-related risk concerns remain conjectural. However, there is little or no scientific evidence to substantiate the concerns. Furthermore, considering the numerous hydraulic drilling of shale gas formations in the Barnett, Marcellus, Haynesville, Sichuan Basins in the US and China, recent studies (Wang et al., 2020a, McIntosh and Ferguson, 2019, Butkovskyi et al., 2017) suggest that little or no direct groundwater or surface water contamination from fracturing fluid, flowback and produced waters. According to Wang et al. (2014), these perceived concerns constitute less than 20, 25, and 33% in the newspaper articles, broadcast news stories, and online news, respectively, and not scientific documented reports. These studies have argued in favour of the insignificant concentration of the chemical additives and their compliance with minimum and acceptable effluent standard guidelines (Table 6). The South African national framework for effluent discharge corresponds with the international policies (DEA, 2014). Table 2.6 shows the typical flowback water limit of pollutants in hydraulic fracturing fluid in the UK.

Although, the hydro-fracturing drilling is estimated to consume about 12,000l of freshwater per meter and considered to have little or no significance as freshwater consumption locally or in region without water crisis (Mauter et al., 2014), it will still strain the available fresh water resource for households, agriculture and industries. In order to mitigate these potential water-

related risks associated with shale gas recovery, the use of flowback, produced and brackish water have been identified as alternative fluid to freshwater usage hence minimizing water crisis for fracking (Estrada and Bhamidimarri, 2016). However, the likely constraints for the alternative fluids may entails high total dissolve solids (TDS) and salinity resulting from mixture of injected fracking fluid with salts and possible heavy metals in the shale formation before returning to the surface (Barbot et al., 2013) as showing in Figure 2.12.

Table 2.6: Typical flowback water limit of pollutants in hydraulic fracturing fluid in the UK (after Estrada and Bhamidimarri, 2016)

Pollutant	Range	Discharge limits	Pollutant	Range	Discharge limits
BOD5	3-2070 mg O2/L	25 mg O2/L UWWT	Naphthalene	0.1-1400 µg/L	2.4 µg/L (AA, ISW)
COD	175-21, 900mg O2/L	125 mg O2/L UWWT			1.2 µg/L (AA, OSW)
Chloride	1670-181,000 mg/L	250 mg/L MAC	Dimethyl phthalate	-	800 µg/L (AA, FW, SW)
Bromine	15.8-1600 mg/L	2 µg/L (AA, FW)			4000 µg/L (MAC, FW,SW)
		5 µg/L (MAC, FW)	Diethyl phthalate	35 µg/L	200 µg/L (AA, FW,SW).
		10 µg/L (MAC, SW)			1000 µg/L (MAC, FW,SW)
Benzylbuthyl phthalate	-	20 µg/L (AA,FW,SW)	Dibuthyl phthalate	11-130 µg/L	8 µg/L (AA, FW,SW)
		100 µg/L (MAC, FW,SW)			40 µg/L (MAC,FW,SW)
Dioctyl phthalate	15 µg/L	20 µg/L (AA, FW,SW	Xylenes	15-5200 µg/L	30 µg/L (AA, ISFW)
		40 µg/L (MAC, FW,SW)			30 µg/L (CW, RTW)
Nonylphenol	-	0.3 µg/L (AA, ISFW)	Nonylphenol	-	2.0 µg/L (MAC, ISFW)
		0.3 µg/L (AA, OSW)			2.0 µg/L (MAC, OSW)

UWWT: Urban Waste Water Treatment; AA: Annual Average Standard according to the Horizontal Guidance to Environmental Permitting; MAC: Maximum Allowable Concentration according to the Horizontal Guidance to Environmental Permitting; FW: freshwater, SW: Surface Water, ISW: Inland Surface Water, OSW: Other Surface Water; CW: Coastal water, RTW: Relevant Territorial Water

The hydro-fracturing drilling is estimated to consume about 12,000l of freshwater per meter. It has little or no significance as freshwater consumption locally or in a region without a water crisis (Mauter et al., 2014). However, It may strain the available freshwater resource for households, agriculture, and industries. To mitigate these potential water-related risks associated with shale gas recovery, the use of flowback, produced, and brackish water has been identified as alternative fluid to freshwater usage hence minimizing water crisis for fracking (Estrada and Bhamidimarri, 2016). However, the likely constraints for the alternative fluids may entail high total dissolved solids (TDS) and salinity resulting from a mixture of injected fracking fluid with salts and possibly heavy metals in the shale formation before returning to the surface (Barbot et al., 2013) as showing in Figure 2.11.
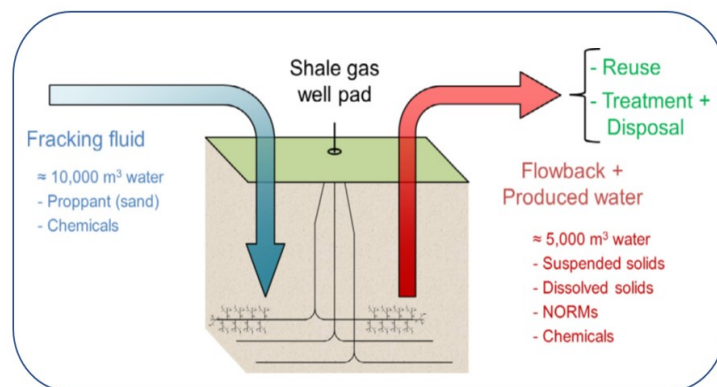
Figure 2.11: Reuse of wastewater as fracking fluid (after Estrada and Bhamidimarri, 2016)

Some studies (Sun et al., 2019, Alessi et al., 2017, Hammond and O'Grady, 2017) have argued that reusing fluid high TDS and salts contents due to damaging effect it has on fracking pumping seal resulting from. On the other hand, some studies have supported the reuse of the fluid directly or blended with freshwater due to compatibility of brackish water with friction reducer agent as long as the TDS concentration is within satisfactory range of 35,000 to 50,000 mg/l (Shamloo et al., 2020, Menefee and Ellis, 2020, Mao et al., 2018). Meanwhile, there is no common accepted limit standard for water quality required for reuse as fracking fluid (Blauch et al., 2009), but information on the concentration limit of parameters are shown in Table 2.7.

Table 2.7: Selected parameter suitability for reuse for fracturing fluid

Parameters	Concentration	Optimization	Water types
TDS	50,000-65,000mg/l	Evaporation with mechanical vapour Compression (MVC)	Flowback water, produced water and brackish water
Chloride	20,000-30,000mg/l	Distillation	
TSS	<50mg/l	MVC	
Hardness	<2500mg/l	Membrane distillation	
Fe	<500mg/l	MVC	
pH	6-8	MVC	
Oil and soluble organics	<25mg/l	Coagulation and flocculation, Forward Osmosis	
sulphate	<100mg/l	Reverse osmosis	
Total bacteria count	<100/100ml	Membrane distillation	
NORM	<500 Bq/l	MVC	
Ammonium	<450 mg/l	Reverse Osmosis	

TDS- total dissolved solid, TSS- Total soluble solid, NORM- naturally occurring radioactive material

For sustainable development of shale gas, best operational practices and policies have suggested practices such as proximity of fracking site from wetlands, multiple well on one pad, surface distance between of 5km between two shale gas. The large distance between two adjacent shale gas play may reduce seismicity resulting from hydraulic fracturing for shale gas

extraction which is a growing concerns just as other anthropogenic activities that have potentials to alters the stress state of the subsurface such as mining, impounding reservoirs, waste-fluid disposal and geothermal probing (Bao and Eaton, 2016, Verdon and Budge, 2018). These previous studies have noted that the pre-existing fault can be activated when pore-fluid pressure increases however, recent studies have revealed that most hydraulic fracturing does not trigger large seismic events (Davies et al., 2013). To date, the largest felt seismic event probably induced by hydraulic fracturing occurred at the Horn River Basin, British Columbia in Canada with a moment magnitude of M3.8. Based on Richter's Magnitude scale having a maximum value of M10, such event magnitude M3.8 is benign and non-damaging compared with other anthropogenic earthquake such as the Denver earthquake with M5.3 induced by waste fluid at the Rocky Mountain Arsenal Colorado.
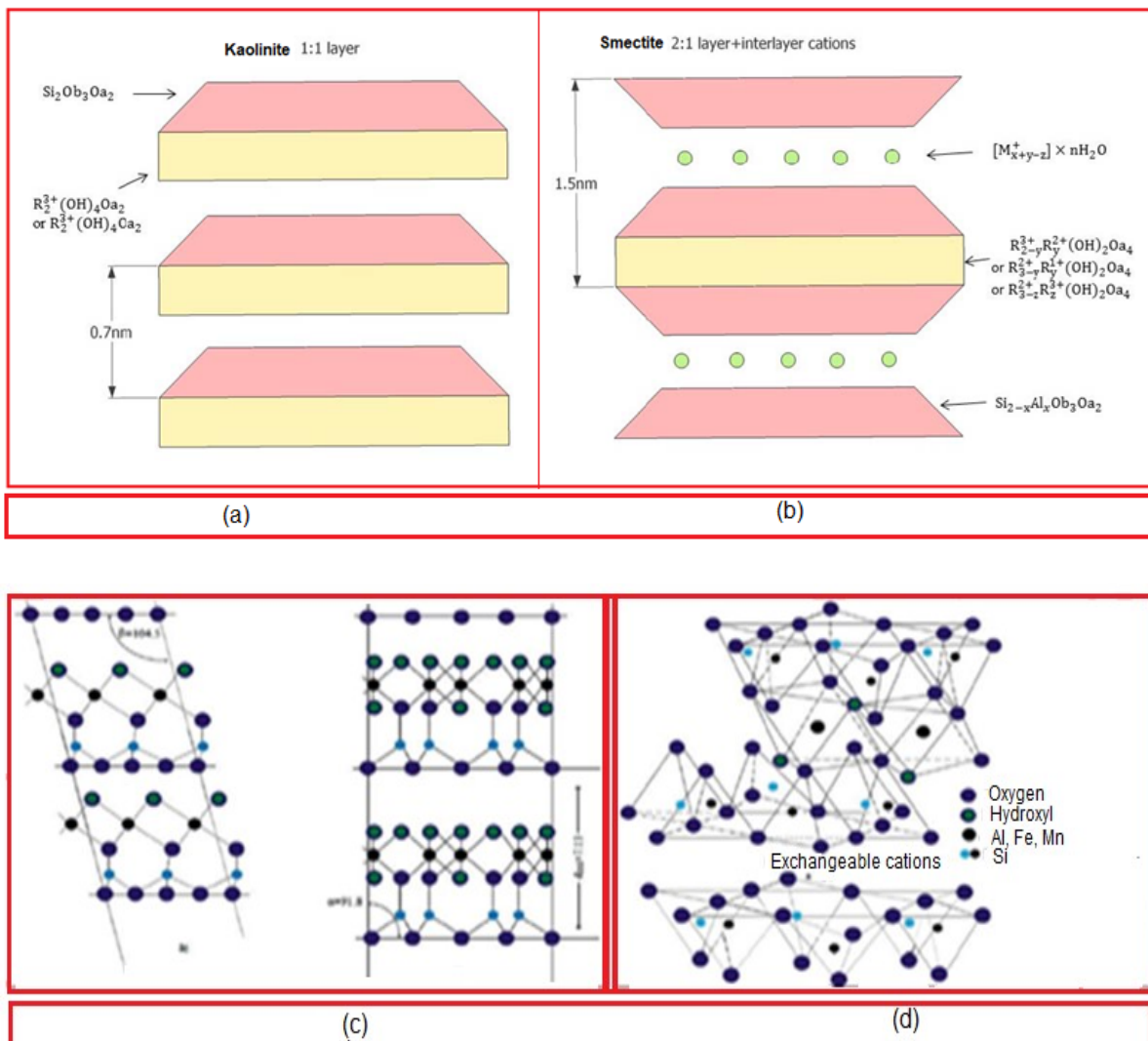
Figure 2.12: Interstitial water in different clay minerals types (a) kaolinite (b) smectite (c) illite (d) Palygorskite (after Akintola, 2018; Bergaya and Lagaly 2013)

2.17   Summary of the Chapter

This chapter presents a critical and systematic evaluation of literature that is relevant to comprehending current and existing information on shale gas reservoirs, as well as research gaps in the study area. The evaluation begins with an overview of the research area's regional and local geological context in the Tuli Basin. In addition, it distinguishes between shale gas and shale rock. Furthermore, the organic matters that serve as the parent materials for shale gas production are studied in terms of production, accumulation, preservation, and deposition environment. The burial and diagenetic transformation of these organic substances to kerogen prone to gas generation is then discussed. Aside from a crucial study of thermal maturity and ways for determining it, storage porosity for generated gas is also discussed.

Sequel to this review, shale gas remains an unconventional resources that can accumulate in an organic-rich shale but varies from area to region due to geologic heterogeneity and petroliferous indications. It implies that contextualising the search for shale gas reduces the risks associated with generalizing the country's prospective resources. Furthermore, the research finds that while a few studies have been conducted in South Africa's main Karoo Basin and other parts of the world, there is no previous or current study on the Karoo-age Limpopo Basins for shale gas potentiality. The Tuli, Tshipise, Ellisras, and Springbok Flat Basins are among these basins. Given the rising demand for electricity and energy crisis resulting from the decision to reduce greenhouse gases emissions from coal plants, there is need for alternative and energy mix, thus investigating source rock potentials to generate shale gas in the Tuli Basin.

CHAPTER THREE

RESEARCH METHODOLOGY

This section provides an information on the systematic approach used to achieve the objectives of the research. The research design focuses on the shale core samples and not on outcropped samples due to the burial diagenetic changes that are of paramount interest in the study. The retrieved core samples are prepared for experimental investigations in line with the aim of the study. Figure 3.1 shows the systematic flowchart of research characterisation according to set objectives.
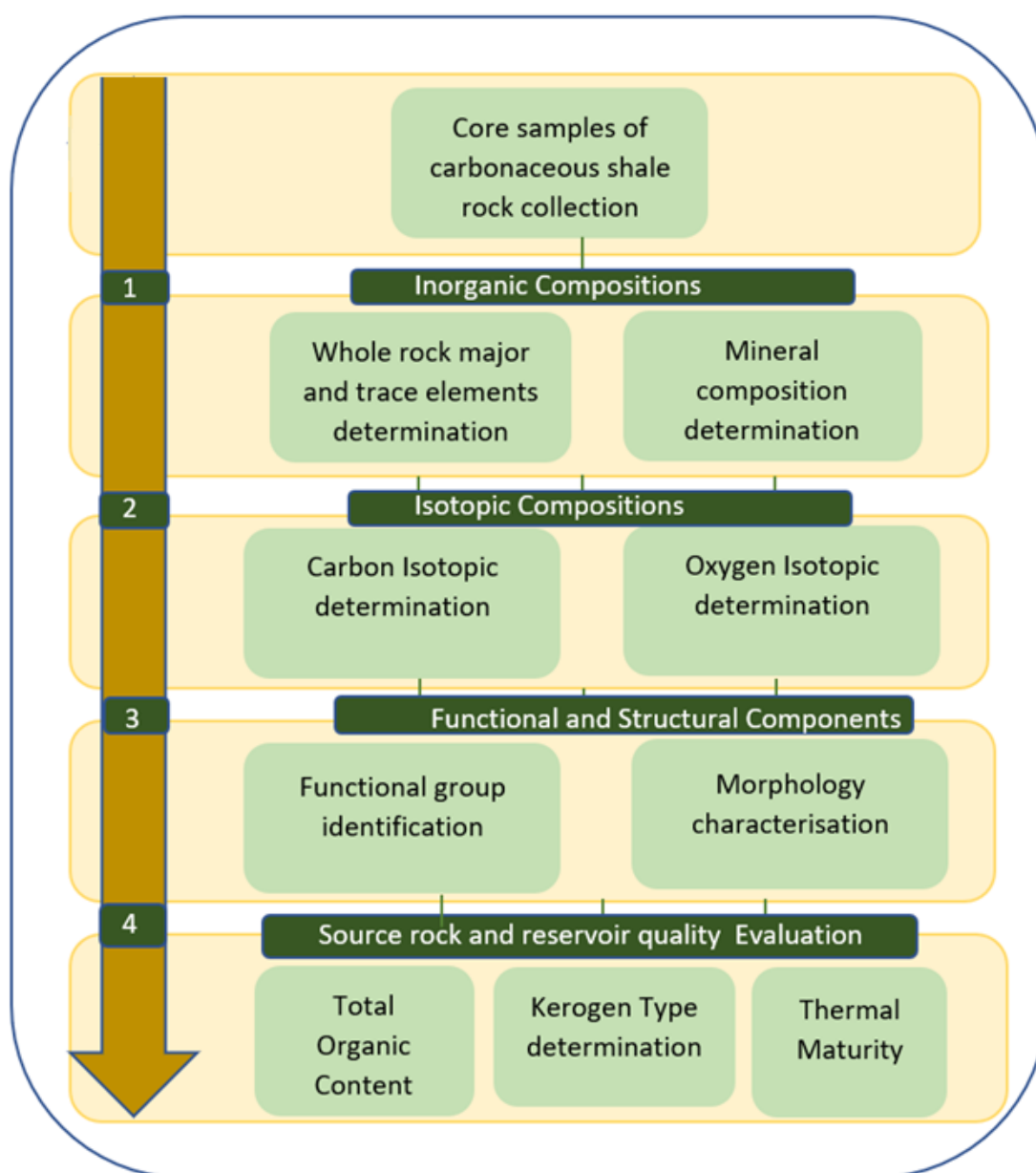
Figure 3.1: Systematic Flowchart of Research Methodology

3.1   Sample Collection and Preparation

The core samples used for this study are collected from three boreholes that penetrated the Mikambeni and Madzaringwe Formations of the Permian Tuli Basin in Limpopo Province of South Africa as shown in Figure 3.1. Several core samples were taken from various depth while a total of 10 representative samples are tagged from SK1 to SK10 in the Mikambeni Formation. In similar manner, the Madzaringwe shales are labelled from SD1 to SD10. The 20 representative core samples spanned a depth range of 370 to 580 m. The Mikambeni shale samples range from 370 to 480m, whereas the Madzaringwe shale samples range from 485 to 580 m.

Based on the lithological facies (Figure 3.2), 20 representative shale samples corresponding to the formations were selected and pulverised in an agate mortar. The shale samples are fissile and sliced as layered surfaces are pulverised for inorganic analysis, functional groups, morphological, total organic composition and source rock analysis.
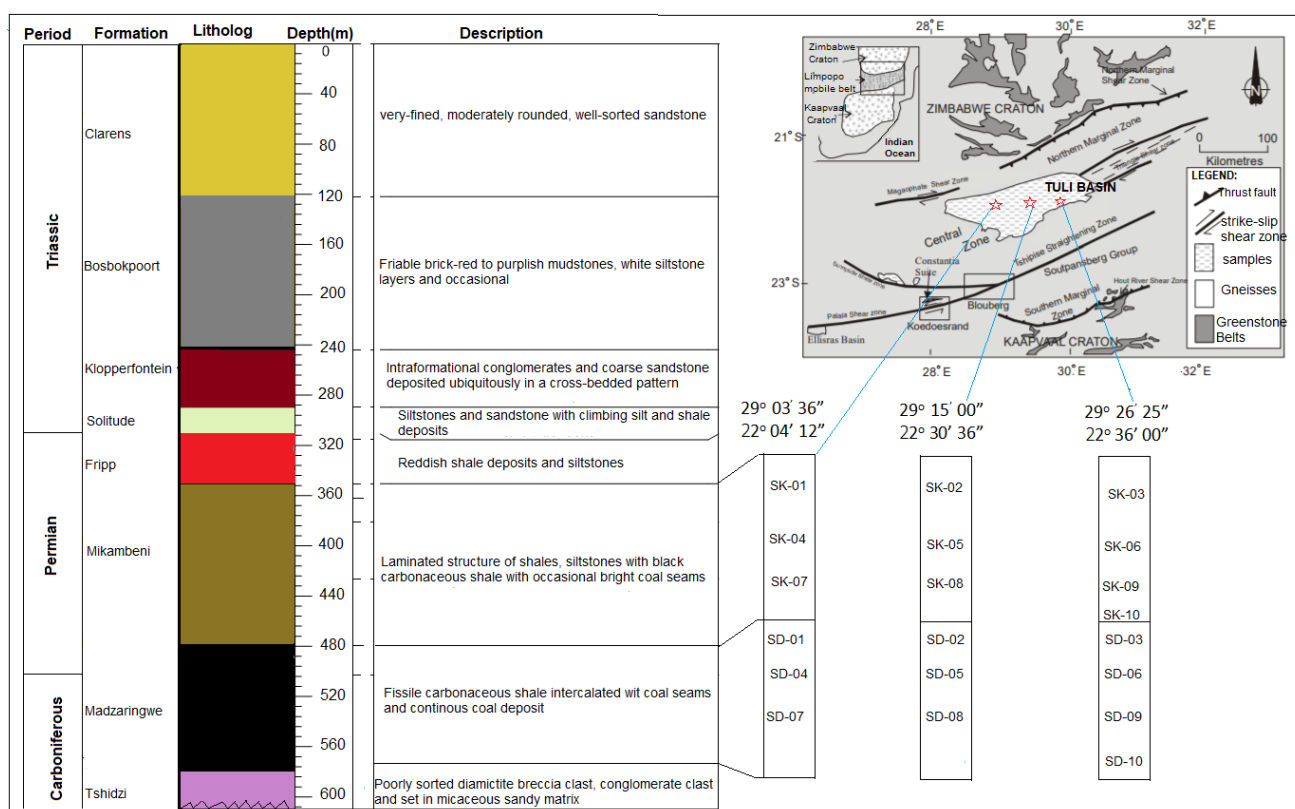
Figure 3.2: Map showing shale samples collection

Figure 3.3: Representative core samples of carbonaceous Shale of the Tuli Basin

3.2   Determination of the Inorganic Compositions

The determination of the inorganic compositions of the carbonaceous shale samples provides detailed information on the mineral and geochemical compositions of the studied samples. The mineral compositions were determined using the X-ray diffraction (XRD) techniques while the geochemical compositions were analysed using the X-ray fluorescence (XRF) and Laser Ablation Inductively Coupled Plasma Mass Spectrometry (LA ICP-MS).

3.2.1   Mineral identification and quantification

Mineralogical identification and quantification of the core samples from the borehole that penetrated the carbonaceous Mikambeni and Madzaringwe shale Formations at different depths was determined using X-ray diffraction (XRD) technique at Council for Scientific and Industrial Research (CSIR) Pretoria. Based on the lithological facies, 20 representative shale samples corresponding to the formations were selected and pulverised in an agate mortar. The clay fractions were dispersed in 0.7 mg/mL of distilled water and put in an ultrasonic water bath for 40 s to prevent flocculation of particles. Afterwards, the air-dried samples were treated with ethylene glycolation to identify smectite minerals and dimethyl sulphoxide to differentiate kaolinite from chlorite. Samples were tightly mounted on oriented sample holder with very little pressure using black loading preparation technique using PANalytical X'Pert Pro-powder diffractometer equipped with X'Celerator detector coupled with receiving slits, variable divergence and Fe-filtered Cu-Kα radiation at the Energy Centre CSIR Pretoria. Whilst the receiving slit was positioned at 0.040°, counting area was from 2 to 80° on a 2θ scale at 1.5s. The interstratified I/S minerals is measured on the less than 2μm fraction of air-dried samples using Cu-Kα radiation. Semi-quantitative mineral measurements were obtained using single line fitting of TOPAS software while the detection limits remain 1% threshold.

3.2.2   Geochemical characterisation

The details of the sample preparation for the X-ray fluorescence (XRF) and Laser Ablation Inductively Coupled Plasma-Mass Spectroscopy (LA-ICP-MS) geochemical procedures are presented in this sub-section. Meanwhile, part of the XRF and ICP-MS geochemical procedures need to be mentioned in this section because the trace and major elements of preparation shared similar preparation procedures. For sample preparation, fusion disks prepared for XRF analysis by an automatic Claisse M4 Gas Fusion instrument and ultrapure Claisse Flux, using a ratio of 1:10 for sample: flux, were coarsely crushed and a chip of sample mounted along with up to 10 other samples in a 2.4cm round resin disk. The mount was mapped and then polished for analysis. The NIST 610 glass (values from Jochum et al., 2011) was used for quantification and analysed every sample, along with BCR-2G and BHVO-2G values from GeoReM (Jochum et al., 2005). A fusion control standard from certified basaltic reference material BCR-2 and BHVO-1 values (Jochum et al., 2016) is also analysed at the beginning of a sequence to verify the effective ablation of fused material. Data processing was done using the LA-ICP-MS data reduction software package LADR from Norris Scientific (Jochum et al., 2011, Jochum et al., 2005, Norris and Danyushevsky, 2018, Jochum et al., 2016). An internal standard element of known concentration is used to correct variations in ablation yield between standards and samples (Longerich et al., 1996). The Al_2O_3 content of each sample, obtained from XRF analysis, was used for this purpose.

Major Elemental Compositions

The geochemical analyses of the major elements of the shale samples were quantitatively estimated using PANalytical X-ray fluorescence (XRF) at the Stellenbosch University, Cape Town. It is equipped with 3kWatt Rhodium (Rh) tube and inserted glass disks containing 1g calcined sample, 8g flux composed of 35% alkali borate ($LiBO_2$) and 64.71% lithium tetraborate ($Li_2B_4O_7$) as oxidant at 1000°C. At this temperature, the weight loss or gain on ignition (LOI) includes the total volatiles content of the rock samples including the water combined to the lattice of silicate minerals, and the gain on ignition related to the oxidation of the rock mostly due to Fe. Pressed powder pellets for XRF analyses were prepared using 3g of sample powder and 6g of boric acid as a binder. The mixture was fused into a steel cup and pressed at a pressure of 30tons in a hydraulic set.

Trace Elemental Compositions

Trace elements in bulk shale samples as well as on single mineral grains were analysed using a resolution 193nm Excimer laser ablation system (ICP-MS), connected to an Agilent 7700 Q

ICP-MS at the Central Analytical Facilities, Stellenbosch University. Before the analysis, Inductively Couple Plasma Mass Spectrometry (ICP-MS) is optimised for sensitivity and low oxide ratios of less than 0.2% by tuning both the ICP and laser parameters while ablating a line on NIST612. Ablation is performed in He gas at a flow rate of 0.35L/min, then mixed with argon (0.9L/min) and Nitrogen (0.003L/min) just before introduction into the ICP plasma. For trace infusions, 2 spots of 104µm are ablated on each sample using a frequency of 8Hz and fluence of ~3.5 J/cm^2.

3.3 Stable Isotopes of Organic Carbon and Oxygen

To remove the organic matter (OM), the core shale samples collected from burial depth of 370 m to 580 m were grounded to 80 to 100µ grain size using agate mortar and treated with hydrochloric acid and hydrogen fluoride to remove carbonates and silicate respectively for about 24 hrs (Rexer et al., 2014). Afterwards, the residual solids were washed severely with distilled water and later treated with Chromium chloride to remove pyrite. Following severely washing of the aliquot with distilled water, the OM samples were separated by mean of 0.6µ filter due to its insolubility and dried in a vacuum at 60°C (Tang et al., 2016). After isolation of OM, a Costech ECS4010 elemental analyser was used to quantitatively combust into CO_2 over a heated copper oxide at 800°C (Rachold and Hubberten, 1999). At the same time, the δ ^{13}C / δ ^{12}C and δO^{18}C/ δ O^{16}C isotope ratios were measured from 0.2 mg of sample using a isotope ratio Finnigan Delta^{plus} mass spectrometer. The carbon isotopes of organic material is expressed in equation [1] and reported in per mil (‰) relative to Pee Dee Belemnite (PDB) reference standard with precision of +/- 0.3‰ while oxygen isotopic compositions are reported relative to standard mean ocean water SMOW (Zhang et al., 2018a).

$$\delta\ 13C(‰) = \left[\frac{(13C/12C)\text{sample}}{(13C/12C)PDB} - 1 \right]\ x\ 10^3 \qquad [1]$$

3.4 Functional Group Identification

The functional group of the studied organic-rich shale was determined by the Fourier Transform Infrared (FTIR) Alpha Bruker spectrophotometer at the University of Venda, South Africa. The pulverised samples were placed in the measurement position of the spectrometer and scanned between the minimum and maximum wavelength range of 500 to 4000cm^{-1} respectively. The absorbance spectral depicts the crystalline phases, reflecting their functional group.

3.5   Scanning Electron Microscopy- Energy Dispersive X-ray

A Zeiss EVO MA15 scanning electron microscope (SEM) equipped with a tungsten filament and a Bruker energy dispersive X-ray (EDX) spectrometer were used for the morphological analysis. The system was operated under a high system vacuum, approximately 7.03 to 007 mbar. The electron beam was generated with an accelerating voltage of 20 kV and a probe current of approximately 2nA. The sample was sprinkled onto a carbon tape substrate and carbon-coated before being loaded into the SEM. A secondary electron detector was used to produce images at 300x, 600x and 900x magnifications. Some of these particles are out of focus, owing to the three-dimensional depth loss of information - focusing one-part results in the other being out of focus on some of these images, particularly at the high magnifications

3.6   Rock-Eval 6 Programmed Pyrolysis and Total Organic Carbon Content (TOC)

In the Rock-Eval 6 Pyrolysis, the organic matter in studied shale samples was cracked isothermally in a programmed temperature pattern to constrain hydrocarbon generation and the Kerogen type. At the Activation Labs Ontario Canada, about 100 mg of pulverized sample in a crucible inserted in an automatic sample holder fitted with the Rock-Eval pyrolyser. At the first stage of pyrolysis, a sample is held isothermally at 300°C for three minutes for volatile free hydrocarbon content (S1) to be released under inert conditions as detected by flame ionization detector (FID). With increasing temperature at the rate of 25°C per minute to a temperature of 650°C, the remaining heavy hydrocarbon is released by cracking of kerogen within the studied sample. This gives rise to the S2 peak. Following the pyrolysis, the sample is placed in the Oxidation Oven and held isothermally at 400°C for three minutes for carbon (IV) content (S3). The temperature is then increased at the rate of 25°C per minute to a final temperature of 800°C and held for five minutes (S4 and S5). The reduced weight results (analysis weights at approximately 10 mg) were reported for parameters where Flame Ionisation Detector (FID) saturation was encountered (S2 and TOC). The TOC content is determined by the addition of the pyrolysable organic carbon and that of oxidised residual organic carbon. Further reduced weight analyses were utilized for improved peak shape and Tmax determinations. The Tmax is the maximum temperature of the S2 peak during the pyrolysis process, indicating the maturity state of an organic matter. The S2 and S3 indicate the amount of hydrogen and oxygen respectively and are used to calculate other parameters. The hydrogen index (HI), oxygen index (OI), production index (PI), vitrinite reflectance (VR$_o$), and oil saturation index (OSI) were calculated using equations 2-6 to determine the quantity, type, generative potential and thermal maturity of the organic matter in studied shale rock.

$$HI = {S2}/{TOC} \; x \; 100 \qquad\qquad [2]$$

$$OI = {S3}/{TOC} \; x \; 100 \qquad\qquad [3]$$

$$PI = \frac{S1}{(S1+S2)} \qquad\qquad [4]$$

$$VRo = (0.0180 \; x \; Tmax) - 7.16 \qquad\qquad [5]$$

$$OSI = {S1}/{TOC} \; x \; 100 \qquad\qquad [6]$$

$$HI = {S2}/{TOC} \; x \; 100$$

CHAPTER FOUR

MINERALOGICAL AND GEOCHEMICAL CHARACTERISTICS OF CARBONACEOUS SHALE ROCKS

An organic-rich shale's inorganic elemental compositions are pervasive and heterogeneous in different areas. This chapter focuses on the inorganic compositions of shale samples to provide essential information about diagenetic alteration, paleo-productivity, paleo-redox state, and hydrothermal activity. In many situations, shale rock consisting of a fine-grained silt made up of quartz, feldspar, clay, and other elements compositions, but the composition varies from area to region due to diverse parent rock minerals. As a result, analytical and empirical techniques were used to characterise the mineralogical and geochemical compositions of the studied carbonaceous shale rocks in this chapter.

4.1   Background of the Study

Understanding the mineralogical and geochemical compositions of an organic-rich shale does not unravel the source rock potential directly but indirectly. Diagenesis involves all change processes that sediment undergoes between the deposition period to before metamorphism (Berner, 2020). These changes include mineralogic, chemical, and physical modification as sediment burial increases in temperature and pressure (Bjørlykke, 2014). Despite the stability of quartz mineral, it is still subject to replacement alteration as cement overgrowth develop on framework quartz grains at temperature >70°C during burial diagenesis (Ma et al., 2021). However, stable limonite mineral (195 – 220°C) as the threshold temperature for diagenetic alteration before metamorphism commences at temperature ≥ 250°C. The thermal maturity of source rock requires sufficient heat and pressure which can be constrained by mineral indicators.

An organic-rich shales' geochemical composition and elemental proxies were used to estimate diagenetic conditions. Several evaluations of the use of elemental concentrations and ratios for paleo-redox (Co, Cr, Mo, U, V, and Re) and paleo-productivity (Sr, Ba, B, Ga, and S) indicators have recently been published (Wei and Algeo, 2019; Algeo and Liu, 2020; Bennett et al., 2020). Some immobile elements, including as La, Th, Co, Sc, Ni, Zr, and Y, show varying concentrations and/or ratios depending on parent rocks and tectonic settings (Cullers and Berendsen, 1998; Cullers, 2002). As a result, the cross and ternary diagrams of these immobile elements might be used to determine the origin and tectonic setting of shale (Tao et al., 2016, 2017; Verma and Armstrong-Altrin, 2016; Deng et al., 2019).

4.2   Purpose of the Study

This chapter aims to characterise the mineralogical and geochemical compositions of the studied shale samples to understand their diagenetic condition, paleo-redox state, and paleo-productivity of the organic-rich shale. To achieve the aim, specific objectives include:

- To assess the mineral components of the Madzaringwe and Mikambeni Formations.
- To characterise the major and trace elemental compositions of the studied formations.

4.3   Results and Interpretations

This section presents the results and interpretations of the mineral components, major elements, and trace element compositions of the studied Mikambeni and Madzaringwe Shale Formations of the Tuli Basin.

4.3.1 X-Ray diffraction data

The X-ray diffraction (XRD) mineralogical data of the studied carbonaceous shale samples are presented in Table 4.1 and Figure 4.1.

The mineralogical powder analysis reveals quartz, albite, microcline, dolomite, pyrite and clay minerals in the studied organic-rich shales samples. The clay mineral component consists of montmorillonite, illite, chlorite, and mixed layered illite/smectite (I/S) in the Mikambeni samples. The average quartz content is 29.42% ranging from 25.10 to 35.60%, present in all samples. The relatively high content of quartz content may be attributed to the preserved detrital silica input from associated siltstone facies since it has high resistance to mechanical alteration although diagenetic quartz can precipitate from the dissolution of feldspar (Baiyegunhi et al., 2017, Johnson et al., 2006a).

Table 4.1: Percentage weight of XRD results in the Mikambeni and Madzaringwe Samples

Sample ID	Formation	Depth (m)	Qtz (%)	Micr (%)	Alb (%)	Chl (%)	Ill (%)	I/S (%)	Mont (%)	Dol (%)	Cal (%)	Pyr (%)
Sk1	Mikambeni	370	25.95	13.05	8.40	2.15	15.20	8.25	21.35	-	5.30	-
Sk2		380	25.10	12.85	7.25	2.70	16.80	9.80	21.90	-	4.40	-
Sk3		390	29.55	8.80	6.05	3.45	14.85	9.70	20.50	-	6.45	1.50
Sk4		410	25.75	10.45	4.90	3.55	15.90	9.05	18.05	-	8.80	3.02
Sk5		430	25.60	9.15	5.05	2.05	18.50	10.40	18.25	10.35	-	1.20
Sk6		440	33.02	9.50	4.45	3.73	19.26	11.98	9.85	7.30	-	1.00
Sk7		450	34.80	8.80	3.05	3.15	19.70	12.20	7.80	11.05	-	-
Sk8		470	35.60	9.75	-	4.05	20.50	13.20	5.40	10.65	-	1.50
Sk9		475	30.68	7.90	2.78	5.56	21.02	13.89	4.30	10.82	-	3.05
Sk10		480	29.07	7.86	1.42	6.54	22.83	14.04	2.49	11.25	-	4.50
SD1	Madzaringwe	485	20.25	14.02	11.4	5.05	15.2	-	20.02	5.10	6.8	1.5
SD2		490	20.1	11.85	8.95	6.1	15.8	-	18.5	7.25	9.6	1.85
SD3		510	20.55	9.08	8.05	7.45	14.05	-	19.5	8.1	9.25	3.3
SD4		520	20.75	8.45	7.2	7.55	15.9	-	18.05	8.02	10.5	3.02
SD5		525	19.6	9.75	6.75	7.95	18.5	-	19.05	6.35	7.43	4.35
SD6		530	25.02	8.5	5.45	8.79	19.26	-	19.85	7.3	1.01	4.5
SD7		545	22.8	8.8	4.05	8.98	19.7	-	19.05	11.05	1.03	4.52
SD8		555	20.6	7.75	6.1	9.05	20.5	-	18.4	10.65	1.00	5.5
SD9		570	24.68	6.8	5.45	10.6	21.02	-	12.05	11.82	1.01	5.85
SD10		580	21.07	5.5	4.75	11.8	22.83	-	14.05	12.25	1.00	6.5

Qtz- Quartz, Micr- Microcline, Alb- Albite, Chl- Chlorite, Ill- Illite, I/S- Mixed Iliite/Smectite, Mont- Montmorillonite, Dol- Dolomite, Calcite-Cal, Pyr- Pyrite
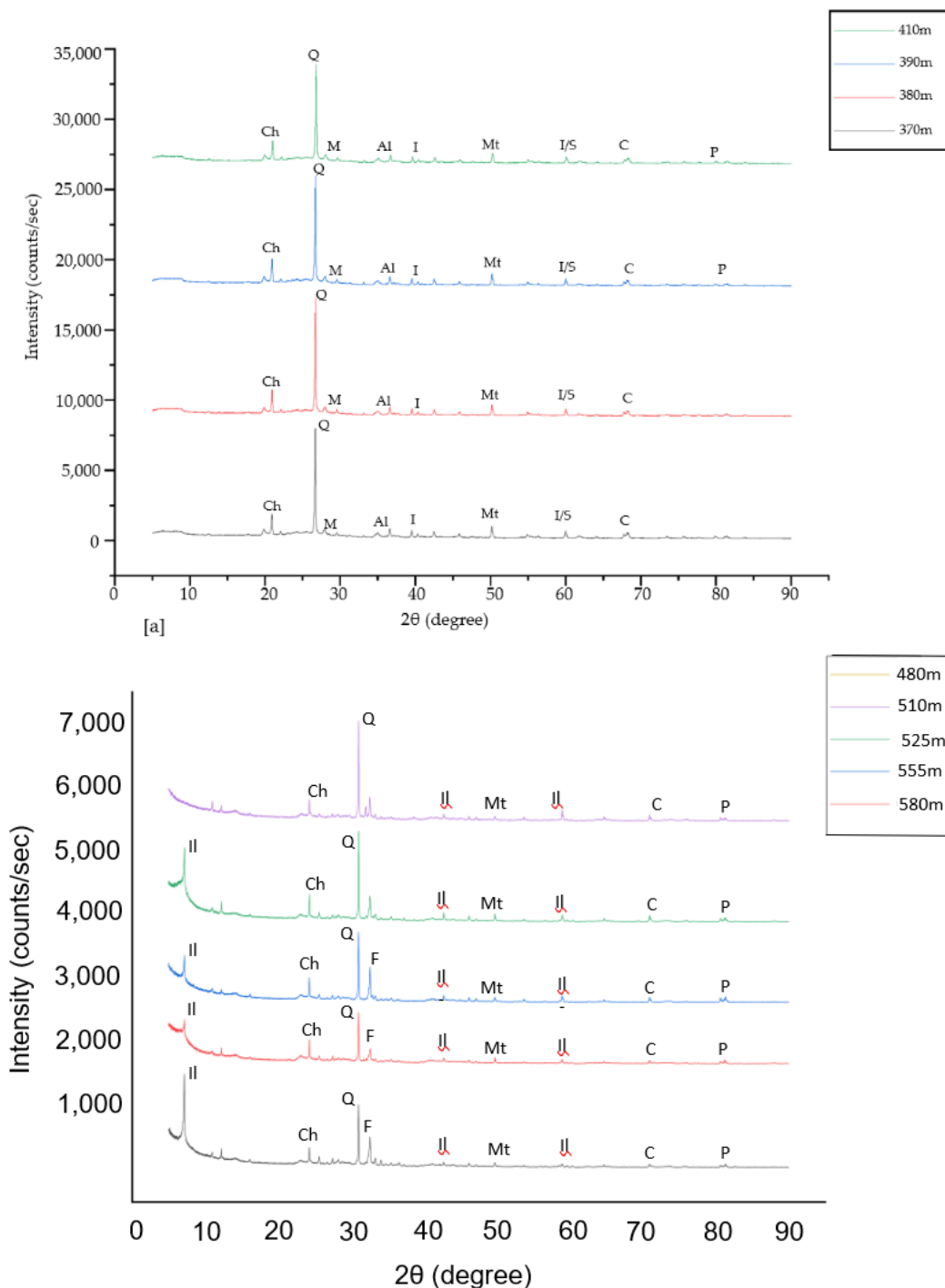
Figure 4.1: X-ray diffractogram patterns of the studied carbonaceous shale (note: ch-chlorite, Q-Quartz, M-Microcline, Al-Albite, I-Illite, Mt-Montmorillinite, I/S-mixed layer Illite-Smectite, C-Calcite, D-Dolomite, P-Pyrite)

The predominant feldspar includes microcline and albite minerals. In comparison to the quartz content, the average amount of microcline and albite was 10.17% and 5.45% although there is no albite mineral present at depth 480m. Feldspars are susceptible to dissolution reaction with increase in burial depth, thus the albite minerals progressively reduces until it eventually lost at depth 480m (Yuan et al., 2019b, Yuan et al., 2017). As burial depth increases, it was noted that the montmorillonite content progressively decreases from 21.35% to 5.40%. On the

63

other hand, the illite and mixed I/S contents increased from 15.20 to 20.50% and 8.25 to 13.20% respectively. This observation may be attributed to the illitization reaction at burial depth temperature less than 200°C in which precursor minerals of K-feldspar or smectite transform to illite or mixed Smectite/illite (S/I) in the presence of sufficient K^+ (Liang et al., 2018a, Berger et al., 1997, Kennedy et al., 2014). Although present in all samples, the chlorite content has an average value of 3.42% and ranged from 2.20 to 5.65 in a random manner. The presence of chlorite mineral suggests a by-product of the montmorillonite-illitization-chloritization alteration process in a closed system having a low ratio of fluid to shale rock (Beaufort et al., 2015). The distribution of dolomite showed a progressive increment in concentration from 5.30 to 11.05% with burial depth. Since the organic-rich shale has a low fluid to rock ratio, the concept of dolomite replacing calcite with the saturated fluid of Mg^{2+} may not be feasible rather precipitation of primary dolomite and stepwise recrystallisation due to bacterial mediation (Montanez and Read, 1992). It is worthy to note that a high fluid-rock ratio is necessary for a steady and saturated supply of Mg^{2+} for dolomitization replacement of calcite which favours permeable sandstone than impermeable buried shales. High burial temperature is insufficient to destroy the evidence of pyrite grain history or origin hence it presence suggested detrital grain devoid of oxidizing setting but associated with anoxic, aridity, or fluvial settings(Johnson et al., 2014, da Costa et al., 2020).

Following the XRD data of the Madzaringwe shale samples, the non-clay mineral consists of quartz, feldspars, dolomite, calcite, and pyrite while the clay mineral that predominates is chlorite, illite, and montmorillonites. The average quartz content is 21.8% ranging from 19.6 to 25.02%, however, the highest quartz content was found at depth 530m. The microcline and feldspar contents have an average of 9.7% and 6.8 respectively. In comparison to the Mikambeni shale, the Madzaringwe shale has lower quartz, plagioclase, and microcline contents. The reason may be attributed to the diagenetic dissolution of plagioclase and microcline as depth increases. However, the quartz may not be expected to dissolute due to its high resistance to alteration, reduction of siltstone input could lower the quartz contents. (Yuan et al., 2019b, Yuan et al., 2017). The mixed I/S content is absent in the Madzaringwe shale but it has the illite content, averaging at 18.3%. This absence of mixed I/S suggests a complete illitization reaction from smectite to illite at greater burial depth. In addition, the montmorillonite content decreases from 20.02% to 15.05% showing a progressive depletion.

4.3.2 Major oxides of geochemical compositions

The result of geochemical compositions of the studied samples showed the presence of major oxides as depicted in Table 4.2 and Appendix-A. It reveals a varying amount of Al_2O_3(19.37–20.32%), CaO (0.20-0.22%), Fe_2O_3 (0.85-0.94%), K_2O (1.59-1.66%), MgO (0.25-0.28%),

Na$_2$O (0.12-0.15%), P$_2$O$_5$ (0.04%), SiO$_2$ (50.37-51.90%), TiO$_2$ (0.69-0.73%) in the studied Mikambeni samples. In addition, the Loss on Ignition (LOI) values averages at 25.10%. In contrast to other elements, silica and alumina showed a relatively higher values which averages at 50.17% and 20.02% respectively suggesting a felsic provenance (Akintola et al., 2021) which is consistent with the discriminate functional plot (Hayashi et al., 1997). Except for the lower value of loss-on-Ignition (LOI) which averages 15.04% in the Madzaringwe Shale, the compositional trend of other important components is comparable. The lower LOI suggests lower carbon content in Madzaringwe compared to the higher carbon content of the Mikambeni Shale.

.

Table 4:2: Major oxides composition of the Mikambeni and Madzaringwe Shale Samples

Sample ID	Depth (m)	Major oxides composition (%)										L.O.I (%)	K_2O /Al_2O_3	Fe/(Fe+Mg)	ICV
		Al_2O_3	CaO	Fe_2O_3	K_2O	MgO	MnO	Na_2O	P_2O_5	SiO_2	TiO_2				
SK1	370	19.99	0.22	0.88	1.64	0.27	0.01	0.14	0.04	51.90	0.71	25.00	0.082	0.55	0.158
SK2	380	20.30	0.21	0.88	1.65	0.28	0.01	0.15	0.04	51.08	0.73	24.94	0.081	0.50	0.157
SK3	390	19.37	0.20	0.85	1.59	0.25	0.01	0.14	0.04	50.86	0.69	25.05	0.082	0.66	0.157
SK4	410	19.66	0.21	0.88	1.59	0.27	0.01	0.12	0.04	50.50	0.70	25.08	0.081	0.79	0.157
SK5	430	20.10	0.21	0.86	1.63	0.28	0.01	0.14	0.04	51.37	0.71	25.06	0.081	0.78	0.156
SK6	440	19.62	0.21	0.87	1.61	0.27	0.01	0.14	0.04	50.78	0.70	25.18	0.082	0.79	0.159
SK7	450	20.27	0.21	0.90	1.66	0.27	0.01	0.14	0.04	51.51	0.73	25.11	0.082	0.79	0.157
SK8	470	20.19	0.21	0.91	1.64	0.27	0.01	0.13	0.04	51.03	0.73	25.05	0.081	0.80	0.157
SK9	475	20.21	0.21	0.91	1.65	0.27	0.01	0.14	0.04	51.10	0.73	25.06	0.082	0.68	0.157
SK10	480	20.32	0.21	0.94	1.66	0.29	0.01	0.14	0.04	51.57	0.73	24.96	0.082	0.80	0.160
SD1	485	29.17	0.28	1.10	0.98	0.12	0.01	0.11	0.22	52.26	1.19	15.04	0.03	0.90	0.09
SD2	490	29.24	0.28	1.16	0.98	0.13	0.01	0.11	0.22	52.45	1.19	15.11	0.03	0.90	0.09
SD3	510	29.16	0.28	1.13	0.98	0.12	0.01	0.10	0.22	52.18	1.20	15.10	0.03	0.90	0.09
SD4	520	29.23	0.29	1.12	0.97	0.13	0.01	0.11	0.21	52.18	1.19	15.06	0.03	0.90	0.09
SD5	525	29.19	0.28	1.13	0.97	0.13	0.01	0.10	0.21	52.26	1.19	14.95	0.03	0.90	0.09
SD6	530	29.12	0.28	1.14	0.98	0.13	0.01	0.10	0.21	52.50	1.19	15.06	0.03	0.90	0.09
SD7	545	29.14	0.29	1.11	0.97	0.13	0,01	0.12	0.21	52.30	1.18	14.97	0.03	0.90	0.09
SD8	555	29.11	0.28	1.12	0.97	0.13	0,01	0.09	0.21	52.34	1.18	15.06	0.03	0.90	0.09
SD9	570	29.25	0.28	1.12	0.98	0.13	0.01	0.10	0.22	52.25	1.18	15.03	0.03	0.90	0.09
SD10	580	29.18	0.28	1.09	0.98	0.13	0.01	0.10	0.21	52.37	1.19	15.03	0.03	0.89	0.09

The plot (Figure 4.2) showed that the studied samples were found to have both quartzose sedimentary and intermediate igneous provenances thus explaining the exceptional higher values of alumina and silica. The intermediate provenance is further revealed by the high Fe/(Fe+Mg) values which exceeded 0.5 and ranged from 0.5 to 0.9, which is comparable to the report of Mesquita et al (2018). According to the study (Mesquita et al., 2018), the granite has calcic amphibole composed of ferro-hornblende and ferro-edenite with Fe/(Fe + Mg) values ranging from 0.53 to 0.81 while the biotite has Fe/(Fe + Mg) ratio > 0.60 thus indicating a mafic input besides the felsic input. Furthermore, the oxide of Al and Ti elements have been used as a veritable tools to interpret deposited sediments due to their immobility nature during transportation from weathered source rock (McLennan et al., 2006, McLennan, 2001, Hayashi et al., 1997) with the elemental proxies ratio of Al_2O_3/ TiO_2 values > 25 indicating sedimentary and intermediate igneous sources. The Index of Compositional Variation (ICV) of the carbonaceous shale samples have an average value < 0.1 which is comparable with the Paleogene-Neogene black shales of Arang, Nyalau Tanjong Balingian Bergih Liang Formations in Malaysia enriched with kerogen capable of generating gas (Baiyegunhi et al., 2018a). The elemental ratio K_2O/Al_2O_3 (0.08) of the studied samples showed values ≤ 0.5 which suggest a highly mature shale since significant amount of Al_2O_3 is typical of immature sediments (Cox et al., 1995).
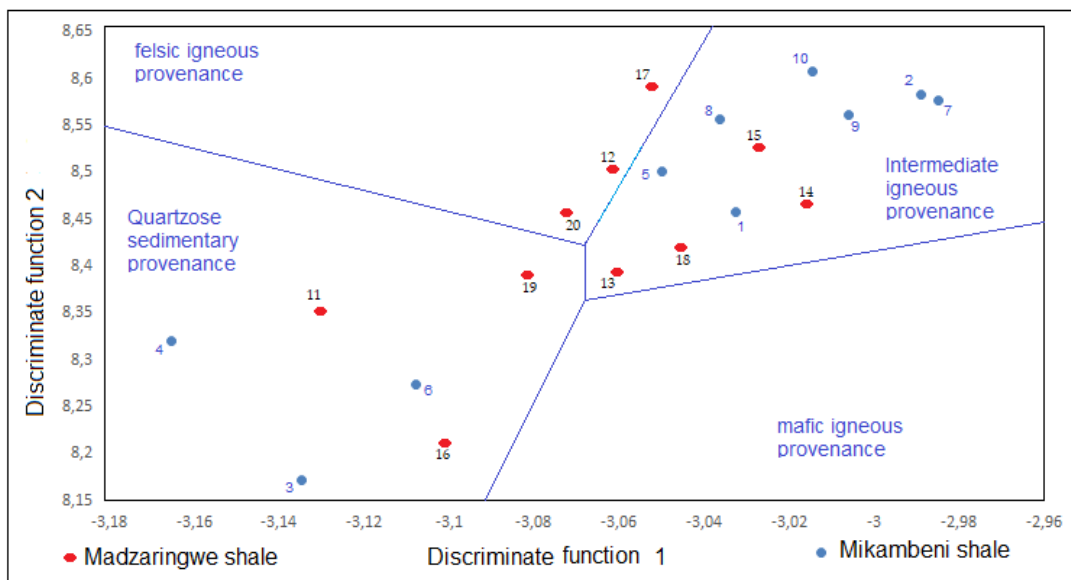
Figure 4.1: Plot of Discrimination functions using major elements index for felsic and mafic provenance and quartzose sedimentary provenance (**Note:** Discrimination Function 1: - 1.733 TiO_2 + 0.607 Al_2O_3 +0.76 Fe_2O_3 (t) - 1.5 MgO + 0.616 CaO + 0.509 Na_2O - 1.224K_2O -0.909. Discrimination Function 2: 0.445 TiO_2 + 0.07 Al_2O_3 - 0.25Fe_2O_3 (t) - 1.142 MgO + 0.438 CaO + 1.475 Na_2O + 1.426K_2O - 6.861)

4.3.3 Trace and rare-earth elemental compositions

The trace and rare earth elements distributions (REE) in the studied samples are presented in Table 4.3 and Appendix-B. The trace element showed relatively high concentration in Ba, Zr, Rb, Zn, Sr, V and Cr with values above 50 ppm while all other elements are lower. In all Mikambeni samples, the highest value of Barium, Ba (294.19 - 331.27 ppm) with an average of 301.29 ppm suggest dissolution of mineral barite in the black shale by action of sulphate-reducing bacteria (Hanor, 2000, Saba, 2015). In combination with Ba, the relatively high concentration of zinc, Zn (82.73-121.63 ppm) with an average of 96.92 ppm indicates paleo-productivity of abundant organic matter the Mikambeni Formation. The association of elements such as Ba, Zn, Pb and Cu with abundance of organic matter have been reported in shale source rock due to high stability thus providing an important forensic tool for paleo-productivity (Li et al., 2017, Wu et al., 2017). The concentration of Ba may be altered by hydrothermal overprint however it is precipitated in connection with organic matter, high concentration of Zn may be related to hydrothermal activities (Hönisch and Hemming, 2004, Charriau et al., 2011). The relatively high concentration of zirconium, Zr (189.02 – 208.61 ppm) with an average of 202.28 ppm suggests shale deposition that is weakly affected by weathering action and diagenesis (Huang et al., 2020). The concentrations of Rubidium, Rb (94.18-102.26 ppm) with an average of 97.52 ppm and Strontium, Sr (92.02-99.62 ppm) with an average of 96.03 ppm are close and suggest saline depositional environment of the organic-rich shale formation (Frape et al., 2003). The concentration of Vanadium, V (81.24-93.72 ppm) with an average of 86.70 ppm and Chromium, Cr (47.50 – 52.85 ppm) with an average of 50.86 ppm fall within the range of value, 50 – 250 ppm which had been indicated for lacustrine oil shale (Frape et al., 2003). The geochemical proxies ratio of V/(V+Ni) and V/Ni for all studied samples exceed 0.54 and 4.25 respectively thus suggesting anoxic condition of depositional environment (Ferriday and Montenari, 2016).

Table 4.3: Trace elements composition of the Mikambeni Shale Samples

Sample ID	Sc	V	Cr	Co	Ni	Cu	Zn	Rb	Sr	Y	Zr	Nb	Mo	Cs	Ba	La	Ce	Pr	Nd
Sk1	12.46	83.66	48.61	11.36	14.63	22.07	94.85	100.27	97.62	31.63	200.85	15.80	3.09	7.50	312.95	52.21	115.79	13.95	47.31
Sk2	12.51	84.40	52.28	10.01	15.07	17.83	92.30	98.37	94.86	30.47	204.16	15.05	2.97	7.61	303.15	50.40	117.57	12.75	45.82
SK3	12.51	84.40	52.28	10.01	15.07	17.83	92.30	98.37	94.86	30.47	204.16	15.05	2.97	7.61	304.15	50.40	117.57	12.75	45.82
SK4	11.89	81.24	48.19	9.72	16.03	19.97	87.16	94.18	96.41	30.61	196.55	15.71	3.36	7.79	313.82	50.43	121.55	12.86	47.42
SK5	11.61	81.82	51.91	13.38	13.27	16.51	82.73	97.03	95.63	30.34	208.43	16.42	2.64	7.62	306.95	50.51	118.91	13.47	45.06
SK6	11.97	93.72	52.10	9.51	16.57	18.90	94.01	96.01	99.61	32.29	201.68	16.10	3.41	8,28	308.03	51.52	123.88	13.98	47.63
SK7	12.63	92.09	52.34	12.46	19.82	26.82	107.59	97.93	95.18	29.99	201.13	17.02	2.74	7.99	312.71	52.27	125.11	13.17	48.61
SK8	12.30	89.95	50.55	9.51	17.14	31.39	94.88	96.52	92.02	31.53	208.61	15.69	3.29	7.97	305.90	51.34	122.01	13.68	47.17
SK9	12.27	84.50	47.50	10.20	18.09	37.58	101.76	94.28	94.46	31.88	189.02	15.30	3.01	7.43	294.16	49.82	119.57	13.19	46.87
SK10	12.41	91.20	52.85	10.13	19.36	33.14	121.63	102.26	99.62	33.22	208.18	17.41	2.85	8.46	331.27	54.21	132.09	13.83	48.15

Sample ID	Sm	Eu	Gd	Tb	Dy	Ho	Er	Tm	Yb	Lu	Hf	Pb	Th	U	V/(V+Ni)	V/Ni	(Eu/Eu*)	(Ce*)	Sr/Rb
Sk1	8.33	1.55	6.47	1.01	5.63	1.18	3.01	0.52	2.77	0.48	5.39	12.84	18.60	5.06	0.85	5.72	0.64	4.39	0.97
Sk2	7.75	1.58	6.33	0.91	5.83	1.09	2.71	0.51	3.15	0.46	5.72	13.52	17.65	4.84	0.85	5.60	0.69	4.67	0.96
SK3	7.75	1.58	6.33	0.91	5.83	1.09	2.71	0.51	3.15	0.46	5.72	13.52	17.65	4.84	0.85	5.60	0.69	4.67	0.96
SK4	8.64	1.64	7.27	0.99	5.52	1.07	3.07	0.48	2.85	0.42	5.83	12.69	17.83	4.91	0.84	5.07	0.63	4.27	1.02
SK5	8.42	1.57	6.71	0.91	5.76	1.23	3.13	0.48	2.90	0.40	5.45	11.25	18.70	5.09	0.86	6.17	0.64	4.40	0.99
SK6	9.22	1.71	6.69	0.92	5.65	1.19	2.90	0.46	3.18	0.42	5.07	12.34	18.94	4.96	0.85	5.66	0.67	4.39	1.04
SK7	8.68	1.40	7.00	1.03	6.23	1.18	3.23	0.46	2.95	0.46	5.42	14.69	18.43	4.83	0.82	4.65	0.55	4.46	0.97
SK8	9.05	1.38	6.82	0.97	5.36	1.17	2.85	0.44	2.90	0.46	5.64	11.56	18.03	5.14	0.84	5.25	0.54	4.32	0.95
SK9	8.42	1.45	7.08	1.11	5.88	1.11	2.95	0.46	3.23	0.43	5.56	12.85	17.79	4.71	0.82	4.67	057	4.31	1.00
SK10	9.18	1.54	6.95	1.13	6.46	1.14	3.27	0.53	3.00	0.47	5.56	16.30	19.10	5.19	0.82	4.71	0.59	4.60	0.97

$Eu^* = (Sm_{CN}*Gd_{CN})^{1/2}$ CN denotes chondrite-normalized value

For the Madzaringwe samples, the highest value of Barium, Ba (513.85 - 560.88 ppm) with an average of 545.77 ppm suggest dissolution of mineral barite in the black shale by action of sulphate-reducing bacteria (Hanor, 2000, Saba, 2015). Furthermore, the sulphate-reducing and methanogenesis bacteria actions are reflected by the increasing concentration of Pb, averaging at 32.75 ppm. The reduction processes were observed in the Mikambeni but at a low rate indicated by the lower value of Ba and Pb concentration. The concentrations of Zn and Cu of the Madzaringwe showed similar trend with the Mikambeni but Zirconium, Zr (314.58- 341.73 ppm) and the Vanadium showed a higher concentration in the Madzaringwe shale. This higher concentration of Zr and V suggest an increasing paleo-productivity of organic matter and brackish deposit (Li et al., 2017, Wu et al., 2017, Frape et al., 2003). The average geochemical proxies ratio of V/(V+Ni) and V/Ni for all studied samples exceed 0.77 and 3.80 ppm respectively, suggesting anoxic condition of depositional environment (Ferriday and Montenari, 2016).

Table 4.4: Trace Elemental Composition of the Madzaringwe Shale Samples

Sample	Sc	V	Cr	Co	Ni	Cu	Zn	Rb	Sr	Y	Zr	Nb	Mo	Cs	Ba	La	Ce	Pr	Nd	
SD1	25.19	151.88	82.80	5.51	45.09	43.09	65.30	69.77	328.15	56.63	314.58	29.64	1.37	9.15	557.17	91.48	168.57	19.27	63.60	
SD2	25.91	153.51	83.96	5.89	51.29	77.11	64.17	69.65	344.91	57.09	328.64	32.17	1.95	9.68	547.99	93.19	172.81	19.43	67.04	
SD3	23.44	150.94	73.08	5.34	39.04	39.92	65.37	67.69	336.77	53.99	317.59	28.83	1.87	9.76	550.62	91.01	170.72	19.21	64.11	
SD4	25.40	156.69	76.64	5.16	39.53	29.04	59.03	68.58	335.61	56.71	325.10	29.21	1.95	9.21	560.83	93.05	173.01	19.35	63.31	
SD5	25.22	156.61	78.22	5.96	43.54	39.45	57.46	70.11	325.77	58.22	315.47	29.52	1.89	9.32	527.61	92.60	170.34	19.62	66.19	
SD6	25.39	155.86	81.64	5.93	48.40	44.27	62,05	68.06	340.61	55.66	316.38	30.08	1.90	9.92	513.85	91.71	164.63	18.33	64.44	
SD7	25.09	156.88	86.66	5.79	45.75	37.30	58.51	73.87	343.57	59.75	341.73	31.51	2.27	9.65	560.88	93.34	173.39	19.40	64.70	
SD8	25.82	153.66	80.84	6.03	44.29	36.21	67.09	68.00	342.15	57.76	319.57	30.33	1.93	9.61	550.97	93.58	168.96	19.28	63.59	
SD9	23.49	155.09	85.37	5.49	43.44	37.23	59.86	68.15	339.71	58.51	328.14	30.40	1.57	9.50	554.09	92.30	175.01	19.51	63.83	
SD10	23.45	156.02	85.12	4.85	39.50	33.12	61.89	73.00	333.74	56.50	316.50	30.53	1.97	9.55	533.70	88.48	174.55	19.61	61.87	
	Sm	Eu	Gd	Tb	Dy	Ho	Er	Tm	Yb	Lu	Hf	Ta	Pb	Th	U	V/(V+Ni)	V/Ni	(Eu/Eu*)	(Ce*)	Sr/Rb
SD1	12.14	2.57	10.75	1.57	9.49	2.07	4.87	0.72	5.30	0.76	8.73	2.01	30.62	29.52	6.67	0.77	3.37	0.05	14.44	4.70
SD2	12.99	2.47	10.47	1.50	9.16	1.95	5.31	0.83	5.13	0.78	7.70	2.20	35.22	30.58	6.73	0.75	2.99	0.05	14.62	4.95
SD3	12.92	2.44	10.69	1.55	9.27	1.95	5.06	0.79	4.90	0.78	8.23	2.14	35.11	29.85	6.45	0.79	3.87	0.05	14.54	4.98
SD4	13.28	2.50	10.85	1.76	9.51	2.09	5.39	0.93	6.00	0.79	8.14	2.11	33.49	31.76	6.47	0.80	3.96	0.05	14.63	4.89
SD5	12.53	2.20	11.94	1.72	9.69	1.99	5.14	0.79	5.49	0.68	8.11	2.14	32.55	30.63	6.65	0.78	3.60	0.04	14.52	4.65
SD6	12.75	2.27	11.01	1.64	9.55	1.99	5.25	0.77	4.49	0.77	8.07	2.02	33.74	29.44	6.35	0.76	3.22	0.04	14.27	5.00
SD7	14.06	2.24	10.76	1.69	9.75	2.00	4.95	0.77	5.31	0.85	7.81	2.18	31.95	31.88	6.65	0.77	3.43	0.04	14.65	4.65
SD8	12.28	2.48	11.76	1.68	10.13	1.96	5.42	0.83	5.68	0.86	8.23	2.11	32.13	30.59	6.33	0.78	3.47	0.05	14.46	5.03
SD9	13.55	2.20	10.48	1.74	9.13	1.89	5.42	0.84	5.10	0.80	8.44	2.13	32.98	29.26	6.53	0.78	3.57	0.04	14.72	4.98
SD10	13.33	2.71	10.35	1.57	8.88	1.91	5.25	0.90	5.39	0.79	8.22	1.99	29.63	29.36	6.24	0.80	3.95	0.05	14.70	4.57

$Eu* = (Sm_{CN}*Gd_{CN})^{1/2}$ CN denotes chondrite-normalized value, $Ce* = (Ce_{CN})^{1/2}$

For both the Madzaringwe and Mikambeni shales, the distribution of the REE is characterised with the light rare earth elements (LREE) from Lanthanum (La) to Europium (Eu) and heavy rare earth elements (HREE) from Gadolinium (Ga) to Lutetium (Lu) (Table 4.3). All the studied sample showed low concentration below 50 ppm except La and Cerium, Ce which have average concentration of above 51.30 and 175.01 ppm respectively suggesting higher concentration of LREE. The sum of LREE is significantly enriched than HREE with the ratio of ΣLREE/ΣHREE value averaging at 11.24 ppm for the Mikambeni shale and 120 ppm for the Madzaringwe shale, showing similar concentration with the black shale of the Niuitang Formation bearing shale gas (Han et al., 2020). The plot of the chondrite normalised REE distribution pattern showed similar concentration of each element with depth of burial suggesting a syngenetic input rather than diagenetic (Figure 4.3). Diagenetic minerals exhibit heterogenous value or concentration as temperature and pressure increase with depth hence least susceptible to diagenesis. Some previous studies (Nagarajan et al., 2017, Kessler and Jong, 2017, Anaya-Gregorio et al., 2018, Jong and Kessler, 2019, Mclennan, 2018) have reported the relative insolubility and immobility of REE during hydrothermal alteration, weathering and low-grade metamorphism.
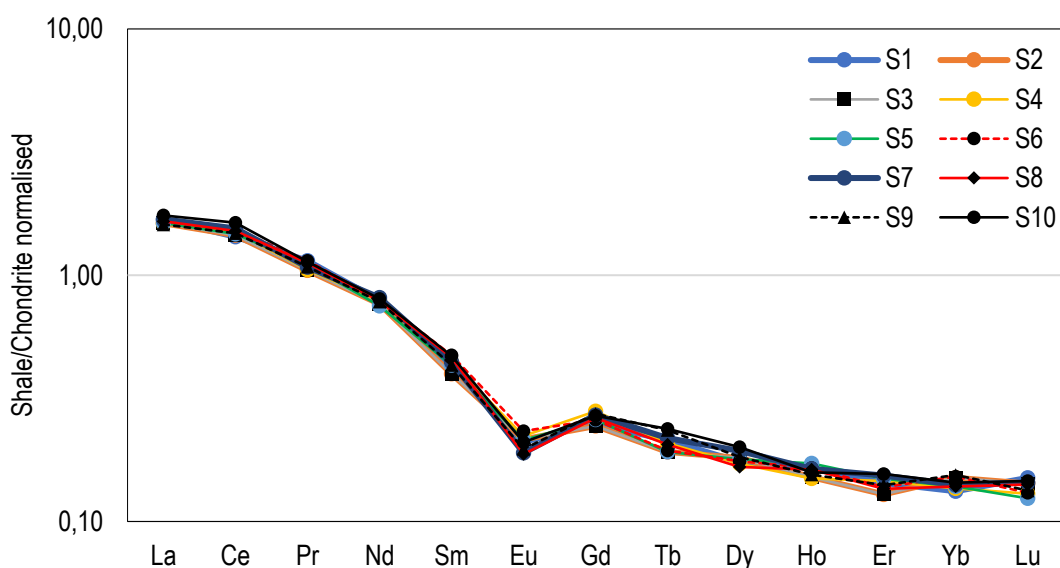
Figure 4.1: Chondrite-normalised REE pattern of the studied carbonaceous shale

The geochemical proxies ratio of Eu/Eu* has values between 0.04 and 0.69 ppm with an average of 0.65 ppm, showing that the Eu is enriched relative to other on chondrite-normalised diagram thus indicating a positive Eu-anomaly and favourable condition for organic matter maturity (Figure 4.3). The interpretation of the anoxic environment is consistent with V/(V+Ni) average value of 0.84 ppm which exceeds 0.54 limit for anoxic condition (Wu et al., 2016, Han et al., 2020). This result is comparable with V/(V+Ni) average value of 0.80 ppm for Niutitang

shale bearing gas (Wu et al., 2016). The positive anomalous concentration of Ce (115.79-132.09 ppm) and enrichment value of Ce* greater than 1 suggest terrigenous input in an anoxic condition (Anawar et al., 2010). In an anoxic condition, sulphate reduction may occur with increasing depth alongside with concomitant precipitation of FeS while Mo may concentrate as a separate phase of insoluble sulphide (Calvert and Pedersen, 1993, Rice and Claypool, 1981). This reduction reaction may have contributed to the presence of Mo with an average value of 3.03 ppm in the studied carboniferous shale samples.

4.4   Discussion

This section provides implications emanating from the mineralogical and geochemical results. The diagenetic alteration of the mineral components in the studied organic-rich shale are well discussed. Furthermore, the geochemical parameters provide elemental proxies from which the paleo-depositional environment and paleo-production of organic materials are discussed.

4.4.1 Diagenetic pathway

With an increase in burial depth resulting from successive overlying sediments of the Solitude, Klopperfontein, Bosbokpoort, and Clarens Formations, the elevated temperature in the studied samples causes further geochemical and mineralogical diagenetic alteration. The gradual decrease in montmorillonite and a parallel progressive increase of illite minerals were observed, while mixed-layered montmorillonite-illite (M-I) mark the extent of progress along with series of reactions between burial depths of about 370 m to 480 m. In Mikambeni shale, the first series of the illitization reaction progress is made possible due to the presence of microcline and montmorillonite minerals as expressed in Equation [7] (Essene and Peacor, 1995). Alternatively, diagenetic illite may have crystallized from geochemical interaction between kaolinite and microcline or potassium ion (K^+), but the absence of kaolinite inhibits that reaction's progress pathway. Retrospective studies (Baiyegunhi et al., 2017, Yuan et al., 2019a) have reported the kaolinite illitization via reactions with k-feldspar, K^+, or H^+ as burial depth increases. However, this reaction mechanism is hindered due to the absence of kaolinite minerals in the studied shale. Kaolinites may have precipitated due to increasing quartz concentrations, but it is likely to be consumed immediately after crystallization as expressed in Equation [8] due to high temperature. Studies (Curtis, 1985, Thyberg and Jahren, 2011, Metwally and Chesnokov, 2012) have unequivocally demonstrated that the kaolinite dissolution in shale rock can take place at a lower temperature than 60°C.

$$Al_2Si_4O_{10}[OH]_2 \cdot nH_2O + KAlSi_3O_8 \rightarrow KAl_3Si_3[OH]_2 + SiO_2 + nH_2O \qquad [7]$$

$$Al^{3+} + SiO_2 + 2.5H_2O \rightarrow 0.5Al_2Si_2O_5(OH)_4 \,(\text{kaolinite}) + 3H^+ \qquad [8]$$
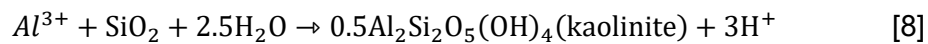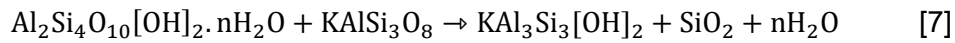
Furthermore, the organic and inorganic interaction promotes the illitization by initiating the release of the H^+ ion from the carboxylic acid functional group as expressed in Equation [9].

$$CH_2O \,(\text{carboxylic group}) + H_2O \rightarrow CO_2 + 4H^+ \qquad [9]$$
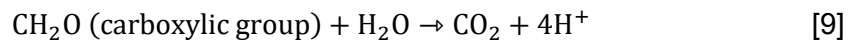
The presence of a carboxyl group increases solubility properties. As such, the labile microcline mineral interacts with the pore water concentrated with carboxylic and phenolic acids to produce silica and potassium cation, which enhances illitization of montmorillonite mineral as represented in Equation [10]. This resulting authigenic silica likely contributes to the increasing quartz content with burial diagenesis, although the presence of preserved detrital quartz inputs cannot be discounted. With the siltstone facies interbedded with the carbonaceous shale, the input of detrital silica is possible since quartz is largely stable at high temperatures. Nonetheless, the increasing quartz contents tend to significantly improve the shale reservoir quality because it imparts a brittleness property and enhances the fracability of shale (Ye et al., 2020).

$$KAlSi_3O_8 \,(\text{microcline}) + H^+ \rightarrow {}^{1}\!/_{2}\,SiO_2 + K^+ \qquad [10]$$
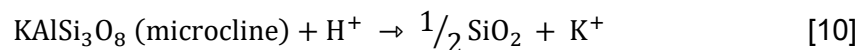
As the reaction continues, more K^+ ions are concentrated via replacement K-feldspar (microcline) by the albite at a higher temperature between 120°C and 180°C as represented in Equation [11] (Curtis, 1985, Bjørlykke and Jahren, 2012). The absence of kaolinite minerals with a parallel increase in chlorite suggests complete dissolution of kaolinite at such a high temperature.

$$KAlSi_3O_8 \,(\text{microcline}) + Na^+ \rightarrow NaAlSi_3O_8 \,(\text{Albite}) + K^+ \qquad [11]$$

With further burial diagenesis, the presence of a high concentration of potassium K^+ fluid promotes the illitization processes of montmorillonite minerals. However, other factors such as time, fluid/rock ratio, nature of starting material, and kinetic mechanism have been considered as important for illitization. It is worth noting that the direct conversion of smectite to illite as expressed in Equation [12] (Huang et al., 1993) does not suggest a solid-state reaction but rather shows the quantitative and compositional changes in shale mineralogy that takes place during burial diagenesis. Importantly, this conversion of smectite to illite reaction has been indicated to take place at similar temperature intervals as the maturation index for organic matter and the release of interstitial water during I-M diagenesis to enhance

hydrocarbon migration (Lynch et al., 1997). By implication, the range for the change in I/S ordering from random to regular during smectite illitization in shales coincides with the temperature range of organic matter maturity and the onset of oil generation in young sedimentary basins.

$$2Na_{0.4}(Al_{1.47} Mg_{0.29}Fe_{0.18})Si_4O_{10}(OH)_2(Smectite) + 0.85K^+ + 1.07H^+$$
$$\rightarrow 1.065K_{0.80} (Al_{1.98}Mg_{0.02})(Si_{3.22}Al_{0.78})O_{10}(OH)_2(illite) \quad [12]$$
$$+ 4.6SiO_2 + 0.36Fe(OH)_3 + 0.56Mg^{2+} + 0.8Na^+ + 0.9H_2O$$
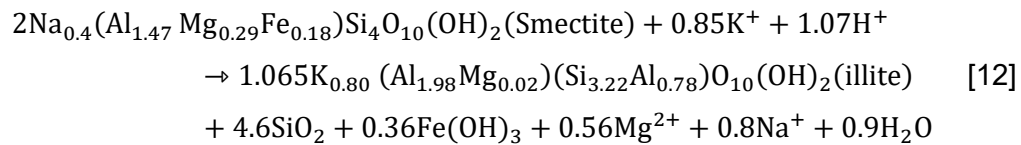
Although present in low quantities, chlorite mineral is increasingly crystallized as a discrete phase rather than evolutionary trend phases of kaolinite and carbonate. The evolutionary phase involves the chloritization phase of kaolinite in the presence of iron- and magnesium-supplied smectite illitization processes at a temperature between 165 and 200°C (Boles and Franks, 1979), but reaction progress is inhibited due to the absence of kaolinite. At a lower temperature of about 120°C and in the presence of carbonate minerals, another chloritization reaction via kaolinite and iron oxide could occur (Muffler and White, 1969, Dowey and Taylor, 2020). The possible explanation for hydrothermal chloritization cannot be discounted in the studied carbonaceous shale owing to the presence of Sagole thermal spring via the Tshipise fault (Johnson et al., 2006b, Olivier et al., 2011). This interpretation is consistent with the chloritization processes reported at the geothermal area of Iceland in which iron-rich smectite (saponite) is transformed into mixed-layer smectite-chlorite (S-C) at about 200 to 230°C (Beaufort et al., 2015). In support of the S-C mixed layer, corrensite is a resulting mineral composed of 50% of each chlorite and smectite mineral (Huggett, 2015). With a further increase in temperature due to burial depth, chlorite crystallizes at temperatures greater than 240°C due to a gradual replacement of iron-rich smectite with daughter chlorite mineral in close zonation contact (Yeblen, 2018). This reaction mechanism suggests a solid-state gradual replacement; however, the reaction pathway may be a continuous series transition instead of a stepwise progression since shale has a low pore fluid to rock ratio due to poor interconnectivity of pores. Stepwise transition is noted to predominate in the system with high pore-fluid-to-rock ratio such as sandstone; hence, chloritization in the studied shale may be a by-product of smectite illitization. Although the rise in temperature of diagenetic chlorite could be promoted by contact diagenesis associated with the Sagole geothermal area, the pore fluid of studied shale is unaffected by the thermal spring due to extremely highly impermeable shale. Carbonate minerals commonly revert to the thermodynamically stable mineral as dolomite replaces limestones in the deep-burial diagenetic realm (Swart, 2015). Calcite dissolution increases with burial dolomitization in the presence of an organic-rich and interstitial fluid via stepwise precipitation of dolomite as expressed in equation [13].

$$CaCO_3 + Fe^{2+} + Mg^{2+} \rightarrow 2CaMg(CO_3)_2 + 2Ca^{2+} \qquad [13]$$
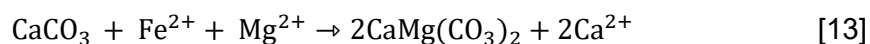
The disappearance of calcite at relatively greater burial depths suggests a low pH medium, while its replacement by dolomite indicates an alkaline setting corresponding to oil window and organic matter maturation at a temperate range of 80–120°C (Montañez, 1994, Machel, 2005, Montañez and Crossey, 2017). Promoted by sulphate reduction of pyrite mineral resulting from microbial activities, an increase in alkalinity medium favours precipitation of dolomite in the presence of Ca and Mg as burial depth increases (Morad, 2009).

4.4.2 Paleo-redox condition of the depositional environment

Elemental proxies of trace elements have proven to be veritable tool to decipher and discriminate paleo environment under which sedimentary deposits were formed owing to their geochemical resilience to weathering, diagenesis and sensitivity to redox reaction. Vanadium and Nickel exhibit similar geochemical behaviour and are considered to be highly stable organo-philic and sulphur-forming elements(Ferriday and Montenari, 2016, Pieta et al., 2019). The elemental ratio of V/(V+Ni) with value greater than 0.5 has been interpreted to represent a reducing environment, while less than 0.5 as an oxidizing environment (Hatch and Leventhal, 1992, Tanwar and Mandal, 2019).

Under this oxic condition, elements such as V, Ni, Fe, Mn, Mo and sulphate are normally present in soluble species in the form of V^{5+}, Ni^{2+}, Fe^{3+}, Mn^{4+}, Mo^{6+} and SO_4^{6+} respectively in water column while the aerobic degradation of organic matter continued until the dissolved oxygen is less than 0.2 ml/L H_2O (Tyson, 2012). Deficiency of oxygen has adduced to climate, sea level changes, tectonic activities and hydrographic factors, resulting to insufficient supply of oxygen to oxidized the organic materials(Dean and Arthur, 1989, Dar et al., 2017). Below this oxygen concentration, anaerobic condition and degradation of organic matter begins as well as reduction of the oxidizing elements to insoluble species of V^{4+}, Ni, Fe^{2+}, Mn^{2+}, thiomolybdate oxyanion(MoO_4^{2-}) and SO_4^{2+} which eventually concentrate in shale sediments (Ferriday and Montenari, 2016).

The anoxic setting is established as all the oxidants in the shale sediments deplete due to further reduction processes relating to burial depth thus promoting the activities of sulphide-reducing bacteria (Capotondi et al., 2016). Studies (Gallagher et al., 2015, Sabino et al., 2020, Natalicchio et al., 2019, Reolid et al., 2019) have highlighted some compounds such as hydrogen sulphide, zinc sulphide, iron sulphide as evidences of reduction process ensued from sulphide-driven bacteria. With further increase in burial depth below the sediment-water interface, the methanogens begin to degrade the organic matter to generate biogenic methane. This is consistent with previous work of Tourtelot (1979) which argued that methane

is unlikely to formed unless all sulphates are depleted while vanadium and nickel being concentrated (Abanda and Hannigan, 2006, Algeo and Maynard, 2004, März et al., 2008, Pi et al., 2013, Ferriday and Montenari, 2016).

4.4.3 Hydrothermal activity and paleo-productivity

Studies (Charriau et al., 2011, Lipinski et al., 2003) have indicated that high amounts of Zn in shale rocks may be related to syn or post-depositional hydrothermal overprint while elements such as Ni, Co and Cu have also been used to indicate hydrothermal overprint in shale formation during the initial stage of deposition (Hatch and Leventhal, 1992, Zhang et al., 2020b, Yin et al., 2020). In a recent work, Yin et al. (2020) used the diagram of Zn-Ni-Co to determine the influence of hydrothermal activities on hydrocarbon source. The average concentrations of elements Zn, Ni, Co and Cu for the Madzaringwe shale are relatively higher than the Mikambeni shales, suggesting heating at depth and re-emergence at upper sedimentation. This slight hydrothermal influence might have emanated from the geothermal spring having temperature ranging from $40^{\circ}C – 100^{\circ}C$ (AE and Olivier, 2010). In Figure 4.4, the plot of the thermometry elements of Zn, Ni and Co shows an influence of heat from hydrothermal overprint. It is unlikely that the hydrothermal fluid could have permeated since shale has an extremely low permeability and porosity (Ren et al., 2016) but heat can be transferred by convection (Raffensperger and Vlassopoulos, 1999).
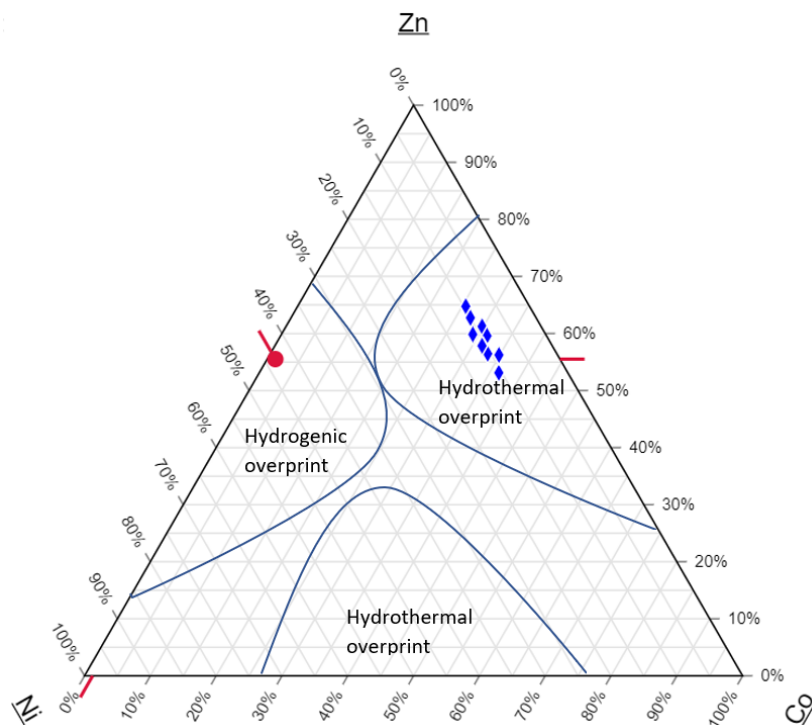
Figure 4.1: Zn-Ni-Co hydrothermal diagram of the represented studied shale samples

The use of Ba as paleo-productivity indicator in sediments exposed to hydrothermal overprint seems unviable due to their susceptibility to alteration (Ferriday and Montenari, 2016). However, the Ba concentration of the studied shales is relatively high, suggesting a non-marine environment since it exceed 400ppm threshold for marine environment in the Madzaringwe shale (Zhao et al., 2016, Wen et al., 2008). Implicitly, high detrital influx with low marine paleo-productivity characterises the studied shale and this interpretation is consistent with the previous study (Chidley, 1985) suggesting accumulation of land-derived plant material. To further corroborate the paleo-productivity condition, the ratio of Sr/Rb elemental proxy in shale is mostly considered as veritable tool to interpret paleo-environmental conditions due to their higher anionic radii and charges (Zuo et al., 2020). Following the Sr/Rb proxy, the studied shale samples indicate a significant amount of organic matter production from brackish water rather than marine since brackish-water represents value greater than 0.6 while marine water are less than 0.6 (Zuo et al., 2020).

4.5   Summary of the Chapter

This chapter reveals that the studied carbonaceous shale samples are composed of quartz, albite, microcline, dolomite, pyrite and clay minerals. The clay mineral component consists of montmorillonite, illite, chlorite, and mixed layered illite/smectite (I/S) in the Mikambeni samples. However, the mixed layered illite/smectite is absent in the Madazringwe samples due to a solid-state gradual diagenetic replacement alteration. Significantly, the alteration of smectite to illite reaction has been interpreted to take place at similar temperature intervals, 190–220°C, as the maturation index for organic matter and the release of interstitial water during I-M diagenesis to enhance gaseous fluid migration. As such, the range for the change in I/S ordering from random to regular during smectite illitization in shales coincides with the temperature range of organic matter maturity and the onset of gaseous hydrocarbon generation in studied formations. The presence of diagenetic chlorite mineral is characteristic of low-grade metamorphism or high diagenetic zone at a temperature around 200–230°C and may correspond to thermal breakdown of kerogen to gas generation.

The increasing quartz mineral tend to significantly improve the shale reservoir quality because it imparts a brittleness property and enhances the fracability of shale during gas exploitation. The quartz is unexpected to dissolute due to its high stability and resistance to diagenetic alteration so its lower concentration reflects a low detrital terrigenous input during sedimentation processes. In contrast to the Mikambeni shale, the Madzaringwe shale has lower quartz, plagioclase, and microcline contents due to the diagenetic dissolution of plagioclase and microcline as depth increases. The pyrite mineral was developed from the availability of hydrogen sulphide that emanates from sulphate-reducing bacteria degrading the

organic-rich shale. The presence of the pyrite mineral precursor a methanogenesis zone for gas generation.

The geochemical compositional trend of most major elements is similar in both Madzaringwe and Mikambeni shales except for the slightly higher alumina value. The presence of the higher alumina content suggests increasing diagenetic clayey production formation. The major elemental components of the in both studied shales include calcium oxide, iron oxide, potassium oxide, magnesia, sodium oxide, phosphorus oxide, silica, and titanium oxide. In contrast to other elements, silica and alumina showed a relatively higher values which averages at 50.17% and 20.02% respectively suggesting a felsic provenance

Based on the geochemical proxies, the reduction process results from microbial activities in an anoxic depositional environment and causes an increase in alkalinity medium that favours precipitation of dolomite in the presence of Ca and Mg as burial depth increases. The elemental ratio K_2O/Al_2O_3 of the studied samples showed values ≤ 0.5 which suggest a highly mature shale since significant amount of Al_2O_3 is typical of immature sediments. Furthermore, the combination of elements such as Ba, Zn, Pb and Cu with abundance of organic matter in shale source rock has a paleo-productivity having a geothermal overprint.

CHAPTER FIVE

STABLE ISOTOPIC, FUNCTIONAL-GROUP AND PORE STRUCTURE CHARACTERISTICS OF CARBONACEOUS SHALE ROCKS

Determining the source rock reservoir quality requires knowledge of the paleo-depositional environment, functional group, and pore types distribution of an organic-rich shale. While the pore type distributions regulate the critical parameters required for source rock development, the information from the paleo-depositional environment and functional group of an organic-rich shale influences the storage site quality to host the expelled gaseous molecules. Depending on the prevailing geological condition and paleo-climatic overprints, sedimentation of an organic-rich shale might occur in a marine, terrestrial, or transitional environment. Under favorable geologic and thermal conditions, organic matter from each depositional environment has various compositions, resulting in different source rock types. Simultaneously, the functional group of organic matter varies depending on the depositional environment. The produced hydrocarbon is contained and stored in the same shale rock when organ matter interacts with it. Because of varied structural deformation and diagenetic conditions in distinct depositional environments, the pore architectures of the source-rock reservoir are heterogeneous. Using carbon and oxygen stable isotopic fractionation, Fourier Transform Infrared Spectrometry (FTIR), and Scanning Electron Microscopy-Energy Dispersive Spectrometry, this chapter characterises the organic-rich shale of the Madzaringwe and Mikambeni Formations of the Tuli Basin to understand their paleo-depositional environment, functional-group, and reservoir pore distribution (SEM-EDX).

5.1 Background to the Study

Stable isotopic measurements have demonstrated that interactions among elements of carbon, oxygen and rocks are significant indicator of paleo-depositional environment for organic-rich shale rock. The organic materials that form kerogen prone to unconventional hydrocarbon have heterogeneous sources, depending primarily on the paleo-depositional environment. Based on a biomarker and petrographic study (Qiao et al., 2021), an organic matter composed of terrigenous conifers plants and lacustrine algal has been reported to produce a Type II-III kerogen prone to oil and gas generation. Instead of shale gas, shale oil emanates from a marine–derived organic matter such as planktonic foraminifera assemblage, structureless (amorphous) and alginite (Hakimi et al., 2016). These organic materials are typical of a marine paleo-depositional environment, producing kerogen Type I-II prone to oil

generation (Hakimi et al., 2016). Unlike the marine paleoenvironment, the fluvio-deltaic settings receive organic material composed of a higher plant with well-developed vascular components due to proximity to the land which are prone to generate Type -III kerogen. Nonetheless, the composition of detrital materials varies in spatial and temporal distributions. Several studies (Cui et al., 2019, Gonzalez et al., 2020) have been conducted on the depositional environment of organic matter for shale gas, information on the Tuli Basin remains elusive.

Organic substances produce characteristic stretching and bending of frequencies between 400 and 4000 cm^{-1}, showing their origin and evolution in terms of the functional group (Zviagina et al., 2004). Hydrocarbons' C-H stretching vibrations have infrared absorption peaks between 2800 and 3300 cm^{-1} wavelength regions, while aromatic compounds have absorption peaks between 680 and 900 cm^{-1} wavelength regions. The FTIR data has shown to be an invaluable tool in the screening of aliphatic organic material, revealing geochemical characteristics such as volatile hydrocarbon, residual hydrocarbon generative potential, aliphatic organic materials, hydrogen index, and total organic carbon (Washburn &Birdwell, 2013). As it absorbs radiation, the FTIR provides information on the functional groups present in the organic molecule, which helps to constrain the origin of organic materials (Baker et al., 2014b). The functional group, in combination with the isotopic composition of organic matter and SEM-EDX, provides an integrated strategy to investigating the provenance of organic matter influx and paleo-depositional settings.

Unconventional shale reservoirs provide a larger emphasis on the creation of organic-matter pore features than typical reservoirs, which rely on framework grains (Löhr et al., 2015). Organic-matter pores are preferred not just because they produce hydrocarbons, but also because they store them. Due to the fine-grained fabric of shale rock, intergranular or intragranular pores between terrigenous clasts are rare or non-existent (Hastings, 2018). Organic-matter pores, inter-grain holes of groundmass minerals, diagenetic fractures, and micro-fractures are all common pores found in shale reservoirs. As a result, determining the pore type of shale is a crucial aspect of determining the quality of an unconventional reservoir.

5.2 Purpose of the study

This chapter aims to determine the pore storage system of the studied carbonaceous shale samples for reservoir quality assessment. To achieve the aim, specific objectives include:

- To examine the paleo-depositional environment of the Mikambeni and Madzaringwe Shale Formations.

- To identify the functional group of methane gas in the studied formations.
- To characterise the pore storage system of the studied formations, hosting the potential generated gas.

5.3   Results and Interpretations

This section presents the results and interpretations of the carbon and oxygen isotopic compositions, functional group, and porosity types of the studied Mikambeni and Madzaringwe Formations.

5.3.1 Carbon and oxygen isotopic compositions of organic-rich shale

The carbon and oxygen isotopic compositions of organic materials associated with the carbonaceous shale samples of the Tuli Basin were presented in Table 5.1. The carbon isotopic composition, $\delta^{13}C$, of the organic-rich shales of the Mikambeni and Madzaringwe Formations ranged from -20.01 to -24.4‰, averaging at -23.1‰ and -21.01 to -24.0‰, averaging at -22.4‰ respectively. It implies that most carbon isotopic signatures of studies samples reflect provenance from terrigenous plants material since it exceeds -22‰ value. However, isotopic fractions found with -20‰ values indicate some influx of organic materials from marine settings.

Table 5.1: Isotopic fractions of $\delta^{13}C$ and $\delta^{18}O$ / $\delta^{16}O$

Formation	Mikambeni									
Samples	SK1	SK2	SK3	SK4	SK5	SK6	SK7	SK8	SK9	SK10
$\delta^{13}C$ (‰)	-24.0	-24.4	-23.1	-23.1	-23.4	-23.4	-22.1	-20.01	-20.5	-20.8
$\delta^{18}O$ (‰)	14.5	14.1	15.1	15.4	16.2	16.5	16.1	16.5	18.3	18.8
$\delta^{16}O$ (‰)	2.82	2.80	3.02	3.08	3.24	3.30	3.22	3.30	3.66	3.76
Formation	Madzaringwe									
Samples	SD1	SD2	SD3	SD4	SD5	SD6	SD7	SD8	SD9	SD10
$\delta^{13}C$ (‰)	-22.4	-22.08	-22.04	-23.1	-24.0	-22.5	-23.02	-22.01	-21.15	-21.06
$\delta^{18}O$ (‰)	9.80	9.45	9.82	9.96	9.75	9.94	9.89	9.87	9.76	9.95
$\delta^{16}O$ (‰)	1.96	1.89	1.96	1.99	1.95	1.98	1.97	1.974	1.95	1.99

This is consistent with the $\delta^{13}C$ values of Whitehill Formation of the MKB found with mixed marine and terrigenous organic carbon material (De Kock, et al., 2017) . This isotopic discrimination indicates higher land plants with vascular tissues to range from -22.4 to -23.1‰ contrary to marine plants such as algae which have a lower isotopic signature -13 to -20‰. The interpretation of terrigenous plant source is consistent with isotopic fractions for carbonaceous Barakar Formation in India, ranging from -23 to -25‰ (Singh et al., 2012).

In contrast, marine plants such phytoplankton contribute carbon enrichment in a typical euxinic depositional environment found with an average $\delta^{13}C$ value around -30‰ (Whiticar, 1996). Notably, the positive excursion of organic carbon isotopes $\delta^{13}C$ suggests a local anoxia deposited around 280 Ma Permian period instead of the large-magnitude negative carbon isotope excursion close to the Ediacaran-Cambrian period (Schröder and Grotzinger, 2007). During this period, a prolonged high burial rate of organic material led to $\delta^{13}C$ enrichment in surface water globally, resulting to isotopically light CO_2 in basins (Schröder and Grotzinger, 2007).
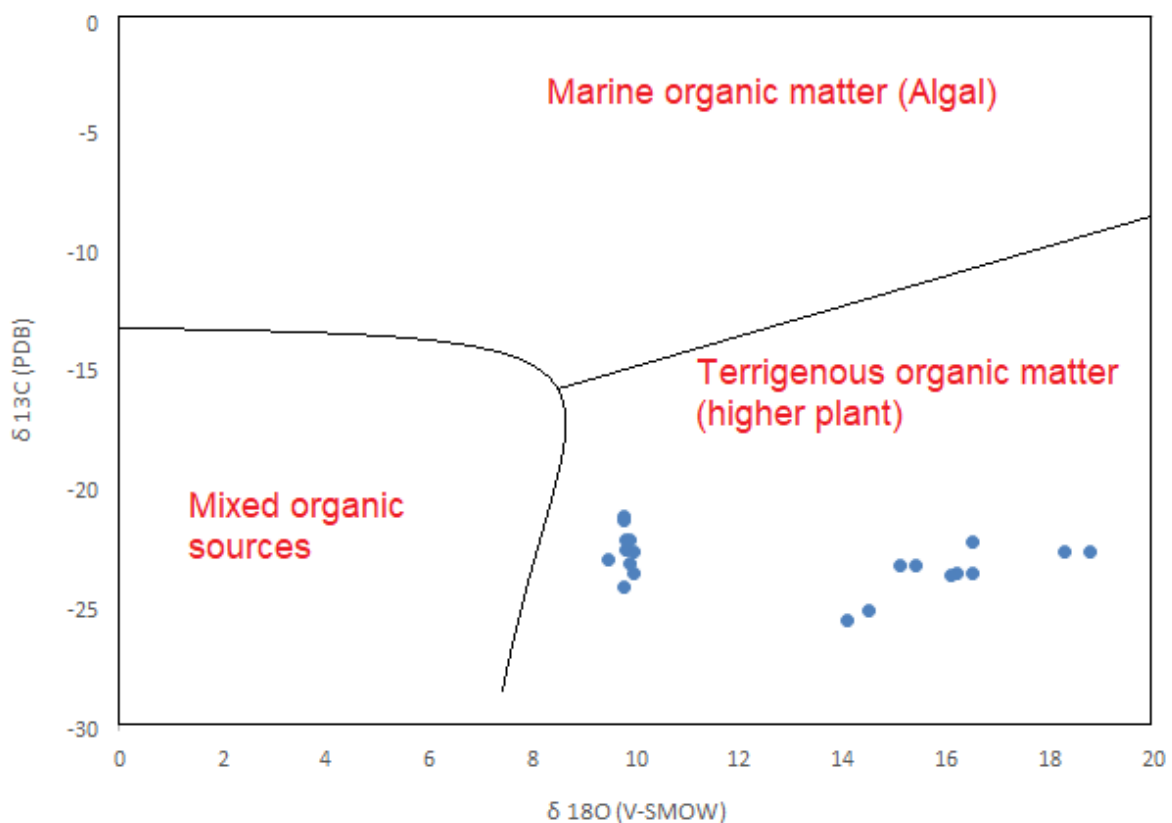
Figure 5.1: Cross-plot of $\delta^{16}O$ vs. $\delta^{13}C$ values for the studied organic-rich shale

At the same time, isotopic fractions $\delta^{18}O$ and $\delta^{16}O$ show a narrow variation in each studied formation, decreasing from Mikambeni to the underlying Madzaringwe Formation. For the $\delta^{18}O$ fractions, it ranges from 14.1 to 18.8 ‰ in the Mikambeni shale and 9.45 to 9.96 ‰ in the Madzaringwe. The plausible explanation for progressive downward decrease in the $\delta^{18}O$ and $\delta^{16}O$ values can be attributed to mineral-water interactions in a closed chemical microsystem of shale caused by thermal alteration as burial depth increases. The explanation is consistent with the negative correlation of $\delta^{18}O$ with loss of ignition of organic matter content (Faure et al., 1995). In Figure 5.2, the plots of $\delta^{18}O$ and $\delta^{16}O$ indicates a mixing of the hydrothermal and meteoric water during the deposition of studied formations (Wang and Guo, 2020). In both

formations, the isotopic signals indicate an oxygen-poor fluvial environment with a threshold $\delta^{18}O$ value less than 20 ‰ and it is also consistent with the previous study of Wang and Guo (2020). As such, the heavy oxygen isotopic composition $\delta^{18}O$ of the Mikambeni and Madzaringwe shales showed depleted values, ranging from 9.45 to 18.8‰, suggesting an anoxic condition. The $\delta^{18}O$ concentrations indicated that the organic matters were acted upon by the microbial activities in a brackish water environment from organic water. The progression of $\delta^{18}O$ concentration with depth suggest depletion of oxygen from oxic condition to anoxic condition (Gong and Hollander, 1997, Freixa et al., 2016).
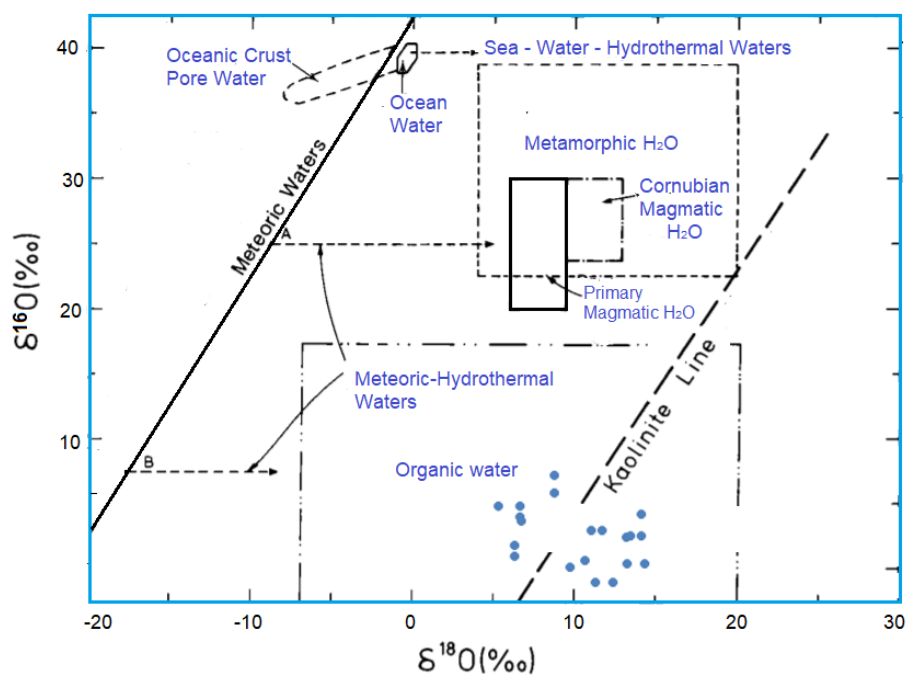
Figure 5.1: Plot of $\delta^{18}O$ vs $\delta^{16}O$ showing origin water types in organic-rich shales

The progression of $\delta^{16}O$ concentration suggest depletion of oxygen from oxic condition to anoxic condition in the Mikambeni sample. It implies a migration of sediment from marine or oxygen-rich environment to terrigenous or oxygen-poor environment. In both Madzaringwe and Mikambeni Formations, the heavy oxygen $\delta^{18}O$ isotopic signals indicate an oxygen-poor fluvial environment with a threshold $\delta^{18}O$ value less than 20 ‰. The $\delta^{18}O$ isotopic fraction indicated a brackish water environment composed of organic matter acted upon by the microbial activities for methanogenesis. The enrichment process of isotope fractionation shows that lighter $\delta^{16}O$ evaporates more easily. The heavier $\delta^{18}O$ is easier to condense out.

5.3.2 Functional group characterisation

The Fourier Transform Infrared (FTIR) spectra of the studied carbonaceous shale depict different absorbance bands of organic and mineral content at various diagnostic wavelengths of infrared spectrum (Figure 5.3).
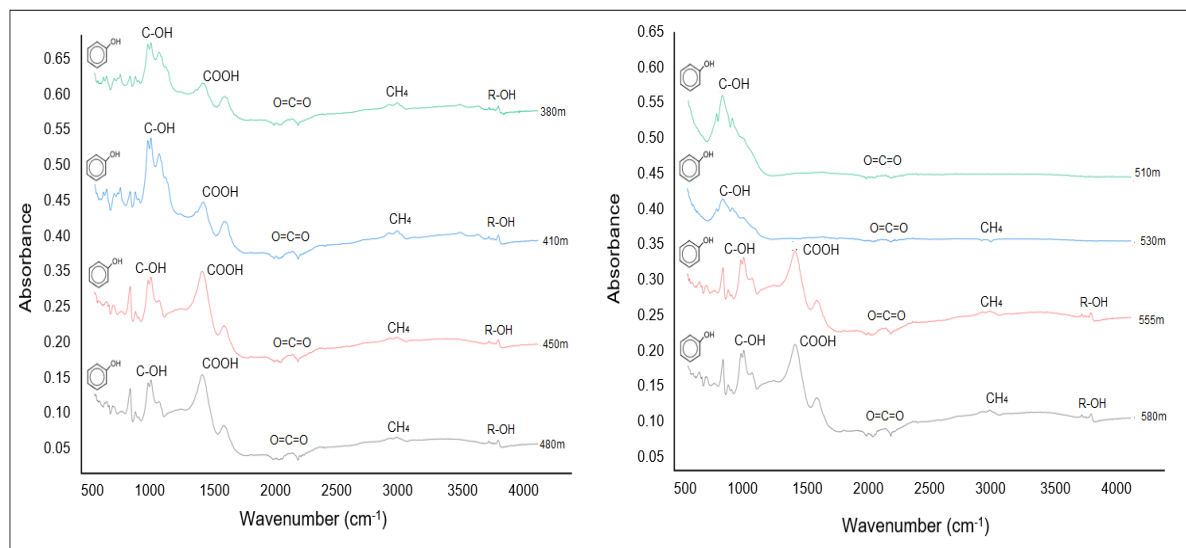
Figure 5.1: FTIR spectra showing functional groups corresponding to organic molecules

Hydrocarbons show infrared absorption peaks between 2800 and 3300 cm^{-1} due to C-H stretching vibrations. The sp^2 C-H hybridization found with absorption peak between 3000 - 3100 cm^{-1} indicates the gaseous hydrocarbon. Some studies (Baker et al., 2014b, Günzler and Gremlich, 2002) reported the gaseous hydrocarbon of CH_4, having infrared absorbance peaks between 2850 and 3000 cm^{-1} due to aliphatic C-H stretching of methyl and methylene vibration while the low absorption peak around 3500 cm^{-1} corresponds to water desorption wavelength (Coenen et al., 2018). Each absorbance band indicates the functional group representing the whole molecular structure of a material (Washburn and Birdwell, 2013). Most of the studied samples exhibit a strong characteristic absorbance peak around 650 and 900 cm^{-1} corresponding to the aromatic phenolic group, C=C-OH, however, the peak reduces as temperature increase depth due to bond deformation(Günzler and Gremlich, 2002). The aromatic C=C absorption suggests the wavelength band of detrital plant lignin-derivative materials, unlike the amide band which is prevalent for marine-derivative materials (Naseem et al., 2016). The peak stretching from around 1000 to 1220 cm^{-1} indicates the C-O stretching and OH deformation of the carboxylic, COOH groups are exhibited samples suggesting decarboxylation of organic matter (Dutta et al., 2013). The deformation of the carboxylic group releases the CO_2 which is recognised from its characteristic strong absorptions around 2000

to 2300 cm^{-1} (Washburn and Birdwell, 2013). However, aliphatic hydrocarbon has been considered to contain more carboxylic- and phenolic-OH functional groups with a micelle-like structure having a relative macromolecular weight ranging from 3,500 to 100,000Da compared with aromatic hydrocarbon(Hillel and Hatfield, 2005). In aromatic hydrocarbon, the voids among the carbon chain serve to act as trapping and binding sites for organic lipids and inorganic materials such as hydrous oxides and clay minerals(Hillel and Hatfield, 2005). At greater burial depths around 485m and 580m, the spectra showed inconspicuous peaks of carboxylic group suggesting over the maturation of organic matter beyond methanogenesis window to coalification.

5.3.3 Porosity-types characterisation

The representative SEM-EDX images of the studied carbonaceous shales depict a combination of organic-matter, groundmass mineral, micro-fracture pore structures reflecting polyframboidal pyrite and carbonate dissolution morphologies (Figure 5.4a-f). The images revealed conspicuous intragranular pores within and between the organic matter and matrix of quartz, feldspars, chlorite, illite, carbonate and pyrite minerals as shown by the XRD and EDX.

As revealed in Figure 5.4a, the bubble-like pore structures located within organic matter as organic-matter pores reflect both gaseous hydrocarbon generation source and storage reservoir. It indicates intra-pores occurring in hollow-fossils and phytoclasts macerals. The nanopore size (100 nm) of the organic-matter pore results from diagenetic alteration due to deep burial upon thermal maturity. The EDX elemental composition of the studied samples showed a significant amount of carbon 69.8%, indicating carbon-rich organic matter in form of carbonaceous compound. The elemental content of carbon dominates the studied Madzaringwe and Mikambeni shale, ranging from 65 to 73%. Similar bubble-like structures with aperture ranging from 10 to 300nm have been reported in organic matters of Barnett shale in the US reputed for shale gas generation (Yang et al., 2019).
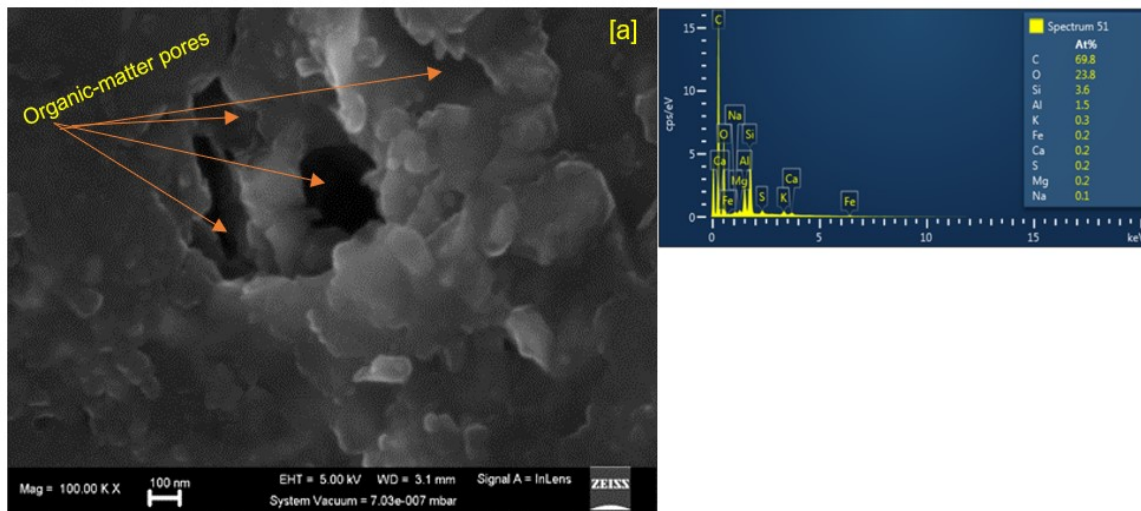
Figure 5.1: (a) SEM-EDX image showing the bubble-like pores of an organic-matter porosity type.

The interstitial organic-matter pores depicted in Figure 5.4b reflect a sheet-like inter-pores between the phytoclast grains. The EDX results show carbon–rich composition above 70% in form of carbonaceous grains. The interparticle pores between carbonaceous grains were occupied by amorphous organic matter. Carbonaceous grains consist of scattered nano-fossils debris that forms supportive framework in organic macerals and tends to form triangular interstitial pores when multiple carbonaceous grains agglomerate.
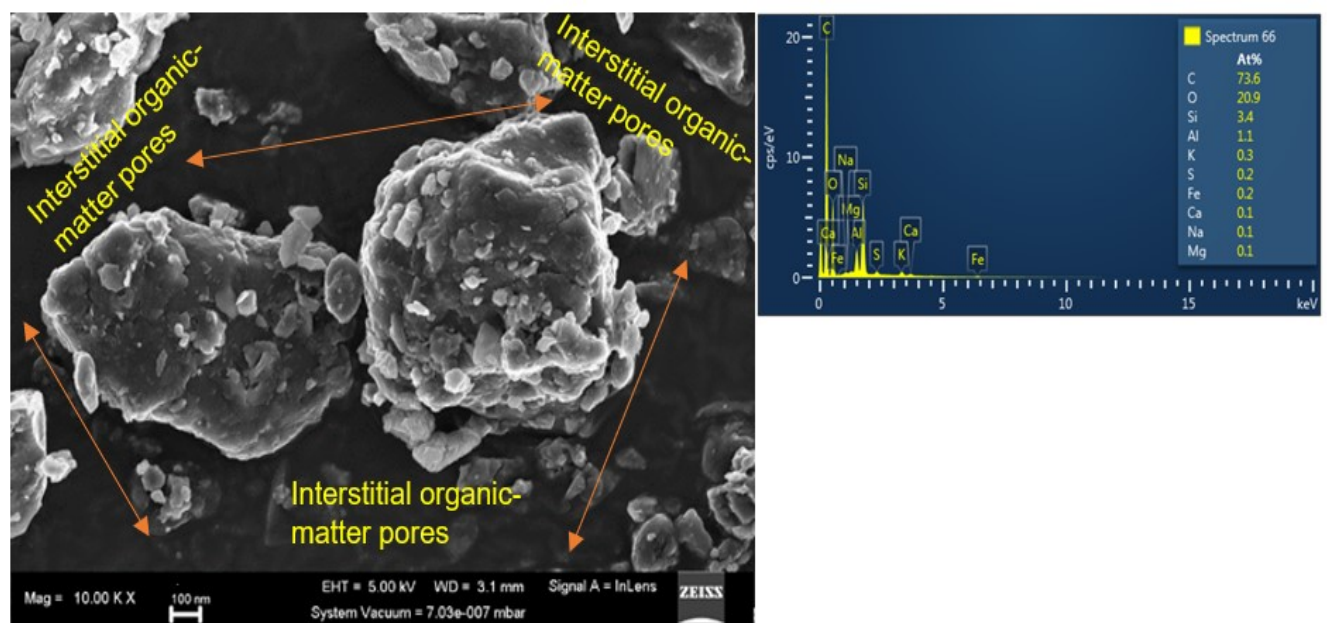
Figure 5.4 (b)SEM-EDX image showing the sheet-like inter-pores of interstitial organic matter porosity type

The groundmass or matrix pores as shown in Figure 5.4c display an irregular-isolated structure between the carbonaceous phytoclast macerals and mineral grains of the studied samples. Based on the XRD data, the groundmass consists of the clay minerals such as illite and chlorite, authigenic quartz and feldspars with a grain and pore size less than 3.2mm and 1μm respectively. The mesopore sizes of are relatively small, range from 20 to 50 nm. The interactive phytoclast macerals grow interactively with the groundmass minerals of clay and siliceous grains. Such morphology indicates a product of recrystallisation and thermal evolution between the groundmass minerals and phytoclast macerals during diagenetic alteration (Yang et al., 2019).

The micro-fracture pores shown in Figure 5.4d displayed a preferred-oriented linear structure suggesting a preponderance of brittle minerals such as quartz under an applied pressure. The pressure might have emanated from tectonic-volcanic structural relations for the development of the Tuli basin. The sedimentation occurred in a separate fault-controlled basin of a comparatively stable miogeosynclinal depression with the intense Karoo volcanic eruption between 200 and 175 Ma ago (Tankard et al., 2012). On the other hand, micro-fracture resulting from diagenetic effect due to increase in temperature and pressure with burial depth tends to contribute to micro-fracture development. Furthermore, the micro-fracture pore structures suggest the easy of fracability of the reservoir at recovery stage indicating a good reservoir storage site.
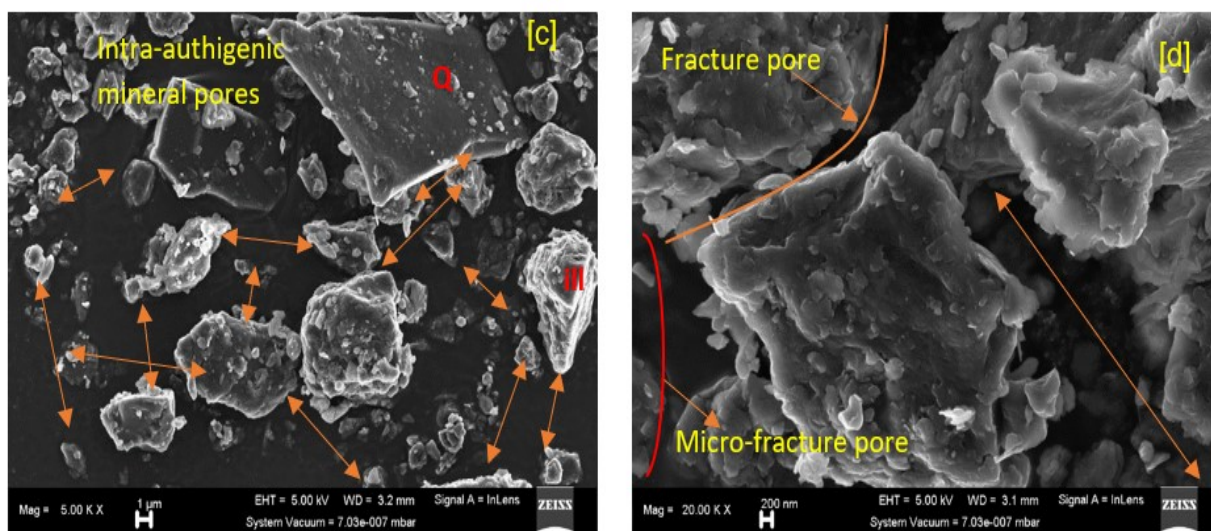
Figure 5.4:(c) SEM-EDX image showing the an irregular-isolated structure of groundmass or matrix porosity type (d) preferred-oriented linear structure of micro-fracture porosity

Non-spherical closely packed polyframboidal pyrite (Figure 5.4e) were observed which is affirmed by the multiple occurrence of Fe-elemental contents on the EDX result. The presence

of the polyframboidal pyrites suggest anaerobic condition which favours organic matter degradation and thermal maturation as burial depth increases (Cruz-Ceballos et al., 2020). Thermal maturity of the organic matter is further supported by the presence of fibrous chlorite and illite minerals (Figure 5.4f) which are index mineral for high diagenetic temperature zone and quality hydrocarbon reservoirs (Worden et al., 2020). The carbonate compound of calcite and dolomite were found to dominate the shale, having carbon elemental content ranging from 65 to 73% (6c). Furthermore, the organic matters were also hosted in the intragranular pores of mineral grain which suggest dissolution cavity of carbonate minerals since intrapore of clay minerals such as feldspar is difficult to observed (Han et al., 2016).
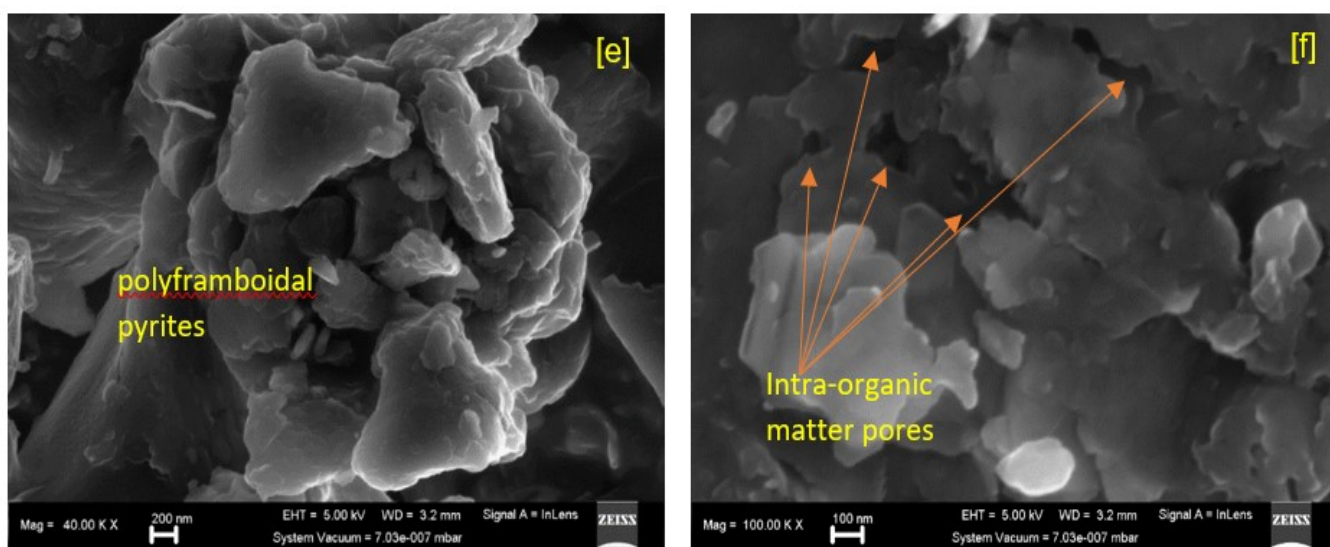
Figure 5.4:(e) SEM-EDX image showing non-spherical closely packed polyframboidal pyrite (f) fibrous chlorite and illite minerals

5.4   Discussion

This section provides a robust discussion on the stable isotopic signals, functional group, and pore structures of the studied organic-rich shale. The stable isotopic signals of carbon and oxygen components offer an insight on provenance of the organic matter in the studied shales. Furthermore, discussion on gas generation capacity based on the aliphatic function group of studied shale is provided. The last section discusses the porosity types in the studied shale samples, serving as reservoir for the potential shale gas.

5.4.1 Origin of the organic material

The formation of solid carbon components involves a multi-stage process of kerogen degradation, initiated by deposition of organic matters (Kotov et al., 2017). Sources of organic matter could be either derived from the ocean, consisting of phytoplanktonic remains, or land,

90

which consists mainly of vascular plant remains. However, accumulation of both marine and land-derived organic matter is common at deltas or floodplains of meandering rivers (Das et al., 2021, Lambert et al., 2016). Under this oxic condition in the water column, the aerobic degradation of organic matter continued until the dissolved oxygen was less than 0.2 mL/L H_2O (Tyson, 2012). The deficiency in oxygen may be due to climatic overprint, sea-level changes, tectonic activities, and hydrographic factors, resulting in an insufficient supply of oxygen to oxidize the organic materials (Dean and Arthur, 1989, Dar et al., 2017). In addition, the faster rate of organic matter accumulation in sediments more than the aerobic degradation and bacterial oxidation processes may contribute to the enrichment of organic carbon beyond its decomposition (Ferriday and Montenari, 2016). Below 0.2 mL/L H_2O oxygen concentration, anaerobic conditions and degradation of organic matter begin, giving rise to the solid carbon-containing components in shale sediments (Ferriday and Montenari, 2016). This anoxic setting is established as all the oxidants in the shale sediments deplete due to further reduction processes caused by increasing burial depth, promoting the activities of sulphide-reducing bacteria (Capotondi et al., 2016). Studies (Gallagher et al., 2015, Sabino et al., 2020, Natalicchio et al., 2019, Reolid et al., 2019) have highlighted minerals and compounds such as pyrite, sphalerite, hydrogen sulphide, and iron sulphide as evidence of the reduction process that ensued from sulphide-driven bacteria. With further increase in burial depth below the sediment–water interface, the methanogens begin to degrade the organic carbon to generate biogenic methane. This is consistent with the previous work of Tourtelot (1979), which argued that methane is unlikely to form unless all sulphates are depleted while vanadium and nickel are concentrated.

The relative amounts of carbon and oxygen isotopic compositions of organic matter is a function of paleo-environmental deposition which is significant to oil and gas exploration. In the studied carbonaceous Madzaringwe and Mikambeni shale, the relationship between of $\delta^{13}C$ and $\delta^{18}O$ / $\delta^{16}O$ of organic material suggests bacterial reduction of organic compounds to CO_2 and hydrogen through an enzymatic reaction in the absence of sulphate. The significant role of the reducing-bacterial involves converting the CO_2 and degradation organic matter into new biomass. This reduction process increases the total organic carbon contents of sedimentary rocks through a biogenic origin (Martini et al., 1996, Wang et al., 2018a). Similarly, the Santa Barbara Basin in the United State was reported to have high total organic carbon contents that resulted from a biogenic mediation of chemoautotrophic and Beggiatoa bacteria activities(Li et al., 2009). Furthermore, an organic isotopic study of the Qiongzhusi Formation in the Sichuan Basin has revealed a high degree of total organic content that is generated by microbial bacterial (Wang et al., 2021).

The oxygen isotopic composition $\delta^{18}O$ / $\delta^{16}O$ of the studied organic matter has revealed a depleted oxygen values from 16.15‰ to 9.82‰, indicating mixture of an organic water with hydrothermal-meteoric water condition. The explanation can be attributed to the relatively high thermal gradients and deep-seated circulation of heat flow provided by meteoric water (Jones, 2017). Meteoric water circulates through the faults and fractures activated by neotectonics (Tshibalo et al., 2010). The relatively high heating flow, 49-58 mWm^{-2} (Jones, 2017) associated with the Tuli Basin emanates from the tectonic-volcanic events not burial depth of the studied sediments around 1000 m. The sedimentation of Mikambeni and Madzaringwe Formations occurred in a separate fault-controlled basin of a comparatively stable miogeosynclinal depression with the intense Karoo volcanic eruption between 200 and 175 Ma ago (Tankard et al., 2012). In any case, the occurrence of thermal springs such as the Sagole and Siloam geothermal springs and heat flow higher than an average value of 120 Js^{-1} suggest the possibility of thermogenic organic matter even at shallow depth (Zhang et al., 2020a, Liu et al., 2021b). However, thermal history seems to support the plausible assumption of their organic matter maturation for shale gas generation.

5.4.2. Methanogenesis potentials of the carbonaceous Shale

The biogenic methanogenesis from diagenetic carbonaceous shale may be attributed both to microbial degradation of organic matters and their thermal maturation as burial depth increases (Figure 5.5). The carboxyl C=O stretching absorption peak, around 1000–1220 cm^{-1}, is stronger in spectra. The presence carboxyl group increases solubility properties. The post-depositional activities of microbial degradation on organic matter of shale deposit tend to produce biogenic methane, sulphide gases, and organic acids fluid capable of dissolving some reactive mineral phases (Montañez and Crossey, 2017). Among the evidence of methanogenesis processes are the imprints of burrowing organisms, which suggest a connection with bioturbation processes capable of expelling biogenic gases from carbonaceous matter in shales (Wang et al., 2019b). The micro-FTIR revealed several linking bonds such as aromatic C=C stretching and amide group N=H bending in the acetic and propionic functional group, thus consistent with the organic macerals rich in protein, carbohydrate, lipids, and lignin (Liu et al., 2019a). At this stage, dewatering of pores first occurs at 10–50 °C, followed by biogenic methane from residual lignin at 50–70°C as shown in Figure 5.5 and characterized by carbonate minerals and acetic organic group. The water absorption spectra stretch between 3500 and 4000 cm^{-1} wavenumber band. This observation alludes to the carbon $\delta^{13}C$ isotopic analysis, which reported an aceticlastic decomposition of aliphatic to aromatic components with the generation of early methane gas (Flores et al., 2008).

Sedimentation and Mineral Changes	Mineral Diagenetic Effect	Organic Functional Group Progresson	Structural Changes	Organic Matter Alteration	Tept. °C		
Fine-grained sediment, organic plant material, inorganic minerals	Bacterial mediation of organic matter, interstitial brackish fluid	Acetic Propionic	Grain-fabric, ichno-relics, amorphous organic compound	Biogenic and microbial gas O$_2$, H$_2$S, CH$_4$	10	Diagenesis / Immature zone / Biomakers	Biogenic methane
Terrigeneous Carbonates			Dolomitic rhombs	Liquid HC			
Kaolinitic alteration Feldspathic dissolution Smectitic		Oxalic	Blocky Anhedra-euhedral	Mixed liquid and gas	50 70	Catagenesis / Oil window	Oil Wet gas
Dolomitic replacement Illitic crystallization Chloritic		Phenolic Carboxylic	Framboidal fibrous-lath like Lamellated	Thermal methane CH$_4$	150 180 230	Metagenesis / Gas window	Dry gas Graphite

Increasing depth and temperature →

Hydrocarbons generated →

Figure 5.1: Methanogenesis potential of the studied carbonaceous shale (modified after Mukhopadhyay,1994)

At greater depth, the organic functional group comprising mainly phenolic and carboxylic, which were observed alongside mineralogical components of illite and chlorite was associated with thermal methanogenesis. At depths greater than 2500m, recent studies (Dowey and Taylor, 2020) (Dowey and Taylor, 2020, Ola et al., 2018, Akintola et al., 2021) have established the presence of diagenetic illite and chlorite minerals to characterized geochemical zones in which the temperature is above 180°C and the low metamorphic zone. Although the studied shale is shallower, the proximity of Sagole and Siloam geothermal fields may play a role in the elevated temperature that caused the diagenetic and thermal maturation of organic matter. The alteration in I-M ordering from random to regular during montmorillonite illitization and chloritization in shales coincides with the temperature range of organic matter maturity and the onset of the oil and gas window in the studied shales. Depending on the nature of the organic matter, marine diatoms and foraminifera undergo a catagenesis at the oil window, while the terrestrial higher plant materials exceed catagenesis to methanogenesis at about 200°C, as indicated by the aliphatic C-H stretching of methyl and methylene vibration (McDonald et al., 2004, Tetiker et al., 2015). The methane is indicated by a strong absorption band around 3000 to 3015cm^{-1} wavelength region.

5.4.3 Shale gas reservoir porosity

It is impractical to characterise gas reservoir in the same way as conventional oil and gas reservoirs because it is both a self-generation and self-storage system. As such, emphasis lies on the porosity than permeability due to recovery technology to produce natural gas from impermeable shale rock (Wood et al., 2015). The enhancement mechanism such as horizontal well-drilling and hydraulic fracturing technologies are recently used to extract natural gas

impregnated in an impermeable organic-rich shale. The knowledge of the pore characteristics is crucial to understanding pore structures and reservoir quality system of the impermeable shale rocks. In the Permian Madzaringwe and Mikambeni Shale samples, the presence of bubble-like structure indicate the organic matter pore types which some studies (Mastalerz et al., 2018b, Yang et al., 2019) described as the dominant spongy-like pore types in the Devonian Marcellus Shale samples. The morphology of the organic matter pore reflects effervescence of gaseous hydrocarbon from thermally matured macerals, creating a bubble-like void which equally host the generated gas. The pore size of the organic matter pores can be less than 2nm when detected by N_2 or CO_2 gas adsorption techniques as compared to high resolution Field Emission-SEM that can detect pores at sizes greater than 5nm in diameter. Although, the gas adsorption techniques might be unable to detect pores occupied by gaseous hydrocarbon or solid bitumen, it can provide information about the pore size, volume and surface area of the shale sample.

The micro-fracture pores developed along a preferred-oriented pores, resulting from depositional diagenetic and tectonic processes. The impact of diagenetic alteration due to increase in temperature and pressure as depth increases causes the brittle quartz minerals to fracture along a preferred orientation (Laubach et al., 2019). Apart from hosting the gaseous hydrocarbon, the micro-fracture pores enhance the mechanical properties although secondary micro-fractures are developed during hydraulic fracturing. In addition, the sedimentation the Tuli Basin occurred in a separate fault-controlled basin of a comparatively stable miogeosynclinal depression with the intense Karoo volcanic eruption between 200 and 175 Ma ago (Tankard et al., 2012). This structural deformation may affect the later fracturing of some diagenetic pores to micro-fracture along a preferred orientation. In contrast to organic matter pores, the micro-fracture pores have larger size >2µm diameter thus enhances pathway for gas molecule within the shale reservoir (Gou et al., 2019). Due to the macropores diameter, the fracture pores have been regarded as controlling structures for accumulation and expulsion of shale gas in a closed system (Martin et al., 1997).

The groundmass or matrix pores of mineral compositions having irregular-isolated structure with pore size ranging from 2 to 50nm diameter based on the SEM-EDX. The polygon and triangular pattern between mineral grains with elliptical shape (Gou et al., 2019). Interaction between mineral and pore fluid during the early diagenesis influence the pattern of groundmass or matrix pores. With increase in the burial depth, the mineral grains of clays, feldspars and quartz are altered, changing their fabrics and pore structures. It is important to note that the groundmass pores tends to have no correlation with the total porosity of an organic-rich shale samples owing to obliteration of primary porosity from diagenetic effect (Mastalerz et al., 2018b).

5.5 Summary of the Chapter

The positive excursion of organic carbon isotopes $\delta^{13}C$ indicate a local anoxic depositional environment around 280 Ma Permian period. During this period, detrital input derived from vascular plants were deposited, enriching the surface or meteoric water. In both Madzaringwe and Mikambeni Formations, the $\delta^{18}O$ and $\delta^{16}O$ isotopic signals indicate an oxygen-poor fluvial environment with a threshold $\delta^{18}O$ value less than 20 ‰. The $\delta^{18}O$ isotopic fraction indicated a brackish water environment composed of organic matter acted upon by the microbial activities for methanogenesis. With an increasing burial depth of sediment and prolonged burial rate, the organic-rich sediment undergoes a diagenetic alteration to insoluble organic compound capable of generating gaseous hydrocarbon. The functional groups of the insoluble organic compound were identified to corresponds to thermal breakdown of kerogen to methane gaseous hydrocarbon at a strong absorption band around 3000–3015 cm^{-1} wavelength region.

Consequently, the produced gaseous hydrocarbon is contained and stored mainly in the organic-matter pores as well as other pore structures. The organic-matter pore features dominated the studied shale samples with a bubble-like voids hosting the generated gas hydrocarbon in micro-nano pores >2nm in diameter. In addition, the micro-fracture pores and the groundmass or matrix pores complemented the reservoir systems of the studied shale formations. In contrast to organic matter pores, the micro-fracture are macropores with size >2μm diameter having a preferred-oriented void spaces, resulting from diagenetic and tectonic processes. Furthermore, the ground mass pores were revealed as isolated voids between micro grains forming an irregular polygon shape with size ranging from 2 to 50nm. The fine-grained fabric has intergranular or intragranular pores between terrigenous clasts despite their scarcity in volume. Finally, the pyrite framboidal structure indicate a sulphate reduction of pyrite mineral reflecting a reduction process by microbial activities in an anoxic environment. The studied shale samples show a potential good source rock for gaseous hydrocarbon as well as a good reservoir system.

CHAPTER SIX

SOURCE-ROCK AND RESERVOIR QUALITY OF THE TULI BASIN FOR POTENTIAL SHALE GAS GENERATION

The source rock for biogenic or thermogenic gaseous hydrocarbon in unconventional system remains an impermeable shale rock which also retained the generated shale gas. Thus, shale gas consists of self-sourced and self-stored biogenic or thermogenic gaseous hydrocarbon in fine-grained shale rock having extremely low permeability. Kerogen, an insoluble organic matter particulate, cracks to generate biogenic or thermogenic gas mainly rich in methane. However, generation of wet gas (ethane, propane, butane and pentane), condensate and crude oil is possible depending on the quantity, quality and maturity of the kerogen. This chapter provides the detail information on the amount, type and maturity of organic matter, whether is sufficient to generate source rock.

6.1   Background to the Chapter

The quantity of organic matter is a measure of the total organic carbon content (TOC) with an excellent threshold value > 4wt% for thermally immature unconventional source rock and > 2wt% for thermally matured unconventional source rock (Peters et al., 2016). TOC measures the sufficiency of organic matter to generate unconventional hydrocarbon but does not measures the quality (gas-prone or oil-prone) or thermal maturity. However, an abundance of organic matter with TOC value > 5% wt % has been considered as an excellent source rock for hydrocarbon generation. Most geochemical approach to quantify organic carbon are based on thermal combustion followed by detection of the generated carbon dioxide using spectroscopy (Egbobawaye, 2017).

The quality of organic matter is a measure of hydrocarbon type, whether gas or oil prone, the source rock can generate. Sedimentary kerogen has different hydrocarbon potentials owing to varying chemical structures of the organic matter. Compositionally, the chemical structure of sapropelic organic matter such as algae, bacteria, phytoplankton, and zooplankton, constitute contributors to kerogen prone to oil generation. The mixture of oil and gas has been attributed to vitrinite and liptinite macerals consisting of higher plant materials, pollens, and spore as found in the Tertiary strata of the Niger Delta Basin (Akinyemi et al., 2020). The kerogen derived mainly from higher terrestrial plants is prone to gas generation and tends to have higher TOC content than those derived from the sapropelic organic matter (Mukhopadhyay et al., 1997, Hu et al., 2018). Although the chemical composition of organic

matter indicates the quality of kerogen, the transportation and deposition environment and sedimentation rate may also influence the organic composition (Playter et al., 2017). Furthermore, organic matter not likely to generate oil or gas is mainly composed of inertinite of coaly substances.

The thermal maturity of organic matter is a measure of kerogen cracking to produce oil, gas, or condensate due to elevated temperature and pressure from burial depth. Cracking process of kerogen does not continue indefinitely with burial depth, but terminates when the kerogen is severely depleted in hydrogen. The Palaeozoic oil field of Illizi Basin in Algeria attained maturity as the thick Jurassic-Cretaceous sediments deposited over the northern Sahara platform (Galeazzi et al., 2010, Zieliński, 2012). Similarly, the Alberta foredeep basin of the Rocky Mountains mobile belt received thick sedimentation of Late Cretaceous. This sedimentation enhances the maturity of the Devonian source rock of Leduc that generates oil and cracked to gas as well (Hackley and Cardott, 2016). It implies that the preservation of organic matter over a considerable geologic period from 250 to 300 Ma largely controls the generation potential of the shale source rocks. At great burial depth over a long geologic period, the biogenic matters undergo thermal degradation, diluting with newly formed hydrocarbon resulting from kerogen degradation (Walters, 2017). Over-maturity of the Ecca Group black shale of Whitehill Formation was attributed to the dolerite intrusion resulting from the Cape orogeny event around 250 Ma ago (Nolte et al., 2019). Besides the increased temperature and pressure resulting from the deep burial of the Whitehill Formation above 2km, the high heat is associated with the dolerite intrusion of the Main Karoo Basin (Nengovhela, 2018). Having noted the essential parameters for quality source rock, the hydrocarbon generation capacity of the carbonaceous shale of the Tuli Basin remains elusive.

6.2   Purpose of the Chapter

This chapter aims to evaluate the source rock potential of the Madzaringwe and Mikambeni shales to generate natural gas in the studied Tuli Basin. To achieve the aim, specific objectives include:

- To examine the sufficiency of organic richness to generate gas source rock.
- To determine the quality of kerogen capacity to generate gas source rock.
- To evaluate the thermal maturity of the kerogen to generate matured or immature gas.

6.3 Results and Interpretations

The total organic carbon (TOC) contents and Rock-Eval 6 pyrolysis were presented in Table 6.1. The TOC value of the Mikambeni shale samples averages at 56.17 wt %, ranging from 53.09 to 58.09 wt%. while the Madzaringwe shale samples ranged from 47.54 to 45.45 wt%, averaging at 47 wt%. TOC contents show a progressive decrease in quantity as depth increases hence the Madzaringwe sample having lower amount of organic carbon content. This progressive decrease indicate cracking of kerogen to hydrocarbon as temperature and pressure increases with depth. In both studied formations, the TOC values exceed the threshold limit of 2 wt%, indicating an excellent source rock for generating oil and gas.

The Rock-Eval VI programmed pyrolysis indicates the hydrocarbon generation potential, kerogen type, and thermal maturity. In the Mikambeni samples, volatile hydrocarbons, S1, range from 3.02 to 3.35 mg HC/g rock, with an average value of 3.2 mg HC/ g rock while the hydrocarbon produced from the thermal break-up of kerogen, S2, range from 101.64 to 122.75 mg HC/grock with an average value of 115.7mg HC/g rock. On the other hand, the Madzaringwe samples have S1 values ranging from 1.62 to 1.98 mg HC/g rock as well as average value of 1.82 mg HC/g rock. At the same time, S2 values range from 15.25 to 16.47mg HC/g rock with an average of 15.69 mg HC/g rock. As such, in both studied formations, the sum of S1 and S2 indicates the hydrocarbon generative potential (GP). The hydrocarbon generative potential for all the studied samples is excellent because it exceeds the minimum threshold value of 2 mg HC/ g rock. S3 values range from 2.10 to 2.35 mg CO_2/g rock and 0.91 to 0.93 mg CO_2/g rock in Mikambeni and Madzaringwe shales respectively. The trend of S3 values show a decrease in CO_2 generation suggesting reduction in microbial activities on organic matter to thermal breakdown of kerogen as depth increases.

Hydrogen index (HI) values in Mikambeni shale samples is relatively high, ranging from 178.6 to 227.2 mg HC/ g TOC compared to the Madzaringwe samples which range from 34.0 to 37.0 mg HC/g TOC. The higher HI values suggest that the TYPE II-III Kerogens are dominant organic matter in the gas shales of Mikambeni while the lower HI values suggest that the TYPE III Kerogens dominate the organic matter of Madzaringwe shales. The HI values are affected by the type and maturity of organic matter, indicating the quality of kerogen. On the other hand, Oxygen index (OI) values range from 3.70 to 4.35 mg HC/g TOC and 2.0 to 3.0 mg HC/g TOC in Mikabeni and Madzaringwe samples respectively. Moreover, the OI values are functions of the volatile hydrocarbons generated in relation to the amount of organic matter in the studied shale samples.

Table 6.1: TOC and Rock-Eval-6 Parameters

Samples	Formation	TOC (wt.%)	S1	S2	S3	Tmax (°C)	VRo (%RoCal)	HI	OI	GP	PI	S2/S3	OSI
				(mg HC/g rock)									
Sk1	Mikambeni	57.61	3.27	113.46	2.30	430	0.58	196.9	4.08	116.73	0.03	49.33	5.68
SK2		56.36	3.02	122.75	2.10	434	0.62	217.8	3.96	125.77	0.02	58.45	5.36
SK3		53.09	3.16	101.64	2.25	431	0.60	191.4	3.95	104.8	0.03	45.17	5.95
SK4		56.98	3.18	119.60	2.20	430	0.58	209.9	3.86	122.78	0.03	54.36	5.58
SK5		57.01	3.08	121.50	2.30	431	0.60	213.1	4.12	124.58	0.02	52.83	5.40
SK6		55.86	3.20	115.28	2.15	433	0.63	206.4	3.70	118.48	0.03	53.62	5.73
SK7		58.09	3.31	103.76	2.31	430	0.58	178.6	4.35	107.07	0.03	44.92	5.70
SK8		53.07	3.35	120.55	2.16	433	0.63	227.2	3.82	123.9	0.03	55.81	6.31
SK9		56.56	3.24	117.67	2.23	432	0.67	208.0	3.91	120.91	0.03	52.77	5.73
SK10		57.05	3.10	120.73	2.35	434	0.65	211.6	4.12	123.83	0.03	51.37	5.43
SD1	Madzaringwe	46.71	1.62	15.95	0.91	468	1.26	34.0	2.0	17.57	0.10	17.52	3.45
SD2		46.75	1.63	15.96	0.91	467	1.24	35.0	3.0	17.59	0.10	17.50	3.49
SD3		47.54	1.75	16.47	0.93	465	1.21	34.0	2.0	18.22	0.10	17.71	3.68
SD4		45.53	1.94	15.25	0.91	464	1.19	37.0	3.0	17.19	0.11	16.76	4.24
SD5		46.72	1.97	15.16	0.92	469	1.28	36.0	2.0	17.13	0.12	16.48	4.22
SD6		46.72	1.69	16.10	0.91	468	1.26	34.0	2.0	17.19	0.10	17.50	4.00
SD7		45.45	1.98	15.98	0.92	470	1.30	37.0	3.0	17.73	0.11	17.37	4.36
SD8		45.68	1.93	15.36	0.91	465	1.21	36.0	2.0	17.29	0.11	16.88	4.22
SD9		46.42	1.96	15.37	0.92	470	1.30	37.0	2.0	17.33	0.11	16.71	4.20
SD10		46.77	1.90	15.37	0.92	466	1.22	37.0	2.0	17.27	0.11	16.71	4.10

GP= S1+S2, PI = S1/(S1+S2), S2/S3 (hydrocarbon product type)

Hydrogen index (HI) values in Mikambeni shale samples is relatively high, ranging from 178.6 to 227.2 mg HC/ g TOC compared to the Madzaringwe samples which range from 34.0 to 37.0 mg HC/g TOC. The higher HI values suggest that the TYPE II-III Kerogens are dominant organic matter in the gas shales of Mikambeni while the lower HI values suggest that the TYPE III Kerogens dominate the organic matter of Madzaringwe shales. The HI values are affected by the type and maturity of organic matter, indicating the quality of kerogen. On the other hand, Oxygen index (OI) values range from 3.70 to 4.35 mg HC/g TOC and 2.0 to 3.0 mg HC/g TOC in Mikabeni and Madzaringwe samples respectively. Moreover, the OI values are functions of the volatile hydrocarbons generated in relation to the amount of organic matter in the studied shale samples.

The maximum temperature, T_{max} and vitrinite reflectance (Cal VR_o) are measures of the thermal maturity of dominant kerogen. In the Mikambeni, T_{max} values range from 430 to 434°C averaging at 431.8°C thus indicating a thermally immature source. This interpretation is consistent with the VR_o ranging from 0.58 to 0.67 %R_oCal. The Production Index (PI) for the studied Mikambeni samples range 0.02 to 0.03, indicating a thermal immaturity and biogenic gas impregnation for source rock. On the other hand, T_{max} values for Madzaringwe shales range from 464 to 470°C averaging at 467.2°C, suggesting a thermally mature source rock. In addition, the vitrinite reflectance (%VR cal.) values range between 1.19 and 1.30%R_o, suggesting a condensate wet gas. Meanwhile, the Production Index (PI) for the studied Madzaringwe samples range 0.028 to 1.11, indicating a thermal maturity and thermogenic gas impregnation for source rock.

6.4   Discussion

This section discusses the generative potential of the studied organic-rich shale formations. The implication of total organic carbon to kerogen richness is well explained. Furthermore, the quality of the organic matter and the type of gas-prone kerogen are discussed. Lastly, the effect of thermal matter on the organic matter in studied shale is presented.

6.4.1 Organic richness of kerogen of the studied source rock

The total organic carbon (TOC) and generative potential yield (S1+S2) show that all the shale samples investigated had an abundance of organic materials as shown in Figure 6.1. To be sufficient for creating hydrocarbons, the amount of organic carbon content must generally exceed the minimal threshold level of 5wt % (Knapp et al., 2020). A suitable quantity of TOC > 2 wt % has been suggested as a threshold limit for an excellent source rock for thermally

matured unconventional gas (Peters et al., 2016). It is important to note that the amount of organic content in a good source rock has nothing to do with the type of hydrocarbon produced or the thermal maturity. The Barnett Shale, for example, has total organic carbon (TOC) levels ranging from 0.85 to 4.9 wt%, which is more than enough to generate hydrocarbons (Jarvie et al., 2005). The Whitehill Formation of the Ecca Group in South Africa possesses 4.5 wt%, making it a good source rock for potential(Nolte et al., 2019). The Prince Albert and Collingham Formations, on the other hand, have 0.37 and 0.62 wt%, respectively, indicating low hydrocarbon generation potential.
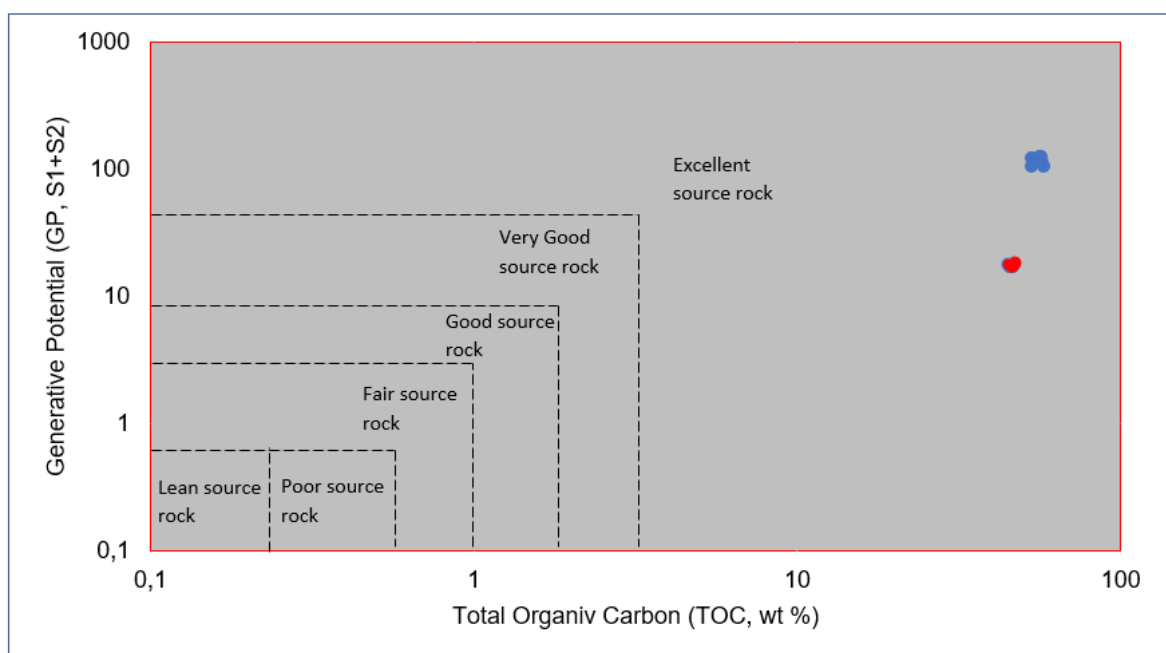
Figure 6.1: Plot of TOC vs. GP showing an excellent source rock for all studied shale samples

The organic materials in all the studied samples emanate from non-marine bottom environments, including fluvio-deltaic and freshwater depositional settings as shown in Figure 6.2. The depositional environment has been interpreted as a braided lacustrine deposit based on the paleo-current directions and facies pattern analysis. (Bordy and Catuneanu, 2002c). Fluvial structures, such as point-bars and channel lags, indicate a relatively low fluvial energy and typical of meandering fluvial or braided stream. The organic material accumulated in flood depositional environment under cool, reducing condition, giving rise carbonaceous shales, siltstones, sporadic coal seamlets with no conglomerate stringers (Chidley, 1985, Bordy, 2000). Given this sedimentary facies, the detritus materials influx from the land and dilute with the organic material to develop the studied formations.

Accumulation of abundant organic matter in the fluvio-deltaic environment is strongly related to pyritic or organic sulphur content (Fe_2S) in studied sediment instead of the total sulphur

content (TS) (Berner and Raiswell, 1983, Hakimi et al., 2016). Promoted by sulphate reduction of pyrite mineral resulting from microbial activities, an increase in alkalinity medium favours precipitation of dolomite in the presence of Ca and Mg as burial depth increases (Morad, 2009). The reduction process of Fe^{3+} to Fe^{2+} in the form of pyrite is evident from the framboidal structure revealed by SEM-EDX microscopy, thus suggesting a reducing or anoxic environment. As such, the framboidal pyrites result from the reduction of organic matter in an organic-rich shale in an anoxic condition. Anoxic conditions are established when all oxidants have been depleted and sufficient amounts of H_2S are produced by sulphate-reducing bacteria, before methane gas generation (Ferriday and Montenari, 2016).
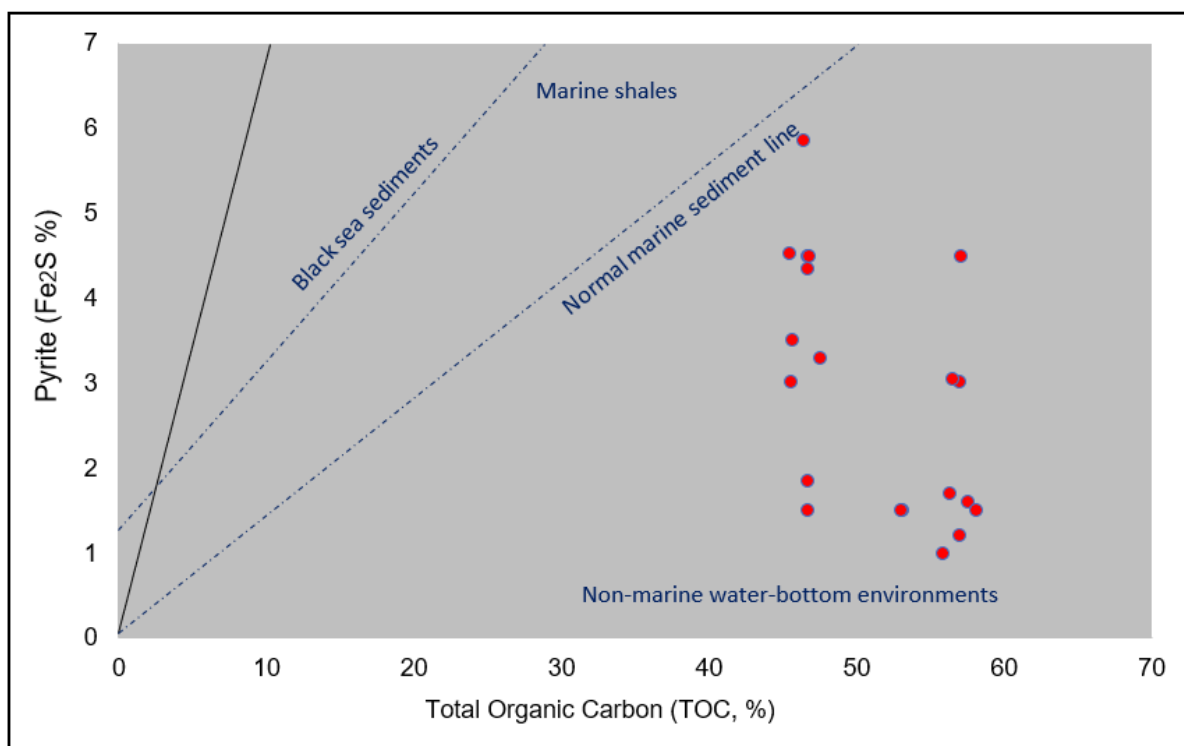
Figure 6.1: Plot of TOC vs. Pyrite showing freshwater depositional environment with marine input studied samples

6.4.2 Quality of kerogen of studied source rock

The quality of organic matter is a measure of gas and/or oil prone source rock, depending on the parent organic matter type incorporated in the shale rocks. Parent organic matter composed of lignin, cellulose and tannins of vascular plant particularly from the periderm and xylem tissues are mainly derived from terrigenous sources (Pournou, 2020). These macerals produce Type-III kerogen, which is gas-prone organic matter, when physicochemical and diagenetic transformations are suitable. The association between S2 and TOC (shown in

Figure 6.3) revealed Type-III kerogen as the major organic matter in the Madzaringwe shale samples, which is noteworthy.

Terrigenous plant materials such as the Permian "*Glossopteris* flora" and "*Dicroidium* flora" have been incorporated in the Madzaringwe Formation. This explanation is consistent with the work of Anderson and Anderson (1985) that reported the occurrence *Glossopteris* and associated taxa in the studied Tuli Basin to the north of the Main Karoo Basin (MKB). Moreover, the stratigraphic correlation between the MKB and the studied basin is supported by the paleo-current system of the Tuli Basin, showing ENE-WSW flow direction towards MKB (Catuneanu et al., 1998, Catuneanu et al., 1999, Bordy, 2000). The Madzaringwe shales, like the Barnette, Fayetteville, and Marcellus shales in the United States, have a similar parent organic material made up of herbaceous, woody, and vitrinite macerals (Broadhead and Gillard, 2007).
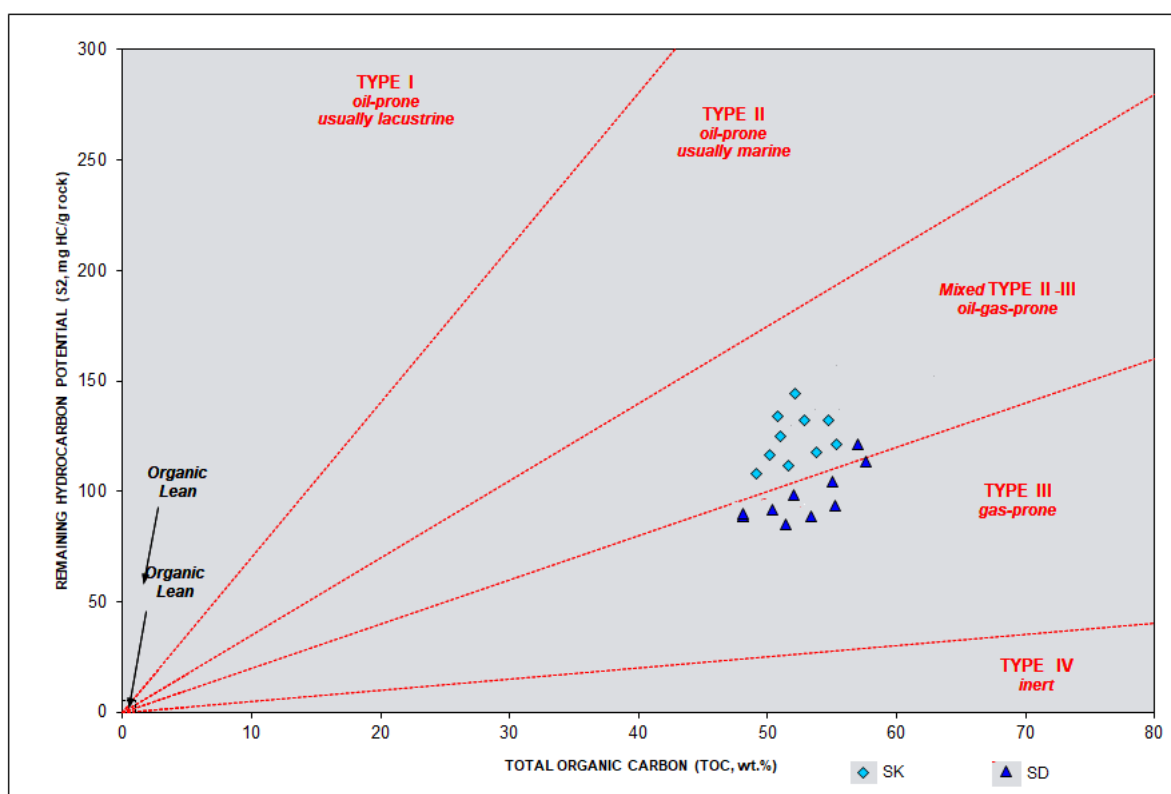
Figure 6.1: Plot of S2 vs. TOC, showing the Kerogen type of the studied shale samples

In addition, the parent organic matter, which includes foraminifera, botryococcus algae, spores, dinoflagellate, pollens, and phytoclasts, comes from marine sources (El Diasty et al., 2020). These macerals create the TYPE-II kerogen in oil-prone organic materials under favorable physicochemical and diagenetic conditions. The Mixed TYPE II-III kerogen, on the other hand, is made up of organic components from both marine and terrestrial sources (Hakimi et al., 2020).

103

The major organic matter in the examined Mikambeni shale samples is mixed TYPE II-III Kerogen, indicating a mixed oil-gas prone organic matter. Marine organic matter may have been included as a result of a brief marine ingression caused by eustatic sea level rise associated with global deglaciation Carboniferous to Early Permian period. The upward-fining facies of fine-grained strata formed of massive or laminated structure of shales, siltstones, and mudstone is supported by this marine ingression. Clastic sediments suggest terrestrial input of organic elements, including abundant plant detritus, fossil leaf imprints of *glossopteris sp.* and seed-bearing plants.

The hydrocarbon contamination and/or staining in source rocks is measured using the relationship between TOC and S1 (Rabbani and Kamali, 2005). As a result, it could occur as an indigenous hydrocarbon discharged from in-situ source rock or as a non-indigenous source migration from a nearby formation. High S1 and low TOC levels can be used to detect migrating oil in each formation. Figure 6.4 shows that all of the examined shale samples have relatively high S1 and TOC values, indicating the presence of indigenous or generated oil (Cardott et al., 2015). It is worth noting that shale samples contaminated with hydrocarbons indicate that oil was created in the source rock prior to the major migration phase (Hakimi et al., 2016). The oil saturation index (OSI) in all of the investigated shale samples is low, ranging from 3.45 to 5.95 but less than 100, indicating minimal oil contamination from the shale source rock.
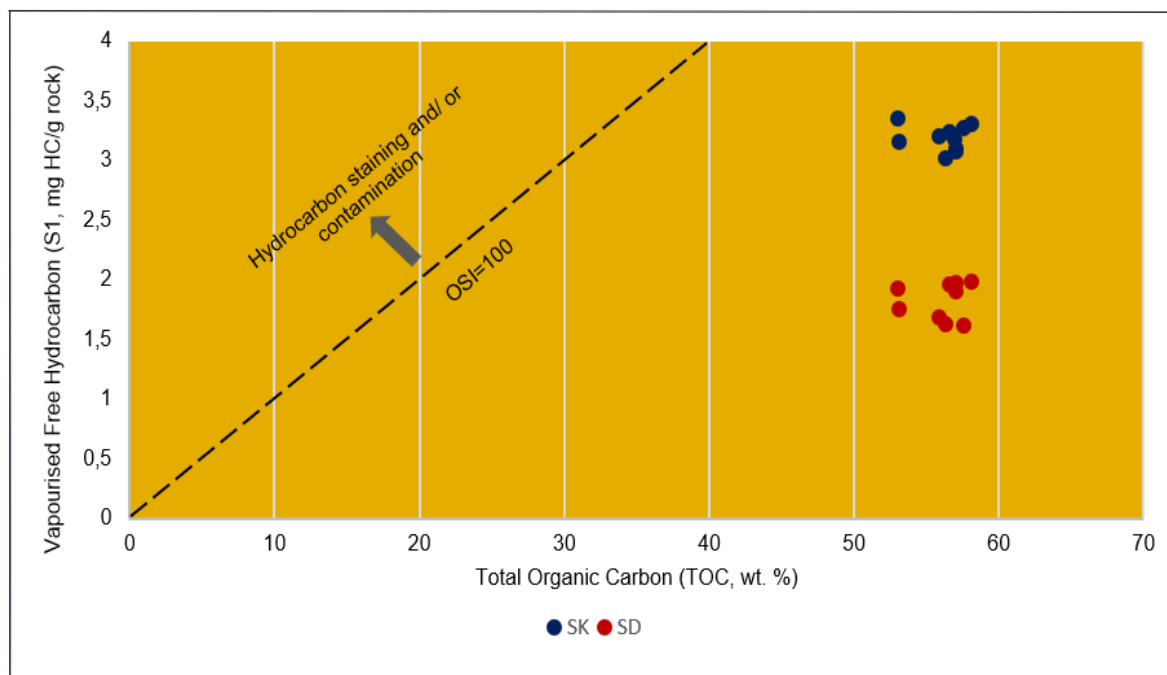
Figure 6.1: Plot of S1 vs. TOC discriminating in-situ and migrated hydrocarbon

6.4.3 Thermal maturity of kerogen of the studied source rock

The thermal maturity of organic matter is a measure of kerogen cracking to produce oil, gas, or condensate due to elevated temperature and pressure from burial depth. The thermal maturity level indicator of kerogen has been evaluated using programmed pyrolysis (Hakimi et al., 2020). Tmax values lower than 435°C indicate immature organic material while values between 435 °C and 455°C are considered mature organic matter (Tissot and Welte, 2013). Tmax values between 455°C to 470°C represents the condensate wet gas zone while over 475°C represents the dry gas zone or over mature organic matter (Tissot and Welte, 2013). Based on the pyrolysis, the Mikambeni shale samples are thermally immature biogenic methane as Tmax values range from 430 to 434°C averaging at 431.8°C as shown in Figure 6.5. Similar, thermally immature biogenic gas has been reported in the Antrim Shale at the United State. The biogenic gas of the Antrim shale of the Michigan Basin in the USA which produces about 12 million m^3/day (Martini et al., 1998, Martini et al., 1996), the studied shale exhibit similar petroliferous characteristics. At a depth less than 600 m, the Antrim shale is enriched with about 20 wt % of TOC while studied shale has 52 wt % with both formations having vitrinite reflectance within the range of 0.4 to 0.65 %Ro. The gases that are co-generated with oil have been thought to form below 160°C while biogenic methane mostly form below 80°C (Stolper et al., 2015, Quigley and Mackenzie, 1988).
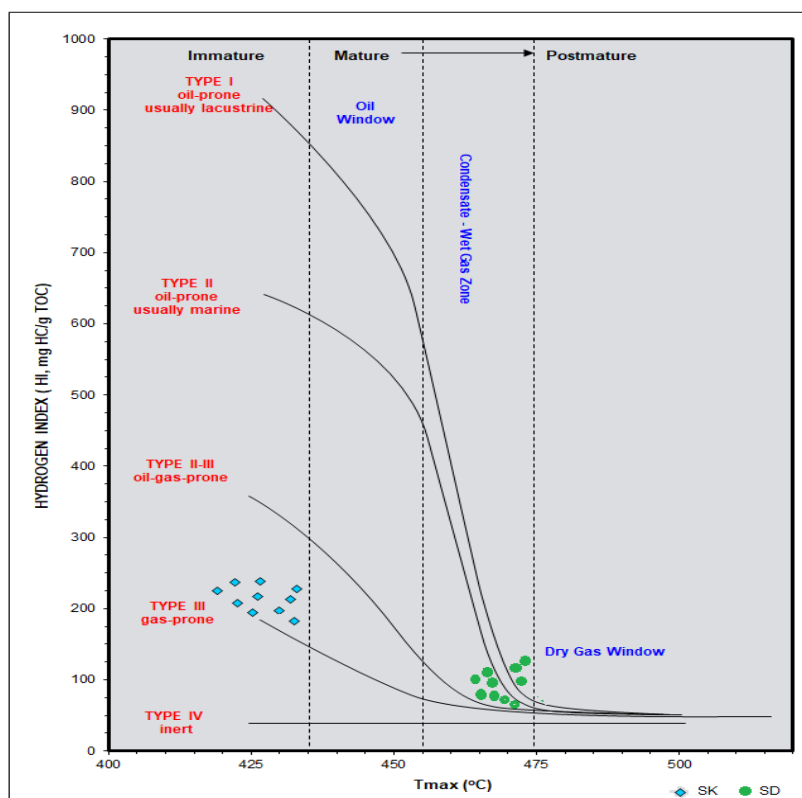
Figure 6.1: Plot of Hydrogen Index (Hi) vs Tmax showing Maturity Level of Studied Shale

On the other hand, the Madzaringwe shale samples contain a thermally mature In the condensate wet gas zone, with Tmax values ranging from 464 to 470°C, with an average of 467.2°C. This is in line with the calculated vitrinite reflectance values. The Madzaringwe shale (< 1000 m) was thought to have insufficient burial depth for the source's thermal maturity. Meanwhile, the investigated Tuli Basin is underlain by a complex network of faults, dolerite dykes, and sills that typified the Limpopo Belt (Bumby et al., 2001, Bumby et al., 2002, Barton and Pretorius, 2007). Dolerite dykes and sills intrusion in this case may produce significant heat for the Madzaringwe Formation's thermal maturity. Using magnetic data and electromagnetic techniques, the dolerite dyke was identified as an anticlinal intrusion with a depth of 2.0 to 3.5 km (Nyabeze and Gwavava, 2016, Nyabeze and Gwavava, 2018), posing a large heat contributor to the fault-controlled Tuli Basin.

Furthermore, the Production Index (PI) analysis reveals a low amount of kerogen conversion to biogenic gas in the Mikambeni shale and a medium level of conversion to condensate wet gas in the Madzaringwe shale throughout the thermal evolution process as shown in Figure 6.6. As thermal modification advances, the PI is a function of the temperature of kerogen breakdown. The Madzaringwe shales have a thermal maturity and wet gas impregnation for source rock, while the Mikambeni shale has a thermally immature and biogenic gas for source rock, according to the PI. Some literature (Li et al., 2015, Stolper et al., 2014, Rice and Claypool, 1981) have linked the existence of biogenic methane gas to shallower depths where organic matter is degraded by methane-producing microorganisms in the absence of sulphate.
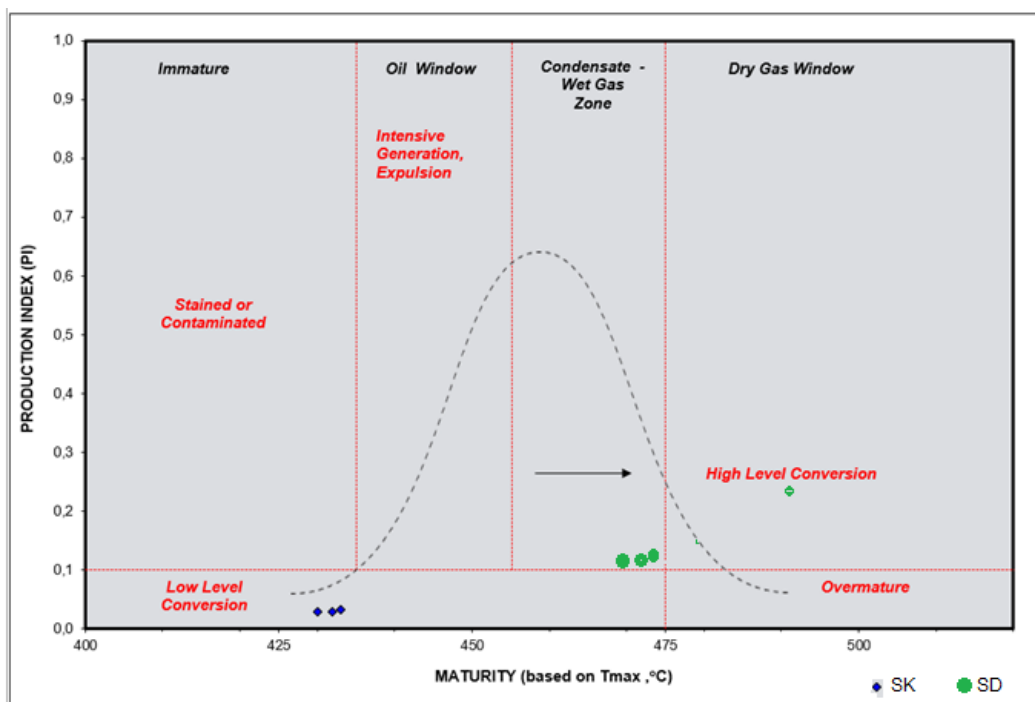
Figure 6.1: Plot of Production Index (PI) vs Tmax showing maturity pathway at low level conversion stage

6.5   Summary of the Chapter

The quantity, quality and thermal maturity of organic matter indicate capacity to generate biogenic gas and condensate wet-gas in the Mikambeni and Madzaringwe shales respectively as shale gas source rock. The quantity of Total Organic Carbon (TOC) content in both studied shale formations exceed the minimum threshold limit for excellent source rock.

Quality of organic matter that formed TYPE II-III kerogen in the Mikambeni shale samples were mainly derived from both terrigenous and marine sources. Influx of marine organic matter may have resulted from a brief marine ingression caused by eustatic sea level rise associated with global deglaciation during the late Carboniferous to Early Permian period. The upward-fining facies of fine-grained strata supports this marine ingression while the clastic sediments suggest terrestrial input of organic elements, including plant detritus and fossil leaf imprints of *glossopteris sp.* plants. On the other hand, the TYPE-III kerogen dominates the Madzaringwe shale samples indicating terrigenous input of organic materials.

Thermal maturity indicators of Tmax, calculated VR_o, and Production Index (PI) have revealed a source rock potential for a thermally immature biogenic gas due to a low level of conversion in the Mikambeni shale formation. Conversely, the Madzaringwe shale formation indicate a potential to generate a condensate wet-gas due to a high level of conversion. Besides the diagenetic burial conversion, the dolerite dykes and sills intrusion may have produced significant heat for the Madzaringwe Formation's thermal maturity. The studied shale formations fulfil the basic prerequisites of successful gas-bearing shales, making it the prime target for potential shale gas prospects in the Northern Limpopo region of South Africa.

CHAPTER SEVEN

CONCLUSIONS AND RECOMMENDATIONS

Source rock and reservoir quality investigation of carbonaceous shale formations of the Tuli Basin for shale gas generation potentiality remain crucial to expanding energy mix. The chapter presents the summary of the research, concluding remarks, the research contribution to the body of knowledge, its limitation, and recommendations for future study.

7.1 Summary of the Research

Shale gas is an unconventional gas that displays signs of future potential for energy generation. Unlike the traditional oil and gas reservoirs, shale gas is characterised by self-generation and self-storage mechanisms because it does not migrate nor diffuse over a long distance owing to the extremely low permeability of the shale. It is relatively clean, lacking heavy hydrocarbon chains in comparison to coal and more efficient than solar and wind energy for power generation since it can power heavy-duty machinery for industrial purposes. Expanding the energy base of the country becomes imperative as demand for energy consumption for industrial and domestic purposes is progressively increasing. Moreover, South Africa's carbon emission from coal-fired power plants stands at an average of 460 million metric tonnes of CO_2 equivalent yearly according to Potsdam Institute for Climate Impact. This emission rate ranked South Africa the leading carbon emitter in Africa and 14th position globally. In South Africa, an endeavour to increase energy supply in the next decade and reduce greenhouse emission from coal powerplants has sparked the interest in the aggressive search for alternative energy, with shale gas being one of the most promising candidates. While addressing problem, the carbonaceous shales of the Tuli Basin situated at Musina area in the north-eastern region of Limpopo Province South Africa were investigated for source rock and reservoir quality for shale gas generation potential.

The aim of this research was to investigate the source rock and reservoir quality for shale gas generation potentials of the Permian Tuli Basin for energy-mix in South Africa. The specific objectives were to assess the diagenetic alteration of the carbonaceous shale, establish the origin of organic matter associated with the carbonaceous shale, determine the pore structure system of the studied shale samples, and evaluate the source rock and reservoir quality of the studied shale.

The materials and methods used in this research involve representative core samples of carbonaceous Madzaringwe and Mikambeni shales of the Tuli Basin. The overlying Mikambeni shale samples covered a depth of 370 to 480m while the underlying Madzaringwe

© University of Venda

shale samples covered a depth of 485 to 580 m. On the retrieved shale samples, the mineralogical and geochemical characterization of the representative studied shale sample were conducted using the X-ray Diffractometer (XRD), and X-ray Fluorescence Spectrometry (XRF) and Laser Ablation-Inductively Couple Plasma Mass Spectrometry (LA-ICP-MS) respectively to understand the inorganic composition, diagenetic alteration, and paleo-productivity condition of the studied shale samples. Afterwards, the stable isotopic fractionation of Carbon, $\delta^{13}C$, and Oxygen $\delta^{18}O$ / $\delta^{16}O$ were determined using a isotope ratio Finnigan Delta^{plus} mass spectrometer to decipher the origin of organic matter present in studied samples. At the same time, the functional groups of the organic matter were identified using Fourier Transform Infra-red spectrometry (FTIR) to provide an insight about the aliphatic methane group potentials present in the studied samples. Consequently, the pore system to store the potential methane groups were characterised using Scanning Electron Microscopy and Bruker energy dispersive X-ray (EDX) spectrometer for the morphological analysis. Finally, the source rock and reservoir quality of studied shale samples were evaluated using the Rock-Eval 6 programmed pyrolysis for shale gas generation potential.

The findings of the research indicate that all studied carbonaceous shale samples are composed of quartz, albite, microcline, dolomite, pyrite, and clay minerals. The clay mineral component consists of montmorillonite, illite, and mixed layered illite/smectite (I/S) in the Mikambeni samples. However, Madzaringwe shale have chlorite minerals but no mixed layered illite/smectite probably due to a solid-state gradual diagenetic replacement alteration. The alteration of smectite to illite reaction has been interpreted to occur at similar temperature of the maturation index for organic matter. As such, the range for the change in I/S ordering from random to regular during smectite illitization in shales coincides with the temperature range of organic matter maturity and the onset of gaseous hydrocarbon generation in studied formations. The presence of chlorite mineral is characteristic of low-grade metamorphism or high diagenetic zone at a temperature around 200–230°C to corresponds to thermal breakdown of kerogen to gas generation

The major elemental components of studied shales include calcium oxide, iron oxide, potassium oxide, magnesia, sodium oxide, phosphorus oxide, silica, and titanium oxide. the elemental proxies ratio of Al_2O_3/TiO_2 values > 25, indicating felsic and intermediate igneous weathering sources for both studies shale samples. The elemental ratio K_2O/Al_2O_3 (0.08) of the studied samples showed values ≤ 0.5 which suggest an immature shale samples since significant amount of Al_2O_3 is typical of immature sediments. Fe/(Fe + Mg) ratio showed values < 0.90, indicating both mafic and felsic input in the Mikambeni Formation while value > 0.90 in the Madzaringwe suggesting more felsic sediment input. The Index of Compositional

Variation (ICV) of the carbonaceous shale samples have an average value < 0.1 suggesting mature sediment in Madzaringwe but immature in Mikambeni since it is greater than 0.1.

The trace element average value for Ba is > 301.29 ppm in the both studied shale formations, suggesting dissolution by action of sulphate-reducing bacteria in anoxic settings. Furthermore, the combination of Ba and Zn concentrations indicate paleo-productivity of abundant organic matter in both studied formations . The interpretation of the anoxic environment is consistent with V/(V+Ni) average value of 0.84 ppm which exceeds 0.54 minimum limit for anoxic condition. The rare earth element proxies ratio of Eu/Eu* has average value of 0.65 ppm in the Mikambeni Formation, showing Eu enrichment relative to other elements on chondrite-normalised diagram. This enrichment indicates a positive Eu-anomaly and favourable condition for immature sediment. The Eu/Eu* has average value of 0.05 ppm in the Madzaringwe Formation indicating matured sediments. The positive anomalous concentration of Ce and enrichment value of Ce* greater than 1, indicating terrigenous input in an anoxic condition in both studied Formation. The relative high Mo concentration > 2.5ppm of Mikambeni, suggests a marine sediment input.

Furthermore, the positive excursion of organic carbon isotopes $\delta^{13}C$ indicate a local anoxic depositional environment around 280 Ma Permian period in both studied Formation. During this period, detrital input derived from vascular plants were deposited, enriching the surface or meteoric water. The progression of $\delta^{16}O$ concentration suggest depletion of oxygen from oxic condition to anoxic condition in the Mikambeni sample. It implies a migration of sediment from marine or oxygen-rich environment to terrigenous or oxygen-poor environment. In both Madzaringwe and Mikambeni Formations, the heavy oxygen $\delta^{18}O$ isotopic signals indicate an oxygen-poor fluvial environment with a threshold $\delta^{18}O$ value less than 20 ‰. The $\delta^{18}O$ isotopic fraction indicated a brackish water environment composed of organic matter acted upon by the microbial activities for methanogenesis.

The functional group of all studied samples show infrared absorption peaks between 2800 and 3300 cm^{-1} wavelength attributed to C-H stretching vibrations. The sp^2 C-H hybridization found with absorption peak between 3000-3100 cm^{-1} wavelength indicates the aliphatic $C-H_4$ stretching of methyl and methylene vibration. At the same time the low absorption peak around 3500 cm^{-1} corresponds to water desorption wavelength. Each absorbance band indicates the functional group representing the whole molecular structure of a material. The studied samples exhibit a strong characteristic absorbance peak around 650 and 900 cm^{-1} wavelength corresponding to the aromatic phenolic group, C=C-OH. However, the peak reduces as temperature increase depth due to bond deformation. The aromatic C=C absorption suggests

the wavelength band of detrital plant lignin-derivative materials, unlike the amide band which is prevalent for marine-derivative materials found in the Mikambeni Shale samples.

Organic-matter, groundmass mineral, micro-fracture pore structures, as well as polyframboidal pyrite and carbonate dissolution morphologies, make up the porosity system of the examined shales sample. The bubble-like pore structures located within organic matter as organic-matter pores reflect both gaseous hydrocarbon generation source and storage reservoir. It indicates intra-pores occurring in hollow-fossils and phytoclasts macerals. The nanopore size (100 nm) of the organic-matter pore results from diagenetic alteration due to deep burial upon thermal maturity. The EDX elemental composition of the studied samples showed a significant amount of carbon 69.8%, indicating carbon-rich organic matter in form of carbonate compound. The groundmass or matrix pores display an irregular-isolated structure between the carbonaceous phytoclast macerals and mineral grains of the studied samples. The mesopore sizes of are relatively small, range from 20 to 50 nm. The micro-fracture pores displayed a preferred-oriented linear structure suggesting a preponderance of brittle minerals such as quartz under an applied pressure. The fracture is interpreted to emanate from diagenetic effect and tectono-volcanic structural event associated with the development of the Tuli basin. Moreover, non-spherical closely packed polyframboidal pyrite were observed, supported by the multiple occurrence of Fe-elemental contents on the EDX result. The presence of the polyframboidal pyrites indicates anaerobic condition which favours organic matter degradation and thermal maturation as burial depth increases.

Finally, the quantity, quality and thermal maturity of organic matter indicate capacity to generate biogenic gas in the Mikambeni shale and condensate wet-gas in the Madzaringwe shale. The quantity of organic richness is a function of the TOC content which exceeded the minimum threshold value of 5 wt% for excellent source rocks in both studied formations. The quality of organic matter in the Mikambeni samples is made up of the TYPE II-III kerogen, consisting of both terrigenous and marine organic sources. On the other hand, the TYPE-III kerogen dominates the Madzaringwe shale samples, indicating terrigenous input of organic materials. Indicators of thermal maturity, Tmax and Calculated VRo, have revealed an immature thermally kerogen that is prone to generate biogenic gas in the Mikambeni shale. Moreover, the thermometric parameters indicate a thermally matured kerogen that is prone to generate condensate wet-gas in the Madzaringwe shale. Furthermore, the gas generative potential (GP) in the studied samples indicate an excellent potential because it exceeds the minimum threshold value of 2 mg HC/ g rock. Lastly, the Madzaringwe shales have a thermal maturity and wet gas impregnation for source rock, while the Mikambeni shale has a thermally immature and biogenic gas for source rock, according to the production index (PI).

7.2   Concluding Remarks

This petroliferous study found a source-reservoir shale in the Mikambeni Shale that is prone to generate a thermally immature biogenic gas, as well as a condensate wet gas in the Madzaringwe Shale Formations of the Tuli Basin.

Based on the mineralogical evaluation of the studied formations, an initial biogenic gas is generated by anaerobic microbes while the diagenetic mineral alteration suggest a more thermally matured Madzaringwe shale compared to the Mikambeni shale. The characterisation revealed the presence of reducing mineral such as pyrite, indicating activities of sulphide-reducing bacteria on parent organic matters to generate biogenic gas. High burial temperature is insufficient to destroy the evidence of pyrite grain history or origin hence it presence indicate a detrital grain devoid of oxidizing setting but associated with anoxic, aridity, and fluvio-deltaic settings. The degradation of the organic matter generates hydrogen sulphide as a by-product of sulphate-reducing bacteria. Meanwhile, the chemical processes causing the formation of methane gas are initiated when all available sulphates are depleted.

Furthermore, the presence of higher amount thermometric minerals such as chlorite and illite in the Madzaringwe shale showed a higher level of thermal maturity compared to Mikambeni shale. In addition, the amount of labile minerals such as the feldspars in the Madzaringwe shale is low compared to the Mikambeni shale, indicating feldspathic dissolution owing to diagenetic alteration as temperature and pressure increase with depth. However, the high quartz minerals in both studied formations tend to significantly improve the shale reservoir quality because it imparts a brittleness property and enhances the fracability of shale during gas exploitation and development. The predominance of quartz minerals is ascribed to their high stability and resistance to diagenetic alteration. Based on the diagenetic alteration of the mineral compositions, the Madzaringwe shale portrays a more thermally matured formation than the Mikambeni shale.

The geochemical proxies of major, trace, and REE elements in the studied formations showed high paleo-productive of organic matter and clastic sediment, derived from both marine and non-marine in the Mikambeni Formation. However, the non-marine input mainly dominates the Madzaringwe Formation. The major elemental proxies of Al_2O_3/TiO_2, K_2O/Al_2O_3, and Fe/(Fe + Mg) have reveal a combination of felsic and intermediate provenance for Mikambeni shale while felsic detrital input dominate the Madzaringwe shale. Furthermore, the proxies indicate the presence of more immature sediment in the Mikambeni compared to the Madzaringwe. Similarly, the trace element proxies of Eu, and Eu/Eu* have average value of

0.05 ppm in the Madzaringwe Formation indicating matured sediments. The positive anomalous concentration of Ce and enrichment value of Ce* greater than 1, indicate terrigenous input in an anoxic condition in both studied Formation. However, the Ba concentration of the studied shales is relatively high, suggesting a non-marine environment since it exceed 400ppm threshold for marine environment for Madzaringwe shale. Implicitly, high detrital influx with low marine paleo-productivity characterises the Madzaringwe shale, suggesting accumulation of land-derived plant material. In addition, the Mikambeni and Madzaringwe shales indicate significant amount of organic matter production from brackish water rather than marine since brackish-water represents a value greater than 0.6 while marine water is less than 0.6 based on the Sr/Rb elemental proxy. Meanwhile, relatively high concentration of vanadium and nickel minerals indicates sulphates depletion process that favours methanogenesis.

The stable carbon and oxygen isotopic fractionations are typical of organic matter derived from terrestrial and marine sources in the studied formations. The $\delta^{13}C$ isotopic fractionation were enriched in both studied formations while $\delta^{16}O$ concentration indicated depletion of oxygen from oxic condition to anoxic condition in the Mikambeni sample. Besides terrigenous input, Mikambeni shale received contribution of organic matter from marine sources due marine ingression caused by eustatic sea level rise. The progression of $\delta^{16}O$ concentration suggest depletion of oxygen from oxic condition to anoxic condition in the Mikambeni sample. In both Madzaringwe and Mikambeni Formations, the heavy oxygen $\delta^{18}O$ isotopic signals indicate an oxygen-poor fluvial environment, indicating a brackish water environment composed of organic matter acted upon by the microbial activities.

The functional group of the studied samples revealed the presence of methane gas, indicated by a strong absorption band around 3000 to 3015 cm^{-1} wavelength region. The pore types that store the available gas include the organic-matter, groundmass mineral, and micro-fracture pore structures. In addition, the presence of polyframboidal pyrite and carbonate dissolution morphologies favours organic matter degradation and thermal maturation as burial depth increases.

The quantity, quality and thermal maturity of organic matter indicate generation of biogenic gas in the Mikambeni shale and condensate wet-gas in the Madzaringwe shale. Variation in generated has been attributed to different diagenetic alteration of kerogen and proximity to heat produced from the intense dolerite dyke and sill intrusions around 200–175 Ma. The amount of organic matter in the studied basin shows an excellent quantity that is sufficient for gas generation since it exceeds the minimum limit of 2 wt%. This excellent quantity of TOC

agrees with the paleo-productivity of organic material and clastic sediment from terrigenous source as well little input from the marine sources.

Furthermore, the quality of organic matter in the studied basin indicated TYPE II-III (mixed of gas and oil prone) in the Mikambeni shale and TYPE III (gas-prone) in the Madzaringwe shale. Variation of kerogen type in the formations is attributed to different kind of parent organic materials. The dominant organic matter in the examined Mikambeni shale samples were derived from the higher vascular terrigenous plants and marine algae, pollens and spore, resulting to a mixed oil-gas prone kerogen-type. Marine organic matter tends to result from a brief marine ingression caused by eustatic sea level rise associated with global deglaciation Carboniferous to Early Permian period. The upward-fining facies of fine-grained strata formed of massive or laminated structure of shales, siltstones, and mudstone is supported by this marine ingression. Clastic sediments suggest terrestrial input of organic elements, including abundant plant detritus, fossil leaf imprints of glossopteris sp. and seed bearing plants. In line with the stable isotope fractionation, the carbon $\delta^{13}C$ and oxygen $\delta^{16}O$ / $\delta^{18}O$ signals revealed origin of organic matter from the terrigenous setting infused with marine inputs.

Finally, the parameters for maturity indicator, Tmax and calculated vitrinite reflectance, revealed that the Mikambeni shale generate a thermally immature biogenic gas due to a relatively shallow burial depth. This is supported by the mineralogical and geochemical findings that showed a less thermally matured components in the Mikambeni shale compared to the Madzaringwe shale. Meanwhile, the oil saturation index (OSI) is low, suggesting an absence of hydrocarbon contamination in both studied formations. On the other hand, the Madzaringwe shale generates thermally mature condensate-wet gas owing to diagenetic alteration of kerogen and proximity to heat produced from the intense dolerite dyke and sill intrusions. Meanwhile, the average Productivity Index (PI) value of 0.1 indicates a moderately mature source rock. In addition, gas generative potential (GP) in the studied basin indicate an excellent potential because it exceeds the minimum threshold value of 2 mg HC/ g rock. Based on these petroliferous evaluations, the carbonaceous shale associated with the Mikambeni and Madzaringwe Formations of the Tuli Basin are found with shale gas generation potential within the domain of thermally immature biogenic gas and thermally mature condensate wet-gas.

7.3 Research Contributions to the Body of Knowledge

The contributions to the body of knowledge of this study are presented in this section as follows:

- Different methods were integrated to investigate shale gas potential in a shallow organic-rich shale basin. As a result of the integration of these methods, including organic, inorganic, structural and functional group characteristics of organic-rich shale, it was possible to identify sulphate-reducing minerals such as pyrite as precursor to shale gas generation

- A detailed knowledge of Kerogen-Types II-III and III in shallow organic-rich shale basin has been provided based on the quality, quantity and thermal maturity of the basin's organic matter. This will be a new reference for other shallow organic shale basin globally when investigating potential shale gas generation.

- Foredeep depozone has been widely explored and its potential for shale gas generation is well-known. However, the capability of back-bulge depozone to generate shale gas has not been given utmost consideration. This study has provided comprehensive and reliable information on geological setting of the back-bulge depozone in terms of its potential to generate shale gas.

7.4 Limitations of the Research

The study encountered some limitations which are highlighted below:

- This research made use of borehole core samples collected from the local study area in Musina and does not transverse through the entire Tuli Basin. It implies that the findings is specific to the studied samples. However, the methods used can be replicated in any other uninvestigated areas.
- Authorization to carry out geophysical, structural, and hydrological investigations at the study area was denied. The sub-surface information in respect of contact zones between the crystalline basement and the sedimentary deposits, structural geology and hydrogeological are lacking. The interpretation of data are based on the generalized and surface structural geology.
- Fresh core logs are not available, hence an estimate of technically recoverable gas cannot be evaluated. Due to degassing, an actual volume of gas is difficult to estimate using un-fresh core logs hence the estimated potential yield could not be determined.

7.5 Recommendations for Future Work

University of Venda

The following suggestions have been given for further investigation and development of this work.

- There is a need to carry out more investigations on carbonaceous shale in other areas of the Tuli Basin to ascertain the homogenous nature and spatial distribution of shale gas potential.
- There is a need to understand the sub-surface conditions such as contact zones between the crystalline basement and the sedimentary deposits, structural geology and hydrogeological conditions using geophysical methods, including electrical resistivity and electromagnetic methods.
- There is a need to sink exploration borehole to obtain fresh core samples to estimate the volume of gas present in the potential shale formations in the Tuli Basin.

REFERENCES

Abanda, P. A. and Hannigan, R. E. (2006). Effect of diagenesis on trace element partitioning in shales. *Chemical Geology,* 230**,** 42-59.

Adeniyi, E. O., Ossa, F. O., Kramers, J. D., De Kock, M. O., Belyanin, G. and Beukes, N. J. (2018). Cause and timing of the thermal over-maturation of hydrocarbon source rocks of the Ecca Group (Main Karoo Basin, South Africa). *Marine and Petroleum Geology,* 91**,** 480-500.

Administration, U. S. E. I. and Kuuskraa, V. (2011). *World shale gas resources: an initial assessment of 14 regions outside the United States*, US Department of Energy.

Ae, T. and Olivier, J. (2010). Sagole spa resort, current and potential uses.

Ahmad, F. (2020). *Experimental investigation of proppant transport and behavior in horizontal wellbores using low viscosity fluids.* Colorado School of Mines.

Ahmed, A., Jahandad, S., Hakimi, M. H., Gharib, A. F., Mehmood, S., Kahal, A. Y., Khan, M. A., Munir, M. N. and Lashin, A. (2022). Organic matter characteristics and conventional oil potentials of shales from the Early Jurassic Datta Formation in the Upper Indus Basin, Northern Pakistan. *Journal of Asian Earth Sciences,* 224**,** 104975.

Akintola, G. O. (2018). *Evaluation of major clay deposits for potential industrial utilization in Vhembe District Municipality, Limpopo Province of South Africa.*

Akintola, G. O., Ikhane, P. R., Amponsah-Dacosta, F., Adeagbo, A. F., Mhlongo, S. E., Edokpayi, J. N., Oladipo, V. O., Jegede, A. O., Akintola, A. I. and Adebisi, N. O. (2021). Geochemical evaluation of the carbonaceous shale of the upper cretaceous Anambra Basin for potential gas generation, Nigeria. *Arabian Journal of Geosciences,* 14**,** 1-14.

Akinyemi, S., Adebayo, O., Nyakuma, B., Adegoke, A., Aturamu, O., Olaolorun, O., Adetunji, A., Hower, J. C., Hood, M. M. and Jauro, A. (2020). Petrology, physicochemical and thermal analyses of selected cretaceous coals from the Benue Trough Basin in Nigeria. *International Journal of Coal Science & Technology,* 7**,** 26-42.

Al-Muntasheri, G. A. (2014). A critical review of hydraulic fracturing fluids over the last decade. SPE Western North American and Rocky Mountain Joint Meeting. Society of Petroleum Engineers.

Al-Selwi, A. and Joshi, M. (2015). Source rock evaluation using total organic carbon (TOC) and the loss-on-ignition (LOI) techniques. *Oil Gas Res,* 1**,** 900-1000.

Alessi, D. S., Zolfaghari, A., Kletke, S., Gehman, J., Allen, D. M. and Goss, G. G. (2017). Comparative analysis of hydraulic fracturing wastewater practices in unconventional shale development: Water sourcing, treatment and disposal practices. *Canadian Water Resources Journal/Revue canadienne des ressources hydriques,* 42**,** 105-121.

© University of Venda

Algeo, T. J. and Maynard, J. B. (2004). Trace-element behavior and redox facies in core shales of Upper Pennsylvanian Kansas-type cyclothems. *Chemical geology,* 206**,** 289-318.

Ali, S. A., Clark, W. J., Moore, W. R. and Dribus, J. R. (2010). Diagenesis and reservoir quality. *Oilfield Review,* 22**,** 14-27.

Alizadeh, A. A., Guliyev, I. S., Kadirov, F. A. and Eppelbaum, L. V. (2017). Economic Minerals of Azerbaijan. *Geosciences of Azerbaijan.* Springer.

Ampomah, W., Balch, R., Cather, M., Rose-Coss, D., Dai, Z., Heath, J., Dewers, T. and Mozley, P. (2016). Evaluation of CO_2 storage mechanisms in CO_2 enhanced oil recovery sites: Application to Morrow sandstone reservoir. *Energy & Fuels,* 30**,** 8545-8555.

Anawar, H. M., Yoshioka, T., Konohira, E., Akai, J., Freitas, M. and Tareq, S. M. (2010). Sources of organic carbon and depositional environment in the Bengal delta plain sediments during the Holocene period. *Limnology,* 11**,** 133-142.

Anaya-Gregorio, A., Armstrong-Altrin, J. S., Machain-Castillo, M. L., Montiel-García, P. C. and Ramos-Vázquez, M. A. (2018). Textural and geochemical characteristics of late Pleistocene to Holocene fine-grained deep-sea sediment cores (GM6 and GM7), recovered from southwestern Gulf of Mexico. *Journal of Palaeogeography,* 7**,** 1-19.

Andreasson, S. (2018). The bubble that got away? Prospects for shale gas development in South Africa. *The Extractive Industries and Society,* 5**,** 453-460.

Baiyegunhi, C., Liu, K. and Gwavava, O. (2017). Diagenesis and reservoir properties of the permian Ecca Group sandstones and mudrocks in the Eastern Cape Province, South Africa. *Minerals,* 7**,** 88.

Baiyegunhi, C., Liu, K., Wagner, N., Gwavava, O. and Oloniniyi, T. (2018a). *Geochemical Evaluation of the Permian Ecca Shale in Eastern Cape Province, South Africa: Implications for Shale Gas Potential*.

Baiyegunhi, C., Liu, K., Wagner, N., Gwavava, O. and Oloniniyi, T. L. (2018b). Geochemical evaluation of the Permian Ecca shale in Eastern Cape Province, South Africa: Implications for shale gas potential. *Acta Geologica Sinica‐English Edition,* 92**,** 1193-1217.

Baker, L., Newell, P. and Phillips, J. (2014a). The political economy of energy transitions: the case of South Africa. *New Political Economy,* 19**,** 791-818.

Baker, M. J., Trevisan, J., Bassan, P., Bhargava, R., Butler, H. J., Dorling, K. M., Fielden, P. R., Fogarty, S. W., Fullwood, N. J. and Heys, K. A. (2014b). Using Fourier transform IR spectroscopy to analyze biological materials. *Nature protocols,* 9**,** 1771.

Bakshi, T. and Vishal, V. (2021). A review on the role of organic matter in gas adsorption in shale. *Energy and Fuels,* 35**,** 15249-15264.

University of Venda

Balashov, V. N., Engelder, T., Gu, X., Fantle, M. S. and Brantley, S. L. (2015). A model describing flowback chemistry changes with time after Marcellus Shale hydraulic fracturingMarcellus Shale Hydraulic Fracturing. *AAPG Bulletin,* 99**,** 143-154.

Bao, X. and Eaton, D. W. (2016). Fault activation by hydraulic fracturing in western Canada. *Science,* 354**,** 1406-1409.

Barbolini, N. and Bamford, M. (2014). Palynology of an Early Permian coal seam from the Karoo Supergroup of Botswana. *Journal of African Earth Sciences,* 100**,** 136-144.

Barbot, E., Vidic, N. S., Gregory, K. B. and Vidic, R. D. (2013). Spatial and temporal correlation of water quality parameters of produced waters from Devonian-age shale following hydraulic fracturing. *Environmental science & technology,* 47**,** 2562-2569.

Barton, J. and Pretorius, W.(2007). Soutpansberg age (1.85 Ga) magmatism and metallogenesis in southern Africa: A result of regional rifting. International Symposium on Plumes, Plates and Mineralisation. 12-19.

Beaufort, D., Rigault, C., Billon, S., Billault, V., Inoue, A., Inoué, S., Patrier, P. and Ferrage, E. (2015). Chlorite and chloritization processes through mixed-layer mineral series in low-temperature geological systems–a review. *Clay Minerals,* 50**,** 497-523.

Belyadi, H., Fathi, E. and Belyadi, F. (2019). *Hydraulic fracturing in unconventional reservoirs: theories, operations, and economic analysis*, Gulf Professional Publishing.

Bergaya, F. and Lagaly, G. (2013). *Handbook of clay science*, Newnes.

Berger, G., Lacharpagne, J.-C., Velde, B., Beaufort, D. and Lanson, B. (1997). Kinetic constraints on illitization reactions and the effects of organic diagenesis in sandstone/shale sequences. *Applied Geochemistry,* 12**,** 23-35.

Berner, R. A. (2020). *Early diagenesis*, Princeton University Press.

Berner, R. A. and Raiswell, R. (1983). Burial of organic carbon and pyrite sulfur in sediments over Phanerozoic time: a new theory. *Geochimica et Cosmochimica Acta,* 47**,** 855-862.

Bestvater, B. P. (2017). *Investigations into enantioselective boro-ion catalysis.* Queen's University (Canada).

Bibi, R., Kang, H. Y., Kim, D., Jang, J., Kundu, G. K., Kim, Y. K. and Kang, C.-K. (2020). Dominance of autochthonous phytoplankton-derived particulate organic matter in a low-turbidity temperate estuarine embayment, Gwangyang Bay, Korea. *Frontiers in Marine Science,* 7**,** 827.

Bjørlykke, K. (2014). Relationships between depositional environments, burial history and rock properties. Some principal aspects of diagenetic process in sedimentary basins. *Sedimentary Geology,* 301**,** 1-14.

Bjørlykke, K. and Jahren, J. (2012). Open or closed geochemical systems during diagenesis in sedimentary basins: Constraints on mass transfer during diagenesis and the

prediction of porosity in sandstone and carbonate reservoirsGeohorizon. *AAPG bulletin,* 96**,** 2193-2214.

Black, D., Booth, P. and De Wit, M. (2016). Petrographic, geochemical and petro-physical analysis of the Collingham Formation near Jansenville, Eastern Cape, South Africa–potential cap rocks to shale gas in the Karoo. *South African Journal of Geology 2016,* 119**,** 171-186.

Blauch, M. E., Myers, R. R., Moore, T., Lipinski, B. A. and Houston, N. A.(2009). Marcellus shale post-frac flowback waters-Where is all the salt coming from and what are the implications. SPE Eastern Regional Meeting. Society of Petroleum Engineers.

Bohlmann, J., Bohlmann, H., Inglesi-Lotz, R. and Van Heerden, J. (2016). An economy-wide evaluation of new power generation in South Africa: The case of Medupi and Kusile. *Energy Policy,* 97**,** 450-460.

Boles, J. R. and Franks, S. G. (1979). Clay diagenesis in Wilcox sandstones of Southwest Texas; implications of smectite diagenesis on sandstone cementation. *Journal of Sedimentary Research,* 49**,** 55-70.

Bordy, E. (2018). Lithostratigraphy of the Tshidzi Formation (Dwyka Group, Karoo Supergroup), South Africa. *South African Journal of Geology,* 121**,** 109-118.

Bordy, E. M. (2000). *Sedimentology of the Karoo Supergroup In the Tuli Basin.* Rhodes University.

Bordy, E. M. and Catuneanu, O. (2001). Sedimentology of the upper Karoo fluvial strata in the Tuli Basin, South Africa. *Journal of African Earth Sciences,* 33**,** 605-629.

Bordy, E. M. and Catuneanu, O. (2002a). Sedimentology and palaeontology of upper Karoo aeolian strata (Early Jurassic) in the Tuli Basin, South Africa. *Journal of African Earth Sciences,* 35**,** 301-314.

Bordy, E. M. and Catuneanu, O. (2002b). Sedimentology of the Beaufort-Molteno Karoo fluvial strata in the Tuli Basin, South Africa. *South African Journal of Geology,* 105**,** 51-66.

Bordy, E. M. and Catuneanu, O. (2002c). Sedimentology of the lower Karoo Supergroup fluvial strata in the Tuli Basin, South Africa. *Journal of African Earth Sciences,* 35**,** 503-521.

Boruah, A. and Ganapathi, S. (2015). Microstructure and pore system analysis of Barren Measures shale of Raniganj field, India. *Journal of Natural Gas Science and Engineering,* 26**,** 427-437.

Boruah, A., Rasheed, A., Mendhe, V. A. and Ganapathi, S. (2019). Specific surface area and pore size distribution in gas shales of Raniganj Basin, India. *Journal of Petroleum Exploration and Production Technology,* 9**,** 1041-1050.

Bosman, K., Baig, A., Viegas, G. and Urbancic, T. (2016). Towards an improved understanding of induced seismicity associated with hydraulic fracturing. *first break,* 34.

Brandl, G. (2002). *The Geology of the Alldays Area: Explanation, Sheet 2228, Scale 1: 250 000*, Council for Geoscience.

Broadhead, R. F. and Gillard, L. (2007). The Barnett Shale in southeastern New Mexico: Distribution, thickness, and source rock characterization. *Work*.

Bumby, A., Eriksson, P., Van Der Merwe, R. and Brümmer, J. (2001). Shear-zone controlled basins in the Blouberg area, Northern Province, South Africa: syn-and post-tectonic sedimentation relating to ca. 2.0 Ga reactivation of the Limpopo Belt. *Journal of African Earth Sciences,* 33, 445-461.

Bumby, A., Eriksson, P., Van Der Merwe, R. and Steyn, G. (2002). A half-graben setting for the Proterozoic Soutpansberg Group (South Africa): evidence from the Blouberg area. *Sedimentary Geology,* 147, 37-56.

Burke, K. and Dewey, J. (1973). Plume-generated triple junctions: key indicators in applying plate tectonics to old rocks. *The Journal of Geology,* 81, 406-433.

Burton Jr, G. A., Basu, N., Ellis, B. R., Kapo, K. E., Entrekin, S. and Nadelhoffer, K. (2014). Hydraulic "fracking": are surface water impacts an ecological concern? *Environmental Toxicology and Chemistry,* 33, 1679-1689.

Butkovskyi, A., Bruning, H., Kools, S. A., Rijnaarts, H. H. and Van Wezel, A. P. (2017). Organic pollutants in shale gas flowback and produced waters: identification, potential ecological impact, and implications for treatment strategies. *Environmental science & technology,* 51, 4740-4754.

Cadle, A., Cairncross, B., Christie, A. and Roberts, D. (1993). The Karoo Basin of South Africa: type basin for the coal-bearing deposits of southern Africa. *International Journal of Coal Geology,* 23, 117-157.

Cai, L., Zeng, Z., Zhang, X., Xiao, G., Guo, X. and Pang, Y. (2020). Hydrocarbon Generation Kinetics of the Gas-Prone Kerogens in the Central Uplift of the South Yellow Sea Basin. *Energy and Fuels,* 34, 12225-12238.

Calvert, S. and Pedersen, T. (1993). Geochemistry of recent oxic and anoxic marine sediments: implications for the geological record. *Marine geology,* 113, 67-88.

Capotondi, L., Girone, A., Lirer, F., Bergami, C., Verducci, M., Vallefuoco, M., Afferri, A., Ferraro, L., Pelosi, N. and De Lange, G. J. (2016). Central Mediterranean Mid-Pleistocene paleoclimatic variability and its association with global climate. *Palaeogeography, Palaeoclimatology, Palaeoecology,* 442, 72-83.

Cardott, B. J., Landis, C. R. and Curtis, M. E. (2015). Post-oil solid bitumen network in the Woodford Shale, USA—a potential primary migration pathway. *International Journal of Coal Geology,* 139, 106-113.

Catuneanu, O. (2004). Retroarc foreland systems—evolution through time. *Journal of African Earth Sciences,* 38, 225-242.

Catuneanu, O., Hancox, P. and Rubidge, B. (1998). Reciprocal flexural behaviour and contrasting stratigraphies: a new basin development model for the Karoo retroarc foreland system, South Africa. *Basin Research,* 10**,** 417-439.

Catuneanu, O., Kun-Jager, E., Rubidge, B. and Hancox, P. (1999). Lateral changes of the Dwyka facies: implications for the initiation of the Cape Orogeny and the associated Karoo foreland system. American Association of Petroleum Geologists Annual Meeting. 11-14.

Catuneanu, O., Wopfner, H., Eriksson, P., Cairncross, B., Rubidge, B., Smith, R. and Hancox, P. (2005). The Karoo basins of south-central Africa. *Journal of African Earth Sciences,* 43**,** 211-253.

Chai, X., Tonjes, D. J. and Mahajan, D. (2016). Methane emissions as energy reservoir: context, scope, causes and mitigation strategies. *Progress in Energy and Combustion Science,* 56**,** 33-70.

Charriau, A., Lesven, L., Gao, Y., Leermakers, M., Baeyens, W., Ouddane, B. & Billon, G. (2011). Trace metal behaviour in riverine sediments: role of organic matter and sulphides. *Applied Geochemistry,* 26**,** 80-90.

Chen, C., Mu, C.-L., Zhou, K.-K., Liang, W., Ge, X.-Y., Wang, X.-P., Wang, Q.-Y. and Zheng, B.-S. (2016a). The geochemical characteristics and factors controlling the organic matter accumulation of the Late Ordovician-Early Silurian black shale in the Upper Yangtze Basin, South China. *Marine and Petroleum Geology,* 76**,** 159-175.

Chen, J., Yang, X., Ma, S., Yang, T. and Niemeijer, A. (2016b). Hydraulic properties of samples retrieved from the Wenchuan earthquake Fault Scientific Drilling Project Hole-1 (WFSD-1) and the surface rupture zone: Implications for coseismic slip weakening and fault healing. *Geochemistry, Geophysics, Geosystems,* 17**,** 2717-2744.

Chen, L., Jiang, Z., Liu, Q., Jiang, S., Liu, K., Tan, J. and Gao, F. (2019). Mechanism of shale gas occurrence: Insights from comparative study on pore structures of marine and lacustrine shales. *Marine and Petroleum Geology,* 104**,** 200-216.

Chen, Y., Mastalerz, M. and Schimmelmann, A. (2012). Characterization of chemical functional groups in macerals across different coal ranks via micro-FTIR spectroscopy. *International Journal of Coal Geology,* 104**,** 22-33.

Chen, Y., Wang, Y., Guo, M., Wu, H., Li, J., Wu, W. and Zhao, J. (2020). Differential enrichment mechanism of organic matters in the marine-continental transitional shale in northeastern Ordos Basin, China: control of sedimentary environments. *Journal of Natural Gas Science and Engineering,* 83**,** 103625.

Cheng, A. H.-D. (2016). *Poroelasticity*, Springer.

University of Venda

Chidley, C. (1985). The geology of the country around Evangelina and Pontdrift (1: 50,000 sheets 2228BD and 2229A). *Unpublished South African Geological Survey Report. Pietersburg, South Africa. 22pp*.

Chima, P., Baiyegunhi, C., Liu, K. and Gwavava, O. (2018). Diagenesis and rock properties of sandstones from the Stormberg Group, Karoo Supergroup in the Eastern Cape Province of South Africa. *Open Geosciences,* 10**,** 740-771.

Clarkson, C. R. and Bustin, R. M. (1996). Variation in micropore capacity and size distribution with composition in bituminous coal of the Western Canadian Sedimentary Basin: implications for coalbed methane potential. *Fuel,* 75**,** 1483-1498.

Clarkson, C. R., Jensen, J. L., Pedersen, P. K. and Freeman, M. (2012). Innovative methods for flow-unit and pore-structure analyses in a tight siltstone and shale gas reservoir. *AAPG bulletin,* 96**,** 355-374.

Cloos, H. (1939). Hebung-Spaltung-Vulkanismus, Elemente einer geomet-risch en Analyse irdischer Grossformen. *Geol. Rund.,* 30**,** 406-527.

Coenen, K., Gallucci, F., Mezari, B., Hensen, E. and Van Sint Annaland, M. (2018). An in-situ IR study on the adsorption of CO_2 and H_2O on hydrotalcites. *Journal of CO_2 Utilization,* 24**,** 228-239.

Cory-Toussaint, D., Taylor, P. J. and Barnhoorn, I. E. (2021). Non-invasive sampling of bats reflects their potential as ecological indicators of elemental exposure in a diamond mining area, northern Limpopo Province, South Africa. *Environmental Science and Pollution Research***,** 1-14.

Cox, K. G., Johnson, R. L., Monkman, L. J., Stillman, C. J., Vail, J. R. & Wood, D. N. (1965). The Geology of the Nuanetsi Igneous Province. *Philosophical Transactions of the Royal Society of London. Series A, Mathematical and Physical Sciences,* 257**,** 71-218.

Cox, R., Lowe, D. R. and Cullers, R. (1995). The influence of sediment recycling and basement composition on evolution of mudrock chemistry in the southwestern United States. *Geochimica et Cosmochimica Acta,* 59**,** 2919-2940.

Cruz-Ceballos, L. F., García-González, M., Cruz-Guevara, L. E. and Avendaño-Sánchez, G. M. (2020). Geochemical Characterization and Thermal Maturation of Cerrejón Formation: Implications for the Petroleum System in the Ranchería Sub-Basin, Colombia. *Geosciences,* 10**,** 258.

Cui, J., Li, S. and Mao, Z. (2019). Oil-bearing heterogeneity and threshold of tight sandstone reservoirs: A case study on Triassic Chang7 member, Ordos Basin. *Marine and Petroleum Geology,* 104**,** 180-189.

Curtis, C. D. (1985). Clay mineral precipitation and transformation during burial diagenesis. *Philosophical Transactions of the Royal Society of London. Series A, Mathematical and Physical Sciences,* 315**,** 91-105.

Da Costa, G., Hofmann, A. and Agangi, A. (2020). A revised classification scheme of pyrite in the Witwatersrand Basin and application to placer gold deposits. *Earth-Science Reviews,* 201**,** 103064.

Dai, S., Bechtel, A., Eble, C. F., Flores, R. M., French, D., Graham, I. T., Hood, M. M., Hower, J. C., Korasidis, V. A. and Moore, T. A. (2020a). Recognition of peat depositional environments in coal: A review. *International Journal of Coal Geology,* 219**,** 103383.

Dai, S., Bechtel, A., Eble, C. F., Flores, R. M., French, D., Graham, I. T., Hood, M. M., Hower, J. C., Korasidis, V. A., Moore, T. A., Püttmann, W., Wei, Q., Zhao, L. and O'keefe, J. M. K. (2020b). Recognition of peat depositional environments in coal: A review. *International Journal of Coal Geology,* 219**,** 103383.

Dar, S. A., Khan, K. and Birch, W. (2017). Sedimentary: Phosphates. *Reference Module in Earth Systems and Environmental Sciences. doi,* 10.

Das, A., Majumder, S., Barman, S., Chatterjee, D., Mukhopadhyay, S., Ghosh, P., Pal, C. N. and Saha, G. (2021). Influence of basin-wide geomorphology on arsenic distribution in Nadia district. *Environmental Research,* 192**,** 110314.

Davies, R., Foulger, G., Bindley, A. and Styles, P. (2013). Induced seismicity and hydraulic fracturing for the recovery of hydrocarbons. *Marine and Petroleum Geology,* 45**,** 171-185.

Davis, L., Graham, A., Parker, H., Abbott, J., Ingber, M., Mammoli, A., Mondy, L., Guo, Q. and Abou-Sayed, A. (2005). Maximizing Storage Rate and Capacity and Insuring the Environmental Integrity of Carbon Dioxide Sequestration in Geological Reservoirs. Texas Tech Univ., Lubbock, TX (United States).

De Kock, M. O., Beukes, N. J., Adeniyi, E. O., Cole, D., Gotz, A. E., Geel, C. and Ossa, F.-G. (2017). Deflating the shale gas potential of South Africa's Main Karoo basin. *South African Journal of Science,* 113**,** 1-12.

Dea, R. (2014). National Guideline for the Discharge of Effluent from Land-Based Sources into the Coastal Environment. Pretoria, South Africa. RP101/2014: Republic of South Africa Department of Environmental Affairs.

Dean, W. E. and Arthur, M. A. (1989). Iron-sulfur-carbon relationships in organic-carbon-rich sequences I: Cretaceous Western Interior Seaway. *American Journal of Science,* 289**,** 708-743.

Decker, J. and Marot, J. (2012). Investigation of hydraulic fracturing in the Karoo of South Africa. Annexure A, Resource Assessment, Petroleum Agency SA.

Denge, E. and Baiyegunhi, C. (2021). Maceral Types and Quality of Coal in the Tuli Coalfield: A Case Study of Coal in the Madzaringwe Formation in the Vele Colliery, Limpopo Province, South Africa. *Applied Sciences,* 11**,** 2179.

Der Berg, V. and Jacobus, H. (1980). *Die sedimentologie van die Soutpansbergsteenkoolveld met spesiale verwysing na steenkoolvorming.* University of the Free State.

Dowey, P. J. and Taylor, K. G. (2020). Diagenetic mineral development within the Upper Jurassic Haynesville-Bossier Shale, USA. *Sedimentology,* 67**,** 47-77.

Du, D., Zhang, G., Zhao, Y., Sun, X. and Zhang, B. (2020). Transient Flow Theory of Multiple-Fractured Horizontal Wells with Complex Mechanisms in Shale Gas Reservoirs. *Geofluids,* 2020.

Du Plessis, W. (2015). Regulation of hydraulic fracturing in South Africa: a project life-cycle approach? *Potchefstroom Electronic Law Journal/Potchefstroomse Elektroniese Regsblad,* 18**,** 1440-1478.

Du Toit, A. L. (1939). *The Geology of South Africa*, Oliver and Boyd.

Dunmade, I., Madushele, N., Adedeji, P. A. and Akinlabi, E. T. (2019). A streamlined life cycle assessment of a coal-fired power plant: the South African case study. *Environmental Science and Pollution Research,* 26**,** 18484-18492.

Dutta, A. (2017). Fourier transform infrared spectroscopy. *Spectroscopic methods for nanomaterials characterization***,** 73-93.

Dutta, S., Hartkopf-Fröder, C., Witte, K., Brocke, R. and Mann, U. (2013). Molecular characterization of fossil palynomorphs by transmission micro-FTIR spectroscopy: Implications for hydrocarbon source evaluation. *International journal of coal geology,* 115**,** 13-23.

Duwiquet, H., Guillou-Frottier, L., Arbaret, L., Bellanger, M., Guillon, T. and Heap, M. J. (2021). Crustal Fault Zones (CFZ) as Geothermal Power Systems: A Preliminary 3D THM Model Constrained by a Multidisciplinary Approach. *Geofluids,* 2021.

Eberhard, A. and Naude, R. (2016). The South African renewable energy independent power producer procurement programme: A review and lessons learned. *Journal of Energy in Southern Africa,* 27**,** 1-14.

Egbobawaye, E. I. (2017). Petroleum Source-Rock Evaluation and Hydrocarbon Potential in Montney Formation Unconventional Reservoir, Northeastern British Columbia, Canada. *Natural Resources,* 8**,** 716.

Eia, U. (2011). International energy outlook. *US Energy Information Administration, Washington, DC*.

El Diasty, W. S., El Beialy, S., Khairy, A., El Attar, R. and Edwards, K. (2020). Palaeoenvironmental and source rock potential of the Turonian–Miocene sequence in the West Esh El Mellaha (SW margin of the Suez rift, Egypt): Insights from palynofacies, palynology and organic geochemistry. *Review of Palaeobotany and Palynology,* 276**,** 104190.

Elliott, E. G., Ettinger, A. S., Leaderer, B. P., Bracken, M. B. and Deziel, N. C. (2017). A systematic evaluation of chemicals in hydraulic-fracturing fluids and wastewater for reproductive and developmental toxicity. *Journal of exposure science & environmental epidemiology,* 27**,** 90-99.

Engelder, T., Cathles, L. M. and Bryndzia, L. T. (2014). The fate of residual treatment water in gas shale. *Journal of Unconventional Oil and Gas Resources,* 7**,** 33-48.

Eriksson, P. (1981). A palaeoenvironmental analysis of the Clarens Formation in the Natal Drakensberg. *South African Journal of Geology,* 84**,** 7-17.

Eskom, I. (2010). The energy efficiency series: Towards an energy efficient mining sector.

Essene, E. and Peacor, D. (1995). Clay mineral thermometry—a critical perspective. *Clays and clay minerals,* 43**,** 540-553.

Estrada, J. M. and Bhamidimarri, R. (2016). A review of the issues and treatment options for wastewater from shale gas extraction by hydraulic fracturing. *Fuel,* 182**,** 292-303.

Faure, K., Armstrong, R. A., Harris, C. and Willis, J. P. (1996). Provenance of mudstones in the Karoo Supergroup of the Ellisras basin, South Africa: Geochemical evidence. *Journal of African Earth Sciences,* 23**,** 189-204.

Faure, K., Harris, C. and Willis, J. P. (1995). A profound meteoric water influence on genesis in the Permian Waterberg Coalfield, South Africa; evidence from stable isotopes. *Journal of Sedimentary Research,* 65**,** 605-613.

Feiyu, W., Jing, G., Weiping, F. and Linyan, B. (2013). Evolution of overmature marine shale porosity and implication to the free gas volume. *Petroleum Exploration and Development,* 40**,** 819-824.

Ferriday, T. and Montenari, M. (2016). Chemostratigraphy and Chemofacies of Source Rock Analogues: A High-Resolution Analysis of Black Shale Successions from the Lower Silurian Formigoso Formation (Cantabrian Mountains, NW Spain). *Stratigraphy & Timescales.* Elsevier.

Fink, J. (2020). *Hydraulic fracturing chemicals and fluids technology*, Gulf Professional Publishing.

Flores, R. M., Rice, C. A., Stricker, G. D., Warden, A. and Ellis, M. S. (2008). Methanogenic pathways of coal-bed gas in the Powder River Basin, United States: the geologic factor. *International Journal of Coal Geology,* 76**,** 52-75.

Fort Worth, T. (2008). USA. 16–18 November 2008. *Richardson, TX, USA: Society of Petroleum Engineers*.

Frape, S., Blyth, A., Blomqvist, R., Mcnutt, R. and Gascoyne, M. (2003). Deep fluids in continents: II Crystalline rocks, In surface and groundwater, weathering, and Soils (ed. JI Drever) Vol. 5. Treatise on Geochemistry. Elsevier-Pergamon, Oxford.

Freixa, A., Rubol, S., Carles-Brangarí, A., Fernàndez-Garcia, D., Butturini, A., Sanchez-Vila, X. and Romaní, A. (2016). The effects of sediment depth and oxygen concentration on the use of organic matter: An experimental study using an infiltration sediment tank. *Science of the total environment,* 540**,** 20-31.

Froidl, F., Littke, R., Grohmann, S., Baniasad, A., Böcker, J., Hartkopf-Fröder, C. and Weniger, P. (2021). Kerogen composition and origin, oil and gas generation potential of the Berriasian Wealden Shales of the Lower Saxony Basin. *International Journal of Coal Geology,* 246**,** 103831.

Fulignati, P. (2020). Clay minerals in hydrothermal systems. *Minerals,* 10**,** 919.

Galeazzi, S., Point, O., Haddadi, N., Mather, J. and Druesne, D. (2010). Regional geology and petroleum systems of the Illizi–Berkine area of the Algerian Saharan Platform: An overview. *Marine and Petroleum Geology,* 27**,** 143-178.

Gallagher, S. J., Kitamura, A., Iryu, Y., Itaki, T., Koizumi, I. and Hoiles, P. W. (2015). The Pliocene to recent history of the Kuroshio and Tsushima Currents: a multi-proxy approach. *Progress in Earth and Planetary Science,* 2**,** 1-23.

Garner, M. (2019). Clay Mineralogy and Porosity Estimates of the Lower Permian Wolfcamp Shale.

Geel, C., De Wit, M., Booth, P., Schulz, H. and Horsfield, B. (2015). Palaeo-environment, diagenesis and characteristics of Permian black shales in the Lower Karoo Supergroup flanking the Cape Fold Belt near Jansenville, eastern Cape, South Africa: Implications for the shale gas potential of the Karoo Basin. *South African Journal of Geology,* 118**,** 249-274.

Geel, C., Schulz, H.-M., Booth, P., Dewit, M. and Horsfield, B. (2013). Shale gas characteristics of Permian black shales in South Africa: results from recent drilling in the Ecca Group (Eastern Cape). *Energy Procedia,* 40**,** 256-265.

Ghanizadeh, A., Bhowmik, S., Haeri-Ardakani, O., Sanei, H. and Clarkson, C. R. (2015). A comparison of shale permeability coefficients derived using multiple non-steady-state measurement techniques: Examples from the Duvernay Formation, Alberta (Canada). *Fuel,* 140**,** 371-387.

Golding, S. D., Boreham, C. J. and Esterle, J. S. (2013). Stable isotope geochemistry of coal bed and shale gas and related production waters: A review. *International Journal of Coal Geology,* 120**,** 24-40.

Gong, C. and Hollander, D. J. (1997). Differential contribution of bacteria to sedimentary organic matter in oxic and anoxic environments, Santa Monica Basin, California. *Organic Geochemistry,* 26**,** 545-563.

Gonzalez, L. D. C., Mastalerz, M. and Mendonça Filho, J. G. (2020). Application of organic facies and biomarkers in characterization of paleoenvironmental conditions and

maturity of sediments from the Codó Formation in the west-central part of the São Luís Basin, Brazil. *International Journal of Coal Geology,* 225**,** 103482.

Gou, Q., Xu, S., Hao, F., Yang, F., Zhang, B., Shu, Z., Zhang, A., Wang, Y., Lu, Y. and Cheng, X. (2019). Full-scale pores and micro-fractures characterization using FE-SEM, gas adsorption, nano-CT and micro-CT: A case study of the Silurian Longmaxi Formation shale in the Fuling area, Sichuan Basin, China. *Fuel,* 253**,** 167-179.

Groenewald, P., Grantham, G. and Watkeys, M. (1991). Geological evidence for a Proterozoic to Mesozoic link between southeastern Africa and Dronning Maud Land, Antarctica. *Journal of the Geological Society,* 148**,** 1115-1123.

Günzler, H. and Gremlich, H.-U. (2002). IR spectroscopy. An introduction.

Guo, C., Chang, H., Liu, B., He, Q., Xiong, B., Kumar, M. & Zydney, A. L. (2018). A combined ultrafiltration–reverse osmosis process for external reuse of Weiyuan shale gas flowback and produced water. *Environmental Science: Water Research & Technology,* 4**,** 942-955.

Guo, P., Wen, H., Gibert, L., Jin, J., Wang, J. and Lei, H. (2021). Deposition and diagenesis of the Early Permian volcanic-related alkaline playa-lake dolomitic shales, NW Junggar Basin, NW China. *Marine and Petroleum Geology,* 123**,** 104780.

Hackley, P. C. and Cardott, B. J. (2016). Application of organic petrography in North American shale petroleum systems: A review. *International Journal of Coal Geology,* 163**,** 8-51.

Hakimi, M. H., Abdullah, W. H., Alqudah, M., Makeen, Y. M. and Mustapha, K. A. (2016). Organic geochemical and petrographic characteristics of the oil shales in the Lajjun area, Central Jordan: origin of organic matter input and preservation conditions. *Fuel,* 181**,** 34-45.

Hakimi, M. H., Ahmed, A., Kahal, A. Y., Hersi, O. S., Al Faifi, H. J. and Qaysi, S. (2020). Organic geochemistry and basin modeling of Late Cretaceous Harshiyat Formation in the onshore and offshore basins in Yemen: Implications for effective source rock potential and hydrocarbon generation. *Marine and Petroleum Geology,* 122**,** 104701.

Hammond, G. P. and O'grady, Á. (2017). Indicative energy technology assessment of UK shale gas extraction. *Applied Energy,* 185**,** 1907-1918.

Han, C., Jiang, Z., Han, M., Wu, M. and Lin, W. (2016). The lithofacies and reservoir characteristics of the Upper Ordovician and Lower Silurian black shale in the Southern Sichuan Basin and its periphery, China. *Marine and Petroleum Geology,* 75**,** 181-191.

Han, S., Zhang, Y., Huang, J., Rui, Y. and Tang, Z. (2020). Elemental Geochemical Characterization of Sedimentary Conditions and Organic Matter Enrichment for Lower Cambrian Shale Formations in Northern Guizhou, South China. *Minerals,* 10**,** 793.

Hannon Jr, M. J., Tucker, Y. T. and Soeder, D. J. (2019). Quantifying the effects of gaseous pore pressure and net confining stress on low-permeability cores using the "RaSSCAL"

steady-state permeameter. *Journal of Petroleum Science and Engineering,* 179**,** 1136-1150.

Hanor, J. S. (2000). Barite–celestine geochemistry and environments of formation. *Reviews in Mineralogy and Geochemistry,* 40**,** 193-275.

Hastings, H. R. (2018). *Microfacies and Wireline Log Analysis of the Upper Leonardian First Bone Spring Carbonate Member, Delaware Basin, Southeast New Mexico.*

Hatch, J. and Leventhal, J. (1992). Relationship between inferred redox potential of the depositional environment and geochemistry of the Upper Pennsylvanian (Missourian) Stark Shale Member of the Dennis Limestone, Wabaunsee County, Kansas, USA. *Chemical Geology,* 99**,** 65-82.

Hayashi, K.-I., Fujisawa, H., Holland, H. D. and Ohmoto, H. (1997). Geochemistry of~ 1.9 Ga sedimentary rocks from northeastern Labrador, Canada. *Geochimica et Cosmochimica Acta,* 61**,** 4115-4137.

Hillel, D. and Hatfield, J. L. (2005). *Encyclopedia of Soils in the Environment*, Elsevier Amsterdam.

Hohner, A. K., Terry, L. G., Townsend, E. B., Summers, R. S. and Rosario-Ortiz, F. L. (2017). Water treatment process evaluation of wildfire-affected sediment leachates. *Environmental Science: Water Research and Technology,* 3**,** 352-365.

Hönisch, B. & Hemming, N. G. (2004). Ground-truthing the boron isotope-paleo-pH proxy in planktonic foraminifera shells: Partial dissolution and shell size effects. *Paleoceanography,* 19.

Hu, T., Pang, X., Jiang, S., Wang, Q., Zheng, X., Ding, X., Zhao, Y., Zhu, C. and Li, H. (2018). Oil content evaluation of lacustrine organic-rich shale with strong heterogeneity: A case study of the Middle Permian Lucaogou Formation in Jimusaer Sag, Junggar Basin, NW China. *Fuel,* 221**,** 196-205.

Huang, W.-L., Longo, J. M. and Pevear, D. R. (1993). An experimentally derived kinetic model for smectite-to-illite conversion and its use as a geothermometer. *Clays and Clay Minerals,* 41**,** 162-177.

Huang, Z., Wang, X., Yang, X., Zhu, R., Cui, J., Shi, W. and Zhu, Y. (2020). Paleoenvironment and Organic Matter Accumulation of the Upper Ordovician-Lower Silurian, in Upper Yangtze Region, South China: Constraints from Multiple Geochemical Proxies. *Energies,* 13**,** 858.

Huggett, J. (2015). Clay minerals, reference module in earth systems and environmental sciences. *Elsevier*.

Hunt, J. M. (1991). Generation of gas and oil from coal and other terrestrial organic matter. *Organic Geochemistry,* 17**,** 673-680.

İnan, S., Goodarzi, F., Mumm, A. S., Arouri, K., Qathami, S., Ardakani, O. H., İnan, T. and Tuwailib, A. A. (2016). The Silurian Qusaiba Hot Shales of Saudi Arabia: an integrated assessment of thermal maturity. *International Journal of Coal Geology,* 159**,** 107-119.

Jackson, R. B., Vengosh, A., Darrah, T. H., Warner, N. R., Down, A., Poreda, R. J., Osborn, S. G., Zhao, K. and Karr, J. D. (2013). Increased stray gas abundance in a subset of drinking water wells near Marcellus shale gas extraction. *Proceedings of the National Academy of Sciences,* 110**,** 11250-11255.

Jakob, M. and Steckel, J. C. (2014). How climate change mitigation could harm development in poor countries. *Wiley Interdisciplinary Reviews: Climate Change,* 5**,** 161-168.

Jali, N. P. (2019). *A study of the non-tax fiscal regime for shale gas development in South Africa.* University of Pretoria.

Jarvie, D. M., Hill, R. J. and Pollastro, R. M. (2005). Assessment of the gas potential and yields from shales: The Barnett Shale model. *Oklahoma Geological Survey Circular,* 110**,** 37-50.

Jarvie, D. M., Hill, R. J., Ruble, T. E. and Pollastro, R. M. (2007). Unconventional shale-gas systems: The Mississippian Barnett Shale of north-central Texas as one model for thermogenic shale-gas assessment. *AAPG bulletin,* 91**,** 475-499.

Jeffrey, L. (2005). Characterization of the coal resources of South Africa. *Journal of the Southern African Institute of Mining and Metallurgy,* 105**,** 95-102.

Johnson, J. E., Gerpheide, A., Lamb, M. P. and Fischer, W. W. 2014. O_2 constraints from Paleoproterozoic detrital pyrite and uraninite. *Bulletin,* 126**,** 813-830.

Johnson, M., Anhauesser, C. and Thomas, R. J. (2006a) The Geology of South Africa. Geological Society of South Africa.

Johnson, M., Van Vuuren, C., Hegenberger, W., Key, R. and Show, U. (1996). Stratigraphy of the Karoo Supergroup in southern Africa: an overview. *Journal of African Earth Sciences,* 23**,** 3-15.

Johnson, M. R., Van Vuuren, C. J., Visser, J. N., Cole, D. I., Wickens, H. D. V., Christie, A. D., Roberts, D. L. and Brandl, G. (2006b). Sedimentary rocks of the Karoo Supergroup. *The Geology of South Africa***,** 461-499.

Jones, M. (2017). Anomalous geothermal gradients and heat flow in the Limpopo Province, South Africa: Implications for geothermal energy exploration. *South African Journal of Geology 2017,* 120**,** 231-240.

Jong, J. and Kessler, F. L. (2019). The Setap Shale Formation on either side of the Baram Line Divide: Facies aspects and tectonic implications.

Kataka, M., Matiane, A. and Odhiambo, B. (2018). Chemical and mineralogical characterization of highly and less reactive coal from Northern Natal and Venda-Pafuri coalfields in South Africa. *Journal of African Earth Sciences,* 137**,** 278-285.

Kazak, E. S. and Kazak, A. V. (2020). Experimental features of cation exchange capacity determination in organic-rich mudstones. *Journal of Natural Gas Science and Engineering,* 83**,** 103456.

Kennedy, M. J., Löhr, S. C., Fraser, S. A. and Baruch, E. T. (2014). Direct evidence for organic carbon preservation as clay-organic nanocomposites in a Devonian black shale; from deposition to diagenesis. *Earth and Planetary Science Letters,* 388**,** 59-70.

Kessler, F. L. and Jong, J. (2017). The roles and implications of several prominent unconformities in Neogene sediments of the greater Miri area, NW Sarawak.

Knapp, L. J., Ardakani, O. H., Uchida, S., Nanjo, T., Otomo, C. and Hattori, T. (2020). The influence of rigid matrix minerals on organic porosity and pore size in shale reservoirs: Upper Devonian Duvernay Formation, Alberta, Canada. *International Journal of Coal Geology,* 227**,** 103525.

Kobylkin, A., Musina, V., Batugin, A., Ponomarev, V., Vorobyeva, O. and Vishnevskaya, E. (2019) Modelling of aerodynamic process for coal waste dump located in geodynamically dangerous zone. IOP Conference Series: Earth and Environmental Science. IOP Publishing, 012087.

Konschnik, K. E. and Boling, M. K. (2014). Shale gas development: a smart regulation framework. *Environmental science & technology,* 48**,** 8404-8416.

Kotov, S., Stolyarov, S., Cazeneuve, E., Walles, F. and Gadzhimirzaev, D. (2017). Looking Beyond the Wellbore: Formation Evaluation Mitigates Risk and Reduces Uncertainty in Multi-Stage Unconventional Completions. Abu Dhabi International Petroleum Exhibition & Conference, 2017. Society of Petroleum Engineers.

Kuila, U. and Prasad, M. (2011). Understanding pore-structure and permeability in shales. SPE Annual Technical Conference and Exhibition. Society of Petroleum Engineers.

Kuuskraa, V., Stevens, S. H. and Moodhe, K. D. (2013). *Technically Recoverable Shale Oil And Shale Gas Resources: An Assessment Of 137 Shale formations in 41 countries outside the United States*, US Energy Information Administration, US Department of Energy.

Lambert, T., Teodoru, C. R., Nyoni, F. C., Bouillon, S., Darchambeau, F., Massicotte, P. and Borges, A. V. (2016). Along-stream transport and transformation of dissolved organic matter in a large tropical river. *Biogeosciences,* 13**,** 2727-2741.

Laubach, S. E., Eichhubl, P., Hilgers, C. and Lander, R. (2010). Structural diagenesis. *Journal of Structural Geology,* 32**,** 1866-1872.

Laubach, S. E., Lander, R., Criscenti, L. J., Anovitz, L. M., Urai, J., Pollyea, R. M., Hooker, J. N., Narr, W., Evans, M. A. and Kerisit, S. N. (2019). The role of chemistry in fracture pattern development and opportunities to advance interpretations of geological materials. *Reviews of Geophysics,* 57**,** 1065-1111.

Li, C., Sessions, A. L., Kinnaman, F. S. and Valentine, D. L. (2009). Hydrogen-isotopic variability in lipids from Santa Barbara Basin sediments. *Geochimica et Cosmochimica Acta,* 73**,** 4803-4823.

Li, N., Feng, Z., Huang, H., Wang, X., Dong, Z. and Chen, Z. (2015). Lithological and diagenetic restrictions on biogenic gas generation in Songliao Basin inferred from grain size distribution and permeability measurement. *Bulletin of Canadian Petroleum Geology,* 63**,** 66-74.

Li, Y., Zhang, T., Ellis, G. S. and Shao, D. (2017). Depositional environment and organic matter accumulation of Upper Ordovician–Lower Silurian marine shale in the Upper Yangtze Platform, South China. *Palaeogeography, Palaeoclimatology, Palaeoecology,* 466**,** 252-264.

Li, Z.-X., Li, Y., Wang, D.-D., Wang, P.-L., Zhang, G.-C., Liu, H.-Y., Liu, Y., Li, X.-J. and Song, G.-Z. (2021). Source-to-sink system for peat accumulation in marginal basins of the South China Sea with the Qiongdongnan Basin as an example. *Australian Journal of Earth Sciences,* 68**,** 421-439.

Liang, C., Cao, Y., Liu, K., Jiang, Z., Wu, J. and Hao, F. (2018a). Diagenetic variation at the lamina scale in lacustrine organic-rich shales: Implications for hydrocarbon migration and accumulation. *Geochimica et Cosmochimica Acta,* 229**,** 112-128.

Liang, C., Jiang, Z., Cao, Y., Wu, J., Wang, Y. and Hao, F. (2018b). Sedimentary characteristics and origin of lacustrine organic-rich shales in the salinized Eocene Dongying Depression. *GSA Bulletin,* 130**,** 154-174.

Liang, M., Wang, Z., Gao, L., Li, C. and Li, H. (2017). Evolution of pore structure in gas shale related to structural deformation. *Fuel,* 197**,** 310-319.

Lianhua, H., Zhichao, Y., Xia, L., Senhu, L., Zhongying, Z., Zhi, Y., Songtao, W., Jingwei, C. and Zhang, L. (2021). Key geological factors controlling the estimated ultimate recovery of shale oil and gas: A case study of the Eagle Ford shale, Gulf Coast Basin, USA. *Petroleum Exploration and Development,* 48**,** 762-774.

Lindeberg, E., Grimstad, A.-A., Bergmo, P., Wessel-Berg, D., Torsæter, M. and Holt, T. (2017). Large scale tertiary CO_2 EOR in mature water flooded Norwegian oil fields. *Energy Procedia,* 114**,** 7096-7106.

Lipinski, M., Warning, B. and Brumsack, H.-J. (2003). Trace metal signatures of Jurassic/Cretaceous black shales from the Norwegian Shelf and the Barents Sea. *Palaeogeography, Palaeoclimatology, Palaeoecology,* 190**,** 459-475.

Littke, R., Krooss, B., Uffmann, A., Schulz, H.-M. and Horsfield, B. (2011). Unconventional gas resources in the Paleozoic of Central Europe. *Oil & Gas Science and Technology– Revue d'IFP Energies nouvelles,* 66**,** 953-977.

Liu, B., Mastalerz, M. and Schieber, J. (2022). SEM petrography of dispersed organic matter in black shales: A review. *Earth-Science Reviews,* 224**,** 103874.

Liu, B., Schieber, J., Mastalerz, M. and Teng, J. (2019a). Organic matter content and type variation in the sequence stratigraphic context of the Upper Devonian New Albany Shale, Illinois Basin. *Sedimentary Geology,* 383**,** 101-120.

Liu, F., Ellett, K., Xiao, Y. and Rupp, J. A. (2013). Assessing the feasibility of CO_2 storage in the New Albany Shale (Devonian–Mississippian) with potential enhanced gas recovery using reservoir simulation. *International Journal of Greenhouse Gas Control,* 17**,** 111-126.

Liu, H., Zhang, S., Song, G., Xuejun, W., Teng, J., Wang, M., Bao, Y., Yao, S., Wang, W. and Zhang, S. (2019b). Effect of shale diagenesis on pores and storage capacity in the Paleogene Shahejie Formation, Dongying Depression, Bohai Bay Basin, east China. *Marine and Petroleum Geology,* 103**,** 738-752.

Liu, J., Liu, T., Liu, H., He, L. and Zheng, L. (2021a). Overpressure caused by hydrocarbon generation in the organic-rich shales of the Ordos Basin. *Marine and Petroleum Geology***,** 105349.

Liu, W., Wu, J., Jiang, H., Zhou, Z., Luo, C., Wu, W., Li, X., Liu, S. and Deng, B. (2021b). Cenozoic exhumation and shale-gas enrichment of the Wufeng-Longmaxi formation in the southern Sichuan basin, western China. *Marine and Petroleum Geology,* 125**,** 104865.

Löhr, S., Baruch, E., Hall, P. and Kennedy, M. (2015). Is organic pore development in gas shales influenced by the primary porosity and structure of thermally immature organic matter? *Organic Geochemistry,* 87**,** 119-132.

Luyt, J. P. (2017). *The tectono-sedimentary history of the coal-bearing Tshipise Karoo basin.* University of Pretoria.

Lynch, F. L., Mack, L. E. and Land, L. S. (1997). Burial diagenesis of illite/smectite in shales and the origins of authigenic quartz and secondary porosity in sandstones. *Geochimica et Cosmochimica Acta,* 61**,** 1995-2006.

Ma, B., Lu, Y., Eriksson, K. A., Peng, L., Xing, F. and Li, X. (2021). Multiple organic–inorganic interactions and influences on heterogeneous carbonate-cementation patterns: Example from Silurian deeply buried sandstones, central Tarim Basin, north-western China. *Sedimentology,* 68**,** 670-696.

Machel, H. G. (2005). Investigations of burial diagenesis in carbonate hydrocarbon reservoir rocks. *Geoscience Canada*.

Malaza, N., Liu, K. and Zhao, B. (2016). Subsidence analysis and burial history of the Late Carboniferous to Early Jurassic Soutpansberg Basin, Limpopo Province, South Africa. *Acta Geologica Sinica‐English Edition,* 90**,** 2000-2007.

Malaza, N. M. (2014). *Basin analysis of the Soutpansberg and Tuli coalfields, Limpopo province of South Africa.* University of Fort Hare.

Mani, D., Kalpana, M., Patil, D. and Dayal, A. (2017). Organic matter in gas shales: origin, evolution, and characterization. *Shale Gas.* Elsevier.

Mao, J., Zhang, C., Yang, X. and Zhang, Z. (2018). Investigation on problems of wastewater from hydraulic fracturing and their solutions. *Water, Air, & Soil Pollution,* 229**,** 246.

Markl, D., Strobel, A., Schlossnikl, R., Bøtker, J., Bawuah, P., Ridgway, C., Rantanen, J., Rades, T., Gane, P. and Peiponen, K.-E. (2018). Characterisation of pore structures of pharmaceutical tablets: A review. *International journal of pharmaceutics,* 538**,** 188-214.

Martin, A. J., Solomon, S. T. and Hartmann, D. J. (1997). Characterization of petrophysical flow units in carbonate reservoirs. *AAPG bulletin,* 81**,** 734-759.

Martini, A., Walter, L., Budai, J., Ku, T. C., Kaiser, C. and Schoell, M. (1998). Genetic and temporal relations between formation waters and biogenic methane: Upper Devonian Antrim Shale, Michigan Basin, USA. *Geochimica et Cosmochimica Acta,* 62**,** 1699-1720.

Martini, A. M., Budai, J. M., Walter, L. M. and Schoell, M. (1996). Microbial generation of economic accumulations of methane within a shallow organic-rich shale. *Nature,* 383**,** 155-158.

März, C., Poulton, S. W., Beckmann, B., Küster, K., Wagner, T. and Kasten, S. (2008). Redox sensitivity of P cycling during marine black shale formation: dynamics of sulfidic and anoxic, non-sulfidic bottom waters. *Geochimica et Cosmochimica Acta,* 72**,** 3703-3717.

Mastalerz, M., Drobniak, A. and Stankiewicz, A. (2018a). Solid bitumen in unconventional systems: Origin, properties, and implications: A review. *International Journal of Coal Geology,* 195**,** 14-36.

Mastalerz, M., Drobniak, A. and Stankiewicz, A. B. (2018b). Origin, properties, and implications of solid bitumen in source-rock reservoirs: a review. *International Journal of Coal Geology,* 195**,** 14-36.

Mauter, M. S., Alvarez, P. J., Burton, A., Cafaro, D. C., Chen, W., Gregory, K. B., Jiang, G., Li, Q., Pittock, J. and Reible, D. (2014). Regional variation in water-related impacts of shale gas development and implications for emerging international plays. ACS Publications.

Mccarthy, K., Rojas, K., Niemann, M., Palmowski, D., Peters, K. and Stankiewicz, A. (2011). Basic petroleum geochemistry for source rock evaluation. *Oilfield Review,* 23**,** 32-43.

Mcdonald, S., Bishop, A. G., Prenzler, P. D. and Robards, K. (2004). Analytical chemistry of freshwater humic substances. *Analytica Chimica Acta,* 527**,** 105-124.

Mcintosh, J. C. and Ferguson, G. (2019). Conventional Oil—The Forgotten Part of the Water-Energy Nexus. *Groundwater,* 57**,** 669-677.

Mclennan, S. M. (2001). Relationships between the trace element composition of sedimentary rocks and upper continental crust. *Geochemistry, Geophysics, Geosystems,* 2.

Mclennan, S. M. (2018). Rare earth elements in sedimentary rocks: influence of provenance and sedimentary processes. *Geochemistry and mineralogy of rare earth elements***,** 169-200.

Mclennan, S. M., Taylor, S. R. and Hemming, S. R. (2006). *Composition, differentiation, and evolution of continental crust: constraints from sedimentary rocks and heat flow*, na.

Menefee, A. H. and Ellis, B. R. (2020). Wastewater management strategies for sustained shale gas production. *Environmental Research Letters,* 15**,** 024001.

Merven, B., Moyo, A., Stone, A. and Dane, A. (2014). Socio Economic Implications of Mitigation in the Power Sector Including Carbon Taxes in South Africa.

Mesquita, C. J. S., Dall'agnol, R. and Almeida, J. D. A. C. D. (2018). Mineral chemistry and crystallization parameters of the A-type Paleoproterozoic Bannach granite, Carajás province, Pará, Brazil. *Brazilian Journal of Geology,* 48**,** 575-601.

Metwally, Y. M. and Chesnokov, E. M. (2012). Clay mineral transformation as a major source for authigenic quartz in thermo-mature gas shale. *Applied Clay Science,* 55**,** 138-150.

Miall, A. D. (1977). A review of the braided-river depositional environment. *Earth-Science Reviews,* 13**,** 1-62.

Miall, A. D. (1985). Architectural-element analysis: a new method of facies analysis applied to fluvial deposits. *Earth-Science Reviews,* 22**,** 261-308.

Mignan, A., Broccardo, M., Wiemer, S. and Giardini, D. (2017). Induced seismicity closed-form traffic light system for actuarial decision-making during deep fluid injections. *Scientific reports,* 7**,** 1-10.

Mignan, A., Broccardo, M., Wiemer, S. and Giardini, D. (2018). Autonomous decision-making against induced seismicity in deep fluid injections. International Symposium on Energy Geotechnics, 2018. Springer, 369-376.

Mitchell, A. H. and Reading, H. G. (1969). Continental margins, geosynclines, and ocean floor spreading. *The Journal of Geology,* 77**,** 629-646.

Montañez, I. and Crossey, L. (2017). Diagenesis. *Encyclopedia of Geochemistry, WM White, Ed., Encyclopedia of Earth Sciences Series*.

Montañez, I. P. (1994). Late diagenetic dolomitization of Lower Ordovician, upper Knox carbonates: A record of the hydrodynamic evolution of the southern Appalachian Basin. *AAPG bulletin,* 78**,** 1210-1239.

Montanez, I. P. and Read, J. F. (1992). Fluid-rock interaction history during stabilization of early dolomites, upper Knox Group (Lower Ordovician), US Appalachians. *Journal of Sedimentary Research,* 62**,** 753-778.

Morad, S. (2009). *Carbonate cementation in sandstones: distribution patterns and geochemical evolution*, John Wiley & Sons.

Mosavel, H., Cole, D. and Siad, A. (2019). Shale gas potential of the Prince Albert Formation: A preliminary study. *South African Journal of Geology 2019,* 122**,** 541-554.

Mtimkulu, M. N. (2010). *A provisional basinal study of the Waterberg-Karoo, South Africa.* University of Pretoria.

Muffler, L. J. and White, D. E. (1969). Active metamorphism of upper Cenozoic sediments in the Salton Sea geothermal field and the Salton Trough, southeastern California. *Geol. Soc. Am., Bull.,* 80.

Mukhopadhyay, P., Goodarzi, F., Kruge, M. A. and Alimi, M. (1997). Comparison of source rock geochemistry of selected rocks from the Schei Point group and Ringnes formation, Sverdrup basin, arctic Canada. *International journal of coal geology,* 34**,** 225-260.

Nagarajan, R., Armstrong-Altrin, J., Kessler, F. and Jong, J. (2017). Petrological and geochemical constraints on provenance, paleoweathering, and tectonic setting of clastic sediments from the Neogene Lambir and Sibuti Formations, northwest Borneo. *Sediment provenance.* Elsevier.

Naseem, A., Tabasum, S., Zia, K. M., Zuber, M., Ali, M. and Noreen, A. (2016). Lignin-derivatives based polymers, blends and composites: A review. *International journal of biological macromolecules,* 93**,** 296-313.

Natalicchio, M., Pierre, F. D., Birgel, D., Brumsack, H., Carnevale, G., Gennari, R., Gier, S., Lozar, F., Pellegrino, L. and Sabino, M. (2019). Paleoenvironmental change in a precession-paced succession across the onset of the Messinian salinity crisis: insight from element geochemistry and molecular fossils. *Palaeogeography, Palaeoclimatology, Palaeoecology,* 518**,** 45-61.

Nengovhela, V. (2018). Petrophysical analysis of thermo-tectonic effects linked to Lower Jurassic dolerite intrusions in sedimentary rocks of the Main Karoo Basin, with implications for shale gas development in South Africa. *Port Elizabeth: Nelson Mandela University*.

Nengovhela, V., Linol, B., Bezuidenhout, L., Dhansay, T., Muedi, T. and De Wit, M. (2021). Shale gas leakage in lower Ecca shales during contact metamorphism by dolerite sill intrusions in the Karoo Basin, South Africa. *South African Journal of Geology 2021,* 124**,** 443-464.

Nhamo, G. (2011). *Green economy and climate mitigation: Topics of relevance to Africa*, African Books Collective.

Nolte, S., Geel, C., Amann-Hildenbrand, A., Krooss, B. M. and Littke, R. (2019). Petrophysical and geochemical characterization of potential unconventional gas shale reservoirs in the southern Karoo Basin, South Africa. *International Journal of Coal Geology,* 212**,** 103249.

Nyabeze, P. and Gwavava, O. (2016). Investigating heat and magnetic source depths in the Soutpansberg Basin, South Africa: exploring the Soutpansberg Basin Geothermal Field. *Geothermal Energy,* 4**,** 1-20.

Nyabeze, P. K. and Gwavava, O. (2018). Modelling and Inversion of Ground Magnetic and Electromagnetic Data for Delineation of Subsurface Structures at Siloam Hot Spring in the Soutpansberg Basin. *Journal of Geoscience and Environment Protection,* 6**,** 109-123.

Ola, P. S., Aidi, A. K. and Bankole, O. M. (2018). Clay mineral diagenesis and source rock assessment in the Bornu Basin, Nigeria: Implications for thermal maturity and source rock potential. *Marine and Petroleum Geology,* 89**,** 653-664.

Olivier, J., Venter, J. and Jonker, C. (2011). Thermal and chemical characteristics of hot water springs in the northern part of the Limpopo Province, South Africa. *Water Sa,* 37**,** 427-436.

Ortlepp, G. (2012). Limpopo coalfield. Mineral Deposits of Southern Africa, 1986. 2057-2061.

Palayangoda, S. S. & Nguyen, Q. P. (2012). An ATR-FTIR procedure for quantitative analysis of mineral constituents and kerogen in oil shale. *Oil Shale,* 29**,** 344.

Pan, Z. and Connell, L. D. (2015). Reservoir simulation of free and adsorbed gas production from shale. *Journal of Natural Gas Science and Engineering,* 22**,** 359-370.

Peters, K., Xia, X., Pomerantz, A. and Mullins, O. (2016. Geochemistry applied to evaluation of unconventional resources. *Unconventional oil and gas resources handbook.* Elsevier.

Pi, D.-H., Liu, C.-Q., Shields-Zhou, G. A. and Jiang, S.-Y. (2013). Trace and rare earth element geochemistry of black shale and kerogen in the early Cambrian Niutitang Formation in Guizhou province, South China: Constraints for redox environments and origin of metal enrichments. *Precambrian Research,* 225**,** 218-229.

Pieta, I. S., Rathi, A., Pieta, P., Nowakowski, R., Hołdynski, M., Pisarek, M., Kaminska, A., Gawande, M. B. and Zboril, R. (2019). Electrocatalytic methanol oxidation over Cu, Ni and bimetallic Cu-Ni nanoparticles supported on graphitic carbon nitride. *Applied Catalysis B: Environmental,* 244**,** 272-283.

Pietersen, K., Chevallier, L., Levine, A., Maceba, T., Gaffoor, Z. and Kanyerere, T. (2020). Prospective policy safeguards to mitigate hydrogeological risk pathways in advance of

shale gas development in the Karoo basin, South Africa. *Groundwater for Sustainable Development*, 100499.

Playter, T., Konhauser, K., Owttrim, G., Hodgson, C., Warchola, T., Mloszewska, A. M., Sutherland, B., Bekker, A., Zonneveld, J.-P. and Pemberton, S. G. (2017). Microbe-clay interactions as a mechanism for the preservation of organic matter and trace metal biosignatures in black shales. *Chemical Geology,* 459, 75-90.

Pollet, B. G., Staffell, I. and Adamson, K.-A. (2015). Current energy landscape in the Republic of South Africa. *International Journal of Hydrogen Energy,* 40, 16685-16701.

Pournou, A. (2020). *Biodeterioration of Wooden Cultural Heritage: Organisms and Decay Mechanisms in Aquatic and Terrestrial Ecosystems*, Springer Nature.

Pradhan, A. and Mbohwa, C. (2014). Development of biofuels in South Africa: Challenges and opportunities. *Renewable and Sustainable Energy Reviews,* 39, 1089-1100.

Qiao, J., Baniasad, A., Zieger, L., Zhang, C., Luo, Q. and Littke, R. (2021). Paleo-depositional environment, origin and characteristics of organic matter of the Triassic Chang 7 Member of the Yanchang Formation throughout the mid-western part of the Ordos Basin, China. *International Journal of Coal Geology,* 237, 103636.

Quigley, T. and Mackenzie, A. (1988). The temperatures of oil and gas formation in the sub-surface. *Nature,* 333, 549-552.

Rabbani, A. R. and Kamali, M. R. (2005). Source rock evaluation and petroleum geochemistry, offshore SW Iran. *Journal of Petroleum Geology,* 28, 413-428.

Rachold, V. and Hubberten, H.-W. (1999). Carbon isotope composition of particulate organic material in East Siberian rivers. *Land-ocean systems in the Siberian Arctic.* Springer.

Raffensperger, J. P. and Vlassopoulos, D. (1999). The potential for free and mixed convection in sedimentary basins. *Hydrogeology Journal,* 7, 505-520.

Ramaano, A. I. (2021a). Potential for tourism to promote indigenous resources for community development in Musina Municipality, Vhembe District, Limpopo Province, South Africa. *Forestry Economics Review*.

Ramaano, A. I. (2021b). Prospects of using tourism industry to advance community livelihoods in Musina municipality, Limpopo, South Africa. *Transactions of the Royal Society of South Africa,* 76, 201-215.

Ren, J., Guo, P., Peng, S. and Yang, C. (2016). Investigation on permeability of shale matrix using the lattice Boltzmann method. *Journal of Natural Gas Science and Engineering,* 29, 169-175.

Reolid, M., Duarte, L. and Rita, P. (2019). Changes in foraminiferal assemblages and environmental conditions during the T-OAE (Early Jurassic) in the northern Lusitanian Basin, Portugal. *Palaeogeography, Palaeoclimatology, Palaeoecology,* 520, 30-43.

Rexer, T. F., Mathia, E. J., Aplin, A. C. and Thomas, K. M. (2014). High-pressure methane adsorption and characterization of pores in Posidonia shales and isolated kerogens. *Energy & Fuels,* 28**,** 2886-2901.

Rice, D. D. and Claypool, G. E. (1981). Generation, accumulation, and resource potential of biogenic gas. *AAPG bulletin,* 65**,** 5-25.

Rogers, H. (2011). Shale gas—the unfolding story. *Oxford Review of Economic Policy,* 27**,** 117-143.

Rolf, T., Coltice, N. and Tackley, P. (2012). Linking continental drift, plate tectonics and the thermal state of the Earth's mantle. *Earth and Planetary Science Letters,* 351**,** 134-146.

Rowan, E. L., Engle, M. A., Kraemer, T. F., Schroeder, K. T., Hammack, R. W. and Doughten, M. W. (2015). Geochemical and isotopic evolution of water produced from Middle Devonian Marcellus shale gas wells, Appalachian basin, PennsylvaniaGeochemistry of Produced Water from Marcellus Shale Water, PA. *Aapg Bulletin,* 99**,** 181-206.

Saba, T. (2015). Hydraulic Fracturing: Data Analysis Methods to Identify Sources of Dissolved Gas and Chemical Compounds in Drinking Water Wells. *Introduction to Environmental Forensics***,** 513-529.

Sabino, M., Schefub, E., Natalicchio, M., Pierre, F. D., Birgel, D., Bortels, D., Schnetger, B. and Peckmann, J. (2020). Climatic and hydrologic variability in the northern Mediterranean across the onset of the Messinian salinity crisis. *Palaeogeography, Palaeoclimatology, Palaeoecology,* 545**,** 109632.

Schieber, J. (1992). A combined petrographical—geochemical provenance study of the Newland Formation, Mid-Proterozoic of Montana. *Geological Magazine,* 129**,** 223-237.

Scholvin, S. 2014. South Africa's energy policy: Constrained by nature and path dependency. *Journal of Southern African Studies,* 40**,** 185-202.

Schröder, S. and Grotzinger, J. (2007). Evidence for anoxia at the Ediacaran–Cambrian boundary: the record of redox-sensitive trace elements and rare earth elements in Oman. *Journal of the Geological Society,* 164**,** 175-187.

Schulz, H.-M., Linol, B., De Wit, M., Schuck, B., Schaepan, I. and Wirth, R. (2018). Early diagenetic signals archived in black shales of the Dwyka and Lower Ecca Groups of the southern Karoo Basin (South Africa): Keys to the deglaciation history of Gondwana during the Early Permian, and its effect on potential shale gas storage. *South African Journal of Geology 2018,* 121**,** 69-94.

Sebag, D., Copard, Y., Di-Giovanni, C., Durand, A., Laignel, B., Ogier, S. and Lallier-Vergès, E. (2006). Palynofacies as useful tool to study origins and transfers of particulate organic matter in recent terrestrial environments: Synopsis and prospects. *Earth-Science Reviews,* 79**,** 241-259.

Shamloo, N., Bakhtavar, E., Hewage, K. and Sadiq, R. (2020). Optimization of hydraulic fracturing wastewater management alternatives: A hybrid multi-objective linear programming model. *Journal of Cleaner Production*, 124950.

Siegel, D., Smith, B., Perry, E., Bothun, R. and Hollingsworth, M. (2015). Pre-drilling water-quality data of groundwater prior to shale gas drilling in the Appalachian Basin: Analysis of the Chesapeake Energy Corporation dataset. *Applied Geochemistry,* 63**,** 37-57.

Singh, P. K., Singh, M., Prachiti, P., Kalpana, M., Manikyamba, C., Lakshminarayana, G., Singh, A. K. and Naik, A. (2012). Petrographic characteristics and carbon isotopic composition of Permian coal: Implications on depositional environment of Sattupalli coalfield, Godavari Valley, India. *International Journal of Coal Geology,* 90**,** 34-42.

Sinha, S. K. and Sharma, A. (2016). Shale Gas in the Energy Basket. *Energy Security and Sustainability.* CRC Press.

Smith, M. B. and Montgomery, C. (2015). *Hydraulic Fracturing*, Crc Press.

Smithard, T., Bordy, E. and Reid, D. (2015). The effect of dolerite intrusions on the hydrocarbon potential of the lower Permian Whitehill Formation (Karoo Supergroup) in South Africa and southern Namibia: A preliminary study. *South African Journal of Geology,* 118**,** 489-510.

Soeder, D. J. 2018. The successful development of gas and oil resources from shales in North America. *Journal of Petroleum Science and Engineering,* 163**,** 399-420.

Srinivasan, K., Krishnamurthy, J. and Kaufman, P. 2019. Concerns and Clarifications for Drilled Uncompleted (DUC) Wells in the Williston Basin. *SPE Reservoir Evaluation & Engineering,* 22**,** 190-202.

Stewart, B. W., Chapman, E. C., Capo, R. C., Johnson, J. D., Graney, J. R., Kirby, C. S. and Schroeder, K. T. (2015). Origin of brines, salts and carbonate from shales of the Marcellus Formation: Evidence from geochemical and Sr isotope study of sequentially extracted fluids. *Applied Geochemistry,* 60**,** 78-88.

Steyn, L. (2015). The hunt for Karoo shale gas begins: The government plans to grant oil companies licences to begin exploring the Karoo for gas from as early as July this year. *Mail & Guardian*.

Stolper, D., Lawson, M., Davis, C., Ferreira, A., Neto, E. S., Ellis, G., Lewan, M., Martini, A. M., Tang, Y. and Schoell, M. (2014). Formation temperatures of thermogenic and biogenic methane. *Science,* 344**,** 1500-1503.

Stolper, D., Martini, A., Clog, M., Douglas, P., Shusta, S., Valentine, D., Sessions, A. and Eiler, J. (2015). Distinguishing and understanding thermogenic and biogenic sources of methane using multiply substituted isotopologues. *Geochimica et Cosmochimica Acta,* 161**,** 219-247.

Strąpoć, D., Mastalerz, M., Dawson, K., Macalady, J., Callaghan, A. V., Wawrik, B., Turich, C. and Ashby, M. (2011). Biogeochemistry of Microbial Coal-Bed Methane. *Annual Review of Earth and Planetary Sciences,* 39**,** 617-656.

Suboyin, A., Rahman, M. M. and Haroun, M. (2020). Hydraulic fracturing design considerations, water management challenges and insights for Middle Eastern shale gas reservoirs. *Energy Reports,* 6**,** 745-760.

Sun, Y., Wang, D., Tsang, D. C., Wang, L., Ok, Y. S. and Feng, Y. (2019). A critical review of risks, characteristics, and treatment strategies for potentially toxic elements in wastewater from shale gas extraction. *Environment international,* 125**,** 452-469.

Swart, P. K. (2015). The geochemistry of carbonate diagenesis: The past, present and future. *Sedimentology,* 62**,** 1233-1304.

Tang, X., Jiang, Z., Jiang, S. and Li, Z. (2016). Heterogeneous nanoporosity of the Silurian Longmaxi Formation shale gas reservoir in the Sichuan Basin using the QEMSCAN, FIB-SEM, and nano-CT methods. *Marine and Petroleum Geology,* 78**,** 99-109.

Tanikawa, W. and Shimamoto, T. (2006). Klinkenberg effect for gas permeability and its comparison to water permeability for porous sedimentary rocks. *Hydrology and Earth System Sciences Discussions,* 3**,** 1315-1338.

Tankard, A. J., Martin, M., Eriksson, K., Hobday, D., Hunter, D. and Minter, W. (2012). *Crustal evolution of southern Africa: 3.8 billion years of earth history*, Springer Science & Business Media.

Tanwar, R. and Mandal, U. K. (2019). Photocatalytic activity of $Ni_{0.5} Zn_{0.5} Fe_3O_4$ at polyaniline decorated BiOCl for azo dye degradation under visible light–integrated role and degradation kinetics interpretation. *RSC Advances,* 9**,** 8977-8993.

Teng, J., Mastalerz, M. and Liu, B. (2021). Petrographic and chemical structure characteristics of amorphous organic matter in marine black shales: Insights from Pennsylvanian and Devonian black shales in the Illinois Basin. *International Journal of Coal Geology,* 235**,** 103676.

Tetiker, S., Yalçın, H. and Bozkaya, Ö. (2015). Approaches to the low grade metamorphic history of the Karakaya complex by chlorite mineralogy and geochemistry. *Minerals,* 5**,** 221-246.

Theloy, C., Leonard, J. E. and Smith, S. C. (2019). An uncertainty approach to estimate recoverable reserves from the Bakken petroleum system in the North Dakota part of the Williston Basin. *AAPG Bulletin,* 103**,** 2295-2315.

Thyberg, B. and Jahren, J. (2011). Quartz cementation in mudstones: sheet-like quartz cement from clay mineral reactions during burial. *Petroleum Geoscience,* 17**,** 53-63.

Tinni, A., Fathi, E., Agarwal, R., Sondergeld, C., Akkutlu, Y. and Rai, C. (2012). Shale permeability measurements on plugs and crushed samples. SPE Canadian Unconventional Resources Conference. OnePetro.

Tissot, B. P. and Welte, D. H. (1978). Sedimentary processes and the accumulation of organic matter. *Petroleum Formation and Occurrence.* Springer.

Tissot, B. P. and Welte, D. H. (2013). *Petroleum formation and occurrence*, Springer Science & Business Media.

Trollip, H., Butler, A., Burton, J., Caetano, T. and Godinho, C. (2014). Energy Security in South Africa.

Tshibalo, A., Olivier, J. and Venter, J. South Africa Geothermal Country Update (2005-2009). Proceedings of the World Geothermal Congress, 2010.

Tuo, J., Wu, C. and Zhang, M. (2016). Organic matter properties and shale gas potential of Paleozoic shales in Sichuan Basin, China. *Journal of Natural Gas Science and Engineering,* 28**,** 434-446.

Tyson, R. (2012). *Sedimentary organic matter: organic facies and palynofacies*, Springer Science & Business Media.

Useia, U. (2013). Technically recoverable shale oil and shale gas resources: an assessment of 137 shale formations in 41 countries outside the United States. *USEIA, USA*.

Van Vuuren, D. P., Stehfest, E., Den Elzen, M. G., Kram, T., Van Vliet, J., Deetman, S., Isaac, M., Goldewijk, K. K., Hof, A. and Beltran, A. M. (2011). RCP2. 6: exploring the possibility to keep global mean temperature increase below 2 C. *Climatic Change,* 109**,** 95.

Vengosh, A., Jackson, R. B., Warner, N., Darrah, T. H. and Kondash, A. (2014). A critical review of the risks to water resources from unconventional shale gas development and hydraulic fracturing in the United States. *Environmental science & technology,* 48**,** 8334-8348.

Vengosh, A., Warner, N., Jackson, R. and Darrah, T. (2013). The effects of shale gas exploration and hydraulic fracturing on the quality of water resources in the United States. *Procedia Earth and Planetary Science,* 7**,** 863-866.

Verdon, J. P. and Budge, J. (2018). Examining the Capability of Statistical Models to Mitigate Induced Seismicity during Hydraulic Fracturing of Shale Gas ReservoirsExamining the Capability of Statistical Models to Mitigate Induced Seismicity. *Bulletin of the Seismological Society of America,* 108**,** 690-701.

Walters, C. C. (2017). Origin of petroleum. *Springer Handbook of Petroleum Technology.* Springer.

Wang, B., Xiong, M., Wang, P. and Shi, B. (2020a). Chemical characterization in hydraulic fracturing flowback and produced water (HF-FPW) of shale gas in Sichuan of China. *Environmental Science and Pollution Research***,** 1-11.

Wang, C., Zhang, B., Hu, Q., Shu, Z., Sun, M. and Bao, H. (2019a). Laminae characteristics and influence on shale gas reservoir quality of lower Silurian Longmaxi Formation in the Jiaoshiba area of the Sichuan Basin, China. *Marine and Petroleum Geology,* 109**,** 839-851.

Wang, F. and Guo, S. (2020). Upper Paleozoic Transitional Shale Gas Enrichment Factors: A Case Study of Typical Areas in China. *Minerals,* 10**,** 194.

Wang, G. and Du, H. (2018). Rheological properties of KCl/Polymer type drilling fluids containing particulate loss prevention material. *Applied Rheology,* 28.

Wang, H., Xiao, E., Li, Y., Latif, K. and Riaz, M. (2018a). New Advances and Existed Problems for the Forming Mechanism of the Microbial Dolomite. *sedimentology,* 2**,** 5.

Wang, J., Liu, M., Bentley, Y., Feng, L. and Zhang, C. (2018b). Water use for shale gas extraction in the Sichuan Basin, China. *Journal of environmental management,* 226**,** 13-21.

Wang, J., Ryan, D. and Anthony, E. J. (2011). Reducing the greenhouse gas footprint of shale gas. *Energy Policy,* 39**,** 8196-8199.

Wang, N., Wen, L., Li, M., Dai, X., Xu, Y., Ming, Y. and Yang, S. (2021). The origin of abnormally 13C-depleted organic carbon isotope signatures in the early Cambrian Yangtze Platform. *Marine and Petroleum Geology,* 128**,** 105051.

Wang, Q., Chen, X., Jha, A. N. and Rogers, H. (2014). Natural gas from shale formation–the evolution, evidences and challenges of shale gas revolution in United States. *Renewable and Sustainable Energy Reviews,* 30**,** 1-28.

Wang, Q., Guo, H., Wang, H., Urynowicz, M. A., Hu, A., Yu, C.-P., Fallgren, P., Jin, S., Zheng, H. and Zeng, R. J. (2019b). Enhanced production of secondary biogenic coalbed natural gas from a subbituminous coal treated by hydrogen peroxide and its geochemical and microbiological analyses. *Fuel,* 236**,** 1345-1355.

Wang, X., Ding, W., Cui, L., Wang, R., He, J., Li, A., Gu, Y., Liu, J., Xiao, Z. and Fu, F. (2018c). The developmental characteristics of natural fractures and their significance for reservoirs in the Cambrian Niutitang marine shale of the Sangzhi block, southern China. *Journal of Petroleum Science and Engineering,* 165**,** 831-841.

Wang, Y., Shardt, N., Lu, C., Li, H., Elliott, J. A. and Jin, Z. (2020b). Validity of the Kelvin equation and the equation-of-state-with-capillary-pressure model for the phase behavior of a pure component under nanoconfinement. *Chemical Engineering Science,* 226**,** 115839.

Warren, J. K. (1983). Pedogenic calcrete as it occurs in Quaternary calcareous dunes in coastal South Australia. *Journal of Sedimentary Research,* 53**,** 787-796.

Washburn, K. E. (2015). Rapid geochemical and mineralogical characterization of shale by laser-induced breakdown spectroscopy. *Organic Geochemistry,* 83**,** 114-117.

Washburn, K. E. and Birdwell, J. E. (2013). Multivariate analysis of ATR-FTIR spectra for assessment of oil shale organic geochemical properties.*Organic geochemistry,* 63**,**1-7.

Wei, J., Wang, Y., Wang, G., Wei, Z. and He, W. (2021). Geochemistry and shale gas potential of the lower Permian marine-continental transitional shales in the Eastern Ordos Basin. *Energy Exploration & Exploitation,* 39**,** 738-760.

Wen, H., Zheng, R., Tang, F., Zheng, A., Sang, T., Chen, S., Li, G. and Li, Z. (2008). Reconstruction and analysis of paleosalanity and paleoenvironment of the Chang 6 member in the Gengwan region, Ordos basin. *Journal of Mineralogy and Petrology,* 28**,** 114-120.

Whiticar, M. J. (1996). Stable isotope geochemistry of coals, humic kerogens and related natural gases. *International Journal of Coal Geology,* 32**,** 191-215.

Wood, J. M., Sanei, H., Curtis, M. E. and Clarkson, C. R. (2015). Solid bitumen as a determinant of reservoir quality in an unconventional tight gas siltstone play. *International Journal of Coal Geology,* 150**,** 287-295.

Worden, R., Utley, J. E., Butcher, A. R., Griffiths, J., Wooldridge, L. and Lawan, A. (2020). Improved imaging and analysis of chlorite in reservoirs and modern day analogues: new insights for reservoir quality and provenance. *Geological Society, London, Special Publications,* 484**,** 189-204.

Wu, C., Tuo, J., Zhang, M., Liu, Y., Xing, L., Gong, J. and Qiu, J. (2017). Multiple controlling factors of lower Palaeozoic organic-rich marine shales in the Sichuan Basin, China: Evidence from minerals and trace elements. *Energy Exploration & Exploitation,* 35**,** 627-644.

Wu, C., Tuo, J., Zhang, M., Sun, L., Qian, Y. and Liu, Y. (2016). Sedimentary and residual gas geochemical characteristics of the Lower Cambrian organic-rich shales in Southeastern Chongqing, China. *Marine and Petroleum Geology,* 75**,** 140-150.

Wu, J., Liang, C., Jiang, Z. and Zhang, C. (2019). Shale reservoir characterization and control factors on gas accumulation of the Lower Cambrian Niutitang shale, Sichuan Basin, South China. *Geological Journal,* 54**,** 1604-1616.

Xi, Z., Tang, S. and Wang, J. (2018). The reservoir characterization and shale gas potential of the Niutitang formation: Case study of the SY well in northwest Hunan Province, South China. *Journal of Petroleum Science and Engineering,* 171**,** 687-703.

Xia, X., Chen, J., Braun, R. and Tang, Y. (2013). Isotopic reversals with respect to maturity trends due to mixing of primary and secondary products in source rocks. *Chemical Geology,* 339**,** 205-212.

Xiong, Y., Zhang, L., Chen, Y., Wang, X., Li, Y., Wei, M., Jiang, W. and Lei, R. (2016). The origin and evolution of thermogenic gases in organic-rich marine shales. *Journal of Petroleum Science and Engineering,* 143**,** 8-13.

Xu, L., Yang, K., Wei, H., Liu, L., Li, X., Chen, L., Xu, T. and Wang, X. (2021). Diagenetic evolution sequence and pore evolution model of Mesoproterozoic Xiamaling organic-rich shale in Zhangjiakou, Hebei, based on pyrolysis simulation experiments. *Marine and Petroleum Geology,* 132**,** 105233.

Yang, Y.-R., Liu, X.-C., Zhang, H., Zhai, G.-Y., Zhang, J.-D., Hu, Z.-F., Bao, S.-J., Zhang, C., Wang, X.-H. and Yang, X. (2019). A review and research on comprehensive characterization of microscopic shale gas reservoir space. *China Geology,* 2**,** 541-556.

Ye, Y., Tang, S. and Xi, Z. (2020). Brittleness Evaluation in Shale Gas Reservoirs and Its Influence on Fracability. *Energies,* 13**,** 388.

Yeblen, D. R. (2018). Electron microscopy applied to nonstoichiometry, polysomatism, and replacement reactions in minerals. *Minerals and Reactions at the Atomic Scale***,** 181-230.

Yin, J., Xu, C., Hao, F., Wang, Q., Miao, Q., Wang, Z. and Zou, H. (2020). Controls on organic matter enrichment in source rocks of the Shahejie Formation in the southwestern Bozhong Sag, Bohai Bay Basin, China. *Palaeogeography, Palaeoclimatology, Palaeoecology,* 560**,** 110026.

Yu, X., Li, S. and Li, S. (2018). Reservoir Diagenesis. *Clastic Hydrocarbon Reservoir Sedimentology.* Springer.

Yuan, G., Cao, Y., Gluyas, J. and Jia, Z. (2017). Reactive transport modeling of coupled feldspar dissolution and secondary mineral precipitation and its implication for diagenetic interaction in sandstones. *Geochimica et Cosmochimica Acta,* 207**,** 232-255.

Yuan, G., Cao, Y., Schulz, H.-M., Hao, F., Gluyas, J., Liu, K., Yang, T., Wang, Y., Xi, K. and Li, F. (2019a). A review of feldspar alteration and its geological significance in sedimentary basins: From shallow aquifers to deep hydrocarbon reservoirs. *Earth-science reviews,* 191**,** 114-140.

Yuan, G., Cao, Y., Zan, N., Schulz, H.-M., Gluyas, J., Hao, F., Jin, Q., Liu, K., Wang, Y. and Chen, Z. (2019b). Coupled mineral alteration and oil degradation in thermal oil-water-feldspar systems and implications for organic-inorganic interactions in hydrocarbon reservoirs. *Geochimica et Cosmochimica Acta,* 248**,** 61-87.

Zaarur, S., Affek, H. P. and Brandon, M. T. (2013). A revised calibration of the clumped isotope thermometer. *Earth and Planetary Science Letters,* 382**,** 47-57.

Zhai, G.-Y., Wang, Y.-F., Zhou, Z., Yu, S.-F., Chen, X.-L. and Zhang, Y.-X. (2018). Exploration and research progress of shale gas in China. *China Geology,* 1**,** 257-272.

Zhang, C., Pathegama Gamage, R., Perera, M. S. A. and Zhao, J. (2017a). Characteristics of clay-abundant shale formations: use of CO2 for production enhancement. *Energies,* 10**,** 1887.

Zhang, F.-Q., Dilek, Y., Chen, H.-L., Yang, S.-F. and Meng, Q.-A. (2017b). Structural architecture and stratigraphic record of Late Mesozoic sedimentary basins in NE China: Tectonic archives of the Late Cretaceous continental margin evolution in East Asia. *Earth-Science Reviews,* 171**,** 598-620.

Zhang, J.-F., Zhai, G.-Y., Wang, D.-M., Bao, S.-J., Chen, K., Li, H.-H., Song, T., Wang, P. and Zhou, Z. (2020a). Tectonic evolution of the Huangling dome and its control effect on shale gas preservation in the north margin of the Yangtze Block, South China. *China Geology,* 3**,** 28-37.

Zhang, K., Liu, R., Liu, Z., Li, B., Han, J. and Zhao, K. (2020b). Influence of volcanic and hydrothermal activity on organic matter enrichment in the Upper Triassic Yanchang Formation, southern Ordos Basin, Central China. *Marine and Petroleum Geology,* 112**,** 104059.

Zhang, M., Tang, Q., Cao, C., Lv, Z., Zhang, T., Zhang, D., Li, Z. and Du, L. (2018a). Molecular and carbon isotopic variation in 3.5 years shale gas production from Longmaxi Formation in Sichuan Basin, China. *Marine and Petroleum Geology,* 89**,** 27-37.

Zhang, S., Hu, X., Han, Z., Li, J. and Garzanti, E. (2018b). Climatic and tectonic controls on Cretaceous-Palaeogene sea-level changes recorded in the Tarim epicontinental sea. *Palaeogeography, Palaeoclimatology, Palaeoecology,* 501**,** 92-110.

Zhang, S., Zhang, B., Bian, L., Jin, Z., Wang, D. and Chen, J. (2007). The Xiamaling oil shale generated through Rhodophyta over 800 Ma ago. *Science in China Series D: Earth Sciences,* 50**,** 527-535.

Zhang, W., Zhu, Q., Zhan, H., Huang, G. and Wang, Q. (2020c). A Critical Review of non-Darcian Flow and Future Challenges. *Earth and Space Science Open Archive ESSOAr*.

Zhang, Y., He, Z., Jiang, S., Lu, S., Xiao, D., Chen, G. and Zhao, J. (2018c). Factors affecting shale gas accumulation in overmature shales case study from lower Cambrian shale in western Sichuan Basin, South China. *Energy & Fuels,* 32**,** 3003-3012.

Zhao, J., Jin, Z., Jin, Z., Geng, Y., Wen, X. and Yan, C. (2016). Applying sedimentary geochemical proxies for paleoenvironment interpretation of organic-rich shale

deposition in the Sichuan Basin, China. *International Journal of Coal Geology,* 163**,** 52-71.

Zhiltsov, S. S. and Semenov, A. (2016a). Shale gas: history of development. *Shale Gas: Ecology, Politics, Economy.* Springer.

Zhiltsov, S. S. and Semenov, A. V. (2016b). The Role of Shale Gas in the Global Energy. *Shale Gas: Ecology, Politics, Economy.* Springer.

Zhu, H., Ju, Y., Qi, Y., Huang, C. and Zhang, L. (2018). Impact of tectonism on pore type and pore structure evolution in organic-rich shale: Implications for gas storage and migration pathways in naturally deformed rocks. *Fuel,* 228**,** 272-289.

Zieliński, M. (2012). Conodont thermal alteration patterns in Devonian and Carboniferous rocks of the Ahnet and Mouydir basins (southern Algeria). *Marine and petroleum geology,* 38**,** 166-176.

Zumberge, J., Ferworn, K. and Brown, S. (2012). Isotopic reversal ('rollover') in shale gases produced from the Mississippian Barnett and Fayetteville formations. *Marine and Petroleum Geology,* 31**,** 43-52.

Zuo, X., Li, C., Zhang, J., Ma, G. and Chen, P. (2020). Geochemical characteristics and depositional environment of the Shahejie Formation in the Binnan Oilfield, China. *Journal of Geophysics and Engineering,* 17**,** 539-551.

APPENDICES

APPENDIX-A: Results of Major Elements

Sample name		Meas. date/time	Al2O3	CaO	Cr2O3	Fe2O3	K2O	MgO	MnO	Na2O	P2O5	SiO2	TiO2	L.O.I.	Sum Of Conc.
PANalytical															
Results quantitative - MajorBasic32+Zn															
Major element analysis by XRF, Rh Tube, 3kWatt															
BDL = Below Detection Limit															
Note: LOI = weight loss or gain at 1000ºC.															
LOI (loss on ignition) includes the total of volatiles content of the rock (including the water combined to the lattice of silicate minerals) and the gain on ignition related to the oxidation of the rock (mostly due to Fe).															
Sample name		**Meas. date/time**	**Al2O3**	**CaO**	**Cr2O3**	**Fe2O3**	**K2O**	**MgO**	**MnO**	**Na2O**	**P2O5**	**SiO2**	**TiO2**	**L.O.I.**	**Sum Of Conc.**
			(%)	(%)	(%)	(%)	(%)	(%)	(%)	(%)	(%)	(%)	(%)	**(%)**	(%)
BH-MD1	MajorBasic32+Zn	2021/01/28 17:27	19,99	0,22	bdl	0,88	1,64	0,27	0,01	0,14	0,04	51,90	0,71	**25,00**	100,80
BH-MD2	MajorBasic32+Zn	2021/01/28 17:37	20,30	0,21	bdl	0,88	1,65	0,28	0,01	0,15	0,04	51,08	0,73	**24,94**	100,27
BH-MD3	MajorBasic32+Zn	2021/01/28 17:46	19,37	0,20	bdl	0,85	1,59	0,25	0,01	0,14	0,04	50,86	0,69	**25,05**	99,05
BH-MD4	MajorBasic32+Zn	2021/01/28 17:56	19,66	0,21	bdl	0,88	1,59	0,27	0,01	0,12	0,04	50,50	0,70	**25,08**	99,06
BH-MD5	MajorBasic32+Zn	2021/01/28 18:06	20,10	0,21	bdl	0,86	1,63	0,28	0,01	0,14	0,04	51,37	0,71	**25,06**	100,41
BH-MD6	MajorBasic32+Zn	2021/01/28 18:15	19,62	0,21	bdl	0,87	1,61	0,27	0,01	0,14	0,04	50,78	0,70	**25,18**	99,43
BH-MD7	MajorBasic32+Zn	2021/01/28 18:25	20,27	0,21	bdl	0,90	1,66	0,27	0,01	0,14	0,04	51,51	0,73	**25,11**	100,85
BH-MD8	MajorBasic32+Zn	2021/01/28 18:34	20,19	0,21	bdl	0,91	1,64	0,27	0,01	0,13	0,04	51,03	0,73	**25,05**	100,21
BH-MD9	MajorBasic32+Zn	2021/01/28 18:44	20,21	0,21	bdl	0,91	1,65	0,27	0,00	0,14	0,04	51,10	0,73	**25,06**	100,32
BH-MD10	MajorBasic32+Zn	2021/01/28 18:53	20,32	0,21	bdl	0,94	1,66	0,29	0,01	0,14	0,04	51,57	0,73	**24,96**	100,87
BH-MK11	MajorBasic32+Zn	2021/01/29 10:45	29,17	0,28	bdl	1,10	0,98	0,12	0,01	0,11	0,22	52,26	1,19	**15,04**	100,48
BH-MK12	MajorBasic32+Zn	2021/01/29 10:54	29,24	0,28	bdl	1,16	0,98	0,13	0,01	0,11	0,22	52,45	1,19	**15,11**	100,88
BH-MK13	MajorBasic32+Zn	2021/01/29 11:04	29,16	0,28	bdl	1,13	0,98	0,12	0,01	0,10	0,22	52,18	1,20	**15,10**	100,48
BH-MK14	MajorBasic32+Zn	2021/01/29 11:13	29,23	0,29	bdl	1,12	0,97	0,13	0,01	0,11	0,21	52,18	1,19	**15,06**	100,50
BH-MK15	MajorBasic32+Zn	2021/01/29 11:23	29,19	0,28	bdl	1,13	0,97	0,13	0,01	0,10	0,21	52,26	1,19	**14,95**	100,42
BH-MK16	MajorBasic32+Zn	2021/01/29 11:32	29,12	0,28	bdl	1,14	0,98	0,13	0,01	0,10	0,21	52,50	1,19	**15,06**	100,72
BH-MK17	MajorBasic32+Zn	2021/01/29 11:42	29,14	0,29	bdl	1,11	0,97	0,13	0,01	0,12	0,21	52,30	1,18	**14,97**	100,43
BH-MK18	MajorBasic32+Zn	2021/01/29 11:52	29,11	0,28	bdl	1,12	0,97	0,13	0,01	0,09	0,21	52,34	1,18	**15,06**	100,50

APPENDIX A: *Continued*

Sample	Method	Date/Time													
BH-MK19	MajorBasic32+Zn	2021/01/29 12:01	29,25	0,28	bdl	1,12	0,98	0,13	0,01	0,10	0,22	52,25	1,18	**15,03**	100,55
BH-MK20	MajorBasic32+Zn	2021/01/29 12:11	29,18	0,28	bdl	1,09	0,98	0,13	0,01	0,10	0,21	52,37	1,19	**15,03**	100,57
Value in RED are outside our calibration range and might be extrapolated.															
Standards analysed with the samples:															
BE-N															
Basalt Reference values			10,05	14,03		12,84	1,40	13,15	0,20	3,18	1,06	38,38	2,59		96,88
BE-N std	MajorBasic32+Zn	2020/02/14 09:38	10,26	14,08	0,05	12,99	1,41	13,26	0,20	3,22	1,08	38,36	2,66		97,57
BE-N std	MajorBasic32+Zn	2020/02/19 09:57	10,21	14,08	0,05	12,97	1,41	13,32	0,20	3,18	1,08	38,56	2,64		97,70
BE-N std	MajorBasic32+Zn	2020/03/11 09:34	10,27	14,12	0,05	12,99	1,40	13,25	0,20	3,20	1,07	38,49	2,66		97,70
BE-N std	MajorBasic32+Zn	2020/03/23 13:16	10,24	14,09	0,05	13,02	1,42	13,26	0,20	3,21	1,08	38,40	2,66		97,63
BE-N std	MajorBasic32+Zn	2020/05/13 11:06	10,20	14,03	0,05	13,01	1,41	13,17	0,20	3,20	1,08	38,43	2,63		97,41
BEN std	MajorBasic32+Zn	2020/05/15 02:47	10,25	14,11	0,05	12,95	1,42	13,32	0,20	3,17	1,08	38,33	2,63		97,51
BE-N std	MajorBasic32+Zn	2020/05/25 12:05	10,25	14,12	0,05	12,99	1,41	13,26	0,20	3,18	1,08	38,51	2,64		97,69
BE-N std	MajorBasic32+Zn	2020/06/03 15:45	10,13	14,12	0,05	13,04	1,41	13,25	0,20	3,22	1,08	38,49	2,66		97,65
BE-N std	MajorBasic32+Zn	2020/06/08 16:12	10,24	14,07	0,04	12,97	1,41	13,19	0,20	3,20	1,08	38,43	2,65		97,48
BE-N std	MajorBasic32+Zn	2020/06/23 10:29	10,20	14,05	0,05	12,98	1,41	13,23	0,19	3,18	1,08	38,32	2,63		97,32
BE-N std	MajorBasic32+Zn	2020/07/29 10:58	10,24	14,12	0,05	13,02	1,41	13,19	0,20	3,21	1,07	38,38	2,65		97,54
BE-N std	MajorBasic32+Zn	2020/07/30 16:03	10,17	14,05	0,05	12,99	1,41	13,21	0,20	3,20	1,09	38,39	2,64		97,40
BE-N std	MajorBasic32+Zn	2020/08/04 15:15	10,23	14,13	0,05	12,99	1,40	13,21	0,20	3,21	1,08	38,50	2,64		97,64
BE-N std	MajorBasic32+Zn	2020/09/18 13:05	10,21	14,10	0,05	13,02	1,41	13,19	0,20	3,17	1,08	38,36	2,65		97,44
BE-N std	MajorBasic32+Zn	2020/09/21 14:39	10,22	14,05	0,05	13,03	1,41	13,25	0,19	3,23	1,08	38,35	2,63		97,49
BE-N std	MajorBasic32+Zn	2020/10/28 16:30	10,24	14,11	0,05	12,99	1,40	13,28	0,20	3,19	1,08	38,55	2,65		97,74
BE-N std	MajorBasic32+Zn	2020/11/11 16:42	10,15	14,06	0,05	13,00	1,40	13,22	0,19	3,21	1,06	38,36	2,63		97,33
BE-N std	MajorBasic32+Zn	2020/12/04 10:17	10,24	14,04	0,05	13,02	1,40	13,22	0,19	3,16	1,07	38,46	2,64		97,49
BE-N STD	MajorBasic32+Zn	2021/01/27 11:17	10,26	14,06	0,05	12,97	1,40	13,21	0,20	3,19	1,07	38,54	2,64		97,59
BE-N STD	MajorBasic32+Zn	2021/01/28 09:07	10,13	14,04	0,05	13,05	1,41	13,22	0,19	3,16	1,07	38,49	2,63		97,44

BE-N STD	MajorBasic32+Zn	2021/01/29 09:50	10,18	14,03	0,05	13,02	1,40	13,19	0,20	3,14	1,07	38,27	2,64		97,19
Average			10,22	14,08	0,05	13,00	1,41	13,23	0,20	3,19	1,08	38,43	2,64	#DIV/0!	97,52
Relative standard deviation (%)			1,65	0,36		1,25	0,58	0,63	1,19	0,41	1,14	0,11	2,10	#DIV/0!	0,66
JB-1			14,53	9,29	0,07	8,97	1,43	7,73	0,16	2,79	0,26	52,17	1,34		98,74
Basalt (depleted) Reference values															
JB-1 std	MajorBasic32+Zn	2020/02/14 09:47	14,00	9,35	0,06	8,93	1,44	7,91	0,15	2,90	0,27	52,91	1,30		99,22
JB-1 std	MajorBasic32+Zn	2020/02/19 10:06	14,10	9,33	0,06	8,92	1,43	7,96	0,16	2,95	0,28	52,88	1,30		99,37
JB-1 std	MajorBasic32+Zn	2020/03/11 09:43	14,05	9,28	0,06	8,95	1,45	7,95	0,16	2,93	0,27	52,88	1,31		99,29
JB-1 std	MajorBasic32+Zn	2020/03/23 13:26	14,07	9,33	0,06	8,95	1,44	7,97	0,16	2,93	0,28	52,85	1,30		99,34
JB-1 std	MajorBasic32+Zn	2020/05/13 11:15	14,04	9,32	0,06	8,95	1,44	7,99	0,16	2,92	0,27	53,01	1,32		99,48
JB-1 std	MajorBasic32+Zn	2020/05/15 03:12	14,09	9,36	0,07	8,95	1,44	7,95	0,16	2,93	0,28	53,01	1,31		99,55
JB-1 std	MajorBasic32+Zn	2020/05/25 12:15	14,05	9,30	0,06	8,97	1,44	7,99	0,16	2,91	0,27	52,77	1,31		99,23
JB-1 std	MajorBasic32+Zn	2020/06/03 15:54	15,04	9,32	0,06	8,98	1,43	7,95	0,16	2,96	0,27	52,13	1,30		99,60
JB-1 std	MajorBasic32+Zn	2020/06/08 16:21	15,04	9,36	0,06	8,97	1,43	7,96	0,16	2,92	0,28	52,15	1,31		99,64
JB-1 std	MajorBasic32+Zn	2020/06/23 10:38	15,08	9,36	0,07	8,95	1,45	7,95	0,16	2,90	0,28	52,19	1,31		99,70
JB-1 std	MajorBasic32+Zn	2020/07/29 11:07	14,06	9,34	0,06	8,96	1,43	7,90	0,16	2,93	0,28	52,99	1,30		99,41
JB-1 std	MajorBasic32+Zn	2020/07/30 16:12	14,02	9,30	0,06	8,96	1,44	7,95	0,16	2,94	0,28	52,15	1,31		98,57
JB-1 std	MajorBasic32+Zn	2020/08/04 15:25	15,01	9,38	0,06	8,95	1,44	7,93	0,16	2,95	0,27	52,03	1,31		99,49
JB-1 std	MajorBasic32+Zn	2020/09/18 13:14	14,95	9,29	0,06	8,98	1,44	7,89	0,16	2,92	0,27	52,19	1,31		99,46
JB-1 std	MajorBasic32+Zn	2020/09/21 14:49	14,94	9,30	0,07	8,97	1,44	7,92	0,16	2,94	0,27	52,01	1,30		99,32
JB-1 std	MajorBasic32+Zn	2020/10/28 16:39	15,07	9,35	0,06	9,00	1,43	7,92	0,16	2,93	0,28	52,15	1,30		99,65
JB-1 std	MajorBasic32+Zn	2020/11/11 16:51	14,93	9,30	0,06	8,98	1,44	7,91	0,17	2,90	0,28	52,00	1,30		99,27
JB-1 std	MajorBasic32+Zn	2020/12/04 10:26	14,97	9,30	0,06	9,01	1,42	7,95	0,16	2,95	0,28	51,98	1,29		99,37
JB-1 STD	MajorBasic32+Zn	2021/01/27 11:27	14,97	9,29	0,06	8,97	1,42	7,92	0,17	2,91	0,27	52,67	1,31		99,96

JB-1 STD	MajorBasic32+Zn	2021/01/28 09:16	14,93	9,30	0,06	8,97	1,42	7,89	0,16	2,95	0,28	51,88	1,30		99,14
JB-1 STD	MajorBasic32+Zn	2021/01/29 09:59	14,93	9,28	0,06	8,97	1,44	7,94	0,16	2,94	0,27	51,97	1,30		99,26
Average			14,59	9,32	0,06	8,96	1,44	7,94	0,16	2,93	0,28	52,42	1,30	#DIV/0!	99,40
Relative standard deviation (%)			0,40	0,33	9,66	0,07	0,40	2,69	0,30	4,98	5,86	0,48	2,63		0,67
BHVO-1															
Basalt Reference values			13,71	11,39	0,04	12,36	0,54	7,22	0,17	2,31	0,27	49,82	2,73	0,52	101,08
BHVO-1 monitor	MajorBasic32+Zn	2020/02/14 09:56	13,97	11,35	0,03	12,25	0,52	7,31	0,17	2,32	0,28	49,40	2,73	0,52	100,85
BHVO-1 monitor	MajorBasic32+Zn	2020/02/19 10:15	14,07	11,44	0,04	12,39	0,52	7,38	0,17	2,33	0,29	49,19	2,73	0,52	101,07
BHVO-1 monitor	MajorBasic32+Zn	2020/03/11 09:52	14,07	11,47	0,04	12,42	0,53	7,29	0,17	2,34	0,29	49,08	2,73	0,52	100,95
BHVO-1 monitor	MajorBasic32+Zn	2020/03/23 13:35	14,01	11,45	0,04	12,44	0,52	7,37	0,17	2,35	0,29	49,23	2,75	0,52	101,14
BHVO-1 monitor	MajorBasic32+Zn	2020/05/13 11:24	14,07	11,46	0,04	12,46	0,53	7,30	0,17	2,36	0,29	49,24	2,74	0,52	101,18
BHVO-1 std	MajorBasic32+Zn	2020/05/15 03:45	13,99	11,47	0,04	12,46	0,52	7,30	0,16	2,32	0,29	49,18	2,74	0,52	100,99
BHVO-1 monitor	MajorBasic32+Zn	2020/05/25 12:24	14,03	11,43	0,04	12,47	0,53	7,33	0,17	2,33	0,28	49,18	2,72	0,52	101,03
BHVO-1 monitor	MajorBasic32+Zn	2020/06/03 16:03	14,05	11,50	0,04	12,50	0,52	7,32	0,17	2,36	0,28	49,18	2,74	0,52	101,18
BHVO-1 monitor	MajorBasic32+Zn	2020/06/08 16:30	14,06	11,48	0,04	12,48	0,52	7,32	0,17	2,37	0,29	49,24	2,73	0,52	101,22
BHVO-1 monitor	MajorBasic32+Zn	2020/06/23 10:47	13,98	11,47	0,04	12,42	0,52	7,34	0,17	2,35	0,29	50,13	2,73	0,52	101,96
BHVO-1 monitor	MajorBasic32+Zn	2020/07/29 11:16	14,09	11,44	0,03	12,47	0,52	7,29	0,17	2,30	0,28	49,20	2,73	0,52	101,04
BHVO-1 monitor	MajorBasic32+Zn	2020/07/30 16:21	14,03	11,46	0,04	12,46	0,53	7,29	0,16	2,34	0,28	49,23	2,73	0,52	101,07
BHVO-1 monitor	MajorBasic32+Zn	2020/08/04 15:34	14,06	11,47	0,04	12,44	0,53	7,30	0,16	2,33	0,29	49,24	2,72	0,52	101,10
BHVO-1 monitor	MajorBasic32+Zn	2020/09/18 13:23	14,06	11,47	0,04	12,46	0,53	7,36	0,17	2,33	0,28	49,22	2,74	0,52	101,18
BHVO-1 monitor	MajorBasic32+Zn	2020/09/21 14:58	14,15	11,41	0,04	12,48	0,52	7,31	0,16	2,33	0,29	49,29	2,73	0,52	101,23
BHVO-1 monitor	MajorBasic32+Zn	2020/10/28 16:48	14,06	11,48	0,04	12,50	0,52	7,31	0,17	2,32	0,29	49,37	2,74	0,52	101,32
BHVO-1 monitor	MajorBasic32+Zn	2020/11/11 17:01	13,95	11,44	0,04	12,48	0,52	7,31	0,16	2,30	0,28	49,17	2,72	0,52	100,89
BHVO-1 monitor	MajorBasic32+Zn	2020/12/04 10:36	13,99	11,44	0,04	12,50	0,52	7,32	0,17	2,30	0,28	49,47	2,74	0,52	101,29

APPENDIX A: *Continued*

BHVO-1 STD	MajorBasic32+Zn	2021/01/27 11:45	13,84	11,45	0,04	12,48	0,53	7,29	0,17	2,32	0,27	50,16	2,73	0,52	101,80
BHVO-1 STD	MajorBasic32+Zn	2021/01/28 09:34	13,84	11,41	0,03	12,51	0,52	7,26	0,17	2,31	0,29	50,18	2,74	0,52	101,78
BHVO-1 STD	MajorBasic32+Zn	2021/01/29 10:17	13,11	11,42	0,04	12,43	0,52	7,26	0,17	2,32	0,29	50,18	2,72	0,52	100,98
Average			13,98	11,45	0,04	12,45	0,52	7,31	0,17	2,33	0,29	49,42	2,73	0,52	101,20
Relative standard deviation (%)			1,93	0,51		0,75	3,09	1,28	1,40	0,87	5,64	0,81	0,09		0,12
JG-1															
Granodiorite Reference values			**14,20**	**2,18**	**0,01**	**2,14**	**3,97**	**0,74**	**0,06**	**3,39**	**0,10**	**72,30**	**0,26**		**99,35**
JG-1 std	MajorBasic32+Zn	2020/02/14 09:10	14,68	2,17	bdl	2,10	4,00	0,66	0,06	3,48	0,09	72,23	0,26		99,73
JG-1 std	MajorBasic32+Zn	2020/02/19 09:30	14,70	2,17	bdl	2,08	3,99	0,67	0,07	3,50	0,09	72,01	0,26		99,54
JG-1 std	MajorBasic32+Zn	2020/03/11 09:07	14,78	2,16	0,01	2,09	4,01	0,67	0,07	3,43	0,09	72,03	0,26		99,60
JG-1 std	MajorBasic32+Zn	2020/03/23 12:49	14,70	2,16	0,01	2,09	3,99	0,68	0,07	3,55	0,09	72,20	0,26		99,80
JG-1 std	MajorBasic32+Zn	2020/05/13 10:28	14,72	2,17	0,01	2,09	3,98	0,67	0,06	3,50	0,09	72,05	0,26		99,60
JG-1 std	MajorBasic32+Zn	2020/05/15 01:15	14,77	2,17	0,01	2,08	4,02	0,67	0,06	3,50	0,09	72,30	0,25		99,92
JG-1 std	MajorBasic32+Zn	2020/05/25 11:18	14,71	2,15	0,01	2,10	3,99	0,66	0,06	3,53	0,09	72,98	0,26		100,54
JG-1 std	MajorBasic32+Zn	2020/06/03 15:07	14,72	2,16	0,01	2,09	4,00	0,68	0,06	3,50	0,09	72,17	0,26		99,74
JG-1 std	MajorBasic32+Zn	2020/06/08 15:35	14,70	2,14	bdl	2,10	4,00	0,68	0,06	3,51	0,09	72,27	0,26		99,81
JG-1 std	MajorBasic32+Zn	2020/06/23 09:53	14,69	2,17	bdl	2,09	4,00	0,68	0,06	3,56	0,09	72,15	0,26		99,75
JG-1 std	MajorBasic32+Zn	2020/07/29 10:21	14,72	2,16	bdl	2,10	3,98	0,67	0,07	3,45	0,09	72,29	0,26		99,79
JG-1 std	MajorBasic32+Zn	2020/07/30 15:26	14,78	2,16	bdl	2,09	3,99	0,67	0,07	3,52	0,09	72,30	0,26		99,93
JG-1 std	MajorBasic32+Zn	2020/08/04 14:39	14,86	2,16	0,01	2,10	4,01	0,66	0,06	3,47	0,10	72,32	0,26		100,01
JG-1 std	MajorBasic32+Zn	2020/09/18 12:28	14,72	2,16	bdl	2,09	3,98	0,66	0,06	3,47	0,10	72,97	0,26		100,47
JG-1 std	MajorBasic32+Zn	2020/09/21 14:02	14,68	2,16	0,01	2,09	3,97	0,68	0,07	3,47	0,09	72,34	0,25		99,81
JG-1 std	MajorBasic32+Zn	2020/10/28 15:53	14,68	2,16	bdl	2,11	3,99	0,66	0,06	3,54	0,09	72,23	0,26		99,78
JG-1 std	MajorBasic32+Zn	2020/11/11 15:47	14,72	2,16	bdl	2,11	4,01	0,67	0,06	3,51	0,09	72,23	0,26		99,82
JG-1 std	MajorBasic32+Zn	2020/12/04 09:41	14,77	2,15	0,01	2,11	4,00	0,66	0,06	3,48	0,09	72,50	0,26		100,09
JG-1 STD	MajorBasic32+Zn	2021/01/27 11:54	14,36	2,16	0,01	2,14	4,00	0,75	0,06	3,42	0,10	72,54	0,26		99,80

JG-1　STD	MajorBasic32+Zn	2021/01/28 09:43	14,74	2,18	0,01	2,12	4,02	0,67	0,06	3,52	0,10	72,27	0,25		99,94
JG-1　STD	MajorBasic32+Zn	2021/01/29 10:26	14,78	2,16	0,01	2,10	4,01	0,68	0,07	3,50	0,10	72,28	0,26		99,95
Average			14,71	2,16	0,01	2,10	4,00	0,67	0,06	3,50	0,09	72,32	0,26	#DIV/0!	99,87
Relative standard deviation (%)			3,59	0,85	6,38	1,94	0,67	8,99	0,00	3,11	5,15	0,03	0,58		0,53
Quality control for 2010-2011															
Average HUSG		1900/01/13 17:55	13,75	1,52	0,00	3,78	4,66	1,04	0,06	2,57	0,21	69,77	0,54	0,73	98,65
STDEV		1900/01/00 04:51	0,20	0,04	0,00	0,14	0,06	0,04	0,01	0,18	0,01	0,54	0,02	0,05	0,71
MIN		1900/01/13 00:57	13,04	1,48	0,00	3,64	4,55	0,94	0,05	2,30	0,20	68,42	0,52	0,53	97,23
MAX		1900/01/14 07:06	14,30	1,63	0,01	4,56	4,80	1,22	0,08	3,30	0,23	70,96	0,60	0,80	100,40
HUSG-1　std	MajorBasic32+Zn	2019/11/01 18:23	14,23	1,55	bdl	3,74	4,67	1,02	0,05	2,81	0,22	70,53	0,56	0,90	100,28
HUSG-1　std	MajorBasic32+Zn	2019/11/04 13:12	14,18	1,55	bdl	3,76	4,65	1,03	0,05	2,82	0,21	70,52	0,56	0,90	100,23
HUSG-1　std	MajorBasic32+Zn	2019/11/19 15:35	14,45	1,55	bdl	3,77	4,67	1,05	0,06	2,80	0,21	70,43	0,55	0,90	100,44
HUSG-1　std	MajorBasic32+Zn	2019/11/28 10:10	14,40	1,55	bdl	3,78	4,68	1,02	0,05	2,79	0,22	70,05	0,55	0,90	99,99
HUSG-1　std	MajorBasic32+Zn	2020/02/14 09:29	14,34	1,56	bdl	3,77	4,70	1,04	0,05	2,77	0,21	70,22	0,55	0,90	100,11
HUSG-1　std	MajorBasic32+Zn	2020/02/19 09:48	14,38	1,56	bdl	3,76	4,66	1,05	0,05	2,80	0,21	70,01	0,55	0,90	99,93
HUSG-1　std	MajorBasic32+Zn	2020/03/11 09:25	14,42	1,57	bdl	3,76	4,69	1,04	0,06	2,79	0,21	69,85	0,56	0,90	99,85
HUSG-1　std	MajorBasic32+Zn	2020/03/23 13:07	14,22	1,56	bdl	3,69	4,66	1,03	0,06	2,77	0,21	69,51	0,55	0,90	99,16
HUSG-1　std	MajorBasic32+Zn	2020/05/13 10:55	14,29	1,56	bdl	3,73	4,67	1,03	0,05	2,78	0,21	69,82	0,55	0,90	99,59
HUSG-1　std	MajorBasic32+Zn	2020/05/15 02:13	14,20	1,57	bdl	3,73	4,67	1,00	0,06	2,82	0,22	69,84	0,55	0,90	99,56
HUSG-1　std	MajorBasic32+Zn	2020/05/25 11:47	14,23	1,57	bdl	3,72	4,64	1,04	0,05	2,77	0,22	69,59	0,55	0,90	99,28
HUSG-1　std	MajorBasic32+Zn	2020/06/03 15:27	14,15	1,55	bdl	3,75	4,65	1,03	0,06	2,79	0,20	69,73	0,54	0,90	99,35
HUSG-1　std	MajorBasic32+Zn	2020/06/08 15:53	14,21	1,56	bdl	3,76	4,64	1,03	0,05	2,77	0,22	69,76	0,55	0,90	99,45
HUSG-1　std	MajorBasic32+Zn	2020/06/23 10:11	14,29	1,55	bdl	3,79	4,67	1,04	0,05	2,76	0,21	69,74	0,56	0,90	99,56
HUSG-1　std	MajorBasic32+Zn	2020/07/29 10:39	14,31	1,55	bdl	3,79	4,67	1,03	0,06	2,76	0,21	69,85	0,55	0,90	99,68
HUSG-1　std	MajorBasic32+Zn	2020/07/30 15:44	14,25	1,57	bdl	3,81	4,67	1,05	0,06	2,78	0,21	69,60	0,55	0,90	99,45

HUSG-1 std	MajorBasic32+Zn	2020/08/04 15:05	14,25	1,55	bdl	3,74	4,65	1,03	0,06	2,80	0,21	69,49	0,54	0,90	99,22
HUSG-1 std	MajorBasic32+Zn	2020/09/18 12:46	14,18	1,54	bdl	3,77	4,66	1,03	0,06	2,79	0,21	69,59	0,54	0,90	99,27
HUSG-1 std	MajorBasic32+Zn	2020/09/21 14:29	14,20	1,55	bdl	3,75	4,64	1,02	0,06	2,84	0,22	69,67	0,54	0,90	99,39
HUSG-1 std	MajorBasic32+Zn	2020/10/28 16:12	14,23	1,55	bdl	3,77	4,66	1,04	0,06	2,75	0,21	69,47	0,54	0,90	99,18
HUSG-1 std	MajorBasic32+Zn	2020/11/11 16:22	14,30	1,55	bdl	3,77	4,67	1,02	0,05	2,83	0,21	69,80	0,54	0,90	99,64
HUSG-1 std	MajorBasic32+Zn	2020/12/04 10:07	14,20	1,55	bdl	3,78	4,67	1,03	0,05	2,76	0,21	69,65	0,54	0,90	99,34
HUSG-1 STD	MajorBasic32+Zn	2021/01/27 11:36	14,24	1,54	bdl	3,79	4,67	1,04	0,05	2,80	0,21	69,73	0,54	0,80	99,41
HUSG-1 STD	MajorBasic32+Zn	2021/01/28 09:25	14,24	1,54	0,00	3,76	4,68	1,03	0,06	2,80	0,21	69,47	0,53	0,80	99,12
HUSG-1 STD	MajorBasic32+Zn	2021/01/29 10:08	14,21	1,56	0,00	3,78	4,68	1,02	0,05	2,79	0,22	69,90	0,53	0,80	99,54
Average			14,26	1,55	0,00	3,76	4,67	1,03	0,05	2,79	0,21	69,83	0,55	0,89	99,60
Relative standard deviation (%)			3,76	2,17	100,00	0,42	0,22	1,20	14,94	8,59	0,05	0,09	0,81	21,64	0,97
WITS-G															
Granite Reference values			11,53	1,51		3,58	4,46	0,10	0,05	2,97	0,04	74,53	0,29	0,08	99,14
WITS-G			11,73	1,44		3,43	4,29	0,21	0,03	2,39	0,05	74,26	0,29	0,07	98,19
WITS-G (AUG)			12,01	1,46		3,51	4,26	0,05	0,02	2,39	0,06	74,56	0,30	0,07	98,69
WITS-G (OCT)			11,52	1,47		3,47	4,33	0,00	0,05	2,37	0,03	73,57	0,28	0,07	97,14
WITS-G (DEC)			11,45	1,47		3,50	4,39	0,06	0,05	2,45	0,04	75,45	0,28	0,07	99,22
Average reference value			<u>11,65</u>	<u>1,47</u>	.	<u>3,50</u>	<u>4,34</u>	<u>0,08</u>	<u>0,04</u>	<u>2,51</u>	<u>0,04</u>	<u>74,47</u>	<u>0,29</u>	<u>0,07</u>	<u>98,48</u>
WITS-G std	MajorBasic32+Zn	2019/11/01 18:14	12,09	1,48	bdl	3,43	4,46	0,02	0,04	2,81	0,04	75,10	0,27	0,07	**99,81**
WITS-G std	MajorBasic32+Zn	2019/11/04 13:03	12,25	1,48	bdl	3,39	4,45	0,02	0,05	2,81	0,04	74,95	0,27	0,07	**99,78**
WITS-G std	MajorBasic32+Zn	2019/11/19 15:26	12,25	1,49	bdl	3,38	4,45	0,02	0,05	2,88	0,04	74,84	0,27	0,07	**99,74**
WITS-G std	MajorBasic32+Zn	2019/11/28 10:01	12,25	1,48	bdl	3,41	4,44	0,02	0,05	2,79	0,04	75,06	0,27	0,07	**99,88**

155

WITS-G std	MajorBasic32+Zn	2020/02/14 09:19	12,26	1,51	bdl	3,39	4,47	0,02	0,05	2,85	0,04	74,90	0,27	0,07	**99,83**
WITS-G std	MajorBasic32+Zn	2020/02/19 09:39	12,25	1,48	bdl	3,40	4,45	0,03	0,05	2,84	0,04	74,60	0,26	0,07	**99,47**
WITS-G std	MajorBasic32+Zn	2020/03/11 09:16	12,25	1,50	bdl	3,39	4,46	0,03	0,05	2,81	0,04	74,88	0,27	0,07	**99,75**
WITS-G std	MajorBasic32+Zn	2020/03/23 12:58	12,19	1,49	bdl	3,41	4,46	0,01	0,05	2,86	0,04	74,84	0,26	0,07	**99,68**
WITS-G std	MajorBasic32+Zn	2020/05/13 10:38	12,25	1,48	bdl	3,40	4,43	0,03	0,05	2,81	0,04	74,84	0,26	0,07	**99,66**
WITS-G std	MajorBasic32+Zn	2020/05/15 01:40	12,23	1,50	bdl	3,40	4,45	0,01	0,05	2,85	0,04	74,98	0,27	0,07	**99,85**
WITS-G std	MajorBasic32+Zn	2020/05/25 11:38	12,23	1,50	bdl	3,40	4,46	0,02	0,05	2,85	0,04	75,17	0,27	0,07	**100,06**
WITS-G std	MajorBasic32+Zn	2020/06/03 15:18	12,27	1,50	bdl	3,40	4,44	0,02	0,05	2,83	0,04	75,25	0,27	0,07	**100,14**
WITS-G std	MajorBasic32+Zn	2020/06/08 15:44	12,26	1,48	bdl	3,42	4,44	0,02	0,05	2,80	0,04	75,10	0,27	0,07	**99,95**
WITS-G std	MajorBasic32+Zn	2020/06/23 10:02	12,33	1,48	bdl	3,43	4,47	0,02	0,04	2,82	0,04	75,05	0,27	0,07	**100,02**
WITS-G std	MajorBasic32+Zn	2020/07/29 10:30	12,28	1,49	bdl	3,42	4,46	0,02	0,05	2,82	0,04	75,00	0,27	0,07	**99,92**
WITS-G std	MajorBasic32+Zn	2020/07/30 15:35	12,26	1,49	bdl	3,40	4,46	0,02	0,04	2,85	0,04	75,01	0,27	0,07	**99,91**
WITS-G std	MajorBasic32+Zn	2020/08/04 14:48	12,28	1,48	bdl	3,41	4,46	0,04	0,05	2,80	0,04	74,91	0,27	0,07	**99,81**
WITS-G std	MajorBasic32+Zn	2020/09/18 12:37	12,23	1,50	bdl	3,41	4,44	0,02	0,05	2,86	0,04	74,11	0,27	0,07	**99,00**
WITS-G std	MajorBasic32+Zn	2020/09/21 14:12	12,20	1,49	bdl	3,41	4,43	0,02	0,05	2,83	0,04	73,90	0,26	0,07	**98,70**
WITS-G std	MajorBasic32+Zn	2020/10/28 16:02	12,29	1,48	bdl	3,41	4,43	0,02	0,05	2,81	0,05	74,00	0,27	0,07	**98,88**
WITS-G std	MajorBasic32+Zn	2020/11/11 15:56	12,23	1,48	bdl	3,40	4,46	0,02	0,05	2,84	0,04	74,99	0,27	0,07	**99,85**
WITS-G std	MajorBasic32+Zn	2020/12/04 09:50	12,22	1,50	bdl	3,39	4,44	0,02	0,05	2,83	0,04	74,92	0,27	0,07	**99,75**
WITS-G STD	MajorBasic32+Zn	2021/01/27 12:03	11,64	1,49	bdl	3,39	4,46	0,01	0,05	2,84	0,04	75,14	0,27	0,07	**99,40**
WITS-G STD	MajorBasic32+Zn	2021/01/28 09:52	12,21	1,50	bdl	3,42	4,46	0,02	0,05	2,87	0,04	74,83	0,26	0,07	**99,73**
WITS-G STD	MajorBasic32+Zn	2021/01/29 10:35	12,23	1,47	bdl	3,40	4,46	0,02	0,05	2,85	0,05	74,23	0,27	0,07	**99,10**
Average			12,24	1,49	#DIV/0!	3,41	4,45	0,02	0,05	2,83	0,04	74,87	0,27	0,07	99,73

APPENDIX-B: Results of the Trace Elements

	Values in ppm	Sc	V	Cr	Co	Ni	Cu	Zn	Rb	Sr	Y	Zr
	Instrument DL	0,014	0,005	0,093	0,018	0,033	0,053	0,034	0,008	0,001	0,001	0,001
	Method DL (fusions)	0,516	0,145	1,444	0,428	1,000	0,932	0,944	0,087	0,035	0,018	0,048
Certified BHVO glass		**33,00**	**308,00**	**293,00**	**44,00**	**116,00**	**127,00**	**102,00**	**9,20**	**396,00**	**26,00**	**170,00**
	BHVO - 1	34,87	323,77	287,30	44,91	123,51	130,96	131,05	9,71	389,84	22,65	155,89
	BHVO - 2	31,17	322,00	292,92	44,45	133,24	130,80	118,05	10,26	393,29	25,32	171,89
	BHVO - 3	30,07	319,62	285,46	43,21	125,33	123,08	114,10	9,82	391,76	24,69	164,57
	BHVO - 4	31,64	322,69	286,24	43,87	120,48	126,58	123,26	9,47	388,54	22,25	156,50
	BHVO - 5	30,76	323,09	289,72	43,80	119,81	126,19	118,54	9,34	391,44	22,41	156,24
	Average Analysed	**31,70**	**322,23**	**288,33**	**44,05**	**124,48**	**127,52**	**121,00**	**9,72**	**390,97**	**23,47**	**161,02**
	% Deviation	*3,9*	*4,6*	*1,6*	*0,1*	*7,3*	*0,4*	*18,6*	*5,7*	*1,3*	*9,7*	*5,3*
Certified BCR glass		**33,00**	**425,00**	**17,00**	**38,00**	**13,00**	**21,00**	**125,00**	**47,00**	**342,00**	**35,00**	**184,00**
	BCR - 1	36,14	422,68	15,11	36,70	12,02	17,28	164,85	47,72	331,90	30,95	170,29
	BCR - 2	32,43	424,44	14,63	36,58	12,71	17,53	152,59	53,19	339,97	34,69	184,16
	BCR - 3	31,24	416,68	14,66	35,58	12,31	16,67	146,74	50,76	328,40	33,63	180,32
	BCR - 4	33,05	421,75	14,94	36,26	11,83	17,59	162,47	48,05	331,35	30,51	170,53
	BCR - 5	32,42	421,83	14,56	36,02	11,73	17,04	156,40	47,71	334,20	30,49	170,74
	Average Analysed	**33,05**	**421,48**	**14,78**	**36,23**	**12,12**	**17,22**	**156,61**	**49,49**	**333,16**	**32,05**	**175,21**
	% Deviation	*0,2*	*0,8*	*13,1*	*4,7*	*6,8*	*18,0*	*25,3*	*5,3*	*2,6*	*8,4*	*4,8*
Certified BHVO powder		**31,42**	**313,80**	**287,60**	**44,90**	**120,00**	**137,20**	**105,10**	**9,52**	**399,20**	**26,23**	**174,60**
	BHVOf - 1	32,27	294,07	270,07	38,88	117,03	122,12	93,89	8,44	342,60	23,69	156,37
	BHVOf - 2	30,41	302,37	285,52	42,52	127,65	124,79	99,95	8,97	370,00	25,82	167,96
	BHVOf - 3	31,46	301,19	275,06	42,63	127,84	145,40	95,25	9,05	363,73	25,49	172,56
	BHVOf - 4	32,01	307,52	278,91	41,86	130,15	134,02	104,18	9,29	371,76	25,61	174,00

	BHVOf - 5	30,80	306,33	279,88	41,90	128,81	135,60	101,76	9,04	372,47	25,88	171,50
	BHVOf - 6	31,69	304,01	293,45	42,26	135,82	132,99	100,77	10,06	374,86	25,90	170,76
	BHVOf - 7	31,44	305,67	278,65	42,13	130,70	133,04	103,25	9,26	372,68	25,73	172,22
	BHVOf - 8	31,01	307,65	283,17	42,99	128,77	131,67	105,28	9,70	372,91	26,66	173,68
	BHVOf - 9	31,17	306,34	282,99	41,25	125,73	126,01	102,17	9,53	373,91	25,26	171,17
	BHVOf - 10	31,14	305,66	288,67	41,60	130,99	128,19	103,75	9,35	373,34	25,67	172,25
	Average Analysed	**31,34**	**304,08**	**281,64**	**41,80**	**128,35**	**131,38**	**101,02**	**9,27**	**368,83**	**25,57**	**170,25**
	% Deviation	*0,3*	*3,1*	*2,1*	*6,9*	*7,0*	*4,2*	*3,9*	*2,6*	*7,6*	*2,5*	*2,5*
Certified BCR powder		**33,53**	**417,60**	**15,85**	**37,33**	**12,57**	**19,66**	**129,50**	**46,02**	**337,40**	**36,07**	**186,50**
	BCRf - 1	34,34	395,23	19,10	33,19	13,83	26,59	126,36	44,25	304,72	33,42	176,53
	BCRf - 2	32,09	399,11	16,99	34,45	13,80	21,83	130,58	46,05	318,20	34,52	182,08
	BCRf - 3	32,73	396,32	18,81	34,10	13,50	30,31	131,94	46,05	314,21	34,02	182,52
	BCRf - 4	33,60	402,70	18,12	35,40	15,23	26,97	139,48	47,17	315,71	34,58	185,63
	BCRf - 5	33,71	403,72	17,24	36,03	15,03	28,69	130,28	45,40	320,23	35,73	186,36
	BCRf - 6	33,02	402,13	19,34	35,02	15,57	26,09	133,62	46,97	319,02	35,14	183,99
	BCRf - 7	32,30	401,09	15,89	34,33	14,33	25,69	128,55	45,57	318,05	35,21	184,94
	BCRf - 8	32,27	396,88	17,27	34,80	14,85	23,63	130,41	47,65	317,88	35,19	183,57
	BCRf - 9	33,33	400,12	15,99	34,50	13,98	23,55	132,86	46,73	317,56	35,01	186,19
	BCRf - 10	32,35	400,28	16,44	34,28	14,25	23,07	133,74	46,42	318,52	35,25	186,18
	Average Analysed	**32,97**	**399,76**	**17,52**	**34,61**	**14,44**	**25,64**	**131,78**	**46,23**	**316,41**	**34,81**	**183,80**
	% Deviation	*1,7*	*4,3*	*10,5*	*7,3*	*14,9*	*30,4*	*1,8*	*0,4*	*6,2*	*3,5*	*1,4*
	MD1 - 1	12,46	83,66	48,61	11,36	14,63	22,07	94,85	100,27	97,62	31,63	200,85
	MD1 - 2	12,39	96,45	53,53	10,89	14,59	23,21	103,38	97,72	103,74	34,24	222,49
	MD10 - 1	12,41	91,20	52,85	10,13	19,36	33,14	121,63	102,26	99,62	33,22	208,18
	MD10 - 2	12,58	86,16	47,29	9,49	17,88	32,30	108,71	96,39	90,45	32,54	198,15
	MD2 - 1	12,51	84,40	52,28	10,01	15,07	17,83	92,30	98,37	94,86	30,47	204,16
	MD2 - 2	13,12	92,06	54,27	11,80	16,75	20,34	107,73	103,10	99,70	32,22	209,37
	MD3 - 1	12,34	75,55	49,68	9,13	15,94	22,15	90,64	90,50	90,35	29,84	185,03
	MD3 - 2	11,29	84,14	53,52	8,38	14,74	19,14	85,30	93,96	95,64	29,84	185,96

158

MD4 - 1	11,89	81,24	48,19	9,72	16,03	19,97	87,16	94,18	96,41	30,61	196,55
MD4 - 2	11,88	81,88	50,14	9,92	16,43	18,03	87,31	97,38	95,89	29,75	191,66
MD5 - 1	11,61	81,82	51,91	13,38	13,27	16,51	82,73	97,03	95,63	30,34	208,43
MD5 - 2	11,69	81,27	48,53	9,71	14,07	17,92	87,86	92,58	85,91	28,08	190,96
MD6 - 1	11,97	93,72	52,10	9,51	16,57	18,90	94,01	96,01	99,61	32,29	201,68
MD6 - 2	11,83	84,03	48,48	10,23	17,25	20,56	96,53	99,94	95,83	32,28	192,02
MD7 - 1	12,63	92,09	52,34	12,46	19,82	26,82	107,59	97,93	95,18	29,99	201,13
MD7 - 2	11,30	85,41	50,71	10,71	18,85	24,40	105,44	100,77	95,89	31,47	208,20
MD8 - 1	12,30	89,95	50,55	9,51	17,14	31,39	94,88	96,52	92,02	31,53	208,61
MD8 - 2	12,46	85,57	49,54	9,90	17,83	27,23	96,64	95,11	97,80	31,86	215,98
MD9 - 1	12,27	84,50	47,50	10,20	18,09	37,58	101,76	94,28	94,46	31,88	189,02
MD9 - 2	10,77	81,73	46,84	10,73	19,49	28,86	109,81	92,46	91,24	28,92	202,06
MK11 - 1	25,19	151,88	82,80	5,51	45,09	43,09	65,30	69,77	328,15	56,63	314,58
MK11 - 2	26,97	155,21	84,90	5,50	41,99	43,42	65,39	70,60	339,13	58,70	332,22
MK12 - 1	25,91	153,51	83,96	5,89	51,29	77,11	64,17	69,65	344,91	57,09	328,64
MK12 - 2	24,59	155,28	86,72	6,58	49,97	74,63	65,63	70,73	339,10	57,17	322,11
MK13 - 1	23,44	150,94	73,08	5,34	39,04	39,92	65,37	67,69	336,77	53,99	317,59
MK13 - 2	24,92	155,02	85,01	5,72	43,59	43,49	64,97	73,02	338,52	58,79	326,11
MK14 - 1	25,40	156,69	76,64	5,16	39,53	29,04	59,03	68,58	335,61	56,71	325,10
MK14 - 2	23,81	151,75	90,00	5,76	38,84	28,00	57,74	68,12	333,20	54,46	312,73
MK15 - 1	25,22	156,61	78,22	5,96	43,54	39,45	57,46	70,11	325,77	58,22	315,47
MK15 - 2	25,98	157,58	83,93	5,86	42,92	39,19	63,27	66,51	336,22	58,08	325,14
MK16 - 1	25,39	155,86	81,64	5,93	48,40	44,27	62,05	68,06	340,61	55,66	316,38
MK16 - 2	26,27	161,25	85,71	6,99	45,45	42,39	67,54	69,93	330,03	56,83	322,13
MK17 - 1	25,09	156,88	86,66	5,79	45,75	37,30	58,51	73,87	343,57	59,75	341,73
MK17 - 2	26,03	148,46	76,88	5,84	41,88	34,00	61,89	69,76	334,74	57,17	322,62
MK18 - 1	25,82	153,66	80,84	6,03	44,29	36,21	67,09	68,00	342,15	57,76	319,57
MK18 - 2	25,63	160,01	90,12	7,27	39,68	39,27	67,13	71,21	340,81	59,25	323,17
MK19 - 1	23,49	155,09	85,37	5,49	43,44	37,23	59,86	68,15	339,71	58,51	328,14
MK19 - 2	26,60	156,39	83,08	5,06	48,03	39,74	60,03	70,80	339,34	56,69	328,70

	MK20 - 1	23,45	156,02	85,12	4,85	39,50	33,12	61,89	73,00	333,74	56,50	316,50
	MK20 - 2	24,36	151,84	75,23	5,36	37,25	32,62	58,17	68,25	341,14	55,58	318,66

APPENDIX-B: *Continued*

	Values in ppm	Nb	Mo	Cs	Ba	La	Ce	Pr	Nd	Sm	Eu	Gd
	Instrument DL	0,000	0,002	0,004	0,004	0,001	0,001	0,001	0,002	0,002	0,001	0,002
	Method DL (fusions)	0,017	0,090	0,043	0,187	0,017	0,017	0,013	0,092	0,097	0,027	0,104
Certified BHVO glass		**18,30**	**3,80**	**0,10**	**131,00**	**15,20**	**37,60**	**5,35**	**24,50**	**6,10**	**2,07**	**6,16**
	BHVO - 1	16,33	4,04	0,11	128,84	14,26	35,03	5,35	24,50	6,13	2,08	6,16
	BHVO - 2	18,10	4,20	0,10	133,23	14,32	38,82	5,33	23,93	6,00	2,06	6,12
	BHVO - 3	17,48	4,04	0,10	128,07	13,96	37,39	5,25	22,55	5,68	2,03	5,74
	BHVO - 4	16,06	3,97	0,11	127,68	14,01	34,62	5,31	24,38	5,98	2,03	6,12
	BHVO - 5	16,08	3,90	0,10	128,44	14,14	34,54	5,35	24,50	6,07	2,06	6,16
	Average Analysed	**16,81**	**4,03**	**0,10**	**129,25**	**14,14**	**36,08**	**5,32**	**23,97**	**5,97**	**2,05**	**6,06**
	% Deviation	*8,1*	*6,1*	*0,1*	*1,3*	*7,0*	*4,0*	*0,6*	*2,2*	*2,1*	*0,9*	*1,6*
Certified BCR glass		**12,50**	**270,00**	**1,16**	**683,00**	**24,70**	**53,30**	**6,70**	**28,90**	**6,59**	**1,97**	**6,71**
	BCR - 1	11,09	247,02	1,11	662,79	23,15	48,80	6,85	28,52	6,41	1,99	6,59
	BCR - 2	12,18	261,54	1,12	681,87	23,50	54,55	6,90	27,59	6,44	1,98	6,50
	BCR - 3	11,85	248,02	1,07	658,41	22,66	52,28	6,60	26,26	5,96	1,91	6,33
	BCR - 4	10,82	245,69	1,11	661,27	22,93	48,37	6,72	28,24	6,46	1,94	6,59
	BCR - 5	10,88	244,33	1,12	657,70	23,02	48,73	6,75	28,47	6,50	1,95	6,71
	Average Analysed	**11,36**	**249,32**	**1,11**	**664,41**	**23,05**	**50,55**	**6,76**	**27,82**	**6,35**	**1,95**	**6,54**
	% Deviation	*9,1*	*7,7*	*4,7*	*2,7*	*6,7*	*5,2*	*0,9*	*3,8*	*3,6*	*0,8*	*2,5*
Certified BHVO powder		**18,53**	**1,06**	**0,10**	**134,40**	**15,44**	**38,08**	**5,42**	**24,78**	**6,17**	**2,05**	**6,29**
	BHVOf - 1	16,13	1,26	0,25	111,84	12,75	34,17	4,84	20,09	5,14	1,88	5,18
	BHVOf - 2	17,71	1,44	0,20	126,58	14,41	37,73	5,31	23,15	5,94	1,97	6,07
	BHVOf - 3	18,25	1,44	0,20	127,50	13,87	37,71	5,39	24,18	5,61	2,11	5,89
	BHVOf - 4	17,90	1,57	0,25	131,27	14,28	38,68	5,45	23,49	5,77	2,15	5,86
	BHVOf - 5	18,68	1,53	0,15	129,42	14,70	38,66	5,40	24,11	5,78	2,07	6,11

BHVOf - 6	17,46	1,30	0,20	128,02	14,59	39,10	5,36	23,45	5,93	2,23	6,40
BHVOf - 7	17,42	1,31	0,22	131,91	14,55	38,03	5,20	24,38	5,96	1,92	6,34
BHVOf - 8	17,92	1,40	0,24	129,89	14,21	38,27	5,33	23,02	5,67	2,11	6,45
BHVOf - 9	17,83	1,29	0,21	133,07	14,69	38,59	5,36	24,02	6,23	2,02	6,12
BHVOf - 10	18,16	1,38	0,19	131,77	14,51	37,84	5,26	23,72	5,99	2,04	5,89
Average Analysed	**17,75**	**1,39**	**0,21**	**128,13**	**14,26**	**37,88**	**5,29**	**23,36**	**5,80**	**2,05**	**6,03**
% Deviation	*4,2*	*31,3*	*105,8*	*4,7*	*7,7*	*0,5*	*2,4*	*5,7*	*5,9*	*0,2*	*4,1*
Certified BCR powder	12,44	250,60	1,16	683,90	25,08	53,12	6,83	28,26	6,55	1,99	6,81
BCRf - 1	11,17	213,99	1,00	593,00	21,74	49,51	6,31	24,37	5,80	1,80	5,89
BCRf - 2	12,15	231,00	0,96	661,50	22,73	52,43	6,56	26,45	6,37	1,94	6,02
BCRf - 3	12,30	232,14	1,08	651,47	23,02	53,34	6,60	27,69	6,63	2,11	6,37
BCRf - 4	12,09	236,94	0,98	669,70	22,54	53,34	6,64	27,12	6,31	1,98	7,33
BCRf - 5	11,93	238,62	0,98	665,26	23,60	54,09	7,08	27,96	6,58	1,98	6,79
BCRf - 6	12,08	235,27	1,10	670,30	23,09	53,56	6,48	28,26	6,32	2,04	6,78
BCRf - 7	12,36	232,27	1,05	669,52	23,36	53,84	6,77	27,88	6,26	1,91	6,84
BCRf - 8	11,72	236,29	1,09	651,85	23,11	52,76	6,66	27,36	6,57	2,03	6,75
BCRf - 9	12,28	232,76	1,08	674,59	23,30	53,34	6,77	27,99	6,29	1,96	6,72
BCRf - 10	11,91	236,25	1,05	663,38	23,33	52,68	6,69	27,23	6,48	1,98	6,48
Average Analysed	**12,00**	**232,55**	**1,04**	**657,06**	**22,98**	**52,89**	**6,66**	**27,23**	**6,36**	**1,97**	**6,60**
% Deviation	*3,6*	*7,2*	*10,5*	*3,9*	*8,4*	*0,4*	*2,5*	*3,6*	*2,8*	*0,8*	*3,1*
MD1 - 1	15,80	3,09	7,50	312,95	52,21	115,79	13,95	47,31	8,33	1,55	6,47
MD1 - 2	16,44	3,50	8,17	332,99	55,95	133,31	14,40	51,01	9,30	1,60	7,43
MD10 - 1	17,41	2,85	8,46	331,27	54,21	132,09	13,83	48,15	9,18	1,54	6,95
MD10 - 2	16,06	3,12	8,09	299,34	52,76	122,58	12,89	45,20	8,25	1,55	7,11
MD2 - 1	15,05	2,97	7,61	303,15	50,40	117,57	12,75	45,82	7,75	1,58	6,33
MD2 - 2	17,60	3,11	8,85	318,01	55,08	129,23	13,82	51,17	9,16	1,76	6,02
MD3 - 1	16,81	2,50	7,18	299,56	48,94	116,97	12,57	44,29	7,27	1,51	6,23
MD3 - 2	14,65	3,20	7,41	290,75	50,12	115,08	12,98	44,74	8,48	1,48	6,59
MD4 - 1	15,71	3,36	7,79	313,82	50,43	121,55	12,86	47,42	8,64	1,64	7,27

161

APPENDIX-B: *Continued*

	MD4 - 2	15,88	2,73	7,52	292,94	49,28	115,74	12,85	45,97	8,10	1,44	6,23
	MD5 - 1	16,42	2,64	7,62	306,95	50,51	118,91	13,47	45,06	8,42	1,57	6,71
	MD5 - 2	15,02	2,98	7,49	303,93	47,54	110,92	12,81	44,27	8,56	1,45	6,68
	MD6 - 1	16,10	3,41	8,28	308,03	51,52	123,88	13,98	47,63	9,22	1,71	6,69
	MD6 - 2	15,65	3,27	8,21	305,85	50,83	121,21	13,20	49,83	9,41	1,49	7,54
	MD7 - 1	17,02	2,74	7,99	312,71	52,27	125,11	13,17	48,61	8,68	1,40	7,00
	MD7 - 2	15,56	3,09	7,71	307,64	52,60	119,56	13,19	46,11	9,58	1,63	6,85
	MD8 - 1	15,69	3,29	7,97	305,90	51,34	122,01	13,68	47,17	9,05	1,38	6,82
	MD8 - 2	15,84	3,42	7,77	303,94	51,84	121,78	13,76	47,79	9,22	1,48	6,72
	MD9 - 1	15,30	3,01	7,43	294,16	49,82	119,57	13,19	46,87	8,42	1,45	7,08
	MD9 - 2	16,06	3,52	7,56	295,76	49,66	117,06	12,63	46,64	8,77	1,53	6,67
	MK11 - 1	29,64	1,37	9,15	557,17	91,48	168,57	19,27	63,60	12,14	2,57	10,75
	MK11 - 2	30,29	1,41	9,71	544,53	90,60	172,25	19,04	65,03	12,78	2,12	10,66
	MK12 - 1	32,17	1,95	9,68	547,99	93,19	172,81	19,43	67,04	12,99	2,47	10,47
	MK12 - 2	29,50	2,12	9,66	573,18	92,93	174,32	18,90	64,45	12,25	2,33	11,01
	MK13 - 1	28,83	1,87	9,76	550,62	91,01	170,72	19,21	64,11	12,92	2,44	10,69
	MK13 - 2	31,37	2,52	10,07	546,03	93,75	175,21	19,82	66,32	13,61	2,39	11,58
	MK14 - 1	29,21	1,95	9,21	560,83	93,05	173,01	19,35	63,31	13,28	2,50	10,85
	MK14 - 2	30,64	1,75	10,18	551,61	93,45	172,33	18,87	65,19	13,83	2,36	11,40
	MK15 - 1	29,52	1,89	9,32	527,61	92,60	170,34	19,62	66,19	12,53	2,20	11,94
	MK15 - 2	30,78	1,74	9,70	558,18	92,75	176,21	19,90	65,56	11,46	2,21	10,63
	MK16 - 1	30,08	1,90	9,92	513,85	91,71	164,63	18,33	64,44	12,75	2,27	11,01
	MK16 - 2	29,53	2,01	10,08	549,04	91,15	169,52	19,03	62,77	12,72	2,33	11,25
	MK17 - 1	31,51	2,27	9,65	560,88	93,34	173,39	19,40	64,70	14,06	2,24	10,76
	MK17 - 2	29,40	2,12	9,46	522,84	91,66	173,46	18,88	62,83	13,49	2,22	10,10
	MK18 - 1	30,33	1,93	9,61	550,97	93,58	168,96	19,28	63,59	12,28	2,48	11,76
	MK18 - 2	30,50	2,11	9,70	562,33	92,51	170,84	19,80	66,37	13,61	2,27	11,00
	MK19 - 1	30,40	1,57	9,50	554,09	92,30	175,01	19,51	63,83	13,55	2,20	10,48
	MK19 - 2	31,61	1,67	10,40	563,27	97,08	171,54	19,72	67,40	13,50	2,45	11,69
	MK20 - 1	30,53	1,97	9,55	533,70	88,48	174,55	19,61	61,87	13,33	2,71	10,35

162

University of Venda

	MK20 - 2										
		29,83	1,55	9,90	543,60	93,84	171,12	20,27	64,23	13,29	2,32	11,57

	Values in ppm	Tb	Dy	Ho	Er	Tm	Yb	Lu	Hf	Ta	Pb	Th
	Instrument DL	0,000	0,001	0,001	0,001	0,001	0,002	0,001	0,001	0,001	0,002	0,001
	Method DL (fusions)	0,015	0,063	0,014	0,048	0,014	0,073	0,016	0,056	0,015	0,060	0,026
Certified BHVO glass		**0,92**	**5,28**	**0,98**	**2,56**	**0,34**	**2,01**	**0,28**	**4,32**	**1,15**	**1,70**	**1,22**
	BHVO - 1	0,93	5,27	0,98	2,57	0,34	2,03	0,28	4,32	1,15	1,74	1,07
	BHVO - 2	0,91	5,20	0,96	2,43	0,33	1,96	0,29	4,32	1,20	1,73	1,21
	BHVO - 3	0,90	4,62	0,95	2,25	0,30	1,74	0,27	3,96	1,15	1,61	1,18
	BHVO - 4	0,92	5,22	0,96	2,54	0,33	2,03	0,29	4,31	1,17	1,68	1,05
	BHVO - 5	0,91	5,29	0,98	2,55	0,34	1,99	0,28	4,32	1,15	1,69	1,06
	Average Analysed	**0,91**	**5,12**	**0,97**	**2,47**	**0,33**	**1,95**	**0,28**	**4,25**	**1,16**	**1,69**	**1,11**
	% Deviation	0,6	3,0	1,0	3,6	1,7	3,0	0,8	1,8	0,8	0,5	8,4
Certified BCR glass		**1,02**	**6,44**	**1,27**	**3,70**	**0,51**	**3,39**	**0,50**	**4,84**	**0,78**	**11,00**	**5,90**
	BCR - 1	1,05	6,29	1,29	3,72	0,52	3,54	0,50	4,83	0,77	10,38	5,21
	BCR - 2	1,00	6,20	1,29	3,37	0,52	3,34	0,49	4,56	0,79	10,44	5,83
	BCR - 3	0,98	5,61	1,26	3,23	0,48	3,00	0,48	4,30	0,75	9,74	5,65
	BCR - 4	1,03	6,35	1,27	3,68	0,54	3,43	0,52	4,79	0,77	10,32	5,19
	BCR - 5	1,03	6,23	1,26	3,64	0,54	3,38	0,52	4,78	0,77	10,23	5,18
	Average Analysed	**1,02**	**6,14**	**1,27**	**3,53**	**0,52**	**3,34**	**0,50**	**4,65**	**0,77**	**10,22**	**5,41**
	% Deviation	0,0	4,7	0,2	4,6	2,0	1,6	0,4	3,8	1,2	7,1	8,3
Certified BHVO powder		**0,95**	**5,27**	**0,98**	**2,50**	**0,33**	**1,99**	**0,28**	**4,44**	**1,17**	**2,04**	**1,23**
	BHVOf - 1	0,83	4,49	0,90	2,07	0,30	1,63	0,26	3,68	1,03	2,09	1,07
	BHVOf - 2	0,91	4,45	1,04	2,36	0,34	1,72	0,28	4,11	1,18	2,18	1,17
	BHVOf - 3	0,83	4,68	0,91	2,45	0,30	1,86	0,28	4,08	1,12	2,45	1,24
	BHVOf - 4	0,87	5,27	0,99	2,57	0,27	2,11	0,31	4,84	1,19	2,31	1,16
	BHVOf - 5	0,84	4,87	1,01	2,44	0,35	1,98	0,28	4,39	1,15	2,49	1,27
	BHVOf - 6	0,90	5,19	1,01	2,46	0,30	2,08	0,23	4,49	1,20	2,20	1,20
	BHVOf - 7	0,94	4,79	0,94	2,26	0,34	2,01	0,28	4,35	1,20	2,06	1,12

	BHVOf - 8	0,90	4,94	1,00	2,23	0,34	1,89	0,27	4,33	1,19	2,28	1,30
	BHVOf - 9	0,96	4,81	0,99	2,33	0,32	1,91	0,29	4,21	1,23	2,32	1,29
	BHVOf - 10	0,91	4,88	1,01	2,35	0,35	1,75	0,28	4,01	1,14	2,10	1,19
	Average Analysed	**0,89**	**4,84**	**0,98**	**2,35**	**0,32**	**1,89**	**0,27**	**4,25**	**1,16**	**2,25**	**1,20**
	% Deviation	6,1	8,2	0,4	6,0	2,5	4,7	1,2	4,3	1,0	10,3	1,9
Certified BCR powder		**1,08**	**6,42**	**1,31**	**3,67**	**0,53**	**3,39**	**0,50**	**4,97**	**0,79**	**10,59**	**5,83**
	BCRf - 1	1,01	5,56	1,21	3,19	0,51	2,78	0,49	4,29	0,73	9,57	5,59
	BCRf - 2	1,03	5,64	1,27	3,38	0,53	2,98	0,52	4,46	0,76	10,03	5,90
	BCRf - 3	1,04	6,42	1,25	3,52	0,46	3,16	0,45	4,37	0,78	10,84	5,86
	BCRf - 4	1,04	5,94	1,29	3,77	0,48	3,50	0,45	4,67	0,78	10,86	5,86
	BCRf - 5	1,05	6,22	1,32	3,55	0,52	3,12	0,44	4,82	0,73	10,70	5,97
	BCRf - 6	0,99	6,01	1,32	3,37	0,53	3,20	0,50	4,58	0,72	10,54	5,74
	BCRf - 7	0,98	6,19	1,25	3,31	0,49	3,31	0,48	4,81	0,79	10,15	5,73
	BCRf - 8	0,95	6,05	1,34	3,22	0,51	3,10	0,52	4,73	0,72	10,03	5,60
	BCRf - 9	1,04	5,94	1,29	3,27	0,50	2,83	0,49	4,35	0,78	10,39	5,90
	BCRf - 10	1,08	5,76	1,33	3,17	0,53	2,85	0,49	4,42	0,77	10,23	5,71
	Average Analysed	**1,02**	**5,97**	**1,29**	**3,38**	**0,50**	**3,08**	**0,48**	**4,55**	**0,76**	**10,33**	**5,79**
	% Deviation	5,2	7,0	1,9	8,0	5,8	9,1	4,4	8,5	3,7	2,4	0,7
	MD1 - 1	1,01	5,63	1,18	3,01	0,52	2,77	0,48	5,39	1,46	12,84	18,60
	MD1 - 2	1,04	5,85	1,27	3,59	0,45	3,25	0,50	6,11	1,69	14,16	19,75
	MD10 - 1	1,13	6,46	1,14	3,27	0,53	3,00	0,47	5,56	1,55	16,30	19,10
	MD10 - 2	0,99	5,40	1,12	2,89	0,50	3,07	0,46	5,67	1,41	15,84	18,95
	MD2 - 1	0,91	5,83	1,09	2,71	0,51	3,15	0,46	5,72	1,39	13,52	17,65
	MD2 - 2	1,10	6,29	1,13	3,24	0,43	3,47	0,42	5,94	1,40	15,03	19,38
	MD3 - 1	0,87	4,97	1,03	3,07	0,47	2,86	0,45	5,35	1,50	10,75	17,43
	MD3 - 2	1,01	5,95	1,17	2,91	0,46	3,21	0,37	5,83	1,28	10,53	18,06
	MD4 - 1	0,99	5,52	1,07	3,07	0,48	2,85	0,42	5,83	1,27	12,69	17,83
	MD4 - 2	0,94	6,08	1,08	2,89	0,50	2,85	0,44	5,30	1,36	12,57	17,96
	MD5 - 1	0,91	5,76	1,23	3,13	0,48	2,90	0,40	5,45	1,47	11,25	18,70

MD5 - 2	0,99	5,12	1,11	3,07	0,51	3,13	0,40	5,59	1,34	10,78	17,19
MD6 - 1	0,92	5,65	1,19	2,90	0,46	3,18	0,42	5,07	1,36	12,34	18,94
MD6 - 2	1,09	5,82	1,19	3,23	0,54	3,01	0,44	5,86	1,41	12,27	18,43
MD7 - 1	1,03	6,23	1,18	3,23	0,46	2,95	0,46	5,42	1,41	14,69	18,43
MD7 - 2	0,98	6,00	1,20	3,14	0,48	2,83	0,42	5,39	1,42	14,03	18,63
MD8 - 1	0,97	5,36	1,17	2,85	0,44	2,90	0,46	5,64	1,28	11,56	18,03
MD8 - 2	0,94	5,14	1,18	2,88	0,50	3,22	0,42	5,12	1,49	11,52	19,00
MD9 - 1	1,11	5,88	1,11	2,95	0,46	3,23	0,43	5,56	1,22	12,85	17,79
MD9 - 2	0,96	5,37	1,07	3,00	0,43	3,02	0,45	5,66	1,27	13,78	18,35
MK11 - 1	1,57	9,49	2,07	4,87	0,72	5,30	0,76	8,73	2,01	30,62	29,52
MK11 - 2	1,67	8,92	2,20	5,66	0,89	6,10	0,73	8,77	2,30	32,19	30,25
MK12 - 1	1,50	9,16	1,95	5,31	0,83	5,13	0,78	7,70	2,20	35,22	30,58
MK12 - 2	1,62	9,59	1,95	5,48	0,94	5,74	0,70	8,75	2,04	37,05	30,48
MK13 - 1	1,55	9,27	1,95	5,06	0,79	4,90	0,78	8,23	2,14	35,11	29,85
MK13 - 2	1,56	9,79	2,02	5,25	0,87	5,40	0,74	8,94	2,05	37,66	31,99
MK14 - 1	1,76	9,51	2,09	5,39	0,93	6,00	0,79	8,14	2,11	33,49	31,76
MK14 - 2	1,71	9,08	1,96	5,17	0,79	5,24	0,73	8,74	2,01	34,10	30,23
MK15 - 1	1,72	9,69	1,99	5,14	0,79	5,49	0,68	8,11	2,14	32,55	30,63
MK15 - 2	1,64	11,14	2,01	5,19	0,94	5,29	0,77	8,34	2,05	34,13	30,17
MK16 - 1	1,64	9,55	1,99	5,25	0,77	4,49	0,77	8,07	2,02	33,74	29,44
MK16 - 2	1,77	9,59	2,01	5,13	0,84	5,88	0,82	8,72	2,07	33,07	29,28
MK17 - 1	1,69	9,75	2,00	4,95	0,77	5,31	0,85	7,81	2,18	31,95	31,88
MK17 - 2	1,62	10,08	2,05	5,13	0,90	5,22	0,80	8,21	2,06	32,89	30,61
MK18 - 1	1,68	10,13	1,96	5,42	0,83	5,68	0,86	8,23	2,11	32,13	30,59
MK18 - 2	1,79	10,53	2,03	5,28	0,84	5,95	0,77	8,77	2,32	36,99	30,88
MK19 - 1	1,74	9,13	1,89	5,42	0,84	5,10	0,80	8,44	2,13	32,98	29,26
MK19 - 2	1,74	10,21	2,09	5,26	1,01	5,40	0,88	8,80	2,29	32,60	31,55
MK20 - 1	1,57	8,88	1,91	5,25	0,90	5,39	0,79	8,22	1,99	29,63	29,36
MK20 - 2	1,69	9,90	1,96	5,21	0,79	5,71	0,83	8,34	2,22	32,12	31,17

Article

Methanogenesis Potentials: Insights from Mineralogical Diagenesis, SEM and FTIR Features of the Permian Mikambeni Shale of the Tuli Basin, Limpopo Province of South Africa

George Oluwole Akintola [1,*], Francis Amponsah-Dacosta [1], Steven Rupprecht [2], Nithyadharseni Palaniyandy [3], Sphiwe Emmanuel Mhlongo [1], Wilson Mugera Gitari [4] and Joshua Nosa Edokpayi [5]

Stable Isotopic Characteristics of the Permian Tuli Basin: Implication for Shale Gas Potentiality, South Africa

George Akintola[1], Francis Amponsah-Dacosta[1], Steven Rupprecht[2], Sphiwe Mhlongo[1]

[1] University of Venda, Department of Earth Sciences, Faculty of Science, Engineering and Agriculture, Thohoyandou 0950 Private Bag X50550, Limpopo Province South Africa
[2] Department of Mining Engineering, University of Johannesburg, Gauteng Province, South Africa
corresponding-author-georgeakintola540@gmail.com

Shale Gas Potential of the Permian Tuli Basin in Limpopo Province, South Africa: Insight from Mineralogical, SEM and Organic Isotopic Constraints

Akintola George.Oluwole[1], Amponsah-Dacosta Francis[1], Rupprecht Steven[2], Mhlongo Sphiwe.Emmanuel[1]

[1] Department of Earth Sciences, Faculty of Science, Agriculture and Engineering, University of Venda, University Road, Thohoyandou 0950

[2] Department of Mining Engineering, University of Johannesburg, Johannesburg 2006,

Keywords: source-rock, shale gas, thermal maturity, kerogen, Tuli basin

Submissions Being Processed for Author George Oluwole Akintola, Ph.D

Page: 1 of 1 (1 total submissions)   Results per page 10

⊞ Action ▲	Manuscript Number ▲▼	Title ▲▼	Initial Date Submitted ▲▼	Status Date ▲▼	Current Status ⓘ ▲▼
Action Links	AES10246	Kerogen Type, Stable Isotopic and Geochemical Evaluation of the Permian Mikambeni Black Shale of Tuli Basin South Africa: Implication for Shale Gas Potential	06 Oct 2021	11 Oct 2021	Editor Assigned

Page: 1 of 1 (1 total submissions)   Results per page 10

<< Author Main Menu

Arabian Journal
of Geosciences

Editorial
Manager

Role: Author   Username: georgeakintola540@gmail.com

← Submissions Being Processed for Author

Page: 1 of 1 (1 total submissions)

Results per page 10 ⌄

| Action ➕	🔽	Manuscript Number ▲	Title ▲	Initial Date Submitted ▲	Status Date ▼	Current Status ▲
Action Links		AJGS-D-22-01886	Petrographic, mineralogical, morphological and organic constraints of the Permian Shale in Limpopo-Area Karoo Basin, South Africa: Implication for Potential Shale Gas Generation	22 Apr 2022	02 May 2022	Under Review

Page: 1 of 1 (1 total submissions)

Results per page 10 ⌄

168

Editorial Manager™

Role: Author   Username: georgeakintola540@gmail.com

← **Submissions Being Processed for Author**

Page: 1 of 1 (1 total submissions)   Results per page 10 ⌄

Action ➕	⟱	Manuscript Number ▲	Title ▲	Initial Date Submitted ▲	Status Date ▼	Current Status ▲
Action Links		AJGS-D-22-01886	Petrographic, mineralogical, morphological and organic constraints of the Permian Shale in Limpopo-Area Karoo Basin, South Africa: Implication for Potential Shale Gas Generation	22 Apr 2022	02 May 2022	Under Review

Page: 1 of 1 (1 total submissions)   Results per page 10 ⌄